UNIVERSIDAD NACIONAL DE SAN MARTÍN
COMISIÓN NACIONAL DE ENERGÍA ATÓMICA
INSTITUTO DE TECNOLOGÍA
"Prof. Jorge A. Sabato"

Estudio de las propiedades de los hadrones livianos en presencia de campos magnéticos intensos mediante modelos efectivos de quarks

por Lic. Máximo Coppola

Director
Norberto N. Scoccola

(*) Tesis para optar al título de *Doctor en Ciencia y Tecnología, Mención Física*

República Argentina
2023

Resumen

Los campos magnéticos intensos de magnitud $\sqrt{eB} \gtrsim \Lambda_{QCD}$ pueden ser relevantes para una serie de escenarios físicos. Dichos campos logran resolver la estructura de quarks de un hadrón, modificando significativamente las propiedades de la materia que interactúa fuertemente. En esta tesis empleamos un modelo efectivo de quarks para investigar el efecto que un campo magnético uniforme externo tiene sobre las propiedades de los hadrones más ligeros, es decir, los mesones pseudoescalares y los nucleones. Específicamente, utilizamos un modelo tipo Nambu–Jona-Lasinio (NJL), en el cual la interacción entre quarks es local preservando la simetría quiral. Para el análisis de las partículas cargadas, presentamos un método basado en el uso de autofunciones tipo Ritus para sistemas magnetizados que nos permite tener completamente en cuenta los efectos debidos a la presencia de fases de Schwinger no nulas que han sido usualmente desestimadas en la literatura. Para regularizar el modelo utilizamos un esquema en el cual sólo las contribuciones que no dependen explícitamente del campo son regularizadas. Esto permite evitar ciertos inconvenientes que aparecen en otro tipo de esquemas alternativos. Además, exploramos la posibilidad de incorporar el efecto de catálisis magnética inversa mediante el uso de un acoplamiento dependiente del campo magnético. Dentro de este marco, nos centramos en la dependencia con el campo magnético de las masas del nonete de mesones pseudoescalares así como de los nucleones, donde estos últimos se construyen como estados ligados quark-diquark. Otras propiedades de los piones también son calculadas, como los acoplamientos quark-pión, las velocidades transversales y las constantes de decaimiento, lo que permite estimar el ancho de decaimiento de los piones cargados magnetizados. El decaimiento se analiza en términos generales mediante el método de Ritus, donde mostramos que aparecen cuatro factores de forma independientes al hadronizar las corrientes de quarks. Además revelamos que, en presencia de campo magnéticos muy intensos, el mecanismo de supresión de helicidad está ausente, y que la distribución angular de las partículas salientes es altamente anisotrópica. El método de Ritus y otras estrategias presentadas en este trabajo para tratar sistemas magnetizados representan una herramienta útil que puede aplicarse al cálculo de propiedades de partículas cargadas a través de diferentes enfoques.

Palabras claves: QCD. Campo magnético. Modelo NJL.

Abstract

Strong magnetic fields of magnitude $\sqrt{eB} \gtrsim \Lambda_{QCD}$ may be relevant for a range of physical scenarios. Such fields can resolve the quark structure of an hadron, significantly modifying the properties of strongly interacting matter. In this thesis we employ an effective quark model to investigate the effect that an external uniform magnetic field has on the properties of the lightest hadrons, i.e. pseudoscalar mesons and nucleons. Specifically, we use a Nambu–Jona-Lasinio (NJL) type model, in which the interaction between quarks is local while preserving chiral symmetry. For the analysis of charged particles, we present a method based on the use of Ritus-type eigenfunctions for magnetized systems which allow us to fully account for the effects due to the presence of Schwinger phases that have been usually disregarded in the literature. To regularize the model we use a scheme in which only the contributions that do not depend explicitly on the field are regularized. This allows us to avoid certain drawbacks that appear in other types of alternative schemes. In addition, we explore the possibility of incorporating the inverse magnetic catalysis effect through the use of a magnetic field dependent coupling. Within this framework, we focus on the magnetic field dependence of the masses of the nonet of pseudoscalar mesons as well as nucleons, where the latter are constructed as bound quark-diquark states. Other pions properties, such as quark-pion couplings, transverse velocities and decay constants, are also calculated, allowing for an estimation of the decay width of magnetized charged pions. The decay is analyzed on general grounds via the Ritus method, where we show that four independent form factors appear when hadronizing quark currents. We further reveal that, in the presence of a very strong magnetic field, the helicity suppression mechanism is absent, and the angular distribution of outgoing particles is highly anisotropic. The Ritus method and other strategies presented in this work to deal with magnetized systems represent a useful tool that can be applied to the calculation of charged particle properties across different approaches.

Keywords: QCD. Magnetic field. NJL model.

Listado de publicaciones

1. M. Coppola, D. Gomez Dumm & N. N. Scoccola, 'Charged pion masses under strong magnetic fields in the NJL model', Physics Letter B **782**, 155 (2018).

2. M. Coppola, D. Gomez Dumm & N. N. Scoccola, 'Pion masses under intense magnetic fields within the NJL model', Proceedings of the XIV Hadron Physics, SLAC eConf C180318 (2018) - arXiv:1805.01549.

3. M. Coppola, D. Gomez Dumm, S. Noguera & N. N. Scoccola, 'Pion-to-vacuum vector and axial vector amplitudes and weak decays of pions in a magnetic field', Physical Review D **99**, 054031 (2019).

4. M. Coppola, D. Gomez Dumm, S. Noguera & N. N. Scoccola, 'Neutral and charged pion properties under strong magnetic fields in the NJL model', Physical Review D **100**, 054014 (2019).

5. M. Coppola, D. Gomez Dumm, S. Noguera & N. N. Scoccola, 'Weak decays of magnetized charged pions in the symmetric gauge', Physical Review D **101**, 034003 (2020).

6. M. Coppola, D. Gomez Dumm, S. Noguera & N. N. Scoccola, 'Magnetic field driven enhancement of the weak decay width of charged pions', Journal of High Energy Physics **2020**, 58 (2020).

7. M. Coppola, D. Gomez Dumm & N. N. Scoccola, 'Diquarks and nucleons under strong magnetic fields in the NJL model', Physical Review D **102**, 094020 (2020).

8. S. S. Avancini, J. C. Sodré, M. Coppola & N. N. Scoccola, 'Light pseudoscalar meson masses under strong magnetic fields within the SU(3) Nambu–Jona-Lasinio model', Physical Review D **104**, 094040 (2021).

Proyectos científico-tecnológicos

- Subsidio para proyectos científicos y tecnológicos (2015), Temas Abiertos - Tipo A, Agencia Nacional de Promoción Científica y Tecnológica. Proyecto PICT-2014-0492. Investigador responsable: Dr. Norberto N. Scoccola
- Subsidio para proyectos científicos y tecnológicos (2018), Temas Abiertos - Tipo A, Agencia Nacional de Promoción Científica y Tecnológica. Proyecto PICT-2017-0571. Investigador responsable: Dr. Norberto N. Scoccola.
- Subsidio para proyectos científicos y tecnológicos (2022), Temas Abiertos - Serie A, Agencia Nacional de Promoción Científica y Tecnológica. Proyecto PICT-2020-SERIEA-01847. Investigador responsable: Dr. Norberto N. Scoccola.

Contents

CHAPTER 1

Introduction

1.1 Quantum chromodynamics

The theory which describes the strong interactions within the framework of the Standard Model is known as quantum chromodynamics (QCD). It was established as such several decades ago, recognizing quarks as the primary constituents of hadrons and gluons as the mediators of the interaction [1–3]. In this formulation, quarks and gluons possess a property known as "color charge", analogous to the electric charge of quantum electrodynamics (QED), which is responsible for strong interactions. The strength of the interaction is measured by g_s, the dimensionless coupling constant of the theory. However, upon quantization, logarithmic divergences in one-loop diagrams of perturbation theory imply that this "constant" actually depends on the typical energy scale μ of the processes under consideration, called the renormalization group scale. This running of the coupling is specified by the beta-function of the renormalization group. The self-interaction between gluons dramatically modifies the running of the QCD coupling $\alpha_s = g_s^2/(4\pi)$, as compared to QED. For high energies the coupling weakens ($\alpha_s \to 0$) and quarks and gluons form (nearly) free states, a property dubbed as asymptotic freedom [4, 5]. On the other hand, perturbation theory suggests that for low energy processes $\alpha_s \to \infty$. Experience indicates that, under ordinary conditions of temperature and density, say $T \lesssim 200$ MeV and $\mu \lesssim 350$ MeV [6], hadrons are the relevant degrees of freedom. This implies that QCD matter must necessarily glue together in such a way as to form color singlet bound states whose net color charge is zero, a phenomenon dubbed as (color) confinement. The value of μ which separates these two regimes is known as the QCD scale Λ_{QCD}. For scale energies below the charm quark mass $\mu < 1.25$ GeV, where only the three lightest flavors are active,

we have $\Lambda_{\mathrm{QCD}} \sim 300$ MeV. The process by which a dimensionless constant such as g_s is replaced by a dimensionful one such as Λ_{QCD} is called dimensional transmutation.

1.2 QCD matter under extreme conditions

Shortly after the advent of QCD, it was conjectured that at sufficiently high temperatures and/or densities states of matter known by the generic name of quark-gluon plasma (QGP) can form, which are characterized by color deconfinement and where quarks and gluons are the dominant degrees of freedom [7–9]. This prompted the theoretical study of the possible phases of QCD under such extreme conditions and revealed a potentially complex phase structure [10, 11]. In fact, the study of the QCD phase diagram continues to present a theoretical and experimental challenge to this day [12]. A schematic view in the temperature and baryon chemical potential μ_B plane is depicted in Figure 1.1.

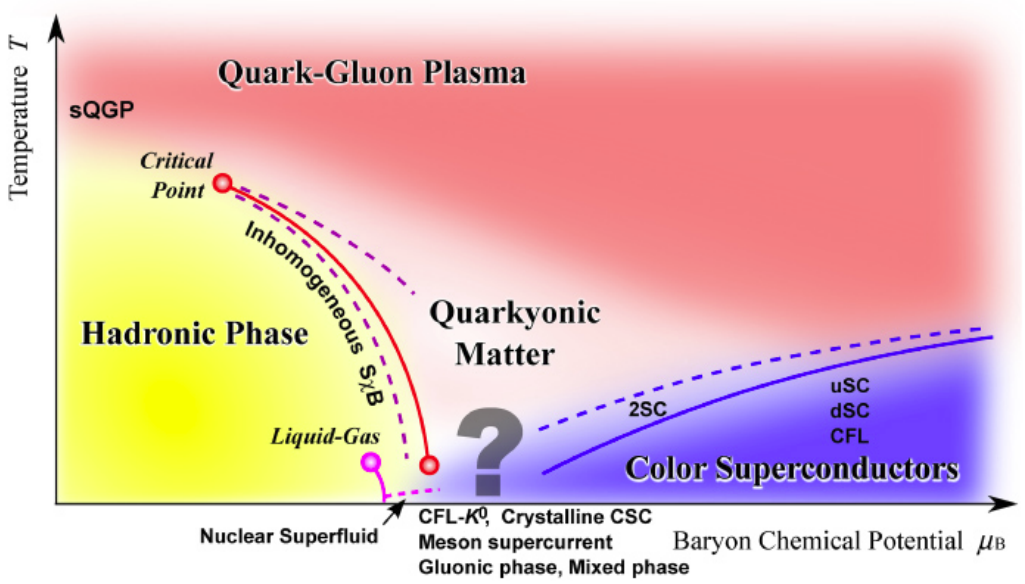

Figure 1.1: Schematic view of the QCD phase diagram at finite temperature and chemical potential (density). Figure from Ref. [10].

The transition between different phases is signaled by critical behavior often associated with the spontaneous breaking of a global symmetry [13]. The order parameter is the quantity that establishes the state of a symmetry: it vanishes when the system shares the symmetry of the Lagrangian and becomes nonzero when the symmetry is spontaneously broken. In order to properly characterize these phases, it is necessary to study the symmetry properties of the theory under groups of unitary transformations acting on the internal degrees of freedom of the theory. The QCD Lagrangian is by construction invariant

under the $SU(3)_c$ color group. For massless quarks, it is also invariant under the flavor chiral group, which can be decomposed into vector and axial groups as $U(N_f)_L \times U(N_f)_L = U(1)_V \times SU(N_f)_V \times U(1)_A \times SU(N_f)_A$. Here N_f is the number of flavors: for full QCD, $N_f = 6$. For massive quarks, chiral symmetry is broken. Nonetheless, it is approximately conserved in the light quark sector. In the vacuum state of QCD, the axial symmetry is broken due to interactions, even for massless quarks. Thus, chiral symmetry is broken and an effective mass for the quarks is dynamically generated [14]. The order parameter that characterizes this spontaneous breaking is the chiral condensate $\langle\bar{\psi}\psi\rangle$. In fact, this breaking is responsible for most of the nucleon mass, while the corresponding light Goldstone bosons [15] are identified with the pions. These dynamical effects are of great importance in the study of the QCD phase diagram, since there are indications that this symmetry is restored in the QGP phase. At the phase transition thermodynamic quantities change characteristically, all related to an anomaly in the pressure. Fluctuations of conserved quantities, such as baryon, electric charge and strangeness number, are sensitive observables in relativistic heavy-ion collisions to probe the QCD phase transition. Furthermore, experimental and theoretical evidence leads to the assumption that the phase transitions of deconfinement and chiral symmetry restoration occur virtually simultaneously at low densities [16–18]. However, the exact mechanism that gives rise to this simultaneous transition is not yet fully understood quantitatively.

The formation of the QGP involves high energy processes, which can only happen under extreme conditions. These conditions are difficult to produce, leaving few physical situations for experimental study. One of the natural scenarios where deconfined QCD phases are believed to be realized is in the hot early Universe, corresponding to the region of low densities and high temperatures in the phase diagram. According to the hot big bang model, the early Universe has experienced (at least) two epochs where phase transitions could occur: the electroweak transition at temperatures around $T_{\rm EW} \sim 100$ GeV, when fermions and gauge bosons became massive particles, and the QCD pseudo-critical transition T_c when quarks confined into hadrons. From lattice QCD (LQCD) simulations, the QCD transition is expected to be a smooth crossover at around $T_c \simeq 156$ MeV [19–22]. However, there are some known mechanisms that could provide a first order QCD transition, see e.g. [23–25]. Another natural scenario corresponds to the cores of so-called compact stars [26, 27]. These neutron stars are extremely stable and dense objects, which constitute one of the possible final scenarios in the life cycle of a star. In them, the density is large enough to form color superconducting states, corresponding to the region of high densities and low temperatures in the phase diagram. At asymptotically large chemical potentials and small temperatures, where perturbative QCD is applicable due to asymptotic freedom, 3-flavor QCD matter is in the so-called color-flavor-locked

phase [28–30]. In this regime chiral symmetry is broken, and the transition temperature to quark matter is found to be first order [31, 32]. At intermediate densities, including those relevant for astrophysics environments, alternative phases proposed in the literature include two-flavor color superconductors, noncolor-flavor-locked mixed phases, crystalline color superconductivity, kaon condensation, gluonic phases, superfluidity, gapless and inhomogeneous phases, see Refs. [6, 33–35] for more details.

As for human-made scenarios, several heavy ion accelerators have been built in the last decades, in which experiments are carried out to reach the phases corresponding to high temperatures and densities in the QCD phase diagram [36, 37]. Large experimental programs have been carried out at the Relativistic Heavy Ion Collider (RHIC) [38, 39] at the BNL laboratory and at the Large Hadron Collider (LHC) [40] under ALICE, ATLAS and CMS experiments as well as the Super Proton Synchrotron (SPS) at CERN. In this type of accelerators, the objective is to collide heavy ions such as lead, silver or gold at center-of-mass energies on the order of $100-200$ GeV or more. Extremely high temperatures are reached during the collision process, above the critical deconfinement temperature T_c [38]. This suggest that a transient QGP is possibly formed, which hadronizes when cooled down. Outcoming particles from the collision carry indirect information about the QGP. Present results suggest that QGP has managed to form for time periods on the order of 10 fm/c [41, 42].

Contrary to original expectations, QGP is not a weakly coupled plasma. It is in fact strongly coupled and near-perfect liquid, with specific viscosity η/s value close to $1/4\pi$ [36, 43]. Interestingly, the AdS/CFT duality between infinitely strongly coupled gauge theories (cousins of QCD) and gravitational descriptions has led to the conjecture that for any relativistic quantum field theory, $\eta/s > 1/4\pi$ [44]. The similarity between both results lends credibility to the idea that holography can provide meaningful insights into QCD. Due to the assumption of infinite coupling strength in the holographic computation, the ideal fluid behavior of the QGP has been interpreted as signaling a strongly interacting system, also supported by the fact that the value of η/s obtained for a gas of quarks and gluons in a weak coupling regime is an order of magnitude larger. Despite its short duration, the QGP exhibits thermodynamic equilibrium properties, further giving evidence confirming the hypothesis that the phase transition between the hadronic and QGP phases is of the crossover type [45]. The conditions produced in current heavy ion accelerators correspond essentially to the vertical axis of the phase diagram, i.e. at low chemical potentials. The quark-hadron crossover transition observed in this regime is expected to change into a first order transition for higher μ_B, with a second order critical endpoint (CEP) in between. The position of the CEP has been extensively studied within different theoretical frameworks (see e.g. Refs. [46–49]) and explored in current accelerators [39, 50].

In fact, its search is one of the benchmarks for future experiments at the Nuclotron-based Ion Collider fAcility (NICA), the Facility for Antiproton and Ion Research (FAIR) and the Japan Proton Accelerator Research Complex (J-PARC), where higher densities can be reached.

While initially the phase diagram was investigated taking density and temperature as variables, in the last decade there has been greatly increased interest in the presence of strong (electro)magnetic fields and their effects [51–53]. Even though the electromagnetic coupling constant e is much smaller than the strong coupling constant g_s, electromagnetism can be relevant for QCD physics if the field strength is so strong that $\sqrt{eE}$, $\sqrt{eB} \sim \Lambda_{QCD}$. Such intense electromagnetic fields appear in many of the aforementioned physical scenarios. Several models predict the generation of strong magnetic fields during the early evolution of the Universe, which are required by present day observations of weak but nonvanishing intergalactic magnetic fields. Such strong fields could have modified the nature of the electroweak phase transition, and their effect could have left traces in certain anisotropies of the cosmic microwave background [54, 55]. On the other hand, at the surface of certain compact stars called 'magnetars', magnetic fields can reach values of the order 10^{15} G [56–58], increasing by a few orders of magnitude to $10^{18} - 10^{20}$ G towards the core [59–62]. See Ref. [63] for a current magnetar catalog and also Ref. [64] for a recent review. The effect of magnetic fields on dense quark matter is also reviewed in Ref. [65]. Regarding human-made scenarios, in the last decade it has been observed that in heavy ion collisions (HIC) the motion of charged spectator particles produces magnetic fields of magnitudes as large as $10^{19} - 10^{20}$ G [66–70]. Although these fields occur essentially at the initial moments of the collision and decay rapidly, at times on the order of 10^{-21} s [67], they could substantially affect the way the QGP hadronizes [51, 71]. Lastly, magnetic fields are also relevant to quasi-relativistic condensed matter systems like graphene [52].

The phase diagram of QCD in the three-dimensional (μ, T, B) space has been studied within several approaches. While the temperature axis can be directly addressed on the lattice, for finite chemical potentials the so-called sign problem hinders density studies, which have been performed mainly through effective models or holographic approaches. Interestingly, while the majority of effective models predict the increase of the pseudocritical transition temperature T_c with the magnetic field [52, 53], accurate LCQD results [73–76] have shown the opposite pattern, i.e. a decrease of T_c with the magnetic field. In fact, as shown in Refs. [72, 77], this behavior is prolonged for very strong magnetic fields, where a first order transition was found at $eB = 9$ GeV^2, implying the existence of a critical end-point somewhere within the range 4 GeV^2 $< eB <$ 9 GeV^2. An updated QCD phase diagram in the temperature and magnetic field plane can be found in Figure 1.2, as proposed by Ref. [72].

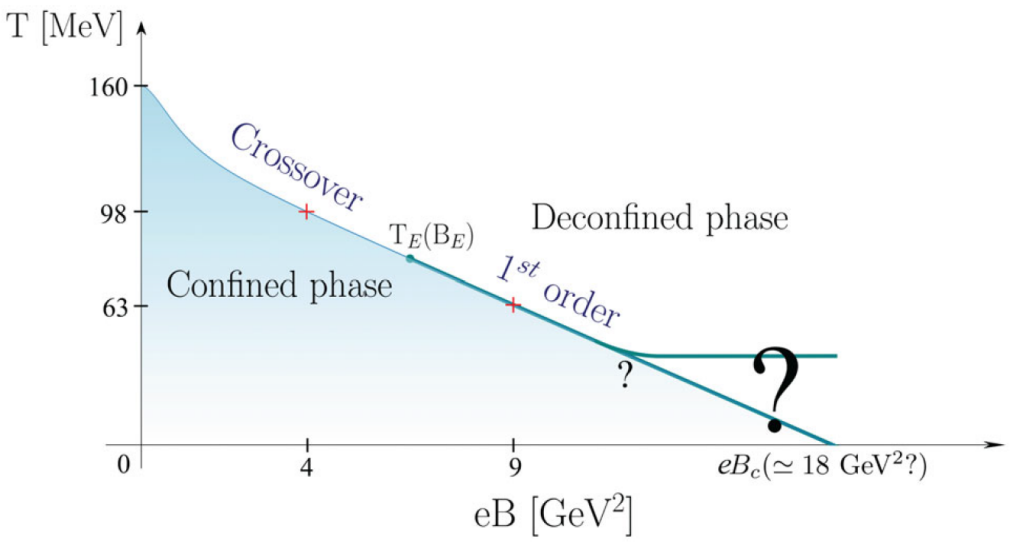

Figure 1.2: QCD phase diagram at finite temperature and magnetic field. The (pseudo)critical temperature decreases as function of B, and the transition switches from a crossover to first order at a critical end point located in the range $4\ \mathrm{GeV}^2 < eB_E < 9\ \mathrm{GeV}^2$. Figure from Ref. [72].

1.3 Magnetic field effects on QCD matter

It is expected that new detectable effects will emerge in the phase diagram and properties of strongly interacting matter due to these extreme magnetic fields, causing numerous phenomenological consequences [52]. These include magnetic catalysis (MC) of the chiral condensate [52, 78]; inverse magnetic catalysis (IMC) of the restoring chiral and deconfinement temperature [73, 74, 79, 80]; chiral magnetic effect [66, 81, 82]; chiral separation effect [83, 84]; chiral magnetic waves [85–89]; vacuum superconductivity [90, 91], as well as many other effects on the properties of the resulting particles that are detected after collisions [71, 92, 93], to name a few. In addition to its importance for the phenomenology of the above-mentioned physical scenarios, magnetic fields also of academic interest on its own because they serve as a probe of the theory of strongly interacting matter. In particular, a comparison between LQCD and effective model results in the presence of external electromagnetic fields allow for a constraint of the latter, acquiring a better understanding of the underlying theory.

For the scope of this thesis, which involves the analysis of light hadron properties, it will be relevant to discuss in some detail the MC and IMC effects. The term magnetic catalysis refers to either the enhancement of an existing condensate or the appearance of a new condensate by the presence of an external magnetic field. In QCD, the generation of the chiral condensate $\langle\bar{\psi}\psi\rangle$ breaks in turn chiral symmetry, generating a dynamical mass. The MC effect was first found in the framework of the NJL [94, 95] and Gross-Neveu model [96, 97]. The basic idea behind MC is that $\langle\bar{\psi}\psi\rangle$ can be thought of as a condensate

of neutral spin-zero fermion-antifermion pairs. Since the magnetic moments of the fermion (with a fixed charge and spin) and the antifermion (with the opposite charge and spin) point in the same direction, both magnetic moments can comfortably align along the magnetic field direction [78].

On more technical grounds, the mechanism behind MC effect was discussed in Refs [98–100], see Ref. [52] for a more general review. The key point revealed in those references is that the magnetic field enhances the pairing between fermions and antifermions in the infrared region, since the dynamics of the pairing is reduced to (1 + 1)-dimensional dynamics. This is connected to the fact that, in the presence of an uniform magnetic field, the transverse momentum of free fermions is quantized into discrete numbers, known as Landau levels (LLs). For the particular case of weak coupling and/or strong magnetic fields, the connection is explicit; the pairing dynamics is dominated by fermions in the lowest Landau level (LLL), which are also subject to the dimensional reduction $D \to D-2$. As a consequence of the pairing, a dynamical mass is generated (mostly in the infrared region) even at the weakest attractive interaction between fermions, which spontaneously breaks chiral symmetry and enhances the chiral condensate. The underlying physics of infrared dynamics becoming stronger because of dimensional reduction is universal, as known from the Bardeen-Cooper-Schrieffer (BCS) theory of superconductivity [101, 102]. In fact, the mechanism of dimensional reduction was proven at asymptotically strong magnetic fields $eB \gg \Lambda_{QCD}^2$, where QCD can be studied rigorously from first-principles [103], obtaining MC. Moreover, the MC effect has been reproduced across many different approaches such as QCD effective models, LQCD, QED, holographic approaches and condensed matter systems [52, 53, 78].

At finite temperature and moderately strong magnetic fields $\sqrt{eB} \gtrsim \Lambda_{QCD}$, a new unexpected behavior was discovered by LQCD [73] for temperatures around T_c, consisting in a decrease, rather than increase, of the quark condensate with B. This phenomenon, not foreseen by effective models, was dubbed as inverse magnetic catalysis. The full mechanism behind IMC at finite temperature is still controversial and under study, see Refs. [79, 104, 105] for some reviews on the subject. This is partially due to the fact that, at these moderate field strengths, QCD is strongly interacting and the Landau level picture is in general not well defined anymore, even though some meaningful identification for the LLL can still be performed [106]. Another controversial aspect exposed by LQCD is that, for heavy pion masses ($m_\pi \gtrsim 500$ MeV), T_c decreases with B even though the condensate is always an increasing function of B at all temperatures, i.e. there is no IMC [107, 108]. It has been suggested that the influence of the magnetic field on the confining properties is the leading effect originating the decrease of T_c as a function of B, a phenomenon dubbed as "deconfinement catalysis". Pertinent confinement observables include the Polyakov

loop [107, 109], string tensions [72, 110–112], flux tubes [113], fluctuations of conserved charges [114] and the ratio of pressure over energy density [75]. The aforementioned suggestion relies on the fact that some of these confining effects happen even in the absence of IMC in the chiral condensate.

A key factor toward the understanding of IMC, first performed in Ref. [115], consists of separating the changes in the quark condensate induced directly through the observable (valence effect), and indirectly through the fermion determinant contributing to the weight of the gauge configurations (sea effect). LQCD results show that the magnetic field enhances the spectral density around zero [109], which according to the Banks-Casher relation [116] is proportional to the quark condensate. This is a purely "valence" effect that can be already observed in the quenched approximation, where the backreaction of charged quarks on the gauge field is ignored, and can be considered the basic mechanism behind magnetic catalysis. In contrast, the sea effect was found to enhance the condensate only well below T_c, whereas around T_c the quark determinant tends to suppress gauge configurations with larger values of the quark condensate [109]. The sea effect is related to the fact that, even though gluons themselves do not carry electric charge, they are affected by B through their coupling to electrically charged quarks. For asymptotically large magnetic fields $eB \gg \Lambda^2_{QCD}$, some light can be shed on the underlying mechanism [103]. There, the dimensional reduction of the LLL dynamics, which is the most relevant level in this regime, leads to a large fermion contribution to the gluon polarization operator. As a result, gluons acquire a mass of order $M_g^2 \propto \alpha_s eB$. Since at leading order the strong coupling decreases logarithmically with B, $\alpha_s(B) = [b \ln(eB/\Lambda^2_{QCD})]^{-1}$ with $b = (11N_c - 2N_f)/6\pi$, this leads to an effective weakening of the interaction between quarks in the presence of an external magnetic field. At moderate field strengths $\sqrt{eB} \gtrsim \Lambda_{QCD}$, the gluonic dependence on B was analyzed on the lattice [117], where it was found that its behavior resembles the one of the chiral condensate. A further analysis of the associated chromo-electromagnetic fields allows for the speculation that the induced chromomagnetic background interferes with the dynamics responsible for symmetry breaking.

Hadron properties are also expected to be affected by this screening effect of gluon interactions. The study of light hadrons under magnetic fields, which is the main topic of this thesis, is important for several reasons. Strong magnetic fields $\sqrt{eB} \sim \Lambda_{QCD}$ can in principle resolve the quark structure of a hadron. Thus, the modifications of their properties in an external magnetic field can help to understand the effects of magnetic fields on the chiral phase transition. In particular, the magnetic field dependence of the masses of the lightest hadrons are expected to play a relevant role for the structure of the phase diagram. Specifically, pions are expected to be dominant in this respect. For example, since neutral pions are Nambu-Goldstone bosons of the chiral symmetry breaking, the decrease

of their mass with B could signal a transition to a deconfined/chirally symmetric phase, as suggested by the simultaneous decrease of T_c with B. Besides, for the chiral partners such as neutral pions and sigma mesons, their mass difference can be also considered as an order parameter to describe the behavior of the chiral crossover, since their screening masses become degenerate when chiral symmetry gets restored. On the other hand, it has been conjectured that strong magnetic fields could reduce the vector meson mass to zero and lead to the condensation of ρ-mesons [118], possibly inducing a transition to a superconducting phase [91]. In this regard, QCD inequalities can be used to show that massless ρ-mesons are only allowed if the (connected) neutral pion mass vanishes as well. Another aspect relevant for the aforementioned physical scenarios concerns the elementary properties of magnetized hadronic degrees of freedom. For cold astrophysical environments, the masses of baryons and mesons enter the nuclear equation of state and influence the mass-radius relations of magnetars [119]. Together with hadronic decay rates, these also affect stability of such compact objects and cooling mechanisms that characterize the emitted neutrino spectrum [120]. As for heavy ion collisions, it has been speculated [121, 122] that long-lived magnetic fields might affect the hadronization process, primarily influencing heavy baryons.

1.4 Theoretical frameworks

Most of the phenomena of QCD matter mentioned in the previous section require treating QCD at energy scales below say 1 GeV, where perturbative methods are not applicable. In this regime, the nonperturbative character of QCD renders calculations extremely difficult. Thus, these low energy processes must be studied through nonperturbative techniques. Ab initio approaches include lattice QCD and functional approaches, such as the functional renormalization group and Dyson-Schwinger Equations [123–126]. In particular, LCQD has significantly improved over the years, along with technological development, proving to be a very useful tool for studying the properties of QCD matter [11, 12, 127]. While the temperature axis can be directly addressed on the lattice, for finite chemical potentials the so-called sign problem hinders density studies, although recent progress has been achieved through the use of different techniques for chemical potentials up to $\mu_B/T < 3$, finding no signal of the CEP [11, 43, 49, 128]. Regarding the inclusion of magnetic fields, even though they can be straightforwardly incorporated to the lattice, other technical problems arise such as the proper handling of lattice artifacts [129], large error bars, the use of higher than physical quark or pion masses due to computational resources, the use of the root trick for staggered quarks and differences in the values of results obtained using different quark implementations.

Another way to deal with nonperturbative QCD relies in the use of a plethora of alternative approaches/models, based on QCD. These include QCD sum rules [130–132], chiral perturbation theory [133, 134], MIT bag model [135–138], quark-meson or linear sigma model [139–141], Sakai-Sugimoto model [142, 143], relativistic Hamiltonian-based formalisms and chiral models, to just name a few.

In this thesis we will make use of the Nambu–Jona-Lasinio (NJL) model, an effective model built upon the chiral symmetries of QCD. It was originally developed in the sixties to study nucleon interactions [14, 144], aiming to explain in a unified manner the large baryon masses as well as the intermediate or small meson masses solely from the isospin symmetry properties of nuclear interactions. The model properly accounts for the spontaneous symmetry breaking mechanism of the axial group, generating dynamical masses for the nucleons and giving rise to Goldstone bosons, associated with pions. Years later, when quarks were recognized as fundamental particles forming hadrons, the model was reinterpreted as an effective theory for quark interactions [145–147]. In this interaction gluon degrees of freedom are frozen, resulting in a lack of confinement. Nevertheless, as long as the quantities under study are not sensitive to the confinement properties, but instead are well described by chiral symmetry properties, reliable calculations can be performed within this model. This shortcoming of the theory can be partially remedied by introducing a dynamic variable known as "Polyakov's loop" [148–151], which is treated as a background field that accounts for gluonic degrees of freedom that can reproduce the deconfinement transition. Another drawback from the model is its nonrenormalizability, due to the approximation of the gluon mediated exchange between quarks as a local point interaction. In this regard, an improvement is seen by considering the nonlocal version of the NJL model [152], although calculations become much more cumbersome.

One of the advantages of the NJL model is that it can be easily extended to include external parameters such as temperature, chemical potential or electromagnetic fields. We will focus on the influence of an external uniform magnetic field. In the context of effective models, it is natural to attribute the IMC failure to the fact that most of these models lack gluonic degrees of freedom and so are unable to account for the backreaction of sea quarks due to the external magnetic field. Several possibilities have been explored in the recent literature to incorporate the IMC effect phenomenologically. Within the NJL model, these improvements include going beyond mean-field calculations [153] or taking into consideration the anomalous magnetic moment of quarks [154–157]. Motivated by the running of the QCD coupling and the fact that gluon screening modifies the coupling as $G \propto \alpha_s/M_g^2 \propto 1/eB$, one of the simplest modifications available consists of introducing a coupling constant $G(B)$ that depends on the magnetic field (and in some cases also on the temperature) and can be fixed by fitting some LQCD results, such as the quark

condensate or the chiral pseudocritical temperature. This strategy has shown that the NJL model can satisfactorily reproduce LQCD results in a broad range of temperature and magnetic fields [158–163]. In this regard, an interesting possibility was proposed in Ref. [164] where $G(B)$ is fitted to reproduce constituent quark masses, which are obtained from the LQCD calculation of baryon masses by assuming in a simplified way that they can be obtained by merely summing the masses of their constituents. Lastly, it is worth mentioning that calculations using the non-local NJL model have shown that IMC and deconfinement catalysis are obtained naturally [165, 166].

1.5 Outline of the thesis

As already mentioned, the study of light hadrons under strong magnetic fields can provide relevant information for the understanding of magnetized QCD matter. The objective of this thesis is to study the effect of an external uniform magnetic field on light hadron properties, particularly pseudoscalar mesons and nucleons. In the framework of the NJL model, mesons are usually described as quantum fluctuations in the random phase approximation (RPA) [145–147], that is, they are introduced via a summation of an infinite number of quark loops. In the presence of a magnetic field, the calculation of these loops requires some special care due to the appearance of Schwinger phases [167] associated with each quark propagator. For neutral mesons these phases cancel out, and as a consequence the usual momentum basis can be used to diagonalize the corresponding polarization function. In contrast, the Schwinger phases do not cancel for charged mesons, leading to a breakdown of translational invariance that prevents to proceed as in the neutral case. In this situation, some existing calculations just neglect the Schwinger phases, taking into account only the translational invariant part of the quark propagator [93, 168, 169]. In this thesis we introduce a method based on the use of Ritus-type eigenfunctions for magnetized systems, which allow us to properly diagonalize charged polarization functions taking fully into account the translational breaking effects induced by Schwinger phases. Although originally introduced to deal with mesons in the NJL model, the method can be applied to charged particles in general, in different magnetized scenarios. In particular, we apply it to the calculation of nucleon masses within the NJL model, constructed as composite quark-diquark bound states.

Regarding the calculation of the pion decay constants, it is important to note that the presence of the external magnetic field opens up new decay channels, parametrized by their corresponding form factors. Even though some of these new decay constants were already recognized in the literature [170, 171], some were not. In this thesis we determine all form factors arising in the presence of an uniform magnetic field by taking into account all

independent tensor structures that can be formed when hadronizing one-pion-to-vacuum matrix elements of quark currents. Using the Ritus method for the calculation of these magnetized matrix elements, we obtain a model-independent expression for the weak decay width of magnetized charged pions $\pi^- \to l\bar{\nu}_l$, as well as the angular distribution of outgoing antineutrinos. Their values can be estimated by providing the magnetic dependence of the pion decay constants, which must be calculated within some QCD approach. We report on estimations from the NJL model.

The thesis is organized as follows. In chapter 2 we introduce the theoretical framework. Since the NJL model is built upon the chiral symmetry of QCD, we first discuss the QCD theory and describe its flavor transformation properties. Afterwards we introduce the NJL model, describing the inclusion of magnetic fields at the mean field level. In chapter 3 we analyze the weak decay of magnetized charged pions solely from quantum field theory grounds. To that end, we provide expressions for the matter fields of the involved particles in the presence of the external field. As mentioned, the external magnetic field opens up new decay channels, so we carefully take into account all possible form factors. In order to provide actual estimates for the decay width and angular distribution, some pion properties such as their masses and decay constants need to be supplied by some QCD approach. In chapter 4 we make use of the two-flavor NJL model to calculate several pion properties, applying the Ritus method to properly address charged particles. The possibility of a magnetic field dependent coupling constant is also explored, in order to account for the IMC effect. In chapter 5 we employ the three-flavor version of the NJL model to extend the meson pole mass calculation to all mesons from the pseudoscalar nonet. Going back to the two-flavor formulation of the model, diquark masses can be straightforwardly obtained by mimicking the pion calculation of chapter 4. Thus, in chapter 6 we analyze diquarks and use them to study nucleon masses. In our approach, nucleons are treated as bound quark-diquark states described by a relativistic Fadeev equation, using the static approximation for quark exchange interactions. The conclusions of this work together with a future outlook is presented in chapter 7. Finally, some technical details of the calculations are discussed in the appendices.

Introducción

Cromodinámica cuántica

La teoría que describe las interacciones fuertes en el marco del Modelo Estándar se conoce como cromodinámica cuántica (QCD). Se estableció como tal hace varias décadas, reconociendo a los quarks como los constituyentes primarios de los hadrones y a los gluones como los mediadores de la interacción [1–3]. En esta formulación, los quarks y gluones poseen una propiedad conocida como "carga de color", análoga a la carga eléctrica de la electrodinámica cuántica (QED), responsable de las interacciones fuertes. La fuerza de la interacción se mide por g_s, la constante adimensional de acoplamiento de la teoría. Sin embargo, tras la cuantización, las divergencias logarítmicas en los diagramas de un lazo de la teoría de perturbaciones implican que esta "constante" depende en realidad de la escala de energía típica μ de los procesos considerados, denominada escala del grupo de renormalización. Este corrimiento del acoplamiento viene especificado por la función beta del grupo de renormalización. La auto-interacción entre gluones modifica dramáticamente el corrimiento del acoplamiento de QCD $\alpha_s = g_s^2/(4\pi)$, en comparación con QED. Para energías altas el acoplamiento se debilita ($\alpha_s \to 0$) y quarks y gluones forman estados (casi) libres, una propiedad denominada libertad asintótica [4, 5]. Por otro lado, la teoría de perturbaciones sugiere que para procesos de baja energía $\alpha_s \to \infty$. La experiencia indica que, en condiciones ordinarias de temperatura y densidad, digamos $T \lesssim 200$ MeV y $\mu \lesssim 350$ MeV [6], los hadrones son los grados de libertad relevantes. Esto implica que la materia QCD debe necesariamente agruparse de manera de formar estados ligados de color singlete cuya carga neta de color es cero, un fenómeno denominado confinamiento (de color). El valor de μ que separa estos dos regímenes se conoce como la escala de QCD Λ_{QCD}, definida como $\alpha_s(\Lambda_{\mathrm{QCD}}) = 1$. Para escalas de energías por debajo de la masa del quark charm $\mu < 1,25$ GeV, donde sólo los tres sabores más ligeros están activos, tenemos $\Lambda_{\mathrm{QCD}} \sim 300$ MeV. El proceso por el cual una constante adimensional como g_s se sustituye por una dimensional como Λ_{QCD} se denomina transmutación dimensional.

Materia de QCD en condiciones extremas

Poco después del advenimiento de QCD, se conjeturó que a temperaturas y/o densidades suficientemente altas podían formarse estados de la materia conocidos con el nombre genérico de plasma de quarks y gluones (QGP), que se caracterizan por el desconfinamiento de color y donde los quarks y gluones son los grados de libertad dominantes [7–9]. Esto impulsó el estudio teórico de las posibles fases de QCD en tales condiciones extremas y reveló una estructura de fases potencialmente compleja [10, 11]. De hecho, el estudio del diagrama de fases de QCD sigue suponiendo un reto teórico y experimental a día de hoy [12]. Una vista esquemática en el plano de temperatura y potencial químico bariónico μ_B se representa en la Figura 1.1

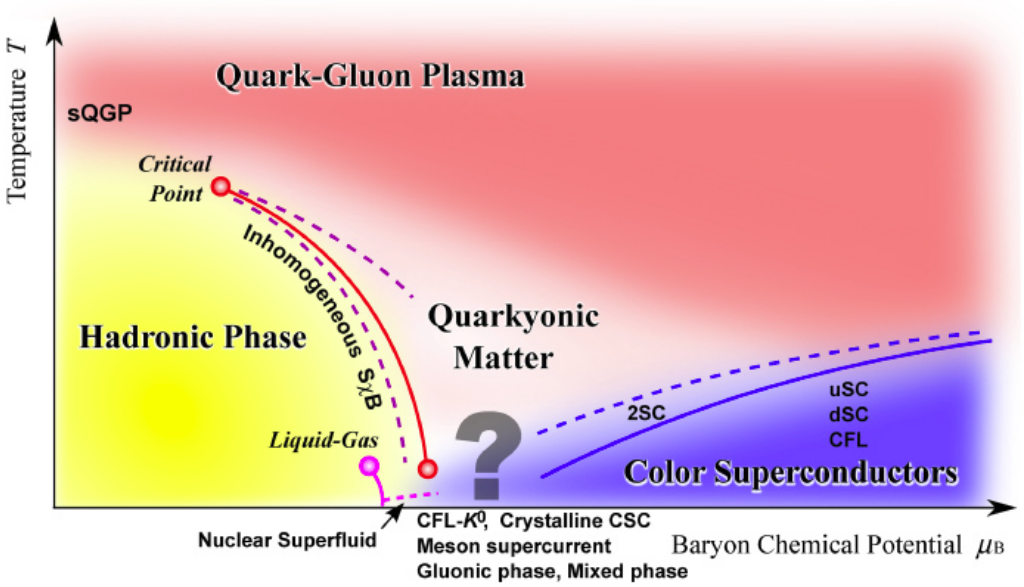

Figura 1.1: Representación esquemática del diagrama de fases de QCD a temperatura y potencial químico bariónico (densidad) finito. Figura extraída de la Ref. [10].

La transición entre diferentes fases está señalada por un comportamiento crítico a menudo asociado con la ruptura espontánea de una simetría global [13]. El parámetro de orden es la cantidad que establece el estado de una simetría: se desvanece cuando el sistema comparte la simetría del Lagrangiano y es finito cuando la simetría se rompe espontáneamente. Para caracterizar adecuadamente estas fases, es necesario estudiar las propiedades de simetría de la teoría bajo grupos de transformaciones unitarias que actúan sobre los grados de libertad internos de la teoría. El Lagrangiano de QCD es por construcción invariante ante el grupo de color $SU(3)_c$. Para quarks sin masa, también es invariante ante el grupo quiral de sabor, que puede descomponerse en grupos vectoriales y axiales como $U(N_f)_L \times U(N_f)_L = U(1)_V \times SU(N_f)_V \times U(1)_A \times SU(N_f)_A$. Aquí N_f es el

número de sabores: en QCD completo, $N_f = 6$. Para quarks masivos, la simetría quiral se rompe. Sin embargo, se conserva aproximadamente en el sector de quarks ligeros. En el estado de vacío de QCD, la simetría axial se rompe debido a las interacciones, incluso para quarks sin masa. Por lo tanto, la simetría quiral se rompe y se genera dinámicamente una masa efectiva para los quarks [14]. El parámetro de orden que caracteriza esta ruptura espontánea es el condensado quiral $\langle\bar{\psi}\psi\rangle$. De hecho, esta ruptura es responsable de la mayor parte de la masa del nucleón, mientras que los correspondientes bosones ligeros de Goldstone [15] se identifican con los piones. Estos efectos dinámicos son de gran importancia en el estudio del diagrama de fases QCD, ya que hay indicios de que esta simetría se restaura en la fase QGP. En la transición de fase las cantidades termodinámicas cambian característicamente, todas relacionadas con una anomalía en la presión. Las fluctuaciones de cantidades conservadas, como el número bariónico, de carga eléctrica y de extrañeza, son observables sensibles en las colisiones relativistas de iones pesados para sondear la transición de fase de QCD. Además, la evidencia experimental y teórica conduce a la suposición de que las transiciones de fase de desconfinamiento y restauración de la simetría quiral se producen prácticamente de forma simultánea a bajas densidades [16–18].Sin embargo, el mecanismo exacto que da lugar a esta transición simultánea aún no se encuentra comprendido cuantitativamente de manera detallada.

La formación del QGP implica procesos de alta energía, que sólo pueden darse en condiciones extremas. Estas condiciones son difíciles de producir, lo que deja pocas situaciones físicas para el estudio experimental. Uno de los escenarios naturales donde se cree que se producen fases desconfinadas de QCD es en el caliente Universo temprano, correspondiente a la región de bajas densidades y altas temperaturas en el diagrama de fases. Según el modelo del big bang caliente, el Universo temprano ha experimentado (al menos) dos épocas en las que podrían producirse transiciones de fase: la transición electrodébil a temperaturas en torno a $T_{\rm EW} \sim 100$ GeV, cuando los fermiones y bosones gauge se convirtieron en partículas masivas, y la transición pseudocrítica de QCD T_c cuando los quarks se confinaron en hadrones. A partir de simulaciones de QCD en la red (LQCD), se espera que la transición de QCD sea un cruce suave (crossover) en torno a $T_c \simeq 156$ MeV [19–22]. Sin embargo, existen algunos mecanismos conocidos que podrían proporcionar una transición QCD de primer orden, véase por ejemplo [23–25]. Otro escenario natural corresponde a los núcleos de las llamadas estrellas compactas [26, 27]. Estas estrellas de neutrones son objetos extremadamente estables y densos, que constituyen uno de los posibles escenarios finales en el ciclo de vida de una estrella. En ellas, la densidad es lo suficientemente grande como para formar estados superconductores de color, correspondientes a la región de altas densidades y bajas temperaturas en el diagrama de fases. A potenciales químicos asintóticamente grandes y temperaturas

pequeñas, donde QCD perturbativo es aplicable debido a la libertad asintótica, la materia de QCD de 3 sabores se encuentra en la llamada fase de bloqueo de color-sabor [28–30]. En este régimen se rompe la simetría quiral, y la temperatura de transición a la materia de quarks es de primer orden [31, 32]. A densidades intermedias, incluyendo aquellas relevantes para ambientes astrofísicos, las fases alternativas propuestas en la literatura incluyen superconductores de color de dos sabores, fases mixtas sin bloqueo de color y sabor, superconductividad de color cristalina, condensación de kaones, fases gluónicas, superfluidez, fases sin brechas e inhomogéneas, ver Refs. [6, 33–35] para más detalles.

En cuanto a escenarios creados por humanos, en las últimas décadas se han construido varios aceleradores de iones pesados, en los que se llevan a cabo experimentos para alcanzar las fases correspondientes a altas temperaturas y densidades en el diagrama de fases de QCD [36, 37]. Grandes programas experimentales se han llevado a cabo en el 'Relativistic Heavy Ion Collider' (RHIC) [38, 39] en el laboratorio BNL y en el 'Large Hadron Collider' (LHC) [40] bajo los experimentos ALICE, ATLAS y CMS, así como el 'Super Proton Synchrotron' (SPS) en el CERN. En este tipo de aceleradores, el objetivo es colisionar iones pesados como plomo, plata u oro a energías del centro de masa del orden de 100-200 GeV o más. Durante el proceso de colisión se alcanzan temperaturas extremadamente altas, por encima de la temperatura crítica de desconfinamiento T_c MeV [38]. Esto sugiere que posiblemente se forme un QGP transitorio, que se hadroniza al enfriarse. Las partículas salientes de la colisión llevan información indirecta sobre el QGP. Los resultados actuales sugieren que el QGP ha logrado formarse durante períodos de tiempo del orden de 10 fm/c [41, 42].

Contrariamente a las expectativas iniciales, el QGP no es un plasma débilmente acoplado. De hecho, está fuertemente acoplado y es casi un líquido perfecto, con una viscosidad específica η/s cercana a $1/4\pi$ [36, 43]. Curiosamente, la dualidad AdS/CFT entre teorías de gauge infinitamente fuertemente acopladas (primas de QCD) y descripciones gravitacionales ha llevado a la conjetura de que para cualquier teoría cuántica de campos relativista, $\eta/s > 1/4\pi$ [44]. La similitud entre ambos resultados da credibilidad a la idea de que la holografía puede proporcionar conocimientos significativos sobre QCD. Debido a la suposición de una fuerza de acoplamiento infinita en el cálculo holográfico, el comportamiento de fluido ideal del QGP se ha interpretado como la señalización de un sistema que interactúa fuertemente, apoyado también por el hecho de que el valor de η/s obtenido para un gas de quarks y gluones en régimen de acoplamiento débil es un orden de magnitud mayor. A pesar de su corta duración el QGP exhibe propiedades de equilibrio termodinámico, lo que aporta pruebas adicionales que confirman la hipótesis de que la transición de fase entre la fase hadrónica y el QGP es del tipo crossover [45]. Las condiciones producidas en los actuales aceleradores de iones pesados corresponden

esencialmente al eje vertical del diagrama de fases, es decir, a bajos potenciales químicos. Se espera que la transición quark-hadrón de tipo crossover observada en este régimen cambie a una transición de primer orden para μ_B más altos, con un punto crítico final (CEP) de segundo orden entre ambos. La posición del CEP se ha estudiado ampliamente en diferentes marcos teóricos (ver por ejemplo Refs. [46–49]) y se ha explorado en los aceleradores actuales [39, 50]. De hecho, su búsqueda es uno de los puntos de referencia para futuros experimentos en el 'Nuclotron-based Ion Collider fAcility' (NICA), el 'Facility for Antiproton and Ion Research' (FAIR) y el 'Japan Proton Accelerator Research Complex' (J-PARC), donde se podrán alcanzar mayores densidades.

Mientras que el diagrama de fases se ha investigado tomando inicialmente como variables la densidad y la temperatura, en la última década ha aumentado enormemente el interés por la presencia de campos (electro)magnéticos fuertes y sus efectos [51–53]. Aunque la constante de acoplamiento electromagnético e es mucho menor que la constante de acoplamiento fuerte g_s, el electromagnetismo puede ser relevante para la física de QCD si la intensidad del campo es tan fuerte que $\sqrt{eE}$, $\sqrt{eB} \sim \Lambda_{\rm QCD}$. Estos campos electromagnéticos intensos aparecen en muchos de los escenarios físicos mencionados. Varios modelos predicen la generación de fuertes campos magnéticos durante la evolución temprana del Universo, que son requeridos por las observaciones actuales de campos magnéticos intergalácticos débiles pero no nulos. Estos campos intensos podrían haber modificado la naturaleza de la transición de fase electrodébil, y su efecto podría haber dejado huellas en ciertas anisotropías del fondo cósmico de microondas [54, 55]. Por otro lado, en la superficie de ciertas estrellas compactas denominadas "magnetares", los campos magnéticos pueden alcanzar valores del orden de 10^{15} G [56–58], aumentando en algunos órdenes de magnitud hasta $10^{18} - 10^{20}$ G hacia el núcleo [59–62]. Véase la Ref. [63] para un catálogo actual de magnetares y también la Ref. [64] para una revisión reciente. El efecto de los campos magnéticos en la materia densa de quarks también se revisa en la Ref. [65]. En cuanto a los escenarios creados por humanos, en la última década se ha observado que en las colisiones de iones pesados (HIC) el movimiento de partículas espectadoras cargadas produce campos magnéticos de magnitudes tan grandes como $10^{19} - 10^{20}$ G [66–70]. Aunque estos campos se producen esencialmente en los momentos iniciales de la colisión y decaen rápidamente, en ocasiones del orden de 10^{-21} s [67], podrían afectar sustancialmente a la forma en que el QGP se hadroniza [51, 71]. Por último, los campos magnéticos también son relevantes para sistemas de materia condensada cuasi relativistas como el grafeno [52].

El diagrama de fases de la QCD en el espacio tridimensional (μ, T, B) se ha estudiado desde varios enfoques. Mientras que el eje de temperaturas puede abordarse directamente en la red, para potenciales químicos finitos el llamado problema del signo dificulta los

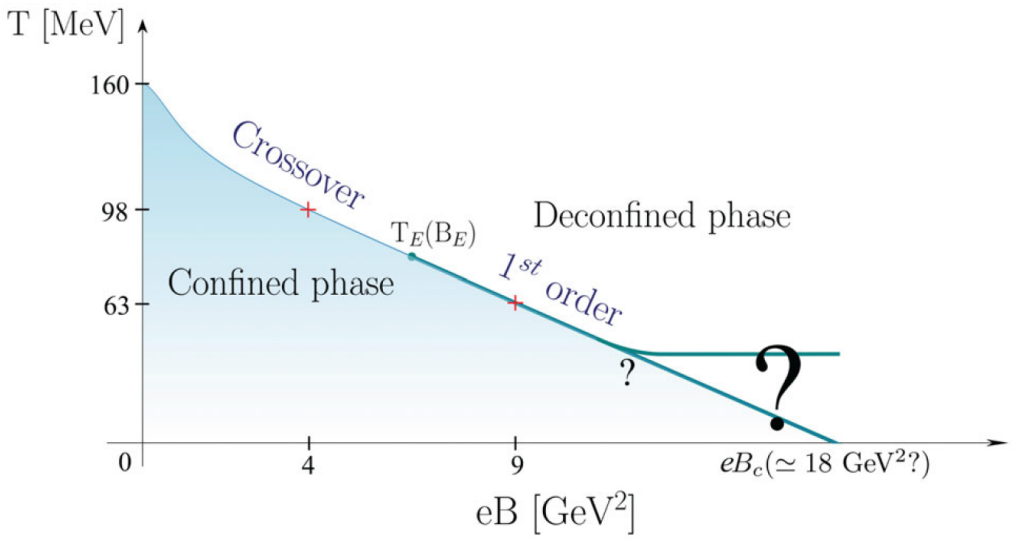

Figura 1.2: Diagrama de fases QCD a temperatura y campo magnético finito. La temperatura (pseudo)crítica disminuye en función de B, y la transición pasa de ser de tipo crossover a primer orden en un punto crítico final situado en el intervalo $4\ \mathrm{GeV}^2 < eB_E < 9\ \mathrm{GeV}^2$. Figura extraída de la Ref. [72].

estudios de densidad, que se han realizado principalmente a través modelos efectivos o enfoques holográficos. Curiosamente, mientras que la mayoría de los modelos efectivos predicen un aumento de la temperatura de transición pseudocrítica T_c con el campo magnético [52, 53], resultados precisos de LCQD [73–76] han mostrado el patrón opuesto, es decir, una disminución de T_c con el campo magnético. De hecho, como se muestra en las Refs. [72, 77], este comportamiento se prolonga para campos magnéticos muy fuertes, donde se encontró una transición de primer orden a $eB = 9\ \mathrm{GeV}^2$, lo que implica la existencia de un punto crítico final en algún lugar dentro del rango $4\ \mathrm{GeV}^2 < eB < 9\ \mathrm{GeV}^2$. Un diagrama de fase QCD actualizado en el plano de temperatura y campo magnético puede encontrarse en la Figura 1.2, propuesta en la Ref. [72].

Efectos del campo magnético sobre la materia de QCD

Es esperable que nuevos efectos detectables en el diagrama de fases y las propiedades de la materia que interactúa fuertemente surjan debido a estos campos magnéticos extremos, provocando numerosas consecuencias fenomenológicas [52]. Entre ellas se incluyen la catálisis magnética (MC) del condensado quiral [52, 78]; la catálisis magnética inversa (IMC) de la temperatura de restauración quiral y de desconfinamiento [73, 74, 79, 80]; el efecto magnético quiral [66, 81, 82]; el efecto de separación quiral [83, 84]; ondas magnéticas quirales [85–89]; superconductividad en el vacío [90, 91], así como muchos otros efectos sobre las propiedades de las partículas resultantes que se detectan tras las colisiones [71,

92, 93], por nombrar algunos. Además de su importancia para la fenomenología de los escenarios físicos mencionados, los campos magnéticos también tienen interés académico por sí mismos, ya que sirven como sonda de la teoría de la materia en interacción fuerte. En particular, la comparación entre resultados de LQCD y modelos efectivos en presencia de campos electromagnéticos externos permite restringir estos últimos, adquiriendo una mejor comprensión de la teoría subyacente.

Para el alcance de esta tesis, la cual involucra el análisis de las propiedades de los hadrones livianos, será pertinente discutir con cierto detalle los efectos MC e IMC. El término catálisis magnética se refiere a la catalización de un condensado existente o a la aparición de un nuevo condensado por la presencia de un campo magnético externo. En QCD, la generación del condensado quiral $\langle\bar{\psi}\psi\rangle$ rompe a su vez la simetría quiral, generando una masa dinámica. El efecto MC se encontró por primera vez en el marco del modelo NJL [94, 95] y Gross-Neveu [96, 97]. La idea básica de la MC es que $\langle\bar{\psi}\psi\rangle$ puede considerarse como un condensado de pares fermión-antifermión neutros de espín cero. Dado que los momentos magnéticos del fermión (con carga y espín fijos) y antifermión (con carga y espín opuestos) apuntan en la misma dirección, ambos momentos magnéticos pueden alinearse cómodamente a lo largo de la dirección del campo magnético [78].

Desde un punto de vista más técnico, el mecanismo que subyace al efecto MC se discutió en las Refs [98–100], véase la Ref. [52] para una revisión más general. El punto clave revelado en esas referencias es que el campo magnético potencia el emparejamiento entre fermiones y antifermiones en la región infrarroja, ya que la dinámica del emparejamiento se reduce a una dinámica $(1 + 1)$-dimensional. Esto está relacionado con el hecho de que, en presencia de un campo magnético uniforme, el momento transversal de los fermiones libres se cuantiza en números discretos, conocidos como niveles de Landau (LLs). Para el caso particular de acoplamiento débil y/o campos magnéticos fuertes, la conexión es explícita; la dinámica de emparejamiento está dominada por fermiones en el nivel más bajo de Landau (LLL), que también están sujetos a la reducción dimensional $D \to D - 2$. Como consecuencia del emparejamiento, se genera una masa dinámica (principalmente en la región infrarroja) incluso para la interacción atractiva más débil entre fermiones, que rompe espontáneamente la simetría quiral y aumenta el condensado quiral. La física subyacente de la dinámica infrarroja que se hace más fuerte debido a la reducción dimensional es universal, como se conoce de la teoría Bardeen-Cooper-Schrieffer (BCS) de la superconductividad [101, 102]. De hecho, el mecanismo de reducción dimensional se demostró a campos magnéticos asintóticamente fuertes $eB \gg \Lambda_{QCD}$, donde QCD puede estudiarse rigurosamente desde primeros principios [103], obteniéndose MC. Además, el efecto MC se ha reproducido a través de muchos enfoques diferentes, tales como modelos efectivos QCD, LQCD, QED, enfoques holográficos y sistemas de materia condensada [52,

53, 78].

A temperatura finita y campos magnéticos moderadamente fuertes $\sqrt{eB} \gtrsim \Lambda_{QCD}$, un nuevo comportamiento inesperado fue descubierto por LQCD [73] para temperaturas alrededor de T_c, consistente en una disminución, en lugar de un aumento, del condensado de quarks con B. Este fenómeno, no previsto por los modelos efectivos, se denominó catálisis magnética inversa. El mecanismo completo detrás de IMC a temperatura finita sigue siendo controvertido y en estudio, veánse las Refs. [79, 104, 105] para algunas revisiones sobre el tema. Esto se debe en parte al hecho de que, a estas intensidades de campo moderadas, la QCD interactúa fuertemente y la imagen de los niveles de Landau ya no está bien definida en general, aunque todavía se puede realizar alguna identificación significativa para el LLL [106]. Otro aspecto controvertido expuesto por LQCD es que, para masas de piones pesadas ($m_\pi \gtrsim 500$ MeV), T_c disminuye con B a pesar de que el condensado es siempre una función creciente de B a todas las temperaturas, es decir, no hay IMC [107, 108]. Se ha sugerido que la influencia del campo magnético sobre las propiedades de confinamiento es el efecto principal que origina la disminución de T_c en función de B, un fenómeno denominado "catálisis de desconfinamiento". Entre los observables de confinamiento pertinentes se incluyen el lazo de Polyakov [107, 109], las tensiones de las cuerdas [72, 110–112], los tubos de flujo [113], las fluctuaciones de las cargas conservadas [114] y la relación entre la presión y la densidad de energía [75]. La sugerencia antes mencionada se basa en el hecho de que algunos de estos efectos de confinamiento ocurren incluso en ausencia de IMC en el condensado quiral.

Un factor clave hacia la comprensión de IMC, realizado por primera vez en la Ref. [115], consiste en separar los cambios en el condensado de quarks inducidos directamente a través del observable (efecto de valencia), e indirectamente a través del determinante fermiónico que contribuye al peso de las configuraciones de gauge (efecto de mar). Los resultados de LQCD muestran que el campo magnético aumenta la densidad espectral alrededor de cero [109], que según la relación Banks-Casher [116] es proporcional al condensado de quarks. Se trata de un efecto puramente de "valencia" que ya puede observarse en la aproximación 'quenched', en la que se ignora la retroreacción de los quarks cargados sobre el campo de gauge, y puede considerarse el mecanismo básico que subyace a la catálisis magnética. En contraste, se encontró que el efecto de mar realza el condensado sólo muy por debajo de T_c, mientras que alrededor de T_c el determinante de quarks tiende a suprimir las configuraciones de gauge con valores mayores del condensado de quarks [109]. El efecto de mar está relacionado con el hecho de que, aunque los gluones en sí mismos no llevan carga eléctrica, se ven afectados por B a través de su acoplamiento a quarks cargados eléctricamente. Para campos magnéticos asintóticamente grandes $eB \gg \Lambda_{QCD}^2$, algo de luz puede arrojarse sobre el mecanismo subyacente [103]. Allí, la reducción dimensional

de la dinámica del LLL, que es el nivel más relevante en este régimen, conduce a una gran contribución fermiónica al operador de polarización del gluón. Como resultado, los gluones adquieren una masa del orden $M_g^2 \propto \alpha_s eB$. Puesto que al orden principal el acoplamiento fuerte disminuye logarítmicamente con B, $\alpha_s(B) = [b \ln(eB/\Lambda_{QCD}^2)]^{-1}$ con $b = (11N_c - 2N_f)/6\pi$, esto conduce a un debilitamiento efectivo de la interacción entre quarks en presencia de un campo magnético externo. A intensidades de campo moderadas $\sqrt{eB} \gtrsim \Lambda_{QCD}$, la dependencia gluónica con B se analizó en la red [117], donde se encontró que su comportamiento se asemeja al del condensado quiral. Un análisis posterior de los campos cromo-electromagnéticos asociados permite especular que el fondo cromo-magnético inducido interfiere con la dinámica responsable de la ruptura de simetría.

Es de esperar que las propiedades de los hadrones también se vean afectadas por este efecto de apantallamiento de las interacciones entre gluones. El estudio de hadrones ligeros bajo campos magnéticos, que es el tema principal de esta tesis, es importante por varias razones. Los campos magnéticos fuertes $\sqrt{eB} \sim \Lambda_{\rm QCD}$ pueden, en principio, resolver la estructura de quarks de un hadrón. Así, las modificaciones de sus propiedades en un campo magnético externo pueden ayudar a comprender los efectos de los campos magnéticos en la transición de fase quiral. En particular, se espera que la dependencia con el campo magnético de las masas de los hadrones más ligeros desempeñe un papel relevante para la estructura del diagrama de fases, siendo los piones dominantes. Por ejemplo, dado que los piones neutros son bosones Nambu-Goldstone de la ruptura de la simetría quiral, la disminución de su masa con B podría señalar una transición a una fase desconfinada/simétrica quiral, como sugiere la disminución simultánea de T_c con B. Además, para las parejas quirales como los piones neutros y los mesones sigma, su diferencia de masa también puede considerarse como un parámetro de orden para describir el comportamiento del cruce quiral, ya que sus masas de apantallamiento se degeneran cuando se restaura la simetría quiral. Por otro lado, se ha conjeturado que campos magnéticos intensos podrían reducir la masa del mesón vectorial a cero y conducir a la condensación de mesones ρ [118], posiblemente induciendo una transición a una fase superconductora [91]. En este sentido, las desigualdades de QCD se pueden utilizar para demostrar que los mesones ρ sin masa sólo se permiten si la masa del pión neutro (conectado) también desaparece. Otro punto relevante para los escenarios físicos mencionados concierne a las propiedades elementales de los grados de libertad hadrónicos magnetizados. En entornos astrofísicos fríos, las masas de bariones y mesones entran en la ecuación de estado nuclear e influyen en las relaciones masa-radio de los magnetares [119]. Junto con las tasas de desintegración hadrónica, también afectan a la estabilidad de estos objetos compactos y a los mecanismos de enfriamiento que caracterizan el espectro de neutrinos emitidos [120]. En cuanto a las colisiones de iones pesados, se ha especulado [121, 122] que los campos

magnéticos de larga duración podrían afectar al proceso de hadronización, influenciando principalmente a los bariones pesados.

Formalismos teóricos

La mayoría de los fenómenos de la materia QCD mencionados en la sección anterior requieren tratar con QCD a escalas de energía por debajo de, digamos, 1 GeV, donde los métodos perturbativos no son aplicables. En este régimen, el carácter no perturbativo de la QCD hace que los cálculos sean extremadamente difíciles. Por lo tanto, estos procesos de baja energía deben estudiarse mediante técnicas no perturbativas. Los enfoques ab initio incluyen QCD en la red y enfoques funcionales, como el grupo de renormalización funcional y las ecuaciones de Dyson-Schwinger [123–126]. En particular, LCQD ha mejorado significativamente a lo largo de los años, junto con el desarrollo tecnológico, demostrando ser una herramienta muy útil para el estudio de las propiedades de la materia de QCD [11, 12, 127]. Mientras que el eje de temperaturas puede ser abordado directamente en la red, para potenciales químicos finitos el llamado problema del signo obstruye el estudio de la densidad, aunque recientemente se ha avanzado en este sentido mediante el uso de diferentes técnicas para potenciales químicos de hasta $\mu_B/T < 3$, no encontrando señal del CEP [11, 43, 49, 128]. En cuanto a la inclusión de campos magnéticos, aunque se pueden incorporar directamente a la red, surgen otros problemas técnicos como el manejo adecuado de artefactos de red [129], grandes barras de error, el uso de masas de quarks o piones superiores a las físicas debido a los recursos computacionales, el uso del truco de la raíz para quarks 'staggered' y diferencias en los valores de los resultados entre diferentes implementaciones de quarks.

Otra forma de tratar con QCD no perturbativa se basa en el uso de una plétora de enfoques/modelos alternativos, basados en QCD. Estos incluyen reglas de suma de QCD [130–132], teoría de perturbación quiral [133, 134], modelo de bolsa del MIT [135–138], modelo quark-mesón o sigma lineal [139–141], modelo Sakai-Sugimoto [142, 143], formalismos relativistas basados en Hamiltonianos y modelos quirales, por nombrar sólo algunos.

En esta tesis haremos uso del modelo Nambu–Jona-Lasinio (NJL), un modelo efectivo construido sobre las simetrías quirales de QCD. Fue desarrollado originalmente en los años sesenta para estudiar las interacciones entre nucleones [14, 144], con el objetivo de explicar de forma unificada las grandes masas de bariones así como las masas intermedias o pequeñas de mesones únicamente a partir de las propiedades de simetría de isospín de las interacciones nucleares. El modelo explica adecuadamente el mecanismo espontáneo de ruptura de simetría del grupo axial, generando masas dinámicas para los nucleones y

dando lugar a los bosones de Goldstone, asociados a los piones. Años más tarde, cuando se reconoció a los quarks como partículas fundamentales que forman hadrones, el modelo se reinterpretó como una teoría efectiva para las interacciones entre quarks [145–147]. En esta interacción los grados de libertad de los gluones están congelados, lo que resulta en una falta de confinamiento. Sin embargo, siempre que las cantidades estudiadas no sean sensibles a las propiedades de confinamiento, sino que estén bien descritas por las propiedades de simetría quiral, se pueden realizar cálculos fiables dentro de este modelo. Esta deficiencia de la teoría puede remediarse parcialmente introduciendo una variable dinámica conocida como "lazo de Polyakov" [148–151], que se trata como un campo de fondo que da cuenta de grados de libertad gluónicos que pueden reproducir la transición de desconfinamiento. Otro inconveniente del modelo es su falta de renormalizabilidad, debido a la aproximación del intercambio entre quarks mediado por gluones como una interacción puntual local. Con respecto a esto, una mejora se observa al considerar la versión no local del modelo NJL [152], aunque los cálculos se vuelven mucho más complejos.

Una de las ventajas del modelo NJL es que puede ampliarse fácilmente para incluir parámetros externos como la temperatura, el potencial químico o los campos electromagnéticos. Nos centraremos en la influencia de un campo magnético uniforme externo. En el contexto de los modelos efectivos, es natural atribuir el fallo del efecto IMC al hecho de que la mayoría de estos modelos carecen de grados de libertad gluónicos y, por tanto, son incapaces de dar cuenta de la retroacción del mar de quarks debida al campo magnético externo. En la literatura reciente se han explorado varias posibilidades para incorporar fenomenológicamente el efecto IMC. Dentro del modelo NJL, estas mejoras incluyen ir más allá de los cálculos de campo medio [153] o tener en cuenta el momento magnético anómalo de los quarks [154–157]. Motivado por el corrimiento del acoplamiento de QCD y el hecho de que el apantallamiento de gluones modifica el acoplamiento según $G \propto \alpha_s/M_g^2 \propto 1/eB$, una de las modificaciones más sencillas disponibles consiste en introducir una constante de acoplamiento $G(B)$ que depende del campo magnético (y en algunos casos también de la temperatura) y puede fijarse ajustando algunos resultados de LQCD, como el condensado de quarks o la temperatura pseudocrítica quiral. Esta estrategia ha demostrado que el modelo NJL puede reproducir satisfactoriamente los resultados de LQCD en un amplio rango de temperatura y campos magnéticos [158–163]. En este sentido, en la Ref. [164] se propuso una interesante posibilidad en la que $G(B)$ se ajusta para reproducir las masas de los quarks constituyentes, obtenidos de resultados de LQCD para las masas de los bariones asumiendo de forma simplificada que las mismas pueden obtenerse meramente sumando de las masas de sus constituyentes. Por último, es interesante mencionar que en la versión no local del modelo se ha mostrado que el efecto IMC y la catálisis de desconfinamiento se obtienen de forma natural [165, 166].

Esquema de la tesis

Como ya se ha mencionado, el estudio de hadrones ligeros bajo fuertes campos magnéticos puede proporcionar información relevante para la comprensión de la materia magnetizada de QCD. El objetivo de esta tesis es estudiar el efecto de un campo magnético uniforme externo sobre las propiedades de los hadrones ligeros, en particular de los mesones pseudoscalares y nucleones. En el marco del modelo NJL, los mesones se describen normalmente como fluctuaciones cuánticas en la aproximación de fase aleatoria (RPA) [145–147], es decir, se introducen a través de una suma de un número infinito de lazos de quarks. En presencia de un campo magnético, el cálculo de estos lazos requiere cierto cuidado especial debido a la aparición de fases de Schwinger [167] asociadas a cada propagador de quark. Para los mesones neutros estas fases se cancelan, y como consecuencia se puede utilizar la base de momento habitual para diagonalizar la función de polarización correspondiente. En cambio, las fases de Schwinger no se cancelan para los mesones cargados, lo que conduce a una ruptura de la invariancia traslacional que impide proceder como en el caso neutro. En esta situación, algunos cálculos existentes simplemente desprecian las fases de Schwinger, teniendo en cuenta sólo la parte invariante traslacional del propagador del quark [93, 168, 169]. En esta tesis introducimos un método basado en el uso de funciones propias de tipo Ritus para sistemas magnetizados, que nos permite diagonalizar adecuadamente las funciones de polarización cargadas teniendo plenamente en cuenta los efectos de ruptura traslacional inducidos por las fases de Schwinger. Aunque originalmente introducido para tratar con mesones en el modelo NJL, el método puede aplicarse a partículas cargadas en general, en diferentes escenarios magnetizados. En particular, lo aplicamos al cálculo de masas nucleónicas dentro del modelo NJL, construidos como estados ligados compuestos quark-diquark.

En cuanto al cálculo de las constantes de desintegración de los piones, es importante señalar que la presencia del campo magnético externo abre nuevos canales de desintegración, parametrizados por sus factores de forma correspondientes. Aunque algunas de estas nuevas constantes de desintegración ya fueron reconocidas en la literatura [170, 171], otras no. En esta tesis determinamos todos los factores de forma que surgen en presencia de un campo magnético uniforme teniendo en cuenta todas las estructuras tensoriales independientes que pueden formarse al hadronizar elementos matriciales entre un pión y vacío de las corrientes de quarks. Utilizando el método de Ritus para el cálculo de estos elementos matriciales magnetizados, obtenemos una expresión independiente del modelo para el ancho de decaimiento débil de los piones cargados magnetizados $\pi^- \to l\bar{\nu}_l$, así como para la distribución angular de los antineutrinos salientes. Sus valores pueden estimarse proporcionando la dependencia magnética de las constantes de desintegración

de los piones, que deben calcularse dentro de alguna aproximación QCD. Presentamos estimaciones obtenidas con el modelo NJL.

La tesis está organizada como se detalla a continuación. En el capítulo 2 introducimos el marco teórico. Dado que el modelo NJL se basa en la simetría quiral de la QCD, primero discutimos la teoría de QCD y describimos sus propiedades de transformación de sabor. Después introducimos el modelo NJL, describiendo la inclusión de campos magnéticos en el nivel de campo medio. En el capítulo 3 analizamos el decaimiento débil de piones cargados magnetizados únicamente a partir de bases de la teoría cuántica de campos. Calculamos la anchura de la desintegración y la distribución angular de los antineutrinos salientes. Para ello, proporcionamos expresiones para los campos de materia de las partículas implicadas en presencia del campo externo. Como ya se ha mencionado, el campo magnético externo abre nuevos canales de desintegración, por lo que tenemos en cuenta todos los factores de forma posibles. Con el fin de proporcionar estimaciones reales para el ancho de desintegración y la distribución angular, algunas propiedades de los piones, tales como sus masas y constantes de desintegración, deben ser proporcionadas por algún enfoque QCD. En el capítulo 4 utilizamos el modelo NJL de dos sabores para calcular varias propiedades de los piones, aplicando el método de Ritus para tratar adecuadamente las partículas cargadas. También se explora la posibilidad de una constante de acoplamiento dependiente del campo magnético, con el fin de tener en cuenta el efecto IMC. En el capítulo 5 empleamos la versión de tres sabores del modelo NJL para extender el cálculo de la masa del polo del mesón a todos los mesones del nonete pseudoescalar. Volviendo a la formulación de dos sabores del modelo, las masas de los diquarks pueden obtenerse de manera sencilla imitando el cálculo piónico del capítulo 4. Así, en el capítulo 6 analizamos los diquarks y los utilizamos para estudiar las masas de los nucleones. En nuestro enfoque, los nucleones se tratan como estados ligados quark-diquark descritos por una ecuación relativista de Fadeev, utilizando la aproximación estática para las interacciones de intercambio de quarks. Las conclusiones de este trabajo, junto con una perspectiva a futuro, se presentan en el capítulo 7. Por último, algunos detalles técnicos de los cálculos se discuten en los apéndices.

CHAPTER 2

Theoretical Formalism: QCD and NJL model

In this chapter we will first describe the basic ideas behind the fundamental theory of strong interactions, namely quantum chromodynamics (QCD). We will pay particular attention to the transformation properties of the QCD Lagrangian under the unitary flavor group, since the corresponding symmetries constitute the basis of the effective Nambu-Jona–Lasinio (NJL) model to be used in this thesis. In fact, this model is built upon the symmetries of QCD so as to reproduce some of its essential characteristics, such as the spontaneous breaking of chiral symmetry. We will introduce the model describing its connection with QCD and surveying its main features. Even though it is in principle a quark model, we will illustrate a bosonization procedure which allows for a description of meson fields. In order to retain predictive power, the parameters of the model are finite and fixed by fitting some phenomenological observables. The effectiveness of the interaction is reflected by the presence of a dimensionful coupling constant, which renders the model nonrenormalizable. Thus we will adopt a regularization scheme to completely define the model, which physically implies disregarding the contribution of high energy processes.

In this thesis we will be interested in the effect of an external uniform magnetic field on some of the properties of QCD matter. We will therefore outline the impact that such field has over the symmetries of strongly interacting systems and the properties of charged particles, which are quantized in the directions perpendicular to the applied field. In this regard, the NJL model can be easily extended to account for the influence of external parameters, such as electromagnetic fields, temperature or chemical potential. Thus we

will lastly describe the magnetized NJL model at the mean field level approximation, paying particular attention to the role of the regularization prescription in this context. Its application on the calculation of hadron properties will be discussed in future chapters.

2.1 General aspects of QCD

At a fundamental level, QCD is formulated in terms of quarks and gluons, represented through fermion and gauge boson fields, respectively. The Lagrangian density which describes the dynamics of these fields along with its interactions is [3]

$$\mathcal{L}_{\rm QCD} \;=\; \bar{\psi}\,(i\not{D} - \hat{m})\,\psi - \frac{1}{4}\,G_a^{\mu\nu}G^a_{\mu\nu}\,, \tag{2.1}$$

where we use for the Minkowski metric the convention $(1,-1,-1,-1)$. The covariant derivative is defined as

$$D_\mu \;=\; \partial_\mu - i\,g_s\,\frac{\lambda_a}{2}\,G^a_\mu\,, \tag{2.2}$$

and the gluon field strength tensor reads

$$G^a_{\mu\nu} \;=\; \partial_\mu G^a_\nu - \partial_\nu G^a_\mu + g_s\,f^{abc}G^b_\mu G^c_\nu\,. \tag{2.3}$$

The ψ field represents quark states, including the corresponding internal degrees of freedom of color and flavor. There are three color states and, for the full theory, six flavor states. These states are described through a tensorial product between both spaces, resulting in 18 spinors. The mass matrix is given in flavor space by $\hat{m} = \mathrm{diag}(m_u, m_d, m_s, m_c, m_b, m_t)$, with $m_u \simeq m_d$. Also, g_s is the coupling constant of QCD, while G^a_μ is the set of massless gauge fields associated to the gluons. Here $a = 1, ..., 8$ and λ^a are Gell-Mann matrices, which satisfy

$$[\lambda^a, \lambda^b] \;=\; 2if^{abc}\lambda^c\,, \qquad \mathrm{Tr_c}(\lambda^a\lambda^b) \;=\; 2\delta^{ab}\,, \tag{2.4}$$

where f^{abc} are the completely antisymmetric structure constants of the $SU(3)$ group.

The $\bar{\psi}(i\gamma_\mu\partial^\mu - \hat{m})\psi$ piece corresponds to the Dirac Lagrangian, which describes the propagation of free quarks. This term is invariant under global transformations of the $SU(3)_c$ group, given by the group of unitary matrices with $+1$ determinant which act on color space. Quark states belong to the (3-dimensional) fundamental representation of this group, while gluons are in the (8-dimensional) adjoint representation. Since $T_a = \lambda_a/2$ are the $SU(3)$ generators in the fundamental representation, we can write an arbitrary global transformation as $U = e^{i\,T_a\theta^a}$, where θ^a are the parameters associated to the generators.

In order for the Lagrangian to be invariant also under local transformations, i.e. $\theta^a(x)$, the partial derivative has to be replaced by the covariant derivative of Eq. (2.2), where gluon fields transform as

$$G^a_\mu \;\longrightarrow\; G^a_\mu - \frac{1}{g_s}\,\partial_\mu\theta^a - f^{abc}\,\theta^b\,G^c_\mu\,. \tag{2.5}$$

Lastly, the Yang-Mills term $G_a^{\mu\nu}G_{\mu\nu}^a$ of Eq. (2.1) describes gluon field dynamics in the absence of quarks. It is formulated as a contraction of field strength tensors so as to be invariant under Lorentz and color groups, mimicking the formulation of quantum electrodynamics (QED). As in QED, the first two terms of Eq. (2.3) describe the field propagation. However, in contrast to QED, invariance requires the addition of an extra term $g_s f^{abc} G_\mu^b G_\nu^c$, due to the fact that the color group is non-abelian. This term represents a self-interaction between gluons, which are coupled through three and four-line vertices.

As known, when studying a process in any renormalizable gauge theory, the inclusion of successive Feynman diagrams in the series expansion can be rearranged so as to express the final result in terms of a 'dressed' coupling constant, which depends on the transferred momentum Q. Consequently, the interaction will behave differently according to the energy scale under study, where the exact functional dependence will depend on the details of the interaction under consideration. In QCD, the self-interaction between gluons dramatically modifies the running of the QCD coupling, $\alpha_s(Q)$. At 1-loop, it is given by

$$\alpha_s(Q^2) \;=\; \frac{g_s^2(Q^2)}{4\pi} \;=\; \frac{4\pi}{\left(11 - \frac{2}{3}N_f\right)\ln\left(Q^2/\Lambda_{\rm QCD}^2\right)}\,, \tag{2.6}$$

where N_f is the flavor number (six in QCD) and $\Lambda_{\rm QCD}$ is the scale parameter of the theory, which can be determined by fitting experimental data at large Q (where perturbation theory is applicable). For five flavors in the $\overline{MS}$ scheme, one finds $\Lambda_{\rm QCD} \simeq 200$ MeV. As can be seen from this expression, $\alpha_s \to 0$ when $Q \to \infty$. This property, known as asymptotic freedom, allows for the study of high energy processes through perturbation theory. On the other hand, for low energy processes $\alpha_s \to \infty$, leading to the confinement of quarks into colorless hadrons (and glueballs). The confinement mechanism has not been satisfactorily understood yet. In particular, for Q below $\Lambda_{\rm QCD}$ we have $\alpha_s > 1$, precluding the possibility of a series expansion in the coupling constant. Since the scale of hadron binding energies lies below this threshold, the study of most hadronic properties must be performed through nonperturbative methods. Some of the most common approaches include simulations in lattice QCD or the development of semi-analytic effective models such as the one used in this thesis, i.e. the NJL model.

It is important to note that, as a consequence of the confinement phenomenon in the vacuum phase, quark masses are not physical observables. Therefore, when quark current masses are used as input parameters of the model, their values are subject to a variable range because they depend on the renormalization scale of the theory. The determination of quark current masses can in fact be performed within certain precision degree by several approaches in the $\overline{MS}$ scheme, resulting in scale dependent quantities. These approaches include Lattice QCD, sum rules, chiral perturbation theory and heavy quark effective

theory. From them it is concluded that up, down and strange quarks are light flavors, with masses below $\Lambda_{\rm QCD}$ [172]. For the low energy properties we will study in this thesis this is the relevant flavor subspace, since we will study the effect of external magnetic fields on light hadron properties for scales below the charm quark mass.

2.1.1 Transformation properties in flavor space

In this subsection we will study the properties of the QCD Lagrangian under transformations in quark flavor space. For massless quarks, $\mathcal{L}_{\rm QCD}$ is invariant under global $U(N_f)_L \times U(N_f)_R = U(N_f)_V \times U(N_f)_A$ transformations, given by

$$U(N_f)_V : \quad \psi \to e^{i\,\tau_a \theta_a^V}\,\psi \ , \qquad U(N_f)_A : \quad \psi \to e^{i\,\gamma_5 \tau_a \theta_a^A}\,\psi \,, \tag{2.7}$$

which correspond to vector and axial transformations, where τ_a with $0 \leq a \leq N_f^2 - 1$ are the generators of $U(N_f)$. This invariance is known as chiral symmetry, and leads to the conservation of the following currents

$$V_a^\mu \ = \ \bar{\psi}\gamma^\mu \tau_a \psi \ , \qquad A_a^\mu \ = \ \bar{\psi}\gamma^\mu\gamma_5 \tau_a \psi \,. \tag{2.8}$$

The associated conserved charges $Q_a^{V,A}$ serve as generators of the corresponding symmetry transformations. Since τ_0 is proportional to the identity, each $U(N_f)$ subgroup can be expressed as the product $U(N_f) = U(1) \times SU(N_f)$. The $U(1)_V$ and $SU(2)_V$ groups are associated to the conservation of the baryon number and isospin, respectively. On the other hand, axial transformations alter the parity associated with a given state. Even though $U(1)_A$ is a symmetry of the classical chiral Lagrangian, it is broken when the theory is quantized. This is due to the fact that the integration measure in the corresponding path integral does not remain invariant under such transformation. This phenomenon is known as axial anomaly [173, 174]. Experimentally, this is evidenced by the fact that one does not observe opposite parity partners to all hadrons, and also manifests in the rather heavy η' meson mass.

It is important to recall that, in general, there is more than one way in which a given symmetry of the Lagrangian (such as chiral symmetry) can manifest itself. The crucial distinction between different modes lies in the vacuum structure. In the Wigner-Weyl mode, the vacuum is also invariant under such symmetry. The ground state is nondegenerated, and therefore an eigenstate of $Q_a^{V,A}$. The spectrum of all eigenstates splits into degenerate multiplets of the symmetry, corresponding to irreducible representations of the symmetry group. On the other hand, in the Nambu-Goldstone mode the vacuum is modified by the interactions, and may only be invariant under a subgroup of the original symmetry group.

This phenomenon is dubbed as spontaneous symmetry breaking. Each broken generator creates a massless excitation which is degenerated with the vacuum, known as Goldstone bosons. This is the content of Goldstone's theorem.

For massive quarks, the conservation of the currents defined in Eq. (2.8) is lost. We have

$$\partial_\mu V_a^\mu \;=\; 2i\,\bar{\psi}\,[\hat{m},\tau_a]\,\psi \;\;, \qquad \partial_\mu A_a^\mu \;=\; 2i\,\bar{\psi}\,\{\hat{m},\tau_a\}\,\gamma_5\,\psi\,. \tag{2.9}$$

However, chiral symmetry is still a useful concept if we restrict to light quarks, because the breaking of the symmetry is small by virtue of the small current masses. We say it is approximately conserved. The light quark subspace includes the up and down sector ($N_f = 2$), and even, although with larger deviations, when strange quarks are included as well ($N_f = 3$).

For $N_f = 2$ we have $m_u \simeq m_d \equiv m_c \neq 0$ and $\hat{m} \simeq \mathrm{diag}(m_u, m_d) \simeq m_c\,\mathbb{1}$. As a result, the vector current is conserved to a good degree of approximation, realized in the Wigner-Weyl mode. This is experimentally evidenced by the degeneration in the masses of baryonic and mesonic isospin multiplets, as well as the existence of approximately conserved currents in processes dominated by the strong interaction.

In contrast, experimental and theoretical evidence indicates that $SU(2)_A$ symmetry is realized in the Goldstone mode. Since the charge operators Q_a^A alter the parity of states, the realization of this symmetry in the Wigner-Weyl mode would imply that for each isospin multiplet there exists another degenerated multiplet with opposite parity, which is not observed in Nature. In addition, hadronic masses are much heavier than current light quark masses, implying the existence of a dynamical mass generation mechanism, which in turn provokes the breaking of the symmetry. These observations suggest that axial symmetry is broken dynamically. In this frame, the Q_a^A generators of the broken symmetry create an isospin triplet of pseudoscalar Goldstone bosons, which can be identified with the pions. This idea is supported by the fact that the components of the pionic triplet have an exceptionally low mass in comparison to other hadrons ($m_\pi/m_N \simeq 0.15$). Their small but nonvanishing mass arises due to the explicit symmetry breaking produced by current quark masses, as seen from Eq. (2.9). Analogously, the pseudoscalar meson octet corresponds to the Goldstone bosons of the three-flavor case. The aforementioned axial anomaly is reflected by the relatively heavy η' meson, which should be much lighter (lighter than the η meson) if it were a Goldstone boson of a spontaneously broken symmetry.

The spontaneous (axial) symmetry breaking of the QCD vacuum and the subsequent generation of a dynamical mass is closely related to the existence of nonvanishing condensates, formed as bilinear products of quark and gluon fields. A relevant one is the chiral

condensate, defined as the expectation value $\langle\bar{\psi}\psi\rangle$, which can be expressed as

$$\langle\bar{\psi}\psi\rangle \;=\; -i\int\frac{d^4p}{(2\pi)^4}\,\mathrm{Tr}_{\mathrm{D,f,c}}\,\mathcal{S}(p)\,, \tag{2.10}$$

where $\mathcal{S}(p)$ is the quark propagator from the full QCD Lagrangian, and the trace is taken over Dirac, flavor and color space. Since the operator $\bar{\psi}\psi$ is not invariant under $SU(2)_A$ transformations, it serves as an order parameter for signaling chiral symmetry breaking. A nonvanishing expectation value would indicate that the QCD vacuum is realized in the Goldstone mode of the axial symmetry. Current theoretical estimations for the chiral condensate suggest that this is effectively the case. For example, according to calculations based on current algebra and QCD sum rules one has $|\langle\bar{f}f\rangle|^{1/3} = 190 - 260$ MeV [175], where f represents u or d flavors. Meanwhile, typical simulations performed in lattice QCD provide $|\langle\bar{f}f\rangle|^{1/3} = 231 \pm 8 \pm 6$ MeV [176].

2.2 NJL model in vacuum

In this thesis we will use NJL effective-type models to calculate several hadronic properties. The main idea behind the model is to respect the flavor symmetries of QCD discussed in the previous section, particularly chiral symmetry and its dynamical breaking. In the NJL model, one argues that the interaction between quarks and antiquarks, which arises from some complicated processes of gluon exchange, can be attractive. Gluon degrees of freedom are assumed to be frozen in the low-energy and long-wavelength limit. Then, similar to Fermi's theory of the weak interaction, the gluon interaction between quarks is modeled as an effective four-point (or more) fermion interaction, see Figure 2.1. These interactions can be thought of to be abstracted from instanton-induced interactions [173, 174].

Since the fundamental quark currents in QCD are color vector currents $J^a_\mu = \bar{\psi}\gamma_\mu T^a\psi$, one can start by considering the simple example of an interaction based on the local coupling between two such currents.

$$\mathcal{L}^c_{\mathrm{int}} \;=\; g\,\left(\bar{\psi}\gamma_\mu T^a\psi\right)^2\,. \tag{2.11}$$

This interaction is invariant under chiral $U(3)_V \times U(3)_A$. It can be though of as abstracted from the QCD Lagrangian by converting the original gauge symmetry $SU(N_c)$ into a global symmetry of color quark currents. By Fierz transformations, this interaction can be rewritten so as to obtain color singlet and color octet terms [146]. In the color singlet channel, new scalar, pseudoscalar, vector and axial-vector interactions appear in flavor

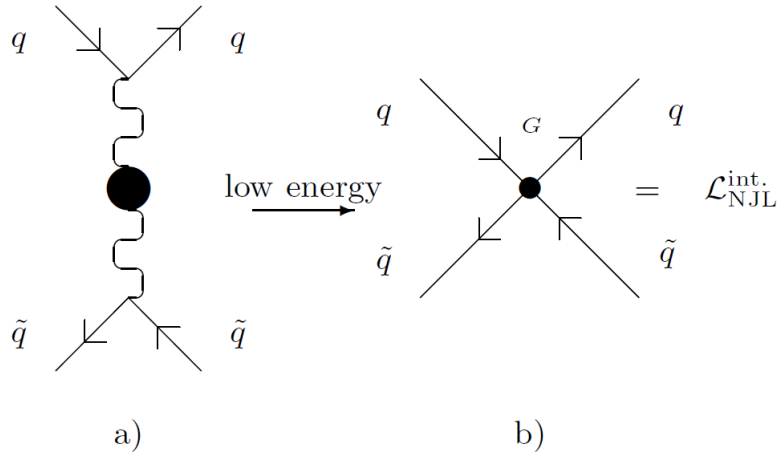

Figure 2.1: Low energy approximation of a nonlocal current-current interaction with a nonperturbative gluon propagator (a) by a local NJL-type interaction (b). Figure adapted from [177].

space, with the quantum numbers (flavor and spin) of the various meson nonets. Similar transformations can be performed for the color axial current. Inspired by this observation, one can construct several four-point interaction terms which are invariant under (global) $SU(3)_c \times U(1)_V \times SU(N_f)_V \times SU(N_f)_A$ [145].

In its simplest form, the two-flavor NJL Lagrangian in Euclidean space is given by a combination of a scalar-isoscalar (Lorentz and isospin invariant, respectively) and a pseudoscalar-isovectorial current

$$\mathcal{L}_E(\psi,\bar{\psi}) \;=\; \bar{\psi}(x)\left(-i\not{\partial} + m_c\right)\psi(x) - G\left\{\left[\bar{\psi}(x)\psi(x)\right]^2 + \left[\bar{\psi}(x) i\gamma_5 \vec{\tau}\psi(x)\right]^2\right\}\,, \tag{2.12}$$

where $\psi = (\psi_u\,,\,\psi_d)^T$ and $\not{\partial} = \gamma_4\partial_4 + \vec{\gamma}\cdot\vec{\nabla}$, with $\gamma_4 = i\gamma_0$. Moreover, G is the effective coupling constant and m_c are the up and down current quark masses, which we will assume equal in this thesis. These are model parameters which have to be fixed by fitting physical observables. It is common to use as observables the pion mass and decay constant, which can be relatively easy calculated within the model, as we will show below.

The connection between Minkowski and Euclidean space is given by a Wick rotation. Starting from the generating functional

$$\mathcal{Z} \;=\; \int \mathcal{D}\bar{\psi}\mathcal{D}\psi\; e^{i\int d^4x\,\mathcal{L}(\psi,\bar{\psi})}\,, \tag{2.13}$$

and making the complex rotation [178] $x_4 = ix^0$ and $x_{i,E} = x^i$ for $i = 1,2,3$ we obtain

$$\mathcal{Z} \;=\; \int \mathcal{D}\bar{\psi}\mathcal{D}\psi\, e^{-\int d^4x_E\,\mathcal{L}_E(\psi,\bar{\psi})}\,, \tag{2.14}$$

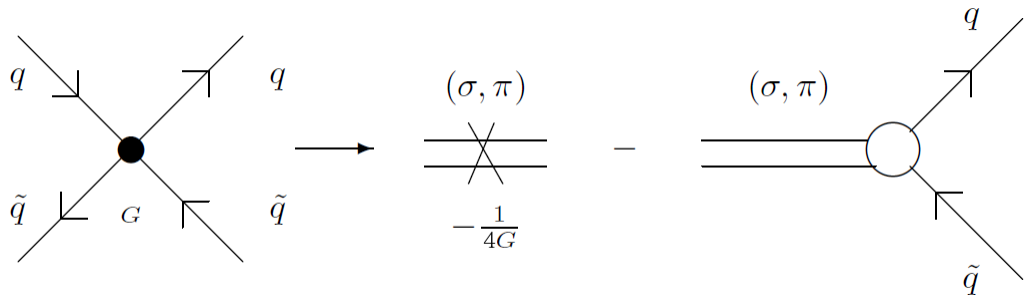

Figure 2.2: Graphical representation of the transformation from fermionic to semibosonized interactions.

where $\mathcal{L}_E = -\mathcal{L}(x^0 \to -ix_4)$. This is the reason why the sign is inverted between the Dirac Lagrangians of Eq. (2.1) (Minkowski) and (2.12) (Euclidean). The Euclidean action serves as a starting point to build an analogy between Euclidean quantum field theory and statistical mechanics. Note that in Euclidean space we use the convention $\{\gamma_\mu, \gamma_\nu\} = -2\delta_{\mu\nu}$. We will omit the Euclidean subindex E in what follows to simplify the notation.

2.2.1 Bosonization formalism

In order to calculate meson properties we resort in what follows to the bosonization formalism [145, 146, 177, 179]. There, quark degrees of freedom, which are not observed at low energies, are integrated out and replaced by meson fields, which represent the physical excitations in that regime. We will exemplify here the two-flavor case.

The idea consists of rewriting the interaction piece of Eq. (2.12) in terms of bosonic fields which represent the scalar and pseudoscalar mesons $\sigma(x)$ and $\vec{\pi}(x)$, respectively. Following the procedure described in Appendix A, one arrives at the semibosonized generating functional

$$\mathcal{Z} \;=\; \int \mathcal{D}\sigma\mathcal{D}\vec{\pi} \int \mathcal{D}\bar{\psi}\mathcal{D}\psi \; e^{-S_F} \; e^{-\frac{1}{4G}\int d^4x\,[\sigma(x)^2+\vec{\pi}(x)^2]} \,. \tag{2.15}$$

The fermionic field contribution has been grouped under the single term

$$S_F \;=\; \int d^4x\, d^4x' \; \bar{\psi}(x) \; \mathcal{D}(x,x') \; \psi(x') \,, \tag{2.16}$$

where the fermionic operator $\mathcal{D}$ is given by

$$\mathcal{D}(x,x') \;=\; \delta^{(4)}(x-x') \left[-i\partial\!\!\!/ + m_c + \sigma(x) + i\gamma_5 \,\vec{\tau}\cdot\vec{\pi}(x)\right] \,. \tag{2.17}$$

A direct product to an identity matrix in color space is understood. Diagrammatically, the procedure corresponds to the rearrangement of the four-point fermionic interaction

into Yukawa-type quark-meson vertices, as illustrated in Figure 2.2 [177].

Since so far the bosonization procedure is exact, the semibosonized Lagrangian possess the symmetries of the original one. Chiral symmetry of the two-flavor NJL model (2.12) is realized in meson field space as the rotation group $O(4)$, which leaves the "length" of the particle vector $(\sigma, \vec{\pi})$ invariant. Hence, all effective potentials of this model depend on the single variable $\sqrt{\sigma^2 + \vec{\pi}^2}$. It should be noted that, so far, the auxiliary fields σ and $\vec{\pi}$ are not dynamic, since no kinetic term of the form $\partial_\mu\sigma\partial_\mu\sigma + \partial_\mu\vec{\pi}\partial_\mu\vec{\pi}$ appears in Eq. (2.15). However, when quark degrees of freedom are integrated out their effect is exerted through quark loops, which dress the boson fields allowing them to describe physical mesons. Both bosonic fields carry the quantum numbers of the composed operators $(\bar{\psi}\psi)$ and $(\bar{\psi}i\gamma_5\vec{\tau}\psi)$, but not their color [180].

In order to completely bosonize the Lagrangian, quark degrees of freedom can be integrated out in terms of a fermionic determinant [178]. Using the property $\ln\det\mathcal{D} = \mathrm{Tr}\ln\mathcal{D}$, the generating functional reads

$$\mathcal{Z} \;=\; \int \mathcal{D}\sigma\mathcal{D}\vec{\pi}\; e^{-S_{\mathrm{bos}}(\sigma,\vec{\pi})}\,, \tag{2.18}$$

where the bosonized action is given by [145]

$$S_{\mathrm{bos}}(\sigma,\vec{\pi}) \;=\; -\mathrm{Tr}\,\ln\mathcal{D} + \int d^4x\left[\frac{\sigma(x)^2+\vec{\pi}(x)^2}{4G}\right]\,. \tag{2.19}$$

The functional trace is taken over coordinate [1], Dirac, color and flavor space. Note that expression (2.18) is completely equivalent to (2.14).

Now, in models where spontaneous symmetry breaking occurs, meson fields can, in general, develop nonvanishing mean field (MF) values. Due to translational invariance, $\sigma(x)$ has a translationally invariant MF value $\bar{\sigma}$, while the pionic MF value vanishes in order to keep the vacuum parity invariant. Expanding the mesonic fields in powers of fluctuacions around their corresponding MF values

$$\sigma(x) \;=\; \bar{\sigma} + \delta\sigma(x)\,, \qquad \vec{\pi}(x) \;=\; \delta\vec{\pi}(x)\,, \tag{2.20}$$

we have

$$\mathcal{D}(x,x') \;=\; \mathcal{D}_{\mathrm{MF}}(x,x') + \delta\mathcal{D}(x,x')\,. \tag{2.21}$$

The MF piece is given by

$$\mathcal{D}_{\mathrm{MF}}(x,x') \;=\; \delta^{(4)}(x-x')\left(-i\partial\!\!\!/ + m_c + \bar{\sigma}\right)\,, \tag{2.22}$$

[1] In coordinate space the functional trace is defined as $\tilde{\mathrm{Tr}} = \int d^4x\, d^4x'\, \delta^{(4)}(x-x')$, being analogous for momentum space.

where an identity matrix in color and flavor space is understood. From Eq. (2.16) we see that the inverse of this operator $\mathcal{S}_{\rm MF}(x,x') = [\mathcal{D}_{\rm MF}(x,x')]^{-1}$ is the quark propagator. Transforming to Fourier space, it can be expressed as

$$\mathcal{S}_{\rm MF}(x,x') \;=\; \int_q e^{iq(x-x')}\;\bar{\mathcal{S}}(q)\;, \qquad \bar{\mathcal{S}}(q) \;=\; \frac{1}{\not{q}+M}\;, \tag{2.23}$$

where we have introduced the shorthand notation

$$\int_q \;=\; \int \frac{d^4q}{(2\pi)^4}\;. \tag{2.24}$$

We can therefore identify the dressed quark mass $M = m_c + \bar{\sigma}$, where we explicitly see that the dynamical generation of the mean field $\bar{\sigma}$ is responsible for the breaking of chiral symmetry.

On the other hand, the second term on the right-hand-side of Eq. (2.21) reads

$$\delta\mathcal{D}(x,x') \;=\; \delta^{(4)}(x-x') \begin{pmatrix} \delta\sigma(x) + i\gamma_5\delta\pi_0(x) & \sqrt{2}i\gamma_5\,\delta\pi^+(x) \\ \sqrt{2}i\gamma_5\,\delta\pi^-(x) & \delta\sigma(x) - i\gamma_5\delta\pi_0(x) \end{pmatrix}\;, \tag{2.25}$$

where $\pi^\pm = (\pi_1 \mp i\pi_2)/\sqrt{2}$. Replacing in the bosonized effective action and expanding in powers of the meson fluctuations around the MF values, we get

$$\begin{aligned} -\ln\det\mathcal{D} \;&=\; -\,\mathrm{Tr}\ln\mathcal{D}_{\rm MF} \;-\; \mathrm{Tr}\ln(1+\mathcal{D}_{\rm MF}^{-1}\,\delta\mathcal{D}) \\ &=\; -\,\mathrm{Tr}\ln\mathcal{D}_{\rm MF} \;-\; \mathrm{Tr}\,(\mathcal{S}_{\rm MF}\,\delta\mathcal{D}) \;+\; \frac{1}{2}\,\mathrm{Tr}\,(\mathcal{S}_{\rm MF}\,\delta\mathcal{D})^2 \;+\; \ldots \end{aligned} \tag{2.26}$$

where $\mathcal{S}_{\rm MF}(x,x') = [\mathcal{D}_{\rm MF}(x,x')]^{-1}$ is the quark propagator. The linear term vanishes and the action can be symbolically written as

$$S^{\rm bos} \;=\; S^{\rm bos}_{\rm MF} \;+\; S^{\rm bos}_{\rm quad} \;+\; \ldots \tag{2.27}$$

2.2.2 Mean field approximation

The zero order contribution in Eq. (2.27) gives the mean field approximation, where all fluctuations are neglected. The MF effective potential reads

$$\Omega_{\rm MF} \;=\; \frac{S^{\rm bos}_{\rm MF}}{V^{(4)}} \;=\; \frac{\bar{\sigma}^2}{4G} - \frac{1}{V^{(4)}}\,\mathrm{Tr}\ln\mathcal{D}_{\rm MF}(x,x')\;. \tag{2.28}$$

In order to proceed we diagonalize by transforming to momentum space, so as to take the logarithm of the eigenvalues. It can be shown that the Fourier transform of an arbitrary

operator is

$$\mathcal{O}(x,x') \;=\; \int_{q,q'} e^{iqx}\,\mathcal{O}(q,q')\,e^{-iq'x'}\,,$$
$$\mathcal{O}(q,q') \;=\; \int d^4x\,d^4x'\,e^{-iqx}\,\mathcal{O}(x,x')\,e^{iq'x'}\,. \tag{2.29}$$

Actually, instead of calculating the trace of $\mathcal{D}_{\rm MF}(x,x')$, it will be more convenient to square this quantity. From the cyclic property of the trace, we can multiply left and right by γ_5, since $\gamma_5^2 = \mathbb{1}$, to obtain

$$\mathrm{Tr}\ln\mathcal{D}_{\rm MF}(x,x') \;=\; \frac{1}{2}\,\mathrm{Tr}\ln\mathcal{A}(x,x')\,, \qquad \mathcal{A}(x,x') \;=\; \delta^{(4)}(x-x')\left(\not{\partial}^2 + M^2\right)\,. \tag{2.30}$$

Applying the transformation (2.29), this operator is diagonalized in Fourier space as

$$\mathcal{A}(q,q') \;=\; (2\pi)^4\,\delta^{(4)}(q-q')\,\left(q^2+M^2\right)\,, \tag{2.31}$$

where we have used that $\not{q}^2 = -q^2$. Since the logarithm of a diagonal matrix is also diagonal, transforming $\ln\mathcal{D}_{\rm MF}(x,x')$ to Fourier space through (2.29) we arrive at

$$\begin{aligned}\mathrm{Tr}\ln\mathcal{D}_{\rm MF}(x,x') \;&=\; \frac{N_cN_f}{2}\,\mathrm{Tr}_{\rm D}\int d^4x\,d^4x'\,\delta^{(4)}(x-x')\int_{q,q'} e^{iqx}\,\ln[\mathcal{A}(q,q')]\,e^{-iq'x'}\\ &=\; \frac{N_cN_f}{2}\,\mathrm{Tr}_{\rm D}\int d^4x\int_q \ln\left(q^2+M^2\right)\,.\end{aligned} \tag{2.32}$$

Finally, the MF free energy is

$$\Omega_{\rm MF} \;=\; \frac{(M-m_c)^2}{4G} - 2N_cN_f\int_q \ln\left(q^2+M^2\right)\,. \tag{2.33}$$

The physical value of M is given by the one which minimizes the free energy. This results in the gap equation

$$M \;=\; m_c + 2G\,\mathrm{Tr}\,\mathcal{S}_{\rm MF}(x,x') \;=\; m_c + 2GMN_cN_fI_1^0\,. \tag{2.34}$$

where we have defined the I_1^0 (divergent) integral

$$I_1^0 \;=\; 4\int_q \frac{1}{q^2+M^2}\,. \tag{2.35}$$

Since in this thesis we will be interested in the effect of external magnetic fields, and we will use a regularization scheme where this $B=0$ contribution is regularized, we have

added a zero superscript to identify this function with the $B = 0$ case for later convenience. For a sufficiently strong coupling G a nontrivial solution $M \neq m_c$ is allowed, even in the chiral limit $m_c \to 0$, producing a gap of $\Delta E = 2M$ in the quark spectrum. In general, the gap equation possess more than one solution. The physical solution will be the one which minimizes the free energy. It is worth remarking that there are alternative methods to derive the gap equation, such as linearizing the quadratic terms in the Lagrangian of Eq. (2.12).

A closely related quantity is the quark or chiral condensate, defined as

$$\langle\bar{\psi}\psi\rangle \equiv -\frac{\delta\Omega_{\rm MF}}{\delta m_c} = \frac{M-m_c}{2G} = -\frac{1}{V^{(4)}}\,{\rm Tr}\,\mathcal{S}_{\rm MF}(x,x') = -MN_cN_f\,I_1^0\,. \tag{2.36}$$

where in the third equality we have made use of the gap equation. Note that this is the average quark condensate, i.e. $\langle\bar{\psi}\psi\rangle = (\langle\bar{u}u\rangle + \langle\bar{d}d\rangle)/2$. In this $B = 0$ case, $\langle\bar{u}u\rangle = \langle\bar{d}d\rangle$. A nonzero quark condensate tells us that the vacuum is filled with quark-antiquark pairs. Equivalently, the gap equation can be written as $M = m_c - 2G\langle\bar{\psi}\psi\rangle$. Thus, M (or $\bar{\sigma}$) servers as an order parameter to determine in which mode the symmetry is realized.

2.2.3 Meson masses

In order to obtain a phenomenological description of mesons, it is necessary to study the theory retaining field fluctuations at quadratic order. From the expansion of Eq. (2.26) we arrive at the quadratic action

$$S^{\rm bos}_{\rm quad} = \frac{1}{2}\,{\rm Tr}\,(\mathcal{S}_{\rm MF}\,\delta\mathcal{D})^2 + \int d^4x\left[\frac{\delta\sigma(x)^2+\delta\vec{\pi}(x)^2}{4G}\right]\,, \tag{2.37}$$

where the operator product in coordinate space is defined as

$$\mathcal{O}_1\mathcal{O}_2(x,x') = \int d^4x''\;\mathcal{O}_1(x,x'')\,\mathcal{O}_2(x'',x')\,. \tag{2.38}$$

Taking some of the traces and rearranging terms, we can express the action in the form

$$S^{\rm bos}_{\rm quad} = \frac{1}{2}\sum_{P=\sigma,\vec{\pi}}\int d^4x\,d^4x'\;\delta P(x)\left[\frac{\delta^{(4)}(x-x')}{2G} - J_P(x,x')\right]\delta P(x')\,, \tag{2.39}$$

where the polarization functions are given by

$$\begin{aligned} J_\sigma(x,x') &= -2N_c\,{\rm Tr}_{\rm D}\left[\mathcal{S}_{\rm MF}(x,x')\,\mathbb{1}\,\mathcal{S}_{\rm MF}(x',x)\,\mathbb{1}\right]\,,\\ J_\pi(x,x') &= 2N_c\,{\rm Tr}_{\rm D}\left[\mathcal{S}_{\rm MF}(x,x')\,\gamma_5\,\mathcal{S}_{\rm MF}(x',x)\,\gamma_5\right]\,. \end{aligned} \tag{2.40}$$

In order to diagonalize the polarization functions, we introduce the Fourier transform of the meson fields

$$\delta P(x) \;=\; \int_p e^{ipx}\; \delta P(p)\,. \tag{2.41}$$

Together with the transformation of the quark propagator in Eq. (2.23), we obtain

$$S^{\rm bos}_{\rm quad} \;=\; \frac{1}{2}\sum_{P=\sigma,\vec{\pi}}\int_p \delta P(-p)\left[\frac{1}{2G} - J_P(p)\right]\delta P(p)\,, \tag{2.42}$$

where

$$\begin{aligned} J_\sigma(p) \;&=\; -\,2N_c\int_r \mathrm{Tr_D}\left[\bar{\mathcal{S}}\left(r+\frac{p}{2}\right)\mathbb{1}\,\bar{\mathcal{S}}\left(r-\frac{p}{2}\right)\mathbb{1}\right]\,,\\ J_\pi(p) \;&=\; 2N_c\int_r \mathrm{Tr_D}\left[\bar{\mathcal{S}}\left(r+\frac{p}{2}\right)\gamma_5\,\bar{\mathcal{S}}\left(r-\frac{p}{2}\right)\gamma_5\right]\,, \end{aligned} \tag{2.43}$$

and $r = (q_f + q_{f'})/2$ is the average of the quarks momenta q_f and $q_{f'}$. Explicit calculation leads to

$$\begin{aligned} J_\sigma(p^2) \;&=\; 2N_c\left[I_1^0 + (p^2+4M^2)\,I_2^0(p^2)\right]\,,\\ J_{\vec{\pi}}(p^2) \;&=\; 2N_c\left[I_1^0 + p^2\,I_2^0(p^2)\right]\,, \end{aligned} \tag{2.44}$$

where I_1^0 was defined in Eq. (2.35) and

$$I_2^0(p^2) \;=\; -2\int_r \frac{1}{[(r+p/2)^2+M^2]\,[(r-p/2)^2+M^2]}\,. \tag{2.45}$$

It is worth remarking that the same result for the polarization functions can be obtained iterating the four-point vertex in the Bethe-Salpeter equation for the mesonic propagator within the random phase approximation [145, 181]. In that case, the pion mass is given by the pole of the mesonic propagator. In our case, the two-point function, given by the bracket term in Eq. (2.42), serves as an inverse meson propagator. Since the mass is defined as the pole of the propagator, one is required to solve

$$1 - 2G\,J_P(p^2 = -m_P^2) \;=\; 0\,. \tag{2.46}$$

In the chiral limit $m_c \to 0$ it can be seen that $m_\pi = 0$, in agreement with Goldstone theorem.

2.2.4 Pion decay constant

Since the pion is a pseudoscalar, its decay constant can be obtained from the matrix element of the axial current between the vacuum and a one-pion state

$$\langle 0|\,\bar{\psi}(x)\gamma_\mu\gamma_5\,\frac{\tau^a}{2}\,\psi(x)\,|\pi^b(\vec{p})\rangle \;=\; -i\,p_\mu\,f_\pi\,e^{ipx}\,\delta^{ab}\,, \tag{2.47}$$

We will come back to this point in more detail in section 3.2. The left hand side of this equation can be calculated within the NJL model by "gauging" the effective action. We postpone the details to section 4.3, where the same procedure will be applied but in the presence of an external magnetic field. It can also be deduced by translating the corresponding diagram, see Refs. [145, 181]. One obtains

$$f_\pi p_\mu \delta^{ab} \;=\; -g_{\pi qq}\int_r \mathrm{Tr}_{\mathrm{D,f,c}}\left[\bar{\mathcal{S}}\left(r+\frac{p}{2}\right)\gamma_5\tau^a\,\bar{\mathcal{S}}\left(r-\frac{p}{2}\right)\gamma_\mu\gamma_5\frac{\tau^b}{2}\right]\,, \tag{2.48}$$

where $g_{\pi qq}$ is the pion-quark-quark coupling constant, calculated as the residue at the pole of the pion two-point function $1/2G - J_\pi(p)$, i.e. $g_{\pi qq} = -\partial J_\pi(p^2)/\partial p^2|_{p^2=-m_\pi^2}$. Explicit calculation of the trace results in

$$f_\pi \;=\; -g_{\pi qq}\,2N_c M\;I_2^0(-m_\pi^2)\,, \tag{2.49}$$

where $I_2^0(p^2)$ has been defined in Eq. (2.45).

Results from current algebra, such as the Goldberger-Treiman (GT) and Gell–Mann-Qakes-Renner (GMOR) relationships, must necessarily hold as a consequence of the chiral symmetry of the model. This can be explicitly demonstrated within the NJL model. Recall that the chiral limit corresponds to $m_c \to 0$, which also implies $m_\pi \to 0$. In fact, explicitly calculating $g_{\pi qq}$ it can be seen that the generalized GT relation is satisfied [182]

$$f_\pi\,g_{\pi qq} \;=\; M_{ch} + \mathcal{O}(m_c)\,. \tag{2.50}$$

The *ch* subscript implies that the chiral limit has been taken. Moreover, making use of this relation together with the gap equation, the generalized GMOR relation [183] is also obtained

$$m_\pi^2\,f_{\pi,ch}^2 \;=\; -2m_c\langle\bar{\psi}\psi\rangle + \mathcal{O}(m_c)\,. \tag{2.51}$$

2.2.5 Regularization procedures

So far, we have seen that the NJL model can be used to obtain a phenomenological description of mesons, yielding results for several meson properties such as masses, couplings

and decay constants. Moreover, it reproduces low energy relationships from current algebra. However, in spite of these satisfactory results, the NJL (effective) model presents several problems:

- It does not confine. This is a consequence of the fact that gluon degrees of freedom have been frozen, as the purely fermionic version of the model cannot reproduce a confinement mechanism. Formally, this is reflected in the fact that the integral in $I_2^0(p^2)$, and hence the polarization functions $J_P(p^2)$, get an imaginary part for $|p^2| > 4M^2$. As a consequence, mesons with masses over $2M$ acquire a finite width, indicating their instability to decay into a free quark-antiquark pair, which is unphysical. Even though the pion is light enough to avoid this problem, the sigma meson exceeds the limiting value if $m_c > 0$. Moreover, if vector mesons are included, it will depend on the parameter set whether their mases are above or below the limiting value. In particular, for $N_f = 3$ the η'-meson mass is generally over the quark threshold, as well as axial-vector mesons. This is rather a feature of states that lie high in energy with respect to the scale of the theory. It was assumed when constructing the NJL model that, for low energy mass spectra and properties, the role of symmetries overrides that of confinement, which is expected to affect the high energy behavior of the theory. In order to deal with the lack of confinement, especially at high temperature, in the literature this problem is usually treated by including a coupling with the Polyakov loop [148–150], which serves as order parameter of the deconfinement transition.

- It is not renormalizable. This is due to the way in which the gluon interaction is modeled, namely as a local point vertex. A regularization scheme specifies a length scale for the theory, which can be expressed as a cutoff on the quark momentum. One may regard the cutoff as an approximate, if crude, implementation of the property of asymptotic freedom of QCD: by suppressing the interaction between quarks for large space-like momentum transfer, one simulates the behavior of the running coupling constant of QCD. In the model, the nonrenormalizability is reflected in the fact that calculated expressions contain divergent integrals, see e.g. Eqs. (2.35) and (2.45). Thus, one should specify how to regularize these divergences. The prescription involves the manipulation of improper integrals and the stage at which the regularization procedure is applied. For example, in order the reach the final expressions (2.44) for the meson polarizations, one has to perform a variable shift along the calculation, which is only valid if the momentum integrals go to infinity. Once the cutoff is introduced the invariance is lost, so it has to be introduced at the end of the calculation. Thus, it is the regularization scheme which determines

the model, and not vice-versa. In the literature several regularization schemes exist, each with its own advantages and drawbacks [145, 179].

In this subsection we deal with the second problem, defining the regularization scheme we choose for (most of) this thesis. A possible regularization consists of incorporating to the divergent integrand a three-dimensional cutoff function $f_\Lambda(|\vec{p}|)$. The function depends on the modulus of the spatial momenta and for high values of $|\vec{p}|$ it tends to zero fast enough so that the integral yields finite. It also contains a cutoff value Λ with units of energy which determines the scale beyond which the strength of interaction becomes negligible. In the model, Λ is taken as an input parameter, usually between 0.5 and 1 GeV.

The choice of this regularization is based on several factors. Its main advantage lies in its simplicity and the fact that it preserves the analytical structure. In addition, as already mentioned, it qualitatively emulates the asymptotic freedom of QCD. Even though it is possible to implement a Lorentz covariant treatment, applying a regulator which depends on the four-components of the momentum, the noncovariance does not represent an inconvenient since our objective is to work in magnetized mediums which already explicitly break Lorentz invariance. The scheme also breaks gauge symmetry. However, as discussed below Eq. (2.11), since in the NJL model the local color symmetry of QCD is replaced by a global symmetry, this scheme brings no further complications. An important aspect is that chiral symmetry and the Goldstone theorem are strictly preserved after regularizing.

For the shape of the cutoff function, we choose a Heaviside step function, i.e. $f_\Lambda(|\vec{q}|) = \Theta(\Lambda - |\vec{q}|)$. This physically intuitive regularization implies that all quark states with momentum $|\vec{q}| < \Lambda$ contribute equally to the vacuum energy, disregarding contributions arising from higher momentum values. Performing the time component integral first, for the regularized version of the I_1^0 and I_2^0 functions defined in Eq. (2.35) and (2.45) (denoted by the 'vac' superscript) we get the well-known results [145]

$$I_1^{\rm vac} \;=\; \frac{1}{2\pi^2}\left[\Lambda\sqrt{\Lambda^2+M^2}+M^2\,\ln\frac{M}{\Lambda+\sqrt{\Lambda^2+M^2}}\right]\,, \tag{2.52}$$

$$I_2^{\rm vac}(p^2) \;=\; \frac{1}{4\pi^2}\int_0^1 dy\left[\frac{\Lambda}{\sqrt{\Lambda^2+M^2+y(1-y)p^2}}+\ln\frac{\sqrt{M^2+y(1-y)p^2}}{\Lambda+\sqrt{\Lambda^2+M^2+y(1-y)p^2}}\right]\,. \tag{2.53}$$

Once the model has been regularized, we can obtain solutions for the dressed quark mass M. To that end, is convenient to adimensionalyze the regularized gap equation

$$M' \;=\; m_c' + g'\,M'\left(\sqrt{1+M'^2}+M'^2\,\ln\frac{M'}{1+\sqrt{1+M'^2}}\right)\,, \tag{2.54}$$

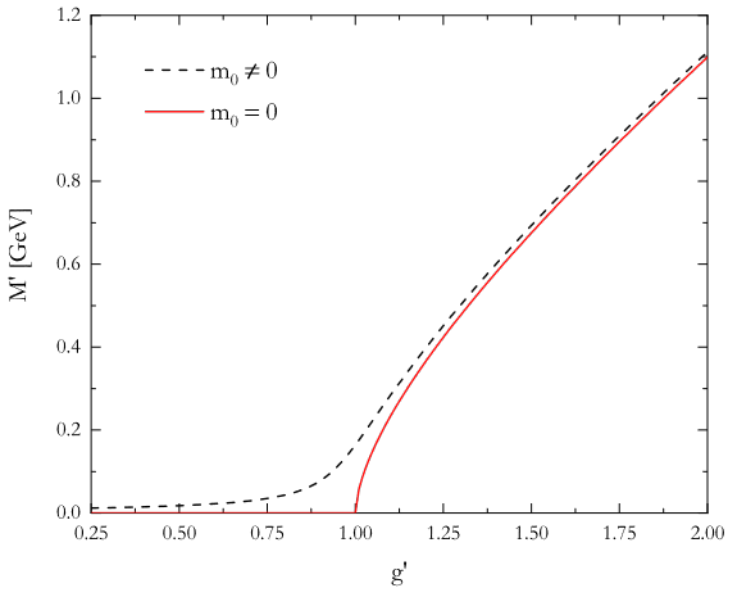

Figure 2.3: Adimensional dressed quark mass $M' = M/\Lambda$ as a function of the dimensionless coupling constant $g' = G\Lambda^2\, N_c N_f/\pi^2$. Chiral (red solid line) and nonchiral (black dashed line) cases are shown.

where we have introduced the dimensionless quantities $M' = M/\Lambda$, $m_c' = m_c/\Lambda$ and $g' = G\Lambda^2\, N_c N_f/\pi^2$. The results are shown in Figure 2.3 for $m_c \neq 0$ as well as for the chiral limit. We see that the dynamical breaking of chiral symmetry depends on the strength of the interaction. For $m_c = 0$ there is a critical value $g_c' = 1$, or equivalently $g_c = \pi^2/(N_c N_f)$ for $g = G\Lambda^2$, which separates two phases were the symmetry is realized in different modes:

- The Wigner-Weyl mode for $g < g_c$. In the chiral limit the dressed mass vanishes, and $SU(2)_A$ symmetry is restored. When $m_c \neq 0$, chiral symmetry is explicitly broken. However, it is approximately conserved due to the smallness of the current mass, reflected by the fact that the value of M stays only slightly above m_c.

- The Nambu-Goldstone mode for $g > g_c$. Here $M > 0$ even in the chiral limit, and steadily increases with g. Quarks acquire a dynamical mass breaking $SU(2)_A$ symmetry, leading to the appearance of Goldstone bosons which are massive (massless) in the nonchiral (chiral) case. The behavior of M does not differ significantly between the chiral and nonchiral case, since in this mode the effect of the current mass is negligible.

As mentioned above, in this thesis we have (mostly) chosen a regularization scheme based on the use of a three-dimensional cutoff step function. It is worth remarking that other regularization procedures can be found in the literature. Within the usual NJL model, covariant schemes include the use of four-momentum cutoff functions, regularization in proper time formalism and the Pauli-Villars method [145, 179]. On the other hand,

there exists a generalization of the model where local interactions are replaced by nonlocal separable ones, which depend on the field values over coordinate (or momentum) space and thus divergences are handled in a more natural way [152]. Even though some results are improved in this version of the model, such as the recovery of a momentum-dependent quark self energy [184], calculations become much more cumbersome.

2.2.6 Parameter fixing

In its simplest form, given by the Lagrangian of Eq. (2.12), the NJL model has three parameters: G, Λ and m_c. Note that for variants of the model with more interactions (such as vector and axial-vector types), additional coupling constants are added. These parameters must be fixed to completely define the model. Usually, this is done by fitting phenomenological observables which the model can reproduce. The typically chosen physical quantities are $\langle\bar{\psi}\psi\rangle$, m_π and f_π, whose fixed values are used to determine G, Λ and m_c by solving the regularized form of Eqs. (2.34), (2.46) and (2.49).

From these three observables, m_π and f_π are experimentally well-measured: $m_{\pi^\pm} = 139.57039 \pm 0.00018$ MeV, $m_{\pi^0} = 134.9768 \pm 0.0005$ MeV and $f_\pi = 92.3198 \pm 0.0919$ MeV [172]. For simplicity we will take $m_\pi = 138$ MeV and $f_\pi = 92.4$ MeV hereafter. On the other hand, the quark condensate is not measured experimentally. Nonetheless, its value can be estimated from several approaches. Calculations based on current algebra and QCD sum rules set the range $|\langle\bar{f}f\rangle|^{1/3} = 190 - 260$ MeV [175] at a scale of 1 GeV, where f represents u or d flavors. A combination of QCD sum rules and chiral perturbation theory yields 242 ± 15 MeV [185] (also at 1 GeV). An approach based on renormalization group equations also results in a large range of $170 - 310$ MeV, which can be narrowed to 244 MeV when estimating the scale of the theory as $\Lambda_{\rm QCD} = 280$ MeV [186]. Meanwhile, simulations performed in $N_f = 2 + 1$ lattice QCD provide $|\langle\bar{f}f\rangle|^{1/3} = 272 \pm 5$ MeV [187], at a higher scale of 2 GeV. We will take variations of this parameter around $|\langle\bar{\psi}\psi\rangle|^{1/3} \sim 245$ MeV.

We have seen that the quark condensate is related to the dressed mass through the gap equation, $M = m_c - 2G\langle\bar{\psi}\psi\rangle$. Thus, we can alternatively use M to refer to the parameter set. Keeping in mind that the nucleon mass is $M_{\rm N} \sim 940$ MeV and they are composed of three valence quarks, the quark mass value can be estimated as $M_{\rm N}/3$, suggesting the approximated value $M \sim 310$ MeV. However, as the quark condensate, this quantity is subject to certain degree of uncertainty. For the aforementioned estimated values of $\langle\bar{\psi}\psi\rangle$, compatibles values of M lie within the range $300 - 500$ MeV.

2.3 Uniform magnetic field

In this thesis we will be interested in the effect of an external uniform magnetic field on hadron properties. Without loss of generality, we can set it in the 3-direction. The background field breaks rotational symmetry into parallel and transverse field directions. In Euclidean space (similarly for Minkowski space) we have $SO(4) \to SO(2)_\perp \times SO(2)_\parallel$, with $SO(2)_\perp$ and $SO(2)_\parallel$ corresponding to rotations in the $x_1 - x_2$ and $x_3 - x_4$ planes, respectively. Moreover, up and down quarks cannot be considered as isospin symmetric anymore due to their different electric charges. Chiral symmetry $SU(2)_V \times SU(2)_A \times U(1)_V$ is broken explicitly to $U(1)_V^3 \times U(1)_A^3 \times U(1)_V$, where the superscript 3 in the vector and axial groups denotes the transformations generated by τ_3 and $\tau_3\gamma_5$, respectively. The magnitude of isospin symmetry breaking is manifested e.g. in the difference between up and down quark chiral condensates. Moreover, due to this reduced symmetry there is only one true Goldstone boson, the neutral pion π^0 (associated to τ_3). In contrast, charged pions are massive even in the chiral limit.

Electromagnetic fields, as gluon fields, are coupled to quarks through the covariant derivative

$$\partial_\mu \;\longrightarrow\; D_\mu \;=\; \partial_\mu - i\hat{Q}\mathcal{A}_\mu \,, \tag{2.55}$$

where $\hat{Q} = \mathrm{diag}(Q_1, Q_2, ..., Q_{N_f})$ is the electric charge matrix which acts on flavor space, with $e > 0$ being the proton electric charge. The corresponding QED Dirac Lagrangian in Euclidean space is

$$\mathcal{L}_\mathrm{D} \;=\; \bar{\psi}(-i\not{D} + \hat{m})\psi \,. \tag{2.56}$$

In the particular case of an external uniform magnetic field, we can disregard the pure gauge term since it is constant. The Dirac equation for a particular flavor reads

$$(-i\not{\partial} - Q_f\not{\mathcal{A}} + m_f)\psi_f \;=\; 0 \,. \tag{2.57}$$

At this stage we choose the Landau gauge $\mathcal{A}_\mu = \delta_{\mu,2}\, Bx_1$. Then, the solutions of Eq. (2.57) can be expanded in terms of the (Euclidean) Ritus spinor eigenfunctions [188–190]

$$\mathbb{E}^s_{\tilde{q}}(x) \;=\; \sum_{\lambda=\pm} \mathcal{B}^s_{\tilde{q}_{s\lambda}}(x)\, P^s_n\, \Delta_\lambda \,, \tag{2.58}$$

where

$$\mathcal{B}^s_{\tilde{q}}(x) \;=\; N_n\, e^{i(q_2x_2+q_3x_3+q_4x_4)}\, D_n(\beta_s) \,, \tag{2.59}$$

and

$$N_n \;=\; \frac{(4\pi B_f)^{\frac{1}{4}}}{\sqrt{n!}}\;, \quad \beta_s \;=\; \sqrt{\frac{2}{B_f}}\,(B_f\,x_1 - s\,p_2)\;, \quad P_n^s \;=\; (1-\delta_{n,0})\mathbb{1} + \delta_{n,0}\Delta_s\,. \tag{2.60}$$

Here $\bar{q} = (n, q_2, q_3, q_4)$ collects the four quantum numbers needed to fully specify the state. Note that $\bar{q}_{s\lambda} = (n_{s\lambda}, q_2, q_3, q_4)$. Other definitions are in order: $s = \mathrm{sign}(Q_f B)$ and $B_f = |Q_f B|$; $\Delta_\lambda = (1 + \lambda\Sigma_z)/2$, with $\Sigma_z = i\gamma^1\gamma^2$, are spin projectors in the magnetic field direction with eigenvalues $\lambda = \pm 1$; n and $n_{s\lambda} = n - (1 - s\lambda)/2$ are non-negative integers, representing the Landau and orbital Landau levels respectively; and $D_n(x)$ are the cylindrical parabolic functions.

The corresponding eigenfunctions fulfill the orthogonality and completeness relations

$$\sum\!\!\!\!\!\!\int_{\bar{q}} \mathbb{E}^s_{\bar{q}}(x)\,\mathbb{E}^s_{\bar{q}}(x')^* \;=\; \delta^{(4)}(x-x')\;, \qquad \int d^4x\,\mathbb{E}^s_{\bar{q}}(x)\,\mathbb{E}^s_{\bar{q}'}(x)^* \;=\; \hat{\delta}_{\bar{q},\bar{q}'}\,P^s_n\;, \tag{2.61}$$

where we have introduced the shorthand notation

$$\sum\!\!\!\!\!\!\int_{\bar{q}} \;=\; \frac{1}{2\pi}\sum_{n=0}^{\infty}\int\frac{dq_2dq_3dq_4}{(2\pi)^3}\;, \qquad \hat{\delta}_{\bar{q},\bar{q}'} \;=\; (2\pi)^4\,\delta_{n,n'}\,\delta(q_2-q_2')\,\delta(q_3-q_3')\,\delta(q_4-q_4')\,. \tag{2.62}$$

Moreover, they satisfy $(\not{\partial} - iQ_f\not{A})^2\,\mathbb{E}^s_{\bar{q}} = (2nB_f + q_3^2 + q_4^2)\,\mathbb{E}^s_{\bar{q}}$, leading to the energy dispersion relation

$$E_f(B)^2 \;=\; -q_4^2 \;=\; m_f^2 + 2nB_f + q_3^2\,. \tag{2.63}$$

As seen, in the presence of a uniform field the momentum of charged particles in the plane perpendicular to $\vec{B}$ is quantized in discrete states known as Landau levels (LL). These are characterized by a non-negative integer n which represents the total quantum angular momentum. For fermions, n is given by a combination of orbital angular momentum and spin. Since $n_{s\lambda} \geq 0$, at the lowest Landau level ($n = 0$) the spin points only in the $\lambda = s$ direction. This information is codified in the projectors P^s_n. All other energy values are degenerated with respect to the two spin orientations in the field direction. Moreover, all values of the squared perpendicular momenta $q_1^2 + q_2^2$ which fall between two successive Landau levels coalesce into a single level. The number of these levels, i.e. the degeneration, is given through integration in polar coordinates by [51, 191]

$$\frac{S}{(2\pi)^2}\int dp_1dp_2 \;=\; \frac{B_f}{(1+\delta_{n,0})\pi}\,S\,, \tag{2.64}$$

where S is the area of the orbit in the $x-y$ plane.

It is worth remarking that, from the four quantum numbers $\bar{q}$ needed to label the

particle-state, only three of them appear in the energy dispersion relation. This is a reflection of gauge invariace, since the remaining number is a gauge-dependent quantity. In our case this number is q_2, associated to translational invariance in the 2-direction present in the Landau gauge.

2.3.1 Magnetized NJL model in mean field approximation

The NJL model has become a popular analytic model in part due to its flexibility, since it has the nice property that it can be easily extended to include the effect of external parameters, such as temperature, chemical potentials and magnetic fields. In the presence of an external uniform magnetic field, one can proceed in general grounds as before, bosonizing and expanding the fields as fluctuations around their MF values. In this subsection we will perform the mean field approximation, deferring the calculation of hadron properties to forthcoming chapters.

The Euclidean Lagrangian density for the NJL two-flavor model in the presence of an electromagnetic field is simply obtained by replacing $\partial_\mu \to D_\mu = \partial_\mu - i\hat{Q}\mathcal{A}_\mu$ in Eq. (2.12), where $\hat{Q} = \mathrm{diag}(Q_u, Q_d)$ with $Q_u = 2e/3$ and $Q_d = -e/3$. Recall that we are considering the particular case of an uniform magnetic field $\vec{B}$ along the positive 3-axis described through the Landau gauge, $\mathcal{A}_\mu = \delta_{\mu,2}\, Bx_1$. We proceed as in the vacuum case; the fermionic action is bosonized introducing $(\sigma, \vec{\pi})$ meson fields, and then expanded in field fluctuations around their MF values $\bar{\sigma}$ and $\bar{\pi}_a = 0$. In fact, the calculation is exactly the same, leading to the free energy of Eq. (2.28). The only difference lies in the derivative inside the flavor-diagonal MF fermion operator in Eq. (2.22), which is now covariant

$$\mathcal{D}_{\mathrm{MF}}(x, x') \;=\; \delta^{(4)}(x - x') \left(-i\not{D} + M\right) \,. \tag{2.65}$$

The mean field quark propagator $\mathcal{S}_{\mathrm{MF}}$ is given by the inverse of (2.65). Since $\mathcal{D}_{\mathrm{MF}}$ is flavor-diagonal, so is $\mathcal{S}_{\mathrm{MF}}$. As is well known, its explicit form can be written in different ways [52, 53]. For convenience we take the form in which it is given by a product of a phase factor and a translational invariant function, namely

$$\mathcal{S}^f_{\mathrm{MF}}(x, x') \equiv \left[\mathcal{D}^f_{\mathrm{MF}}(x, x')\right]^{-1} \;=\; e^{i\Phi_f(x,x')} \int_q e^{iq(x-x')}\, \bar{\mathcal{S}}^f(q) \,, \tag{2.66}$$

for each flavor.

The breaking of translational symmetry, induced by the gauge choice, is manifested in the presence of the so-called Schwinger phase $\Phi_f(x, x') = Q_f B(x_1 + x'_1)(x_2 - x'_2)/2$, which also comprises the gauge dependence of the propagator. We express $\bar{\mathcal{S}}^f(q)$ in the

Schwinger form [52, 53]

$$\bar{\mathcal{S}}^f(q) \;=\; \int_0^\infty d\tau\, e^{-\tau \Upsilon_f(\tau,q)} \left\{ (M - q_{\parallel}\gamma_{\parallel})\, [1 + is\,\gamma_1\gamma_2\, \tanh(\tau B_f)] - \frac{q_\perp \gamma_\perp}{\cosh^2(\tau B_f)} \right\} . \quad (2.67)$$

Since the magnetic fields breaks rotational symmetry, we have accordingly collected "perpendicular" and "parallel" contributions in separated vectors: $\gamma_\perp = (\gamma_1, \gamma_2)$ and $\gamma_{\parallel} = (\gamma_3, \gamma_4)$. Similarly, $q_\perp = (q_1, q_2)$ and $q_{\parallel} = (q_3, q_4)$. Moreover, we have defined the function

$$\Upsilon_f(\tau, q) \;=\; M^2 + q_{\parallel}^2 + \frac{\tanh(\tau B_f)}{\tau B_f}\, q_\perp^2 - i\epsilon\,, \quad (2.68)$$

where the limit $\epsilon \to 0$ is implicitly understood. Notice that the integral in Eq. (2.67) is divergent and has to be properly regularized, as we discuss below.

In order to obtain the gap equation, we proceed as before by diagonalizing $\mathcal{D}_{\text{MF}}$ in the free energy (2.28), so as to take the logarithm of the eigenvalues. However, the Fourier transformation is not convenient now due to the breakdown of translational invariance (induced by the gauge choice). As seen before for the Dirac Lagrangian, in a magnetic field the corresponding eigenfunctions are the Ritus ones. Theferore, to diagonalize the fermion operator one has to transform to Ritus space. It can be shown that the Ritus transform of an arbitrary operator is

$$\begin{aligned} \mathcal{O}(x,x') \;&=\; \sum\!\!\!\!\!\!\int_{\bar{q},\bar{q}'} \mathbb{E}^s_{\bar{q}}(x)\, \mathcal{O}_{\bar{q},\bar{q}'}\, \mathbb{E}^s_{\bar{q}'}(x')^* \,, \\ \mathcal{O}_{\bar{q},\bar{q}'} \;&=\; \int d^4x\, d^4x'\, \mathbb{E}^s_{\bar{q}}(x)^*\, \mathcal{O}(x,x')\, \mathbb{E}^s_{\bar{q}'}(x') \,, \end{aligned} \quad (2.69)$$

The eigenfunctions satisfy $\not{D}^2\, \mathbb{E}^s_{\bar{q}}(x) = \epsilon_{\bar{q}}\, \mathbb{E}^s_{\bar{q}}(x)$, with eigenvalues $\epsilon_{\bar{q}} = q_{\parallel}^2 + 2nB_f$.

Again, instead of $\mathcal{D}_{\text{MF}}$ it will be more convenient to deal with the $\mathcal{A}_{\text{MF}}$ operator defined in Eq. (2.30), replacing $\partial_\mu \to D_\mu$. Applying the transformation (2.69) and using the orthogonality relation (2.61), in Ritus space this operator reads

$$\mathcal{A}_{\bar{q},\bar{q}'} \;=\; \int d^4x\, d^4x'\, \mathbb{E}^s_{\bar{q}}(x)^*\, \delta^{(4)}(x-x') \left(\epsilon_{\bar{q}} + M^2\right) \mathbb{E}^s_{\bar{q}'}(x') \;=\; \hat{\delta}_{\bar{q},\bar{q}'} P^s_n \left(\epsilon_{\bar{q}} + M^2\right) , \quad (2.70)$$

which is diagonal as expected. Since the logarithm of a diagonal matrix is also diagonal,

transforming $\ln \mathcal{D}_{\rm MF}(x,x')$ to Ritus space through Eq. (2.69) we arrive at

$$\begin{aligned}\mathrm{Tr}\ln\mathcal{D}_{\rm MF}(x,x') &= \frac{N_c}{2}\sum_f \mathrm{Tr}_{\rm D}\int d^4x\, d^4x'\,\delta^{(4)}(x-x')\sum\!\!\!\!\!\!\int_{\bar q,\bar q'}\mathbb{E}^s_{\bar q}(x)\,\ln(\mathcal{A}_{\bar q,\bar q'})\,\mathbb{E}^s_{\bar q'}(x')^* \\ &= \frac{N_c}{2}\sum_f \mathrm{Tr}_{\rm D}\int d^4x\sum\!\!\!\!\!\!\int_{\bar q}\mathbb{E}^s_{\bar q}(x)\,\mathbb{E}^s_{\bar q}(x)^*\,\ln\left(\epsilon_{\bar q}+M^2\right)\,, \end{aligned} \tag{2.71}$$

Since the eigenvalues do not depend on the gauge-dependent coordinate q_2, we can integrate in that variable and then take the Dirac trace, using

$$\int\frac{dq_2}{2\pi}\,\mathbb{E}^s_{\bar q}(x)\,\mathbb{E}^s_{\bar q}(x)^* = B_f P^s_n\,, \qquad \mathrm{Tr}_{\rm D}\,P^s_n = 2(2-\delta_{n,0})\,. \tag{2.72}$$

Finally, the magnetized MF free energy is [145]

$$\Omega_{\rm MF} = \frac{(M-m_c)^2}{4G} - N_c\sum_{f,n}\frac{B_f}{2\pi}\,(2-\delta_{n,0})\int\frac{dq_3dq_4}{(2\pi)^2}\,\ln\left(q_\parallel^2+2nB_f+M^2\right)\,. \tag{2.73}$$

Since $\mathrm{Tr}\ln\mathcal{D}_{\rm MF} = \ln\det\mathcal{D}_{\rm MF}$, the same result can be obtained exploiting the fact the determinant is the sum over the eigenvalues, taking into account the corresponding degeneracies.

Minimizing the free energy with respect to M and using the Schwinger parametrization to move to proper time representation, we obtain the gap equation

$$M = m_c + 2G\,\mathrm{Tr}\,\mathcal{S}_{\rm MF}(x,x') = m_c + 4GMN_c\left(\frac{I^{\rm B}_{1u}+I^{\rm B}_{1d}}{2}\right)\,, \tag{2.74}$$

where

$$I^{\rm B}_{1f} = \frac{B_f}{4\pi^2}\int_0^\infty\frac{dz}{z}\,e^{-zM^2}\coth(zB_f)\,, \tag{2.75}$$

is a divergent integral. The contribution from each flavor arises independently because the magnetic field differentiates between particles of different charges.

On the other hand, at the MF level the chiral condensate for each flavor is given by

$$\phi_f = \langle\bar f f\rangle_B = -\frac{\Omega^{\rm bos}_{\rm MF}}{\delta m_f} = -\frac{N_c}{V^{(4)}}\,\mathrm{Tr}_{\rm D}\int d^4x\,\mathcal{S}^f_{\rm MF}(x,x) = -N_cM\,I^{\rm B}_{1f}\,. \tag{2.76}$$

2.3.2 Regularization scheme in the presence of a magnetic field

As we have seen, when a background magnetic field is introduced the vacuum energy acquires a LL structure, and additional care is required in the treatment of the divergences, such as the momentum integral of Eq (2.75). In the literature, a widely used choice to

regularize such divergences is the introduction of regulating functions of the form $h_\Lambda(Q)$, with $Q = \sqrt{2nB_f + p_3^2}$. The form of these cutoff functions include Lorenztian [168, 169, 192–197], Woods-Saxon [154, 170, 198–200], Gaussian [201–203], Fermi-Dirac [204–206], 3D [207–209] and 4D cutoff regularizations. Unlike the $B = 0$ case, where there is a single divergent integral, the sum over Landau levels implies a regularization for each integral and for each flavor state, so it is natural that the regulator depends on the energy through these quantum numbers. An example which highlights the importance of a correct regularization procedure is the calculation of thermodynamical quantities. Since several thermodynamic quantities involve derivatives of the thermodynamic potentials, they are strongly dependent on the regularization and can lead to the existence of unphysical oscillations, leading to unreliable results. This is particularly dramatic when studying color superconducting phases in dense magnetized mediums, since these unphysical oscillations can be easily confused with actual de Haas-van Alfven oscillations [210, 211].

A nice review on the importance of the regularization prescription can be found in Ref. [212]. There, the authors compare the NJL average and difference condensate against lattice results for all regularization schemes found the literature: form factors, proper time and Pauli-Villars. When all form factors are considered, it is clearly seen that the magnitude of the nonphysical oscillations is proportional to the sharpness of the regulating function, in agreement with previous studies [194, 207, 213, 214]. For some of these sharp functions, a reasonable agreement with lattice results is only found for small magnetic fields, $eB < 0.3$ GeV^2 [73]. On the other hand, the use of a too smooth function leads to values of the average quark condensate which are quite above the phenomenological range.

One possible scheme where these unphysical oscillations are completely removed is the 'magnetic field independent regularization' (MFIR) scheme. The idea is to avoid the magnetic dependence in the regularization by regularizing only the vacuum, where one has more control over the model and we have seen that some meson properties are recovered. To that end, one simply adds and subtract the $B = 0$ limit of the corresponding divergent integral, separating the integral into vacuum and magnetic pieces. The magnetic term is finite, and only the vacuum term needs to be regularized by implementing one of the aforementioned regularization schemes; these include form factors, proper time and Pauli-Villars. When the calculation is performed using the LL representation of the quark propagator, the finiteness of the magnetic term in the free energy can be elegantly proven following the steps of the dimensional regularization prescription of QCD, performing the sum over all Landau levels [215]. On the other hand, the proper-time formalism is more convenient for this scheme since the $B \to 0$ limit can be easily taken [216]. For example,

the limit of I_{1f}^{B} in Eq. (2.75) is

$$I_{1f}^{0} \;=\; \frac{1}{4\pi^2}\int_0^\infty \frac{dz}{z^2}\, e^{-zM^2}\,, \tag{2.77}$$

which, as expected, coincides with Eq. (2.35) when one goes back to the momentum representation. As a drawback, this formalism is not available in the nonlocal generalizations of the model, where the effective mass depends on the momentum.

In the aforementioned review of Ref. [212], it is seen that for the MFIR scheme the unphysical oscillations are effectively removed from the condensate for all types of form factors. Moreover, the use of the MFIR scheme tends to provide condensate values which are in closer agreement with lattice QCD calculations, as compared to non-MFIR schemes such as the magnetic dependent proper time [100, 164, 203, 217, 218] and Pauli-Villars [153, 219–224] regularizations. The authors conclude that, from for all the regularizations considered, the noncovariant 3D-cutoff, the covariant 4D-cutoff and Pauli-Villars are the ones that better describe the lattice results. Apart from the condensate, the MFIR scheme has also been shown to avoid unphysical oscillations for other quantities in the context of magnetized quark matter in the presence of color superconductivity, thus avoidining the misinterpretation of unreal van Alphen-de Haas transitions [206, 207, 225, 226]. An improvement within the MFIR scheme was recently suggested in Ref. [163] for the calculation of many mean-field observables. However, this modification is not relevant for the quantities we will study in this thesis, namely quark condensates, hadron masses and pion decay constants, so we can safely omit it.

In order to implement the MFIR scheme, we add and subtract the $B = 0$ contribution (2.77) to the gap equation (2.74). Then, the divergent integral can be separated into magnetic and vacuum pieces. After regularizing the vacuum term we obtain

$$I_{1f}^{\mathrm{reg}} \;=\; I_{1f}^{\mathrm{mag}} + I_{1}^{\mathrm{vac}}\,. \tag{2.78}$$

For a sharp 3D cutoff, I_1^{vac} is given by Eq. (2.52), while the finite magnetic contribution can be written as [212, 227]

$$\begin{aligned} I_{1f}^{\mathrm{mag}} \;&=\; \frac{1}{4\pi^2}\int_0^\infty \frac{dz}{z}\, e^{-zM^2}\left[B_f\coth(zB_f)-\frac{1}{z}\right] \\ &=\; \frac{B_f}{2\pi^2}\left[\ln\Gamma(x_f)+x_f-\left(x_f-\frac{1}{2}\right)\ln x_f-\frac{\ln 2\pi}{2}\right]\,, \end{aligned} \tag{2.79}$$

with $x_f = M^2/(2B_f)$. Since the condensate is driven by the same divergent integral, the

regularized version in the MFIR scheme reads

$$\phi_f^{\rm reg} \;=\; \phi_f^{\rm vac} + \phi_f^{\rm mag} \;, \qquad \begin{cases} \phi_f^{\rm vac} &= -N_c M I_1^{\rm vac} \\ \phi_f^{\rm mag} &= -N_c M I_{1f}^{\rm mag} \end{cases} \;. \tag{2.80}$$

For the NJL, in the case of a small coupling $g' \ll 1$ the dynamical mass squared will be much smaller than the magnetic field, $M^2 \ll B_f$. Then, for $M \ll \Lambda$ there is a nontrivial solution for arbitrarily small g even in the chiral limit, given by [100]

$$M \;=\; \sqrt{\frac{B_f}{\pi}}\, e^{-\frac{\pi^2}{N_c N_f B_f G}} \;, \tag{2.81}$$

analogous to the gap obtained in BCS theory [51, 99, 101]. A nontrivial solution exits in fact for all g, as shown in Ref. [99]. Thus, in contrast to the $B = 0$ case analyzed in subsection 2.2.5, where chiral symmetry can be broken only for $g' > 1$, the presence of a magnetic field always leads to the generation of a dynamical mass, even at the weakest attractive interaction between fermions. Moreover, the magnetic field enhances the gap, and therefore the condensate, reproducing the familiar magnetic catalysis effect.

CHAPTER 3

Leptonic decay of magnetized charged pions

The objective of this thesis is to determine the effect that an external magnetic field has over several hadron properties. Although we will mainly investigate their masses, another important property we are interested in is the decay of pions, with particular focus on the weak decay $\pi^- \to l + \bar{\nu}_l$ (the effects are similar for π^+). The details of pion decay in the presence of a magnetic field are not fully understood yet, see Refs. [170, 171, 228] for some approaches on the charged case. Thus, before considering a particular QCD-like approach, in this chapter we will study the generalities of this decay in order to determine which hadronic observables must be known in order to calculate the corresponding decay width. These observables, such as masses and decay constants, will be calculated in the next chapter for the particular case of the NJL model, allowing for an estimation of the corresponding decay width.

The width associated to the decay $\pi^- \to l + \bar{\nu}_l$ is proportional to the squared modulus of the amplitude, which can be written in a general form as

$$\begin{aligned} \langle\, l,\, \bar{\nu}_l | L_W | \pi^- \,\rangle \;=\; -\frac{G_F}{\sqrt{2}} \cos\theta_c \int d^4x\, \langle 0 | \bar{\psi}_u(x)\, \gamma^\mu (1-\gamma_5)\, \psi_d(x) | \pi^- \rangle \;\times \\ \langle\, l,\, \bar{\nu}_l | \bar{\psi}_l(x)\, \gamma^\mu (1-\gamma_5)\, \psi_{\nu_l}(x) | 0 \rangle \,, \end{aligned} \tag{3.1}$$

where L_W is the usual axial-vector four-fermion effective weak interaction Lagrangian [229]. Here $G_F = 1.1663788 \times 10^{-5}$ GeV^{-2} is the Fermi constant and θ_c is the Cabibbo angle, related to the ud element of the CKM matrix by $\cos\theta_c = V_{ud} = 0.97373$ [172]. While the leptonic matrix element can be calculated using magnetized fields from QED, the

hadronic element involves (in the initial pion state) strong interactions in a low energy regime, which can not be treated perturbatively. Instead, it can be parameterized in terms of decay form factors, taking into account the Lorentz structure and the symmetries of the theory.

First, we will obtain an expression for each involved matter field in the presence of an external uniform magnetic field, necessary to calculate the matrix elements. Next, we will show that the presence of the external field opens up the possibility for new decay channels, reflected in the existence of new axial and vector decay constants which appear when hadronizing the pion-to-vacuum matrix elements of quark currents. Taking into account these new decay constants, we will finally calculate the partial decay width for the magnetized $\pi^- \to l + \bar{\nu}_l$ decay. Throughout this chapter we will work in Minkowski space with metric convention $g^{\mu\nu} = \text{diag}(1, -1, -1, -1)$, as well as $\epsilon^{0123} = +1$ for the totally antisymmetric tensor $\epsilon^{\mu\nu\alpha\beta}$. For a space-time coordinate four-vector we adopt the notation $x^\mu = (x^0, \vec{x})$. Results from this chapter are based on Refs. [230, 231].

3.1 Matter quantum fields in the presence of a uniform magnetic field

3.1.1 Gauge choice and quantum numbers

In this chapter we will study the effect of an external uniform magnetic field on the weak charged pion decay $\pi^- \to l + \bar{\nu}_l$. Without loss of generality, we take the field as oriented in the 3-direction, $\vec{B} = B\,\hat{3}$. Moreover, we consider two gauge choices: the Landau gauge (LG) and symmetric gauge (SG). The comparison between the results obtained with each of these gauges will serve as a verification of the gauge invariance of our result. As briefly mentioned in the previous chapter, in the presence of an external uniform magnetic field the quantum numbers which define charged particle states differ from those in the absence of the field. This is due to the fact that, in the plane perpendicular to $\vec{B}$, the momentum is quantized in Landau levels. Quantum numbers are given by the eigenvalues of operators which commute with the corresponding Hamiltonian. We recall that if a physical quantity has an associated quantum mechanical operator $\mathcal{O}$, the field theoretical realization of this operator is given by

$$\hat{\mathcal{O}} \;=\; \int_V d^3x \;:\psi(x)^\dagger\,\mathcal{O}\,\psi(x)\;:\,, \tag{3.2}$$

where $\psi(x)$ is the corresponding particle field.

Some of these numbers are actually gauge-dependent. In order to specify them, one has to choose a particular gauge. For charged pions and leptons it can be shown that, in both gauges, the 3-component of the canonical momentum commutes with the associated Hamiltonian (Klein-Gordon and Dirac, respectively). From the eigenvalues of the Hamiltonian itself, it can be seen that the Landau level corresponds to another quantum number, needed to completely define energy states. Regarding the third quantum number, it is actually gauge-dependent. In the LG the 2-component of the canonical momentum also commutes with the Hamiltonian, while for the SG the corresponding operator is the canonical total angular momentum. It is worth remarking that even though the *mechanical* momentum and the *mechanical* total angular momentum are gauge-covariant operators, they do not commute with the associated Hamiltonians and therefore do not correspond to conserved quantities [231].

Using Cartesian coordinates $\vec{x} = (x^1, x^2, x^3)$ in the LG we have

$$\mathcal{A}^\mu = \delta^{\mu,2}\,Bx^1 \;\;\Rightarrow\;\; D^\mu = \partial^\mu + isB_e\,x^1\,\delta^{\mu,2}\,, \tag{3.3}$$

where $s = \text{sign}(\sigma B)$ and $B_e = e|B|$ for a particle of charge $Q = \sigma e$, $e > 0$ being the proton charge and $\sigma = \pm$. In this gauge, the relevant quantum numbers of the charged

particles involved are the 2− and 3− components of the canonical momentum together with the corresponding Landau level. For antineutrinos, they are the usual three Cartesian momentum components.

On the other hand, for the SG we have $\vec{A} = \vec{B} \times \vec{r}/2$. In this gauge it is convenient to use cylindrical coordinates $\vec{x} = (\rho\cos\phi, \rho\sin\phi, x^3)$. The vector potential is then given by

$$\mathcal{A}^\mu = \frac{B\rho}{2}(\cos\phi\,\delta^{\mu,2} - \sin\phi\,\delta^{\mu,1}) \;\Rightarrow\; D^\mu = \partial^\mu + i\,\frac{sB_e\rho}{2}(\cos\phi\,\delta^{\mu,2} - \sin\phi\,\delta^{\mu,1})\,. \tag{3.4}$$

One can define a complete basis of states of well defined energy by taking as quantum numbers the Landau level, the 3-component of the canonical momentum and the 3-component of the canonical total angular momentum j_3. For antineutrinos, having zero electric charge, we take k^3, j_3 and $k_\perp = \sqrt{(k^1)^2 + (k^2)^2}$, where $\vec{k}$ is the antineutrino linear momentum.

The shorthand notation used for the quantum numbers and other related labels of the π^-, l^- and $\bar{\nu}_l$ particles in each gauge is summarized in Table 3.1. There, ℓ, n, $\imath$, and υ are non-negative integers, while $\jmath$ is an integer. To this set of quantum numbers one has to add the polarization $\tau = 1, 2$ of the charged lepton (we assume the antineutrino to be purely righthanded). Notice that, although not indicated explicitly, the pion mass m_{π^-} is a function of the magnetic field B. The explicit form of the π^-, l^- and $\bar{\nu}_l$ fields will be given in the following subsections.

3.1.2 Neutral pion and neutrino quantum fields

The expressions for neutral fields are not modified by the presence of the external magnetic field. Thus, they can be written in terms of the usual creation and annihilation operators of definite momentum states. Following the conventions given e.g. in Ref. [232], the neutral pion field is given by

$$\phi_{\pi^0}(x) \;=\; \int \frac{d^3p}{(2\pi)^3 2E_{\pi^0}} \left[a_{\pi^0}(\vec{p})\; e^{-ip\cdot x} + a_{\pi^0}(\vec{p})^\dagger\; e^{ip\cdot x}\right]\,, \tag{3.5}$$

where $p = (E_{\pi^0}, \vec{p})$, with $E_{\pi^0} = \sqrt{m_{\pi^0}^2 + |\vec{p}|^2}$. It is worth mentioning that, in the presence of an external field, one could also take into account corrections leading to an anisotropic dispersion relation [170]. The operators $a_{\pi^0}(\vec{p})$ and $a_{\pi^0}(\vec{p})^\dagger$ satisfy the commutation rule

$$[a_{\pi^0}(\vec{p}), a_{\pi^0}(\vec{p}')^\dagger] \;=\; 2E_{\pi^0}\,(2\pi)^3\,\delta^{(3)}(\vec{p} - \vec{p}')\,. \tag{3.6}$$

	Pion (π^-)	Lepton (l^-)	Antineutrino ($\bar{\nu}_l$)
PM	p^3	q^3	k^3
LL	ℓ	n	—
Energy	$\sqrt{m_{\pi^-}^2+(2\ell+1)B_e+(p^3)^2}$	$\sqrt{m_l^2+2nB_e+(q^3)^2}$	$\sqrt{k_\perp^2+(k^3)^2}$
Four-QN	$\bar{p}=(E_{\pi^-},\breve{p})$	$\bar{q}=(E_l,\breve{q})$	$\bar{k}=(E_{\bar{\nu}_l},\breve{k})$

Landau Gauge			
QN	$\breve{p}=(\ell,p^2,p^3)$	$\breve{q}=(n,q^2,q^3)$	$\breve{k}=(k^1,k^2,k^3)$
Diff.	$\int d\breve{p}_\chi=\sum_{\ell=0}^{\infty}\int dp^2dp^3$	$\int d\breve{q}_\chi=\sum_{n=0}^{\infty}\int dq^2dq^3$	$\int d\breve{k}_\chi=\int dk^1dk^2dk^3$
Deltas	$\delta_{\breve{p},\breve{p}'}=\delta_{\ell,\ell'}\prod_{i=2,3}\delta(p^i-p^{i\prime})$	$\delta_{\breve{q},\breve{q}'}=\delta_{n,n'}\prod_{i=2,3}\delta(q^i-q^{i\prime})$	$\delta_{\breve{k},\breve{k}'}=\delta^{(3)}(\vec{k}-\vec{k}\,')$

Symmetric Gauge			
QN	$\breve{p}=(\ell,\imath,p^3)$	$\breve{q}=(n,\upsilon,q^3)$	$\breve{k}=(\jmath,k_\perp,k^3)$
Diff.	$\int d\breve{p}_\chi=\sum_{\ell,\imath=0}^{\infty}\int dp^3$	$\int d\breve{q}_\chi=\sum_{n,\upsilon=0}^{\infty}\int dq^3$	$\int d\breve{k}_\chi=\sum_{\jmath=-\infty}^{\infty}2\pi\int dk^3dk_\perp k_\perp$
Deltas	$\delta_{\breve{p},\breve{p}'}=\delta_{\ell,\ell'}\,\delta_{\imath,\imath'}\,\delta(p^3-p'^3)$	$\delta_{\breve{q},\breve{q}'}=\delta_{n,n'}\,\delta_{\upsilon,\upsilon'}\,\delta(q^3-q'^3)$	$\delta_{\breve{k},\breve{k}'}=\frac{\delta_{\jmath\jmath'}}{2\pi}\frac{\delta(k_\perp-k'_\perp)}{k_\perp}\,\delta(k^3-k'^3)$
j_3	$-s(\ell-\imath)$	$-s(n-\upsilon-1/2)$	$\jmath-1/2$

Table 3.1: Shorthand notation for particle quantum numbers. PM stands for parallel momentum, QN for quantum numbers and LL for Landau level, while diff. is an abbreviation of differential.

On the other hand, the massless neutrino field can be written in the helicity basis as

$$\psi_{\nu_l}(x) \;=\; \int\frac{d\breve{k}_\chi}{(2\pi)^3 2E_{\nu_l}}\left[b_{\nu_l}(\breve{k},L)\;U_{\nu_l}(x,\breve{k},L)+d_{\nu_l}(\breve{k},R)^\dagger\;V_{\nu_l}(x,\breve{k},R)\right]\,, \tag{3.7}$$

where $E_{\nu_l}=E_{\bar{\nu}_l}=\sqrt{k_\perp^2+(k^3)^2}$. In the expansion we have taken into account that neutrinos (antineutrinos) are left-handed (right-handed). The corresponding creation and annihilation operators satisfy

$$\begin{aligned}\left\{b_{\nu_l}(\breve{k},L),b_{\nu_l}(\breve{k}\,',L)^\dagger\right\} &= \left\{d_{\nu_l}(\breve{k},R),d_{\nu_l}(\breve{k}\,',R)^\dagger\right\} \;=\; 2E_{\nu_l}\,(2\pi)^3\,\delta_{\breve{k},\breve{k}'}\,,\\ \left\{b_{\nu_l}(\breve{k},L),d_{\nu_l}(\breve{k}\,',R)^\dagger\right\} &= \left\{d_{\nu_l}(\breve{k},L)^\dagger,b_{\nu_l}(\breve{k}\,',R)^\dagger\right\} \;=\; 0\,.\end{aligned} \tag{3.8}$$

The definition of $\delta_{\breve{k},\breve{k}'}$ can be read from Table 3.1. Since neutrinos are neutral, the explicit form of the spinors U_{ν_l} and V_{ν_l} does not depend on the gauge. However, they do depend

on the chosen coordinates. In the LG we have

$$U_{\nu_l}(x,\breve{k},L) \;=\; e^{-ik\cdot x}\,u_{\nu_l}(\breve{k},L) \quad , \qquad V_{\nu_l}(x,\breve{k},R) \;=\; e^{ik\cdot x}\,v_{\nu_l}(\breve{k},R)\,. \tag{3.9}$$

where $u_{\nu_l}(\breve{k},L)$ and $v_{\nu_l}(\breve{k},R)$ are the usual Weyl spinors

$$u_{\nu_l}(\breve{k},L) \;=\; v_{\nu_l}(\breve{k},R) \;=\; \frac{1}{\sqrt{E_{\nu_l}+k^3}}\begin{pmatrix} -k^1+ik^2 \\ E_{\nu_l}+k^3 \\ 0 \\ 0 \end{pmatrix}\,. \tag{3.10}$$

On the other hand, for the SG

$$U_{\nu_l}\left(x,\breve{k},L\right) \;=\; -\;i^{\jmath}\;e^{-i(E_{\nu_l}x^0-k^3x^3)}\;e^{-i\jmath\,\phi}\begin{pmatrix} \sqrt{E_{\nu_l}-k^3}\;J_{\jmath}(k_\perp\rho) \\ i\sqrt{E_{\nu_l}+k^3}\;e^{i\phi}\;J_{\jmath-1}(k_\perp\rho) \\ 0 \\ 0 \end{pmatrix}\,, \tag{3.11}$$

$$V_{\nu_l}\left(x,\breve{k},R\right) \;=\; -\;(-i)^{\jmath}\;e^{i(E_{\nu_l}x^0-k^3x^3)}\;e^{-i\jmath\,\phi}\begin{pmatrix} \sqrt{E_{\nu_l}-k^3}\;J_{\jmath}(k_\perp\rho) \\ -i\sqrt{E_{\nu_l}+k^3}\;e^{i\phi}\;J_{\jmath-1}(k_\perp\rho) \\ 0 \\ 0 \end{pmatrix}\,, \tag{3.12}$$

where $J_\jmath(x)$ are Bessel functions of the first kind. In the SG it can be shown that the eigenvalue of the canonical total angular momentum operator $\hat{j}_3$ acting on a neutrino state is $j_3^{(\nu_l)}=-(\jmath-1/2)$, while for an antineutrino state one has $j_3^{(\bar{\nu}_l)}=\jmath-1/2$ [231].

Lastly, it is worth noticing that these neutrino spinors satisfy the orthogonality relations

$$\begin{aligned} &\int d^3r\,U_{\nu_l}(x,\breve{k},L)^\dagger\;U_{\nu_l}(x,\breve{k}',L) = \int d^3x\,V_{\nu_l}(x,\breve{k},R)^\dagger\;V_{\nu_l}(x,\breve{k}',R) = 2E_{\nu_l}\,(2\pi)^2\delta_{\breve{k},\breve{k}'}\,,\\ &\int d^3x\,U_{\nu_l}(x,\breve{k},L)^\dagger\;V_{\nu_l}(x,\breve{k}',R) = \int d^3x\,V_{\nu_l}(x,\breve{k},R)^\dagger\;U_{\nu_l}(x,\breve{k}',L) = 0\,. \end{aligned} \tag{3.13}$$

3.1.3 Charged pion quantum field

The charged pion fields can be written as (see Table 3.1 for some shorthand notations)

$$\phi^s_{\pi^\sigma}(x) \;=\; \phi^s_{\pi^{-\sigma}}(x)^\dagger \;=\; \int\frac{d\breve{p}}{(2\pi)^3\,2E_{\pi^\sigma}}\left[a_{\pi^\sigma}(\breve{p})\;\mathcal{B}^s_{\breve{p}}(x)+a_{\pi^{-\sigma}}(\breve{p})^\dagger\;\mathcal{B}^{-s}_{\breve{p}}(x)^*\right]\,. \tag{3.14}$$

The operators satisfy the commutation relations

$$\left[a_{\pi^\sigma}(\breve{p}), a_{\pi^{\sigma'}}(\breve{p}')^\dagger\right] \;=\; 2E_{\pi^\sigma}\,(2\pi)^3\,\delta_{\breve{p},\breve{p}'}\,\delta_{\sigma,\sigma'}\;. \tag{3.15}$$

It should be noticed that, with these conventions, the creation and annihilation operators turn out to have different dimensions from the ones usually defined in the absence of the external magnetic field – see Eq. (3.6). In addition, the gauge-dependent Ritus-type basis functions $\mathcal{B}^s_{\bar{p}}(x)$ are solutions of the eigenvalue Klein-Gordon equation for a point-like spin 0 particle in the presence of an electromagnetic field

$$D_\mu D^\mu\;\mathcal{B}^s_{\bar{p}}(x) \;=\; -\left[E^2_{\pi^\sigma} - (2\ell+1)B_e - (p^3)^2\right]\mathcal{B}^s_{\bar{p}}(x)\;. \tag{3.16}$$

They can be chosen to satisfy

$$\sum\!\!\!\!\!\!\int_{\bar{p}} \mathcal{B}^s_{\bar{p}}(x)\,\mathcal{B}^s_{\bar{p}}(y)^* \;=\; \delta^{(4)}(x-y)\;, \qquad \int d^4x\;\mathcal{B}^s_{\bar{p}}(x)\,\mathcal{B}^s_{\bar{p}'}(x)^* \;=\; \hat{\delta}_{\bar{p},\bar{p}'}\;, \tag{3.17}$$

where, similar to Eq. (2.62), we have introduced the shorthand notation

$$\sum\!\!\!\!\!\!\int_{\bar{p}} \;=\; \int \frac{dp^0 d\breve{p}_\chi}{(2\pi)^4}\;, \qquad \hat{\delta}_{\bar{p},\bar{p}'} \;=\; (2\pi)^4\,\delta(p^0-p'^0)\,\delta_{\breve{p},\breve{p}'}\;. \tag{3.18}$$

For the LG we have

$$\mathcal{B}^s_{\bar{p}}(x) \;=\; N_\ell\; e^{-i(E_{\pi^\sigma}x^0 - p^2x^2 - p^3x^3)}\,D_\ell(\beta_s)\;, \tag{3.19}$$

where

$$N_\ell \;=\; \frac{(4\pi B_e)^{\frac{1}{4}}}{\sqrt{\ell!}}\;, \qquad \beta_s \;=\; \sqrt{\frac{2}{B_e}}\left(B_e\,x^1 - s\,p^2\right)\;, \tag{3.20}$$

and $D_\ell(x)$ are the cylindrical parabolic functions, with the standard convention $D_{-1}(x)=0$.

On the other hand, in the SG the Ritus-type basis functions read

$$\mathcal{B}^s_{\bar{p}}(x) \;=\; \sqrt{2\pi}\;e^{-i(E_{\pi^\sigma}x^0 - p^3x^3)}\,e^{-is(\ell-\imath)\phi}\,R_{\ell,\imath}\left(\frac{B_e\rho^2}{2}\right)\;, \tag{3.21}$$

where

$$R_{\ell,\imath}(x) \;=\; N_{\ell,\imath}\,x^{\frac{\ell-\imath}{2}}\,e^{-\frac{x}{2}}\,L^{\ell-\imath}_\imath(x)\;, \qquad N_{\ell,\imath} \;=\; \sqrt{\frac{B_e\,\imath!}{\ell!}}\;, \tag{3.22}$$

with $L^\alpha_\imath(x)$ the associated Laguerre polynomials. In this gauge it can be shown that the eigenvalue of the canonical total angular momentum operator $\hat{j}_3$ acting on a charged pion state is $j_3^{(\pi^\sigma)} = -s(\ell-\imath)$ [231]. Thus, we take $\chi=\imath$ as the third quantum number.

Lastly, in order to define the decay width it will be useful to calculate the particle number associated with the state $|\pi^\sigma(\breve{p})\rangle = a_{\pi^\sigma}(\breve{p})^\dagger|0\rangle$ in a gauge-dependent volume V_χ

$$n_{\pi^\sigma} \;=\; \int_{V_\chi} d^3x\, \langle \pi^\sigma(\breve{p})|\, j^0_{\pi^\sigma}(x)|\pi^\sigma(\breve{p})\rangle \;, \tag{3.23}$$

where $j^0_{\pi^\sigma}$ is the current density

$$j^0_{\pi^\sigma}(x) \;=\; i\left[\phi_{\pi^\sigma}(x)^\dagger \partial^0 \phi_{\pi^\sigma}(x) - \partial^0\phi_{\pi^\sigma}(x)^\dagger\, \phi_{\pi^\sigma}(x)\right] \;. \tag{3.24}$$

In absence of external fields, the usual normalization is $\rho = n/V = 2E$. When the external field is present, the choice of normalization depends on the gauge. In the LG it is convenient to consider an infinite cylinder of section $S = L_2L_3$ lying along the 1-axis; then $n_{\pi^\sigma} = 2E_{\pi^\sigma} 2\pi L_2 L_3$. On the other hand, in the SG we consider a cylinder of infinite radius lying along the 3-axis; then $n_{\pi^\sigma} = 2E_{\pi^\sigma} 4\pi^2 L_3$.

3.1.4 Charged lepton field

The charged lepton field can be written as (see Table 3.1 for some shorthand notations)

$$\psi_l^{s_l}(x) \;=\; \sum_{\tau=1,2} \int \frac{d\breve{q}}{(2\pi)^3 2E_l} \left[b\,(\breve{q},\tau)\; U_l^{s_l}\,(x,\breve{q},\tau) + d\,(\breve{q},\tau)^\dagger\; V_l^{-s_l}\,(x,\breve{q},\tau)\right] \;, \tag{3.25}$$

where the creation and annihilation operators satisfy

$$\begin{aligned} \left\{b(\breve{q},\tau), b(\breve{q}\,',\tau')^\dagger\right\} \;&=\; \left\{d(\breve{q},\tau), d(\breve{q}\,',\tau')^\dagger\right\} \;=\; 2E_l\,(2\pi)^3\,\delta_{\breve{q},\breve{q}'}\,\delta_{\tau,\tau'} \;, \\ \left\{b(\breve{q},\tau), d(\breve{q}\,',\tau')^\dagger\right\} \;&=\; \left\{b(\breve{q},\tau)^\dagger, d(\breve{q}\,',\tau')^\dagger\right\} \;=\; 0 \;. \end{aligned} \tag{3.26}$$

The spinors $U_l^{s_l}$ and $V_l^{-s_l}$ can be written as

$$U_l^{s_l}\,(x,\breve{q},\tau) \;=\; \mathbb{E}^{s_l}_{\breve{q}}(x)\; u_l^{s_l}\,(\breve{q},\tau) \;, \qquad V_l^{-s_l}\,(x,\breve{q},\tau) \;=\; \tilde{\mathbb{E}}^{-s_l}_{\breve{q}}(x)\; v_l^{-s_l}\,(\breve{q},\tau) \;, \tag{3.27}$$

where the spinors $u_l^{s_l}$ and $v_l^{-s_l}$ are given in the Weyl basis by

$$u_l^{s_l}\,(\breve{q},\tau) \;=\; \frac{1}{\sqrt{2(E_l+m_l)}} \begin{pmatrix} (E_l + m_l + s_l\sqrt{2nB_e}\;\tau_2 - q^3\tau_3)\,\Phi^{(\tau)} \\ (E_l + m_l - s_l\sqrt{2nB_e}\;\tau_2 + q^3\tau_3)\,\Phi^{(\tau)} \end{pmatrix} \;, \tag{3.28}$$

$$v_l^{-s_l}\,(\breve{q},\tau) \;=\; \frac{1}{\sqrt{2(E_l+m_l)}} \begin{pmatrix} (E_l + m_l - s_l\sqrt{2nB_e}\;\tau_2 - q^3\tau_3)\,\tilde{\Phi}^{(\tau)} \\ -(E_l + m_l + s_l\sqrt{2nB_e}\;\tau_2 + q^3\tau_3)\,\tilde{\Phi}^{(\tau)} \end{pmatrix} \;, \tag{3.29}$$

with $\Phi^{(1)} = -\tilde{\Phi}^{(2)} = (1,0)^\dagger$ and $\Phi^{(2)} = \tilde{\Phi}^{(1)} = (0,1)^\dagger$. They satisfy the relations

$$\begin{aligned}\sum_{\tau=1,2} u_l^{s_l}(\breve{q},\tau)\,\bar{u}_l^{s_l}(\breve{q},\tau) &= \hat{\not{q}}_{s_l} + m_l\,,\\ \sum_{\tau=1,2} v_l^{-s_l}(\breve{q},\tau)\,\bar{v}_l^{-s_l}(\breve{q},\tau) &= \hat{\not{q}}_{-s_l} - m_l\,,\end{aligned} \tag{3.30}$$

where $\hat{q}^\mu_{s_l} = (E_l, 0, -s\sqrt{2nB_e}, q^3)$. In Eq. (3.27), $\mathbb{E}^{s_l}_{\bar{q}}(x)$ and $\tilde{\mathbb{E}}^{-s_l}_{\bar{q}}(x)$ are Ritus spinor eigenfunctions that satisfy the eigenvalue equation

$$\begin{cases} i\not{D}\ \mathbb{E}^{s_l}_{\bar{q}}(x) = \hat{\not{q}}_{s_l}\ \mathbb{E}^{s_l}_{\bar{q}}(x) & \Rightarrow\quad (i\not{D})^2\ \mathbb{E}^{s_l}_{\bar{q}}(x) = [E_l^2 - 2nB_e - (q^3)^2]\ \mathbb{E}^{s_l}_{\bar{q}}(x)\,,\\ i\not{D}\ \tilde{\mathbb{E}}^{-s_l}_{\bar{q}}(x) = -\hat{\not{q}}_{-s}\ \tilde{\mathbb{E}}^{-s_l}_{\bar{q}}(x) & \Rightarrow\quad (i\not{D})^2\ \tilde{\mathbb{E}}^{-s_l}_{\bar{q}}(x) = [E_l^2 - 2nB_e - (q^3)^2]\ \tilde{\mathbb{E}}^{-s_l}_{\bar{q}}(x)\,. \end{cases} \tag{3.31}$$

They can be written as

$$\mathbb{E}^{s_l}_{\bar{q}}(x) = \sum_{\lambda=\pm} \mathcal{B}^{s_l}_{\bar{q}_{s_l\lambda}}(x) P_n^{s_l}\,\Delta^\lambda\,, \qquad \tilde{\mathbb{E}}^{-s_l}_{\bar{q}}(x) = \sum_{\lambda=\pm} \mathcal{B}^{-s_l}_{\bar{q}_{-s_l\lambda}}(x)^* P_n^{-s_l}\Delta^\lambda\,, \tag{3.32}$$

where $\Delta^\lambda = (1+\lambda\Sigma_z)/2$, with $\Sigma_z = i\gamma^1\gamma^2$, are spin projectors in the magnetic field direction and $\mathcal{B}^{s_l}_{\bar{q}}(x)$ are the gauge-dependent Ritus-type basis functions defined in Eqs. (3.19) and (3.21) for the LG and SG, respectively. Moreover, we have used the shorthand notation $\bar{q}_{s_l\lambda} = (q^0, n_{s_l\lambda}, \chi, q^3)$ where χ is a gauge-dependent quantum number and $n_{s_l\lambda} = n - (1 - s_l\lambda)/2$ is a non-negative integer index representing the orbital Landau level. In the particular case of the lowest Landau level (LLL), $n = 0$, the relation $n_{s_l\lambda} \geq 0$ implies that only one polarization state $\lambda = s_l$ is allowed. This information is codified in the projectors $P_n^{s_l} = (1 - \delta_{n,0})\mathbb{1} + \delta_{n,0}\Delta^{s_l}$. Therefore, we see that the structure of the lepton spinors in Eq. (3.27) is similar to the neutrino one in Eq. (3.9) except that, for the coordinate piece, instead of plane waves one has to use the Ritus basis due to the presence of the magnetic field. Compared to charged pions, we see that both particles share the same scalar basis functions $\mathcal{B}^s_{\bar{q}}(x)$, as could be expected from the fact that the Dirac equation also satisfies the Klein-Gordon equation. Nonetheless, the lepton has an additional Dirac structure, codified in the spin-polarization projectors $P_n^s\Delta^\lambda$.

Similarly to the neutrino case, see Eq. (3.13), it can be seen that the lepton spinors in Eq. (3.27) satisfy the orthogonality relations

$$\begin{aligned}\int d^3x\, U_l^{s_l}(x,\breve{q},\tau)^\dagger\, U_l^{s_l}(x,\breve{q}',\tau') &= \int d^3x\, V_l^{-s_l}(x,\breve{q},\tau)^\dagger\, V_l^{-s_l}(x,\breve{q}',\tau') = 2E_l(2\pi)^3\delta_{\breve{q},\breve{q}'}\,\delta_{\tau,\tau'}\,,\\ \int d^3x\, U_l^{s_l}(x,\breve{q},\tau)^\dagger\, V_l^{-s_l}(x,\breve{q}',\tau') &= \int d^3x\, V_l^{-s_l}(x,\breve{q},\tau)^\dagger\, U_l^{s_l}(x,\breve{q}',\tau') = 0\,,\end{aligned} \tag{3.33}$$

and

$$\int d^3x\, \bar{U}_l^{s_l}(x,\breve{q},\tau)\, U_l^{s_l}(x,\breve{q}',r') = -\int d^3x\, \bar{V}_l^{-s_l}(x,\breve{q},\tau)\, V_l^{-s_l}(x,\breve{q}',\tau') = 2m_l(2\pi)^3\delta_{\breve{q},\breve{q}'}\,\delta_{\tau,\tau'}\,,$$
$$\int d^3x\, \bar{U}_l^{s_l}(x,\breve{q},\tau)\, V_l^{-s_l}(\tilde{x},\breve{q}',\tau') = \int d^3x\, \bar{V}_l^{-s_l}(x,\breve{q},\tau)\, U_l^{s_l}(\tilde{x},\breve{q}',\tau') = 0\,, \tag{3.34}$$

where $\delta_{\breve{q},\breve{q}'}$ can be found in Table 3.1 and $\tilde{x} = (x^0, -\vec{x}\,)$. Moreover, as already stated in Eq. (2.61), the Ritus spinor eigenfunctions satisfy relations similar to (3.17)

$$\sum\!\!\!\!\!\!\int_{\bar{q}} \mathbb{E}_{\bar{q}}^{s_l}(x)\,\mathbb{E}_{\bar{q}}^{s_l}(x')^* \;=\; \delta^{(4)}(x-x')\,, \qquad \int d^4x\, \mathbb{E}_{\bar{q}}^{s_l}(x)\,\mathbb{E}_{\bar{q}'}^{s_l}(x)^* \;=\; \hat{\delta}_{\bar{q},\bar{q}'}\,P_n^{s_l}\,. \tag{3.35}$$

The gauge-dependent quantum number χ needed to complete $\bar{q}$ was implicitly defined in the basis functions $\mathcal{B}_{\bar{q}}^{s_l}(x)$. We comment on it explicitly. In the LG, it is the 2-component of the canonical momentum, $\chi = q^2$. Meanwhile, in the SG it can be shown that the eigenvalue of the canonical total angular momentum operator $\hat{j}_3$ acting on a lepton state is $j_3^{(l)} = -s(n-\upsilon-1/2)$, while for an antilepton state one has $j_3^{(\bar{l})} = s(n-\upsilon-1/2)$ [231]. Thus, $\chi = \upsilon$.

3.2 Pion-to-vacuum amplitudes in the presence of a uniform magnetic field

In this section we analyze the general form of the vacuum-to-pion matrix elements of vector and axial-vector quark currents, which are involved in the weak decay of pions. Let us start by considering the hadronic matrix elements for the case of a neutral pion in the absence of external fields. The matrix element of the hadronic current is given by

$$H_L^{0,\mu}(x,\vec{p}) = H_V^{0,\mu}(x,\vec{p}) - H_A^{0,\mu}(x,\vec{p}) = \langle 0|\bar{\psi}(x)\gamma^\mu(1-\gamma_5)\frac{\tau_3}{2}\,\psi(x)|\pi^0(\vec{p}\,)\rangle \tag{3.36}$$

where $\psi(x) = (\psi_u(x), \psi_d(x))^T$ is the two-flavor quark field and τ_3 is a Pauli matrix acting on flavor space. In order to deal with these matrix elements it is possible to hadronize the quark currents, i.e. to consider matrix elements of hadronic field operators carrying appropriate Lorentz indexes and quantum numbers. In the low energy limit (typically, below the ρ meson threshold), the relevant hadronic field is the pion field $\phi_{\pi^0}(x)$, and in absence of external fields the only available vector-like differential operator is the momentum operator $\hat{p}^\mu = i\partial^\mu$. Since the pion field is pseudoscalar, only the matrix

element of the axial-vector hadronic current can be nonzero. In this way, one has

$$\begin{aligned}\langle 0|\bar{\psi}(x)\gamma^{\mu}\frac{\tau_3}{2}\psi(x)|\pi^0(\vec{p})\rangle &= 0\,,\\ \langle 0|\bar{\psi}(x)\gamma^{\mu}\gamma_5\frac{\tau_3}{2}\psi(x)|\pi^0(\vec{p})\rangle &= f(\hat{p}^2)\,\partial^{\mu}\langle 0|\phi_{\pi^0}(x)|\pi^0(\vec{p})\rangle\,.\end{aligned} \tag{3.37}$$

The function $f(\hat{p}^2)$ contains all the information of nonperturbative QCD contributions. Using the explicit form of $\phi_{\pi^0}(x)$ – see Eq. (3.5) – and the commutation rules for the corresponding creation and annihilation operators – see Eq. (3.6)– one immediately finds

$$\begin{aligned}H_V^{0,\mu}(x,\vec{p}) &= 0\,,\\ H_A^{0,\mu}(x,\vec{p}) &= -if(p^2)\,p^{\mu}e^{-ip\cdot x}\,.\end{aligned} \tag{3.38}$$

As usual, the four-momentum p^{μ} is defined by $p^{\mu} = (E_{\pi},\vec{p})$, with $E_{\pi} = \sqrt{m_{\pi}^2 + |\vec{p}|^2}$. Similar expressions can be obtained for charged pions. It can be seen that the invariance of strong interactions under discrete transformations, such as parity $\mathcal{P}$, charge conjugation $\mathcal{C}$ and temporal inversion $\mathcal{T}$, implies that $f(p^2)$ is a real function. In the absence of external fields, the pion decay constant is given by $f_{\pi} = f(m_{\pi}^2) \simeq 92.32$ MeV [172].

We turn now to the situation in which a static external electromagnetic field is present. In this case, other tensor structures are possible. For a particle of charge Q the relevant basic tensors are the gauge covariant derivative D^{μ} and the gauge invariant electromagnetic field strength $F^{\mu\nu}$, defined as

$$D^{\mu} = \partial^{\mu} + i\,Q\,\mathcal{A}^{\mu}\,, \qquad F^{\mu\nu} = \partial^{\mu}\mathcal{A}^{\nu} - \partial^{\nu}\mathcal{A}^{\mu}\,. \tag{3.39}$$

Taking them as building blocks, one can in principle obtain an infinite number of differential operators with different Lorentz tensor structures. However, for the particular case of a uniform static magnetic field $\vec{B}$, it is well-known - see e.g. Refs. [188, 227] - that only a few independent tensors exist. Noting that $F^{0i} = 0$ and $F^{ij} = F_{ij} = -\epsilon_{ijk}B^k$, we get

$$[D^{\mu}, D^{\nu}] = iQF^{\mu\nu} = -iQ\,\epsilon^{0\mu\nu k}\,B^k\,, \qquad k = 1,2,3\,. \tag{3.40}$$

For definiteness, and without losing generality, in what follows we take $B^k = B\,\delta^{k,3}$. Using the above relations one can prove that there are in fact only two independent scalars, apart from the particle electric charge Q and $F^{\mu\nu}F_{\mu\nu} = 2B^2$. These can be taken to be

$$D_{\parallel}^2 = (D^3)^2 - (D^0)^2\,, \qquad D_{\perp}^2 = -(D^1)^2 - (D^2)^2\,. \tag{3.41}$$

In addition, it is possible to find four independent four-vectors. One possible choice is the

set

$$\begin{aligned} D^\mu &= (D^0, \vec{D}) \,, \\ -i\, F^{\mu\nu} D_\nu &= -i\, B\ (0, D^2, -D^1, 0) \,, \\ F^{\mu\nu} F_{\nu\alpha} D^\alpha &= -B^2\ (0, D^1, D^2, 0) \,, \\ \frac{1}{2}\, \epsilon^{\mu\nu\alpha\beta} F_{\nu\alpha} D_\beta &= B\ (D^3, 0, 0, D^0) \,. \end{aligned} \tag{3.42}$$

Notice that the last of these tensors transforms in fact as an axial-vector.

3.2.1 Neutral pion case

From the above expressions for Lorentz scalars and four-vectors, we can write now a general form for the hadronic currents we are interested in. We consider first the case of the neutral pion, for which $Q = 0$ and the operator D^μ reduces to the usual derivative ∂^μ. Taking into account once again the intrinsic parity of the pion field, the corresponding matrix element can be parametrized as

$$\begin{aligned} H_L^{0,\mu}(x, \vec{p}) \;=\; & \left[\epsilon^{\mu\nu\alpha\beta} F_{\nu\alpha} D_\beta \, \frac{\hat{f}_{\pi^0}^{(V)}}{2B} - D^\mu \, \hat{f}_{\pi^0}^{(A1)} + i\, F^{\mu\nu} D_\nu \, \frac{\hat{f}_{\pi^0}^{(A2)}}{B} - F^{\mu\nu} F_{\nu\alpha} D^\alpha \, \frac{\hat{f}_{\pi^0}^{(A3)}}{B^2} \right] \times \\ & \langle 0 | \phi_{\pi^0}(x) | \pi^0(\vec{p}) \rangle \,, \end{aligned} \tag{3.43}$$

where $\hat{f}_{\pi^0}^{(V)}$ and $\hat{f}_{\pi^0}^{(Ai)}$ are complex functions depending on the magnetic field and the scalar differential operators $\partial_\parallel^2$ and $\partial_\perp^2$. The hadronic matrix elements can be readily obtained using Eqs. (3.5) and (3.6). It is convenient to define the following "parallel" and "perpendicular" combinations

$$\begin{aligned} H_{\parallel,L}^{0,\,\epsilon}(x, \vec{p}) &\equiv H_L^{0,0}(x, \vec{p}) + \epsilon\, H_L^{0,3}(x, \vec{p}) \,, \\ H_{\perp,L}^{0,\,\epsilon}(x, \vec{p}) &\equiv H_L^{0,1}(x, \vec{p}) + i\epsilon\, H_L^{0,2}(x, \vec{p}) \,, \end{aligned} \tag{3.44}$$

where $\epsilon = \pm$. As in the $B = 0$ case, it is important to consider the constraints on the form factors arising from the discrete symmetries of the interaction Lagrangian in the presence of the magnetic field. This is discussed in some detail in Appendix B, where it is shown that these symmetries lead to $f_{\pi^0}^{(A2)} = 0$ while the remaining form factors turn out to be real. In this way, we conclude that the most general form of the vector and axial-vector pion-to-vacuum matrix elements, in the presence of an external uniform magnetic field

along the 3-axis, are

$$H^{0,\epsilon}_{\parallel,L}(x,\vec{p}) \;=\; i\left[f^{(A1)}_{\pi^0} - \epsilon\, f^{(V)}_{\pi^0}\right]\left(E_{\pi^0} + \epsilon\, p^3\right)\, e^{-ip\cdot x}\,,$$
$$H^{0,\epsilon}_{\perp,L}(x,\vec{p}) \;=\; i\left[f^{(A1)}_{\pi^0} - f^{(A3)}_{\pi^0}\right](p^1 + i\epsilon p^2)\, e^{-ip\cdot x}\,, \tag{3.45}$$

where all form factors are real functions of $p_\perp^2 = (p^1)^2 + (p^2)^2$ and $p_\parallel^2 = E_{\pi^0}^2 - (p^3)^2$, with $p_\parallel^2 - p_\perp^2 = p^2 = m_{\pi^0}^2$. The results in Eq. (3.45) are in agreement with the observation made in Ref. [170] that, due to the explicit breaking of rotational invariance caused by the magnetic field, one can define for the neutral meson two different form factors related to the axial current - see also Ref. [103]. One of them can be associated with the direction parallel to $\vec{B}$, and the other one with the perpendicular directions. In addition, according to Eq. (3.45) we find that a new form factor $f^{(V)}_{\pi^0}$ related to the vector current can be defined as well, as first stated in Ref. [230].

3.2.2 Charged pion case

We consider now the case of the charged pion π^σ, with $\sigma = \pm$ (electric charge $Q = \sigma e$). In this case the matrix element is given by

$$H^{\sigma,\mu}_L(x,\breve{p}) \;=\; H^{\sigma,\mu}_V(x,\breve{p}) - H^{\sigma,\mu}_A(x,\breve{p}) \;=\; \langle 0|\bar{\psi}(x)\gamma^\mu(1-\gamma_5)\tau^{-\sigma}\psi(x)|\pi^\sigma(\breve{p})\rangle\,, \tag{3.46}$$

where $\tau^\pm = (\tau_1 \pm i\tau_2)/2$. In analogy with Eq. (3.43), we can parametrize this element as

$$H^{\sigma,\mu}_L(x,\breve{p}) \;=\; \left[\epsilon^{\mu\nu\alpha\beta}F_{\nu\alpha}D_\beta\,\frac{\hat{f}^{(V)}_{\pi^\sigma}}{2B} - D^\mu\,\hat{f}^{(A1)}_{\pi^\sigma} + is\,F^{\mu\nu}D_\nu\,\frac{\hat{f}^{(A2)}_{\pi^\sigma}}{B} - F^{\mu\nu}F_{\nu\alpha}D^\alpha\,\frac{\hat{f}^{(A3)}_{\pi^\sigma}}{B^2}\right]\times$$
$$\sqrt{2}\,\langle 0|\phi_{\pi^\sigma}(x)|\pi^\sigma(\breve{p})\rangle\,. \tag{3.47}$$

Here $\hat{f}^{(V)}_{\pi^\sigma}$ and $\hat{f}^{(Ai)}_{\pi^\sigma}$ are functions of the scalar operators $D_\parallel^2$ and $D_\perp^2$ defined in Eq. (3.41), while $s = \mathrm{sign}(\sigma B)$. The form factors $f^{(V)}_{\pi^\sigma}$ and $f^{(A2)}_{\pi^\sigma}$ were already defined in Ref. [171]. On the other hand, $f^{(A3)}_{\pi^\sigma}$ is new, first defined in [230]. As in the case of the neutral pion, it will be convenient to deal with the linear combinations defined in Eq. (3.44). The hadronic matrix element can be readily obtained using the expressions given in previous subsections. Let us define it in a general way as $\langle 0|\phi_{\pi^\sigma}(x)|\pi^\sigma(\breve{p})\rangle \equiv \mathcal{B}^s_{\breve{p}}(x)$, where $\mathcal{B}^s_{\breve{p}}(x)$ are the gauge-dependent Ritus-type basis function that satisfy the eigenvalue equation (3.16).

Then, it is not hard to prove that in any gauge we obtain

$$H^{\sigma,\epsilon}_{\parallel,L}(x,\breve{p}) \;=\; i\sqrt{2}\,\left(f^{(A1)}_{\pi^\sigma}-\epsilon f^{(V)}_{\pi^\sigma}\right)\left(E_{\pi^\sigma}+\epsilon p^3\right)\;\mathcal{B}^s_{\bar{p}}(x)\,,$$
$$H^{\sigma,\epsilon}_{\perp,L}(x,\breve{p}) \;=\; s\epsilon\sqrt{2}\left(f^{(A1)}_{\pi^\sigma}-s\epsilon f^{(A2)}_{\pi^\sigma}-f^{(A3)}_{\pi^\sigma}\right)\sqrt{(2\ell+1-s\epsilon)B_e}\;\mathcal{B}^s_{\bar{p}-s\epsilon}(x)\,, \tag{3.48}$$

where the form factors $f^{(V)}_{\pi^\sigma}$ and $f^{(Ai)}_{\pi^\sigma}$ turn out to be gauge-independent functions of m_{π^σ}, p^3, ℓ and B. Moreover, $\bar{p}-s\epsilon$ refers to the fact that one should take $\ell-s\epsilon$ for the Landau level. As in the case of the neutral pion, the discrete symmetries of the interaction Lagrangian in the presence of the magnetic field lead to some restrictions on the form factors $f^{(V)}_{\pi^\sigma}$ and $f^{(Ai)}_{\pi^\sigma}$. Indeed, as shown in Appendix B, they have to be real and independent of the sign of the pion charge. Moreover, it can be seen that the vector form factor $f^{(V)}_{\pi^\sigma}$ should be odd under the exchange $B\to -B$, while the axial-vector form factors $f^{(Ai)}_{\pi^\sigma}$ $(i=1,2,3)$ should be even functions of B.

3.3 Weak decay width of charged pions under a uniform magnetic field

3.3.1 Decay width and kinematics

Let us analyze the decay width for the process $\pi^-\to l\,\bar{\nu}_l$, with $l=\mu,e$, in the presence of the external magnetic field. On general grounds, it is given by

$$\Gamma^-_l(B) \;=\; \lim_{T\to\infty}\frac{1}{n_{\pi^-}}\sum_{\tau=1,2}\int\frac{d\breve{q}_\chi}{(2\pi)^3 2E_l}\int\frac{d\breve{k}_\chi}{(2\pi)^3 2E_{\bar{\nu}_l}}\,\frac{|(\mathcal{S}-1)_{fi}|^2}{T}\,, \tag{3.49}$$

where $(\mathcal{S}-1)_{fi}$ is the relevant $\mathcal{S}$-matrix element between the initial and final states, and n_{π^-} is the particle number associated with the initial π^- state - see text below Eq. (3.24). The shorthand notation $d\breve{q}_\chi$ and $d\breve{k}_\chi$ refers to the fact that one should sum or integrate over the relevant quantum numbers of each particle, which are gauge-dependent quantities - see Table 3.1. Thus, one has

$$\Gamma^-_l(B) \;=\; \lim_{S_\chi,T\to\infty}\frac{1}{2E_{\pi^-}}\int\frac{d\breve{q}_\chi}{(2\pi)^3 2E_l}\int\frac{d\breve{k}_\chi}{(2\pi)^3 2E_{\bar{\nu}_l}}\sum_{\tau=1,2}\frac{|\langle\, l(\breve{q},\tau)\,\bar{\nu}_l(\breve{k},R)|L_W|\pi^-(\breve{p})\,\rangle|^2}{2\pi S_\chi T}\,, \tag{3.50}$$

where T and S_χ are the time and space interval in which the interaction is active. Here S_χ is a gauge-dependent quantity, with $S_\chi=L_2L_3$ in the LG and $S_\chi=2\pi L_3$ in the SG. At the end of the calculation, the limit $S_\chi,T\to\infty$ will be taken. The decay amplitude can be separated in hadronic and leptonic elements according to Eq. (3.1). The leptonic

piece can be calculated using the notation introduced in previous subsections, resulting in

$$\langle\, l(\breve{q},\tau)\,\bar{\nu}_l(\breve{k},R)|L_W|\pi^-(\breve{p})\,\rangle \;=\; -\frac{G_F}{\sqrt{2}}\,\cos\theta_c\,\times \\ \int d^4x\, H_L^{-,\mu}(x,\breve{p})\;\bar{U}_l^-(x,\breve{q},\tau)\,\gamma_\mu\,(1-\gamma_5)\,V_{\nu_l}(x,\breve{k},R)\;, \quad (3.51)$$

where $H_L^{-,\mu}(x,\breve{p})$ stands for the matrix element of the hadronic current, defined in Eq. (3.46). Using the final expressions of Eq. (3.48) for these currents, together with the explicit form of the antineutrino and charged lepton spinors, given in subsection 3.1.2 and subsection 3.1.4 respectively, we get

$$\langle\, l(\breve{q},\tau)\,\bar{\nu}_l(\breve{k},R)|L_W|\pi^-(\breve{p})\,\rangle \;=\; (2\pi)^3\,\delta_{\chi,\chi'}\,\delta(E_{\pi^-}-E_l-E_{\bar{\nu}_l})\,\delta(p^3-q^3-k^3)\;\mathcal{M}(\breve{p},\breve{q},\breve{k},\tau)\;, \quad (3.52)$$

where the polarization amplitudes $\mathcal{M}(\breve{p},\breve{q},\breve{k},\tau)$ (implicitly evaluated at the constraints imposed by these delta functions) will be given below. As expected from the symmetries of the Lagrangian, energy is conserved together with the momentum in the field direction. There is also a remaining conservation of the quantum number χ codified in the $\delta_{\chi,\chi'}$ function. We recall that this quantum number depends on the gauge and therefore does not represent a physical quantity. In the LG it corresponds to the 2-component of the canonical momentum and therefore $\delta_{\chi,\chi'} = \delta(p^2-q^2-k^2)$, while in the SG it is an integer related to the canonical total angular momentum in the field direction, leading to $\delta_{\chi,\chi'} = \delta_{j_3^{(\pi^\sigma)},\, j_3^{(l)}+j_3^{(\bar{\nu}_l)}}$.

The decay width is obtained by inserting Eq. (3.52) into Eq. (3.50). As customary, we replace (similarly for $\delta^2_{\chi,\chi'}$)

$$\begin{aligned}\left[2\pi\,\delta(E_{\pi^-}-E_l-E_{\bar{\nu}_l})\right]^2 \;&\to\; \lim_{T\to\infty}\;\; 2\pi\,T\;\;\delta(E_{\pi^-}-E_l-E_{\bar{\nu}_l})\;,\\ \Big[2\pi\,\delta\Big(p^3-q^3-k^3\Big)\Big]^2 \;&\to\; \lim_{L_3\to\infty}\,2\pi\,L_3\,\delta\Big(p^3-q^3-k^3\Big)\;. \end{aligned} \quad (3.53)$$

Taking the limit of infinite space-time volume we finally get

$$\Gamma_l^-(B) \;=\; \frac{1}{16\pi E_{\pi^-}}\sum_{n=0}^{\infty}\int\frac{d\breve{q}_\chi\,d\breve{k}_\chi}{(2\pi)^3E_lE_{\bar{\nu}_l}}\,\delta_{\chi,\chi'}\,\delta(E_{\pi^-}-E_l-E_{\bar{\nu}_l})\,\delta(p^3-q^3-k^3)\;\overline{\left|\mathcal{M}_{\pi^-\to l\,\bar{\nu}_l}\right|^2}\;, \quad (3.54)$$

where

$$\overline{\left|\mathcal{M}_{\pi^-\to l\,\bar{\nu}_l}\right|^2} \;=\; \sum_{\tau=1,2}\left|\mathcal{M}(\breve{p},\breve{q},\breve{k},\tau)\right|^2\;. \quad (3.55)$$

The calculation of the polarization amplitudes leads to

$$\begin{aligned}\mathcal{M}(\breve{p},\breve{q},\breve{k},1) &= i\,G_F\cos\theta_c\sqrt{\frac{2}{E_l+m_l}}\left[(E_l+m_l-q^3)\,A(\breve{p},\breve{q},\breve{k})-s\sqrt{2nB_e}\,B(\breve{p},\breve{q},\breve{k})\right],\\ \mathcal{M}(\breve{p},\breve{q},\breve{k},2) &= \quad G_F\cos\theta_c\sqrt{\frac{2}{E_l+m_l}}\left[(E_l+m_l+q^3)\,B(\breve{p},\breve{q},\breve{k})-s\sqrt{2nB_e}\,A(\breve{p},\breve{q},\breve{k})\right],\end{aligned} \tag{3.56}$$

where we have defined the functions

$$\begin{aligned}A(\breve{p},\breve{q},\breve{k}) &\equiv a_{\pi^-}(E_{\pi^-}+p^3)\,\sqrt{E_{\bar{\nu}_l}-k^3}\;I_{1\chi}+s\,d_{\pi^-}\sqrt{2(\ell+1+s)B_e}\,\sqrt{E_{\bar{\nu}_l}+k^3}\;I_{2\chi}\,,\\ B(\breve{p},\breve{q},\breve{k}) &\equiv b_{\pi^-}(E_{\pi^-}-p^3)\,\sqrt{E_{\bar{\nu}_l}+k^3}\;I_{4\chi}+s\,c_{\pi^-}\sqrt{(2\ell+1-s)B_e}\,\sqrt{E_{\bar{\nu}_l}-k^3}\;I_{3\chi}\,.\end{aligned} \tag{3.57}$$

In these functions, the decay coefficients are

$$\begin{aligned}a_{\pi^-} &\equiv f_{\pi^-}^{(A1)}-f_{\pi^-}^{(V)}\,, & b_{\pi^-} &\equiv f_{\pi^-}^{(A1)}+f_{\pi^-}^{(V)}\,,\\ c_{\pi^-} &\equiv f_{\pi^-}^{(A1)}-s\,f_{\pi^-}^{(A2)}-f_{\pi^-}^{(A3)}\,, & d_{\pi^-} &\equiv f_{\pi^-}^{(A1)}+s\,f_{\pi^-}^{(A2)}-f_{\pi^-}^{(A3)}\,,\end{aligned} \tag{3.58}$$

while the spatial integrals read

$$\begin{aligned}I_{1\chi} &= f_{1\chi}\,\mathcal{I}_\chi\Big(\ell,n-\frac{1-s}{2}\Big)\,, & I_{2\chi} &= f_{2\chi}\,\mathcal{I}_\chi\Big(\ell+s,n-\frac{1-s}{2}\Big)\,,\\ I_{3\chi} &= f_{3\chi}\,\mathcal{I}_\chi\Big(\ell-s,n-\frac{1+s}{2}\Big)\,, & I_{4\chi} &= f_{4\chi}\,\mathcal{I}_\chi\Big(\ell,n-\frac{1+s}{2}\Big)\,.\end{aligned} \tag{3.59}$$

Here, $\mathcal{I}_\chi$ and $f_{j\chi}$ are gauge dependent functions of the remaining spatial integral. In the

LG they are given by

$$\begin{aligned}
\underline{\text{LG}}: \quad & \bullet\, f_{1\chi} \;=\; f_{3\chi} \;=\; \frac{ik^1+k^2}{k_\perp}\,, \qquad f_{2\chi} \;=\; f_{4\chi} = 1\,, \\
& \bullet\, \mathcal{I}_\chi(\ell,n) \;=\; -iN_\ell\, N_n \int_{-\infty}^{\infty} dx^1\, e^{-ik^1x^1} \times \\
& \qquad\qquad D_\ell\left(\sqrt{2B_e}x^1 - s\sqrt{\frac{2}{B_e}}\,p^2\right) D_n\left(\sqrt{2B_e}x^1 - s\sqrt{\frac{2}{B_e}}\,q^2\right) \\
& \qquad = \; -i\,2\pi\, e^{\frac{-is\,k^1(p^2+q^2)}{2B_e}}\, e^{-\frac{\kappa}{2}} \times \begin{cases} \sqrt{\dfrac{\ell!}{n!}}\left(\dfrac{-ik^1+s\,k^2}{\sqrt{2B_e}}\right)^{n-\ell} L_\ell^{n-\ell}(\kappa) & \text{if } n \geq \ell \\ \sqrt{\dfrac{n!}{\ell!}}\left(\dfrac{-ik^1-s\,k^2}{\sqrt{2B_e}}\right)^{\ell-n} L_n^{\ell-n}(\kappa) & \text{if } \ell \geq n\,, \end{cases}
\end{aligned} \tag{3.60}$$

while in the SG they read

$$\begin{aligned}
\underline{\text{SG}}: \quad & \bullet\, f_{j\chi} \;=\; 1\,, \quad j = 1,...4\,, \\
& \bullet\, \mathcal{I}_\chi(\ell,n) \;=\; (-i)^\jmath\, 2\pi \int_0^\infty d\rho\; \rho\; R_{\ell,\imath}(\rho)\; R_{n,\upsilon}(\rho)\; J_{(\ell-\imath)-(n-\upsilon)}(k_\perp\rho) \\
& \qquad = \; (-i)^\jmath\, 2\pi\, (-1)^{\imath+\upsilon} \sqrt{\frac{\imath!\, n!}{\ell!\, \upsilon!}}\, \kappa^{\frac{(\ell-\imath)-(n-\upsilon)}{2}}\, e^{-\kappa}\, L_\imath^{\upsilon-\imath}(\kappa)\, L_n^{\ell-n}(\kappa)\,.
\end{aligned} \tag{3.61}$$

where we have introduced the dimensionless variable $\kappa = k_\perp^2/(2B_e)$. Details for the spatial integrals can be found in Apps. C of Refs. [230, 231]. Note that since $Q_l = Q_{\pi^-}$, we have grouped the notation of $s_Q = \text{sign}(QB)$ for charged pions and leptons under a single symbol s.

3.3.2 Lowest energy state

As it is usually done, in what follows we will concentrate on the situation in which the decaying pion is in the lowest energy state (LES). This corresponds to the case $\ell = 0$ and $p^3 = 0$. The expressions for $\mathcal{I}_\chi$ involve factorials of ℓ. Therefore, $\ell = 0$ entails

$$\mathcal{I}_\chi(-1,n) \;=\; 0\,. \tag{3.62}$$

If $s < 0$ this implies $I_{2\chi} = 0$, and therefore the decay width does not depend on the combination $f_{\pi^-}^{(A1)} - f_{\pi^-}^{(A2)} - f_{\pi^-}^{(A3)}$. We reach the same conclusion for $s > 0$, since $I_{3\chi} = 0$ in that case.

Let us take for definiteness $B > 0$. Then $s < 0$ and the decay amplitudes simplify to

$$\mathcal{M}(\breve{p}_{LES}, \breve{q}, \breve{k}, 1) \;=\; G_F \cos\theta_c \; (-1)^{n+1} \, 2\pi \, \sqrt{\frac{2(E_{\bar{\nu}_l} - k^3)}{E_l + m_l}} \; \frac{\kappa^{\frac{n-1}{2}}}{\sqrt{n-1!}} \; M_\chi \times$$
$$\Big[a_{\pi^-} E_{\pi^-} (E_l + m_l - q^3) - b_{\pi^-} E_{\pi^-} (E_{\bar{\nu}_l} + k^3) + c_{\pi^-} 2B_e (\kappa - n) \Big] \;, \quad (3.63)$$

$$\mathcal{M}(\breve{p}_{LES}, \breve{q}, \breve{k}, 2) \;=\; iG_F \cos\theta_c \; (-1)^{n} \, 2\pi \, \sqrt{\frac{E_{\bar{\nu}_l} - k^3}{B_e (E_l + m_l)}} \; \frac{\kappa^{\frac{n-1}{2}}}{\sqrt{n!}} \; M_\chi \times$$
$$\Big\{ a_{\pi^-} E_{\pi^-} \, 2nB_e - (E_l + m_l + q^3) \Big[b_{\pi^-} E_{\pi^-} (E_{\bar{\nu}_l} + k^3) - c_{\pi^-} \, 2B_e (\kappa - n) \Big] \Big\} \;, \quad (3.64)$$

where

$$\underline{\text{LG}}: \quad M_\chi \;=\; e^{\frac{i\,k^1 (p^2 + q^2)}{2B_e}} \; i^n \left(\frac{k^1 - ik^2}{k^1 + ik^2} \right)^{\frac{n}{2}} \; e^{-\frac{\kappa}{2}} \;,$$

$$\underline{\text{SG}}: \quad M_\chi \;=\; (-i)^{\jmath - 1} \sqrt{\frac{\imath!}{\upsilon!}} \; (-1)^{\imath + \upsilon} \; \kappa^{(\upsilon - \imath)/2} \; e^{-\kappa} L_\imath^{\upsilon - \imath}(\kappa) \;. \quad (3.65)$$

Regarding the decay width, for $\ell = p^3 = 0$ energy conservation implies

$$\delta \left(E_{\pi^-} - E_l - E_{\bar{\nu}_l} \right) \;=\; \frac{E_l E_{\bar{\nu}_l}}{E_{\pi^-} \bar{k}^3} \, \Theta(n_{\max} - n) \; \Theta(k_\perp^{\max} - k_\perp) \; \Big[\delta\Big(k^3 - \bar{k}^3 \Big) + \delta\Big(k^3 + \bar{k}^3 \Big) \Big] \;, \quad (3.66)$$

where $\Theta(x)$ is the Heaviside step function and we have defined

$$n_{\max} \;=\; \frac{m_{\pi^-}^2 - m_l^2 + B_e}{2B_e} \;, \quad (3.67)$$

$$k_\perp^{\max} \;=\; E_{\pi^-} - \sqrt{m_l^2 + 2nB_e} \;, \quad (3.68)$$

$$\bar{k}^3 \;=\; \frac{1}{2E_{\pi^-}} \sqrt{\left[E_{\pi^-}^2 - 2B_e (n - \kappa) - m_l^2 \right]^2 - 8B_e E_{\pi^-}^2 \kappa} \;. \quad (3.69)$$

The difference between both gauges is condensed in the $|M_\chi|^2$ coefficient, which appears when calculating the squared modulus of the amplitude in Eq. (3.54). In the LG we easily get $|M_\chi|^2 = e^{-\kappa}$. In the SG the calculation is more difficult due to the sum over the charged lepton quantum number υ. However, it is shown in Ref. [231] that

$$\sum_{\upsilon=0}^{\infty} \left| (-i)^{\jmath - 1} \sqrt{\frac{\imath!}{\upsilon!}} \; (-1)^{\imath + \upsilon} \; \kappa^{\frac{\upsilon - \imath}{2}} \; e^{-\kappa} \, L_\imath^{\upsilon - \imath}(\kappa) \right|^2 \;=\; e^{-\kappa} \;. \quad (3.70)$$

Putting all these results together, after some algebra one finally arrives at

$$\Gamma_l^-(B) \;=\; \frac{G_F^2\cos^2\theta_c}{2\pi\, E_{\pi^-}^2}\, B_e \sum_{n=0}^{n_{\max}} \int_0^{\kappa_{\max}} d\kappa\; \frac{1}{\bar{k}^3}\, \frac{\kappa^{n-1}}{n!}\; e^{-\kappa}\; A_{\pi^-}^{(n)}(\kappa)\,, \tag{3.71}$$

where $\kappa_{\max} = (k_\perp^{\max})^2/(2B_e)$ and

$$\begin{aligned} A_{\pi^-}^{(n)}(\kappa) \;=\; & \Big[E_{\pi^-}^2 - 2B_e(n-\kappa) - m_l^2\Big] \times \\ & \left[\frac{m_l^2}{2}\,(n|a_{\pi^-}|^2 + \kappa|b_{\pi^-}|^2) + B_e(n-\kappa)(n|a_{\pi^-} - c_{\pi^-}|^2 + \kappa|b_{\pi^-} - c_{\pi^-}|^2)\right] + \\ & 2B_e\,\kappa\,\left\{E_{\pi^-}^2\Big[n|a_{\pi^-} - b_{\pi^-}|^2 - (n-\kappa)|b_{\pi^-} - c_{\pi^-}|^2\Big] + (n-\kappa)\, m_l^2 |c_{\pi^-}|^2\right\}. \end{aligned} \tag{3.72}$$

It should be noted that the width does not depend on $\imath$ (related to the total angular momentum $j_3^{(\pi^-)}$) in the SG, nor on p^2 in the LG. Since the calculation was carried out using two different gauges, their coincidence provides an explicit confirmation of the gauge independence of our expression for the decay width. Moreover, it is worth remarking that under the exchange $B \to -B$, which implies $s \to -s$ and $f_{\pi^-}^{(V)} \to -f_{\pi^-}^{(V)}$, we have checked that the above expression for the partial decay width remains invariant, as expected. Moreover, it can be seen that in the $B \to 0$ limit one recovers the usual expression for the decay width in the absence of external fields, see Ref. [230] for details.

3.3.3 Strong magnetic field: LLL and chiral limit

It is interesting at this point to study the case of a large external magnetic field. As stated, since the pion is built with charged quarks, the pion mass will depend in general on the magnetic field. Now, if the mass growth is relatively mild, for large magnetic fields one should get $B_e > m_{\pi^-}^2 - m_l^2$. In fact, this is what is obtained from lattice QCD calculations [129] as well as from effective approaches like the Nambu–Jona-Lasinio model [233], for values of the magnetic field say $B_e \gtrsim 0.05$ GeV^2. According to Eq. (3.67), this implies $n_{\max} = 0$; hence the outgoing muon or electron (assuming that the energy is below the τ production threshold) has to lie in its lowest Landau level $n = 0$. As mentioned in subsection 3.1.4, only one polarization state is allowed in this case. Since we are considering $s = -1$, this corresponds to $\tau = 2$. This can also be easily seen from Eqs. (3.56) and (3.57), since $\mathcal{I}_\chi(\ell, -1) = 0$ implies $\mathcal{M}(\breve{p}, \breve{q}_{LLL}, \breve{k}, 1) = 0$. In this case the

expression for the partial width simplifies to

$$\Gamma^{-}_{l,\,LLL}(B) \;=\; \frac{G_F^2\cos^2\theta_c}{2\pi E_{\pi^-}}\int_0^{E_{\pi^-}-m_l} dk_\perp\,\frac{k_\perp}{\bar{k}^3}\,e^{-\frac{k_\perp^2}{2B_e}}\,\times \\ \left[m_l^2\left(E_{\bar{\nu}_l}|b_{\pi^-}|^2-\frac{k_\perp^2}{E_{\pi^-}}|c_{\pi^-}|^2\right)+E_l\,k_\perp^2\,|b_{\pi^-}-c_{\pi^-}|^2\right]\,. \tag{3.73}$$

We can compare this result with the expression quoted in Eq. (5) of Ref. [171], which also corresponds to the limit of a large external magnetic field. The authors of that work make some approximations for the motion of a charged pion in the presence of the magnetic field, concluding that only one of the two possible antineutrino polarizations can contribute to the decay amplitude. Moreover, based on considerations of angular momentum conservation, they assume that the antineutrino momentum in the perpendicular plane $\vec{k}_\perp$ vanishes. It can be seen that if one imposes such condition in Eq. (3.73), the result quoted in Ref. [171] are recovered. However, we find that if the effect of the magnetic field is fully taken into account in the charged pion field, conservation laws do not imply $\vec{k}_\perp = 0$. In fact, an integration over all possible values of the antineutrino momentum has to be performed, as in Eq. (3.73). Another important difference between our work and the analysis in Ref. [171] is that our calculations include a perpendicular piece of the hadronic amplitude (related to c_{π^-}), which arises due to the presence of a π^- zero point motion in the perpendicular plane, even in the $\ell = 0$ state.

A final observation concerns the situation in which $B_e > m_{\pi^-}^2 - m_l^2$ and also $B_e \gg m_l^2$. In this case, in addition to $n = 0$, we can neglect the charged lepton mass in the amplitude, obtaining

$$\mathcal{M}(\breve{p}_{LES},\breve{q}_{LLL},\breve{k})_{\rm ch} \;=\; -\,iG_F\cos\theta_c\,2\pi\sqrt{2E_l(E_{\nu_l}+k^3)}\;M_\chi\,\times \\ \Big[1-{\rm sign}(k^3)\Big]\;\Big[b_{\pi^-}\,E_{\pi^-}-c_{\pi^-}\;(E_{\nu_l}-k^3)\Big]\,, \tag{3.74}$$

and therefore

$$\Gamma^{-}_{l,\,LLL}(B)_{\rm ch} \;=\; \frac{G_F^2\cos^2\theta_c}{\pi}\,\frac{B_e^2}{E_{\pi^-}}\left[1-\left(1+\frac{E_{\pi^-}^2}{2B_e}\right)e^{-\frac{E_{\pi^-}^2}{2B_e}}\right]\left|f_{\pi^-}^{(V)}-f_{\pi^-}^{(A2)}+f_{\pi^-}^{(A3)}\right|^2\,. \tag{3.75}$$

As seen, while for $k^3 > 0$ the amplitude vanishes, for $k^3 < 0$ in general *it does not*. This can be understood in terms of helicity conservation. The helicity of a lepton state can be calculated using Eq. (3.2) together with the lepton field defined in Eq. (3.25). In the chiral limit $m_l \to 0$, for a charged lepton in the LLL we get [231]

$$\gamma_5\;|l(\breve{q}_{LLL})\rangle_{\rm ch} \;=\; s\,{\rm sign}(q^3)\;|l(\breve{q}_{LLL})\rangle_{\rm ch}\,. \tag{3.76}$$

Noting that $q^3 = -k^3$, when $s = -1$ we see that for $k^3 > 0$ the outgoing charged lepton would be right-handed, which is forbidden by helicity conservation since antineutrinos are always right-handed. This is very different from what happens in the absence of a magnetic field. For $B = 0$, momentum conservation together with helicity conservation imply that the total decay amplitude of a pion at rest must vanish as $m_l \to 0$, as can be checked in Eq. (3.75) since all form factors except $f_{\pi^-}^{(A1)}$ cancel when $B \to 0$. At large magnetic field, however, momentum conservations are different, and helicity conservation only implies that the projection of the antineutrino momentum in the direction of $\vec{B}$ must be opposite to $\vec{B}$.

Clearly, the relevance of Eq. (3.75) depends on whether these form factors are non-negligible for magnetic fields that are much larger than the lepton mass squared. While this is likely to happen for the π^- decay to $e\,\bar{\nu}_e$, in the case of the muon (and of course, the tau) the situation is less clear, and the corrections arising from a finite lepton mass should be taken into account. Interestingly, it is possible to obtain relatively simple expressions for the $\pi^- \to l\bar{\nu}_l$ decay width at leading order in the ratio m_l/E_{π^-}. From Eq. (3.73) one gets

$$\Gamma^-_{l,\,LLL}(B) \;\simeq\; \Gamma^-_{l,\,LLL}(B)_{\rm ch} + \frac{G_F^2\cos^2\theta_c}{2\pi}\,\frac{B_e}{E_{\pi^-}}\,e^{-\frac{E_{\pi^-}^2}{2B_e}}\,\times \\ \left[f_1\,|b_{\pi^-}|^2 - 2f_2\,{\rm Re}(b^*_{\pi^-}\,c_{\pi^-}) + f_3\,|c_{\pi^-}|^2\right] m_l^2 \;+\; \mathcal{O}\!\left(\frac{m_l^3}{E_{\pi^-}^3}\right)\,, \tag{3.77}$$

where

$$\begin{aligned} f_1 &= (1+\alpha)^2 - (1+2\alpha)\,e^{\alpha} + 2\alpha^2\left(I(\alpha) - \ln\frac{m_l}{E_{\pi^-}}\right)\,, \\ f_2 &= \alpha(2+\alpha) - 2\alpha\,e^{\alpha} + 2\alpha(\alpha-1)\left(I(\alpha) - \ln\frac{m_l}{E_{\pi^-}}\right)\,, \\ f_3 &= \alpha^2 + 2\alpha - 2 + 2(1-\alpha)\,e^{\alpha} + 2\alpha(\alpha-2)\left(I(\alpha) - \ln\frac{m_l}{E_{\pi^-}}\right)\,, \end{aligned} \tag{3.78}$$

with $\alpha = E_{\pi^-}^2/(2B_e)$ and $I(\alpha) = \int_0^1 dx(e^{\alpha x}-1)/x$. It can be seen that for $m_l = m_\mu = 105.65$ MeV and $B_e \gtrsim 0.3$ GeV^2, Eq. (3.77) approximates the full result in Eq. (3.73) within 15% accuracy.

3.3.4 Angular distribution of outgoing antineutrinos

We have seen in Eq. (3.74) that, in the large magnetic field limit, the amplitude vanishes for $k^3 > 0$. This implies a highly anisotropic distribution of outgoing antineutrinos, which is not explicitly seen in the final expression of the decay width. This in contrast to the

$B = 0$ case, where the distribution is isotropic. In fact, denoting $w = \cos\theta = k^3/|\vec{k}|$, the differential decay rate for the pion LES can be written as

$$\frac{d\Gamma_l^-(B)}{dw} = \frac{G_F^2\cos^2\theta_c}{4\pi}\sum_{n=0}^{n_{\max}}\frac{(1-r)^2}{r\,(1-w^2)^2}\frac{u^{n-1}}{n!}\,e^{-u}\left[|w|\frac{A_{\pi^-}^{(n)}(u)}{\bar{k}^3(u)} + w\,B_{\pi^-}^{(n)}(u)\right], \tag{3.79}$$

where

$$r = \frac{1}{E_{\pi^-}}\sqrt{E_{\pi^-}^2 - (E_{\pi^-}^2 - 2nB_e - m_l^2)\,(1-w^2)}\,, \qquad u = \frac{E_{\pi^-}^2}{2B_e}\frac{(1-r)^2}{(1-w^2)}\,, \tag{3.80}$$

and the function $B_{\pi^-}^{(n)}(u)$ is defined as

$$B_{\pi^-}^{(n)}(u) = E_{\pi^-}\Big[\Big(u|b_{\pi^-}|^2 - n|a_{\pi^-}|^2\Big)\,m_l^2 + 2B_e(n-u)\Big(u|b_{\pi^-} - c_{\pi^-}|^2 - n|a_{\pi^-} - c_{\pi^-}|^2\Big)\Big]\,. \tag{3.81}$$

The term proportional to $B_{\pi^-}^{(n)}(u)$ in Eq. (3.79) does not contribute to the total decay width since it vanishes after integration over w, recovering the result in Eq. (3.71).

In particular, when $B_e \gg m_l^2$ and $B_e > m_{\pi^-} - m_l$, we have $n = 0$ only and $m_l = 0$ approximately. In this chiral case, helicity conservation implies that all antineutrinos should be produced with momenta in the half-space $k^3 < 0$, see Eq. (3.74). Indeed, the normalized differential decay width is given by

$$\frac{1}{\Gamma_{l,\,LLL}^-(B)_{\rm ch}}\frac{d\Gamma_{l,\,LLL}^-(B)_{\rm ch}}{dw} = \begin{cases} 2\lambda^2\dfrac{(1+w)}{(1-w)^3}\dfrac{e^{-\lambda(1+w)/(1-w)}}{1-(1+\lambda)\,e^{-\lambda}} & \text{if } \ w \le 0 \\ 0 & \text{if } \ w > 0 \end{cases}, \tag{3.82}$$

where $\lambda = E_{\pi^-}^2/(2B_e)$.

We conclude that, in contrast to the isotropy seen at $B = 0$, the presence of an external magnetic field induces an anisotropy in the angular distribution of outgoing antineutrinos. The anisotropy is sharpened for strong fields and lower lepton masses (closer to the chiral limit), where antineutrinos are mostly produced with momenta in the half-space opposite to the direction of $\vec{B}$. In addition, it is worth noticing that for large values of B most antineutrinos come out with low $|k^3|$, i.e. in directions approximately perpendicular to the magnetic field.

CHAPTER 4

Pion properties under strong magnetic fields in the SU(2) NJL model

The influence of magnetic fields on the lightest scalar and pseudoscalar mesons (σ and $\vec{\pi}$) has been calculated mostly using two-flavor schemes, such as chiral perturbation theory [234–237], the linear sigma model [238–240], two-flavor quark-meson model [228], relativistic Hamiltonian-based formalisms [236, 241], effective chiral confinement Lagrangian approach [242, 243], QCD sum rules [244], holographic Sakai-Sugimoto model [245], the two-flavor NJL model [156, 157, 161, 162, 168–170, 218, 222–224, 246–249], or its nonlocal version [250, 251]. See also [53] for a comprehensive review on effective models under strong magnetic fields. In this chapter we will study the behavior of several pion properties in the presence of a static uniform magnetic field within the framework of the two-flavor NJL model, using a magnetic field-independent regularization scheme. These properties include their masses and decay constants, which in turn allow us to estimate partial decay widths and angular distributions, according to results from chapter 3. Once again, we will consider the particular case of an uniform magnetic field $\vec{B}$ along the positive 3-axis. We will perform calculations only in the Landau gauge.

Pions are described as quantum fluctuations, constructed through quark bubble summation in the frame of the random phase approximation (RPA) [145, 181]. For neutral pions, the polarization function is translational invariant since Schwinger phases cancel out, and it can be diagonalized by transforming to the usual momentum basis in Fourier space. In contrast, for charged pions Schwinger phases do not cancel and the polarization function

is not translational invariant. For simplicity, many works in the literature simply disregard the Schwinger phases, allowing for a diagonalization in the usual Fourier space [168, 169, 247]. In Ref. [222], the use of a derivative expansion approach has been proposed as an improved approximation to deal with this issue. Nevertheless, such an approach should be expected to be less reliable as the mass of the meson and/or the magnetic field increase. The aim of the present chapter is to introduce a method that allows us to fully take into account the translational-breaking effects introduced by the Schwinger phases. To that end, the treatment of charged pions will be carried out on the basis of the Ritus-type eigenfunction approach to magnetized relativistic systems, introduced in previous chapters, which allows for a proper diagonalization of the system.

As expected, it will be seen that for nonzero magnetic field the π^0 meson can still be treated as a pseudo Nambu-Goldstone boson, with the corresponding form factors satisfying various chiral relations. For definite parametrizations of the model, we will obtain numerical results for the aforementioned pion properties and compare them with previous calculations given in the literature. Results from this chapter are based on Refs. [233, 252, 253].

4.1 Pion masses

In contrast to the previous chapter were we worked in the framework of Minkowski space-time, we perform model calculations within the Euclidean metric as in chapter 2, replacing $x^0 = -ix_4$, $p^0 = -ip_4$ and $\gamma^0 = -i\gamma_4$. In this metric all indexes are down since their placement is irrelevant. Then, the Euclidean Lagrangian density for the NJL two-flavor model in the presence of an electromagnetic field is

$$\mathcal{L} \;=\; \bar{\psi}\left(-i\,\not{D} + m_c\right)\psi - G\left[(\bar{\psi}\,\psi)^2 + (\bar{\psi}\,i\gamma_5\vec{\tau}\,\psi)^2\right] \;, \tag{4.1}$$

where $\psi = (\psi_u, \psi_d)^T$ is the two-flavor quark field and m_c is the current quark mass, which is assumed to be equal for u and d quarks. The interaction between the fermions and the electromagnetic field $\mathcal{A}_\mu$ is driven by the covariant derivative $D_\mu = \partial_\mu - i\,\hat{Q}\mathcal{A}_\mu$, where $\hat{Q} = \mathrm{diag}(Q_u, Q_d)$ with $Q_u = 2e/3$ and $Q_d = -e/3$. We will consider the particular case of an uniform magnetic field $\vec{B}$ along the positive 3-axis. In the Landau gauge, $\mathcal{A}_\mu = Bx_1\,\delta_{\mu,2}$.

We already showed in subsection 2.3.1 how to proceed in this case, obtaining the gap equation in the mean field approximation. However, in order to make this chapter more self-contained for the reader convenience, we will outline the main steps repeating some of the formulas. Since we are interested in studying meson properties, it is convenient to bosonize the fermionic action, introducing scalar $\sigma(x)$ and pseudoscalar $\vec{\pi}(x)$ fields and integrating out the fermion fields. The bosonized Euclidean action – see Eq. (2.19) – can be written as

$$S_{\mathrm{bos}} \;=\; -\mathrm{Tr}\,\ln\mathcal{D} + \frac{1}{4G}\int d^4x\;\left[\sigma(x)\sigma(x) + \vec{\pi}(x)\cdot\vec{\pi}(x)\right] \;, \tag{4.2}$$

where Tr refers to a trace in all spaces; color, flavor, Dirac and coordinates. The fermionic operator reads

$$\mathcal{D}(x,x') \;=\; \delta^{(4)}(x-x')\,\left[-i\,\not{D} + m_c + \sigma(x) + i\,\gamma_5\,\vec{\tau}\cdot\vec{\pi}(x)\right] \;, \tag{4.3}$$

where a direct product to an identity matrix in color space is understood.

We proceed by expanding the bosonized action in powers of fluctuations $\delta\sigma(x)$ and $\delta\pi_i(x)$ around their corresponding mean field (MF) values. As usual, we assume that the field $\sigma(x)$ has a nontrivial translational invariant MF value $\bar{\sigma}$, while the vacuum expectation values of pseudoscalar fields are zero in order to keep the vacuum parity-invariant. Thus we write

$$\mathcal{D}(x,x') \;=\; \mathcal{D}_{\mathrm{MF}}(x,x') + \delta\mathcal{D}(x,x') \;. \tag{4.4}$$

The MF piece is flavor-diagonal. It can be written as

$$\mathcal{D}_{\rm MF}(x,x') \;=\; {\rm diag}\left(\mathcal{D}^u_{\rm MF}(x,x')\,,\,\mathcal{D}^d_{\rm MF}(x,x')\right)\,, \tag{4.5}$$

where

$$\mathcal{D}^f_{\rm MF}(x,x') \;=\; \delta^{(4)}(x-x')\left(-i\partial\!\!\!/ - Q_f A\!\!\!/ + M\right)\,. \tag{4.6}$$

The quark effective mass M is given by $M = m_c + \bar{\sigma}$. On the other hand, the operator $\delta\mathcal{D}$ was given in Eq. (2.25). Replacing Eq. (4.4) in the bosonized effective action and expanding in powers of the meson fluctuations around the MF values – see Eq. (2.26) – the action can be symbolically written as

$$S^{\rm bos} \;=\; S^{\rm bos}_{\rm MF} \,+\, S^{\rm bos}_{\rm quad} \,+\, \ldots \tag{4.7}$$

where the linear term vanishes.

In the previous expansion we have introduced the mean field quark propagators for each flavor $\mathcal{S}^f_{\rm MF}(x,x') = \left[\mathcal{D}^f_{\rm MF}(x,x')\right]^{-1}$, since $\mathcal{D}_{\rm MF}$ is diagonal in flavor space. Their explicit form can be written in different ways [52, 53]. For convenience we take the Schwinger form, given in Eqs. (2.66-2.68). We recall some shorthand notation: $s_f = {\rm sign}(Q_f B)$ and $B_f = |Q_f B|$; $\gamma_\perp = (\gamma_1,\gamma_2)$ and $\gamma_{\rm II} = (\gamma_3,\gamma_4)$; similarly $q_\perp = (q_1,q_2)$ and $q_{\rm II} = (q_3,q_4)$.

The zero order contribution in Eq. (2.26) gives the mean field approximation. The MF free energy $\Omega_{\rm MF} = S^{\rm bos}_{\rm MF}/V^{(4)}$ is given by Eq. (2.28). The fermion operator $\mathcal{D}_{\rm MF}$ can be diagonalized by transforming to Ritus space, resulting in expression (2.73) for $\Omega_{\rm MF}$. Minimizing the free energy with respect to M and using Schwinger parametrization to move to proper-time representation, we obtain the gap equation (2.74)

$$M \;=\; m_c + 2G\,{\rm Tr}\,\mathcal{S}_{\rm MF}(x,x') \;=\; m_c + 4GMN_c\left(\frac{I^{\rm B}_{1u}+I^{\rm B}_{1d}}{2}\right)\,, \tag{4.8}$$

where $I^{\rm B}_{1f}$ is a divergent integral, see (2.75). The contribution from each flavor arises independently because the magnetic field differentiates between particles of different charges. Regularization through the MFIR scheme leads to $I^{\rm B}_{1f} \to I^{\rm reg}_{1f}$, where

$$I^{\rm reg}_{1f} \;=\; I^{\rm vac}_1 + I^{\rm mag}_{1f}\,. \tag{4.9}$$

Namely, the divergent integral is separated into a finite magnetic field dependent contribution, given in Eq. (2.79), and a regularized vacuum ($B = 0$) piece which does depend on the regularization prescription. Choosing the standard procedure in which one introduces a 3D momentum cutoff Λ, we recover the expression given in Eq. (2.52).

On the other hand, the MF chiral condensate for each flavor is given by (2.76)

$$\phi_f \;=\; \langle \bar{f} f \rangle_B \;=\; -\frac{\Omega^{\rm bos}_{\rm MF}}{\delta m_f} \;=\; -\frac{N_c}{V^{(4)}}\,{\rm Tr}_{\rm D}\int d^4x\;\mathcal{S}^f_{\rm MF}(x,x) \;=\; -N_c M\, I^{\rm B}_{1f}\,. \tag{4.10}$$

After regularization using the MFIR scheme with a 3D cutoff, we obtain (2.80)

$$\phi^{\rm reg}_f \;=\; \phi^{\rm vac}_f + \phi^{\rm mag}_f\,, \qquad \begin{cases} \phi^{\rm vac}_f &= -N_c M\, I^{\rm vac}_1 \\ \phi^{\rm mag}_f &= -N_c M\, I^{\rm mag}_{1f} \end{cases}\,. \tag{4.11}$$

4.1.1 Pion polarization functions

The quadratic contribution in Eq. (4.7) is given by

$$S^{\rm bos}_{\rm quad} \;=\; \frac{1}{2}\sum_{P=\sigma,\pi^0,\pi^\pm}\int d^4x\,d^4x'\;\delta P(x)^*\left[\frac{\delta^{(4)}(x-x')}{2G} - J_P(x,x')\right]\delta P(x')\,, \tag{4.12}$$

where $\pi^\pm = (\pi_1 \mp i\pi_2)/\sqrt{2}$ and

$$\begin{aligned} J_{\pi^0}(x,x') \;&=\; N_c\sum_f {\rm Tr}_{\rm D}\left[\,\mathcal{S}^f_{\rm MF}(x,x')\,\gamma_5\,\mathcal{S}^f_{\rm MF}(x',x)\,\gamma_5\,\right]\,, \\ J_{\pi^-}(x,x') \;&=\; 2N_c\,{\rm Tr}_{\rm D}\left[\,\mathcal{S}^d_{\rm MF}(x,x')\,\gamma_5\,\mathcal{S}^u_{\rm MF}(x',x)\,\gamma_5\,\right]\,, \\ J_{\pi^+}(x,x') \;&=\; 2N_c\,{\rm Tr}_{\rm D}\left[\,\mathcal{S}^u_{\rm MF}(x,x')\,\gamma_5\,\mathcal{S}^d_{\rm MF}(x',x)\,\gamma_5\,\right]\,. \end{aligned} \tag{4.13}$$

The expression for J_σ is obtained from that of J_{π^0} replacing $\gamma_5 \to -i\,\mathbb{1}$. Since $J_{\pi^+}(x,x') = J_{\pi^-}(x',x)$, both charged pions have the same mass, and we can proceed by considering only the negatively charged pion π^-.

Before proceeding to each individual case, it is interesting to note some properties from general structure of the polarization functions, which can be studied through the general definition

$$c_{f,f'}(x,x') \;\equiv\; 2N_c\,{\rm Tr}_{\rm D}\left[\mathcal{S}^f_{\rm MF}(x,x')\,\gamma_5\,\mathcal{S}^{f'}_{\rm MF}(x',x)\,\gamma_5\,\right]\,, \tag{4.14}$$

for two quarks of flavors f and f'. We start by replacing into this expression the quark propagator of Eq. (2.66). This leads to

$$c_{f,f'}(x,x') \;=\; e^{i\Phi_P(x,x')}\int_v e^{iv(x-x')}\,c_{f,f'}(v)\,, \tag{4.15}$$

where $\Phi_P(x,x') = Q_P B(x_1+x'_1)(x_2-x'_2)/2$ involves the difference of flavor charges, $Q_P = Q_f - Q_{f'}$. Similarly to the quark propagator, the polarization function can also

be written as the product of a Schwinger phase and a gauge and translational invariant function. The gauge transformation properties of the polarization function are gathered in the Schwinger phase. The momentum function is given by

$$c_{f,f'}(v) \;=\; 2N_c \int_r \mathrm{Tr}_{\mathrm{D}} \left[\bar{\mathcal{S}}^f(r_+)\, \gamma_5\, \bar{\mathcal{S}}^{f'}(r_-)\, \gamma_5 \right] , \tag{4.16}$$

where $r_\pm = r \pm v/2$. Here $r = (q_f + q_{f'})/2$ and $v = q_f - q_{f'}$ are the average and difference of the quarks momenta q_f and $q_{f'}$.

We will perform the calculation in the most general possible scenario, assuming different quark masses (this will be relevant for the next chapter). To proceed, we first insert the quark propagators of Eq. (2.67) and take the Dirac trace

$$\begin{aligned} c_{f,f'}(v) \;=& 8N_c \int_r \int_0^\infty d\tau_1 \int_0^\infty d\tau_2 \; e^{-\tau_1 \Upsilon_f(\tau_1, r_+) - \tau_2 \Upsilon_f(\tau_2, r_-)} \Bigg[(1 + s_f s_{f'} t_{1f} t_{2f'}) \times \\ & \left(M_f M_{f'} + r_\parallel^2 - \frac{v_\parallel^2}{4} \right) + (1 - t_{1f}^2)(1 - t_{2f'}^2) \left(r_\perp^2 - \frac{v_\perp^2}{4} \right) \Bigg] . \end{aligned} \tag{4.17}$$

where we have defined $t_{1f} = \tanh(\tau_1 B_f)$ and $t_{2f'} = \tanh(\tau_2 B_{f'})$. By shifting variables according to $\tau_1 = yz$ and $\tau_2 = (1-y)z$, after some rearranging we arrive at

$$\begin{aligned} c_{f,f'}(v) \;=\; & 8N_c \int_0^\infty dz \int_0^1 dy \; z\, e^{-z\phi_0(v)} \int_r e^{-z\phi_1(r,v)} \Bigg[(1 + s_f s_{f'} t_f t_{f'}) \times \\ & \left(M_f M_{f'} + r_\parallel^2 - \frac{v_\parallel^2}{4} \right) + (1 - t_f^2)(1 - t_{f'}^2) \left(r_\perp^2 - \frac{v_\perp^2}{4} \right) \Bigg] . \end{aligned} \tag{4.18}$$

where now

$$t_f \;=\; \tanh(yzB_f) \,, \qquad t_{f'} \;=\; \tanh[(1-y)zB_{f'}] \,, \qquad t_\pm \;=\; \frac{t_f}{B_f} \pm \frac{t_{f'}}{B_{f'}} \,. \tag{4.19}$$

Moreover, we have defined the functions

$$\begin{aligned} \phi_0(v) \;&=\; yM_f^2 + (1-y)M_{f'}^2 + y(1-y)v_\parallel^2 + \frac{t_+^2 - t_-^2}{z\, t_+} \frac{v_\perp^2}{4} \,, \\ \phi_1(r,v) \;&=\; \left[r_\parallel - (1-2y)\frac{v_\parallel}{2} \right]^2 + \frac{t_+}{z} \left(r_\perp + \frac{t_-}{t_+} \frac{v_\perp}{2} \right)^2 . \end{aligned} \tag{4.20}$$

To perform the momentum integrals we make use of the following relations

$$\int_r e^{-z\phi_1(r,v)} = \frac{1}{16\pi^2\, z\, t_+}\,, \tag{4.21}$$

$$\int_r e^{-z\phi_1(r,v)}\, r_\parallel^2 = \left[\frac{1}{z} + (1-2y)^2\,\frac{v_\parallel^2}{4}\right]\frac{1}{16\pi^2\, z\, t_+}\,, \tag{4.22}$$

$$\int_r e^{-z\phi_1(r,v)}\, r_\perp^2 = \left[\frac{1}{t_+} + \left(\frac{t_-}{t_+}\right)^2\frac{v_\perp^2}{4}\right]\frac{1}{16\pi^2\, z\, t_+}\,. \tag{4.23}$$

Finally, a straightforward calculation leads to

$$c_{f,f'}(v_\perp^2, v_\parallel^2) = \frac{N_c}{2\pi^2}\int_0^\infty dz \int_0^1 dy\, \frac{e^{-z\phi_0(v)}}{t_+}\left\{(1 + s_f s_{f'} t_f t_{f'})\times \right.$$
$$\left. \left[M_f M_{f'} + \frac{1}{z} - y(1-y)v_\parallel^2\right] + (1-t_f^2)(1-t_{f'}^2)\left[\frac{1}{t_+} - \left(1 - \frac{t_-^2}{t_+^2}\right)\frac{v_\perp^2}{4}\right]\right\}. \tag{4.24}$$

We have remarked in the function dependence that, in the pion case, the invariant polarization function is only a function of $v_\perp^2$ and $v_\parallel^2$.

4.1.2 Neutral pion mass

For the calculation of pion masses, we start by the simpler case of the neutral pion π^0. Actually, the analysis of the π^0 pole mass in the presence of a magnetic field within the MFIR scheme has already been carried out in Refs. [161, 248]. However, in those works the authors use a representation of the quark propagator different from the Schwinger one in Eqs. (2.66-2.67). Thus, we find it opportune to verify that both representations lead to the same results for the π^0 mass. Moreover, it will serve us to highlight the differences with the treatment of the charged pion. The study of the σ sigma meson mass can be performed in an entirely equivalent way, and will not be considered here.

In the neutral case, the contributions of Schwinger phases to each term of the sum cancel out since they correspond to the same quark flavor. As a consequence, the polarization function is translational invariant because it depends only on the difference $x - x'$, which leads to the conservation of momentum. If we take now the Fourier transform of the π^0 fields to the momentum basis given in Eq. (2.41), the corresponding transform of the polarization function will be diagonal in momentum space. Thus, the π^0 contribution to

the quadratic action in the momentum basis can be written as

$$S_{\pi^0} \;=\; \frac{1}{2}\int_p \delta\pi^0(-p)\,\left[\frac{1}{2G} - J_{\pi^0}(p_\perp^2,p_\parallel^2)\right]\delta\pi^0(p)\,, \tag{4.25}$$

where the polarization function reads

$$J_{\pi^0}(p_\perp^2,p_\parallel^2) \;=\; \frac{c_{u,u}(p_\perp^2,p_\parallel^2)+c_{d,d}(p_\perp^2,p_\parallel^2)}{2}\,. \tag{4.26}$$

Here $c_{f,f}(p_\perp^2,p_\parallel^2)$ is obtained taking equal flavors in Eq. (4.24). Explicitly,

$$\begin{aligned} c_{f,f}(p_\perp^2,p_\parallel^2) \;=\; & \frac{N_c B_f}{2\pi^2}\int_0^1 dy\int_0^\infty dz\, e^{-z\left[M^2+y(1-y)p_\parallel^2\right]}\, e^{-\gamma_f(y,z)\frac{p_\perp^2}{B_f}}\,\times \\ & \left\{\left[M_f^2+\frac{1}{z}-y(1-y)p_\parallel^2\right]\coth(zB_f)+\frac{B_f}{\sinh^2(zB_f)}\left[1-\gamma_f(y,z)\,\frac{p_\perp^2}{B_f}\right]\right\}\,, \end{aligned} \tag{4.27}$$

where

$$\gamma_f(y,z) \;=\; \frac{\sinh(yzB_f)\sinh[(1-y)zB_f]}{\sinh(zB_f)}\,. \tag{4.28}$$

This expression can be also derived from Eq. (2.14) of Ref. [254].

As done at the MF level, we regularize the integral in Eq. (4.27) using the MFIR scheme. Specifically, we subtract the corresponding unregulated contribution in the $B=0$ limit, given by

$$c^0_{f,f}(p^2) \;=\; \frac{N_c}{2\pi^2}\int_0^\infty \frac{dz}{z}\int_0^1 dy\, e^{-z\left[M^2+y(1-y)\,p^2\right]}\left[M^2+\frac{2}{z}-y(1-y)\,p^2\right]\,, \tag{4.29}$$

and add it in a regularized form $c^{\rm vac}_{f,f}(p^2)$. The regularized flavor polarization function is then

$$c^{\rm reg}_{f,f}(p_\perp^2,p_\parallel^2) \;=\; c^{\rm vac}_{f,f}(p^2)+c^{\rm mag}_{f,f}(p_\perp^2,p_\parallel^2)\,, \tag{4.30}$$

where $c^{\rm mag}_{f,f}(p_\perp^2,p_\parallel^2)=c_{f,f}(p_\perp^2,p_\parallel^2)-c^0_{f,f}(p^2)$ and $c^{\rm vac}_{f,f}$ is chosen to be regularized using a 3D momentum cutoff scheme, as in the case of the gap equation. In that case one has

$$c^{\rm vac}_{f,f}(p^2) \;=\; 2N_c\left[I_1^{\rm vac}+p^2 I_2^{\rm vac}(p^2)\right]\,, \tag{4.31}$$

where $I_1^{\rm vac}$ and $I_2^{\rm vac}(p^2)$ are given in Eqs. (2.52) and (2.53), respectively. Choosing the frame in which the π^0 meson is at rest, its pole mass can be obtained by solving the equation

$$\frac{1}{2G} - J^{\rm reg}_{\pi^0}(0,-m^2_{\pi^0}) \;=\; 0\,. \tag{4.32}$$

For the calculation of the meson masses we can take $p_\perp^2 = 0$ and $p_\parallel^2 < 0$. Assuming $|p_\parallel| < 2M_f$, one can integrate by parts to write the magnetic piece of the $c_{f,f}$ functions in the form of Eq. (4.31)

$$c_{f,f}^{\rm mag}(p_\perp^2 = 0, p_\parallel^2) \;=\; 2N_c \left[I_{1f}^{\rm mag} + p_\parallel^2 \, I_{2f}^{\rm mag}(p_\parallel^2) \right] \,, \tag{4.33}$$

where $I_{1f}^{\rm mag}$ is given in Eq. (2.79) and

$$\begin{aligned} I_{2f}^{\rm mag}(p_\parallel^2) &= -\frac{B_f}{8\pi^2} \int_0^\infty dz \int_0^1 dy \, e^{-z[M^2 + y(1-y)p_\parallel^2]} \left[\coth(zB_f) - \frac{1}{zB_f} \right] \\ &= \frac{1}{8\pi^2} \int_0^1 dy \left[\psi(\bar{x}_f) - \ln(\bar{x}_f) + \frac{1}{2\bar{x}_f} \right] \,. \end{aligned} \tag{4.34}$$

Here, $\bar{x}_f = [M^2 + y(1-y)p_\parallel^2]/(2B_f)$ and $\psi(x)$ is the digamma function. It is interesting to note that this expression of $J_{\pi^0}^{\rm mag}(0, p_\parallel^2) = [c_{u,u}^{\rm mag}(0, p_\parallel^2) + c_{d,d}^{\rm mag}(0, p_\parallel^2)]/2$ is in agreement with the one obtained in Ref. [248], where the calculation has been done using an expansion in Landau levels for the quark propagators instead of considering the Schwinger form of Eq. (2.67). Since both calculations use the 3D cutoff regularization for the $B = 0$ piece, it is checked that different representations of the quark propagator lead to the same result for the (finite) magnetic dependent piece of the polarization function, as expected.

4.1.3 Charged pion mass

We turn now to the determination of charged pion masses. Contrary to the π^0 case, Schwinger phases do not cancel here due to the charge difference in the quark flavors involved. Therefore, the polarization function of Eq. (4.13) is not translational invariant, and consequently it will not become diagonal when transformed to the Fourier momentum basis. Instead, we expand the charged pion field as

$$\pi^\pm(x) \;=\; \sum\!\!\!\!\!\!\int_{\bar{p}} \mathcal{B}_{\bar{p}}^s(x) \, \pi^\pm(\bar{p}) \,, \tag{4.35}$$

where we have used the shorthand notation of Eq. (2.62). The Euclidean Ritus-type basis function $\mathcal{B}_{\bar{p}}^s(x)$ are given in Eq. (2.59) for the Landau gauge. Here, $\bar{p} = (\ell, p_2, p_3, p_4)$, where ℓ labels the charged meson Landau level, and $s = \text{sign}(Q_{\pi^\pm} B)$. The corresponding piece of the action then reads

$$S_{\pi^\pm} \;=\; \frac{1}{2} \sum\!\!\!\!\!\!\int_{\bar{p},\bar{p}'} \left(\delta\pi^\pm(\bar{p}) \right)^* \left[\frac{1}{2G} \, \hat{\delta}_{\bar{p},\bar{p}'} - J_{\pi^\pm}(\bar{p}, \bar{p}') \right] \delta\pi^\pm(\bar{p}') \,, \tag{4.36}$$

where from Eq. (4.15)

$$J_P(\bar{p},\bar{p}') \;=\; \int_v c_{f,f'}(v)\, h_P(\bar{p},\bar{p}',v)\;, \quad P=\pi^{\pm}\,, \tag{4.37}$$

which depends on the function $c_{f,f'}(v_\perp^2, v_\parallel^2)$ defined in Eq. (4.24) and on the spatial integral

$$h_P(\bar{p},\bar{p}',v) \;=\; \int d^4x\, d^4x'\, e^{i\Phi_P(x,x')}\, e^{iv(x-x')}\, \mathcal{B}^s_{\bar{p}}(x)^*\, \mathcal{B}^s_{\bar{p}'}(x')\,. \tag{4.38}$$

For $P=\pi^-$, $f=d$ and $f'=u$, while for $P=\pi^+$ flavors are interchanged, $f=u$ and $f'=d$.

Most of the coordinate integrals are trivial and provide deltas

$$\begin{aligned} h_P(\bar{p},\bar{p}',v) \;=\; & (2\pi)^6\, \delta^{(2)}(p_\parallel - v_\parallel) \sum_{i=2}^{4} \delta(p_i - p_i')\, N_\ell N_{\ell'}\, \frac{2}{B_P} \times \\ & \int dx_1\, e^{iv_1(x_1-x_1')} D_\ell(\beta_s) D_{\ell'}(\beta_s') \Big|_{x_1'=-x_1+\frac{2s}{B_P}(p_2-v_2)}\,, \end{aligned} \tag{4.39}$$

where $B_P = |Q_P B|$, $\beta_s = \sqrt{2B_P}\, x_1 - s\sqrt{2/B_P}\, p_2$ and $\beta_s' = \sqrt{2B_P}\, x_1' - s\sqrt{2/B_P}\, p_2$. In order to perform the remaining coordinate integral, we make use of the following property of the cylindrical parabolic functions

$$\begin{aligned} & \int d\psi\, e^{i\gamma\psi} D_\ell(\eta-\psi)\, D_{\ell'}(\eta+\psi) \;= \\ & \qquad \sqrt{2\pi}\, e^{-\frac{\gamma^2+\eta^2}{2}} \;\times\; \begin{cases} (-1)^\ell\, \ell!\, (i\gamma+\eta)^{\ell'-\ell}\; L_\ell^{\ell'-\ell}(\eta^2+\gamma^2) & \text{if } \ell' \geq \ell \\ (-1)^{\ell'}\, \ell'!\, (-i\gamma+\eta)^{\ell-\ell'}\; L_{\ell'}^{\ell-\ell'}(\eta^2+\gamma^2) & \text{if } \ell \geq \ell'\,. \end{cases} \end{aligned} \tag{4.40}$$

Taking polar coordinates $v_\perp = (\tilde{v}_\perp \cos\varphi, \tilde{v}_\perp \sin\varphi)$ we get (note that $\tilde{v}_\perp^2 = v_\perp^2$)

$$\begin{aligned} h_P(\bar{p},\bar{p}',v) \;=\; & (2\pi)^6\, \delta^{(2)}(p_\parallel - v_\parallel) \sum_{i=1}^{3} \delta(p_i - p_i')\, (-1)^{\ell'}\, e^{-\frac{v_\perp^2}{B_P}}\, \frac{4\pi}{B_P} \times \\ & \left(-\frac{2v_\perp^2}{B_P}\right)^{\frac{|\ell-\ell'|}{2}} e^{is(\ell-\ell')\varphi} \;\times\; \begin{cases} \sqrt{\dfrac{\ell!}{\ell'!}}\; L_\ell^{\ell'-\ell}\left(\dfrac{2v_\perp^2}{B_P}\right) & ,\; \ell' \geq \ell \\ \sqrt{\dfrac{\ell'!}{\ell!}}\; L_{\ell'}^{\ell-\ell'}\left(\dfrac{2v_\perp^2}{B_P}\right) & ,\; \ell \geq \ell' \end{cases}\,, \end{aligned} \tag{4.41}$$

where $L_n^a(x)$ are generalized Laguerre polynomials. The parallel Dirac delta $\delta^{(2)}(p_\parallel - v_\parallel)$ is a consequence of the translational invariance in the parallel directions, since Schwinger

phases do not depend on them. Now, according to Eq. (4.37), we have to perform the momentum integrals over v. The main point here is that $c_{f,f'}(v) = c_{f,f'}(v_\parallel^2, v_\perp^2)$ is actually a function of the squared parallel and perpendicular momenta, see Eq. (4.24). Therefore, the integration over the angle provides an extra delta function

$$\int_0^{2\pi} d\varphi \, e^{is(\ell-\ell')\varphi} \;=\; 2\pi \, \delta_{\ell,\ell'} \,, \tag{4.42}$$

which implies that the polarization function is diagonal in the chosen basis. In fact, we arrive at $J_P(\bar{p}, \bar{p}\,') \;=\; \hat{\delta}_{\bar{p},\bar{p}'} J_P(\ell, \Pi^2)$, where $\Pi^2 = (2\ell+1)B_P + p_\parallel^2$ is introduced for later convenience and

$$J_P(\ell, \Pi^2) \;=\; \int_0^\infty d\tilde{v}_\perp \, \tilde{v}_\perp \, \rho_\ell(\tilde{v}_\perp^2) \, c_{f,f'} \left(\tilde{v}_\perp^2, \Pi^2 - (2\ell+1)B_P \right) \,, \tag{4.43}$$

with

$$\rho_\ell(v_\perp^2) \;=\; (-1)^\ell \, \frac{2}{B_P} \, e^{-\frac{v_\perp^2}{B_P}} \, L_\ell\left(\frac{2v_\perp^2}{B_P} \right) \,. \tag{4.44}$$

Since

$$\int_0^\infty d\tilde{v}_\perp \, \tilde{v}_\perp \, \rho_\ell(\tilde{v}_\perp^2) \;=\; 1 \,, \tag{4.45}$$

$\rho_\ell(\tilde{v}_\perp^2)$ resembles a normalized distribution function for the perpendicular momenta. Using the explicit form of $c_{f,f'}(v_\parallel^2, v_\perp^2)$ given in Eq. (4.24) we can perform the last integral through the use of the following properties – see lines 6 and 7 of 7.414 of Ref. [255]

$$\begin{aligned} \int_0^\infty dx \, e^{-bx} \, L_\ell(x) \;&=\; \frac{(b-1)^\ell}{b^{\ell+1}} \,, \\ \int_0^\infty dx \, x \, e^{-bx} \, L_\ell(x) \;&=\; \frac{(b-1)^{\ell-2} \, (b-1-\ell)}{b^{\ell+2}} \,. \end{aligned} \tag{4.46}$$

Finally, one gets

$$\begin{aligned} J_P(\ell, \Pi^2) \;=\; \frac{N_c}{2\pi^2} \int_0^\infty dz \int_0^1 dy \, \frac{e^{-zM^2}}{\alpha_+} \, e^{-zy(1-y)\left[\Pi^2 - (2\ell+1)\, B_P\right]} \left(\frac{\alpha_-}{\alpha_+} \right)^\ell \times \\ \left\{ \left[M^2 + \frac{1}{z} - y(1-y)(\Pi^2 - (2\ell+1)\, B_P) \right] (1 + s_f \, s_{f'} \, t_f \, t_{f'}) + \right. \\ \left. \frac{(1-t_f^2)(1-t_{f'}^2)}{\alpha_+ \, \alpha_-} \, \left[\alpha_- + (\alpha_- - \alpha_+) \, \ell \right] \right\} , \end{aligned} \tag{4.47}$$

where t_f and $t_{f'}$ were defined in Eq. (4.19) while

$$\alpha_\pm \;=\; \frac{B_f\, t_{f'} + B_{f'}\, t_f \pm B_P\, t_f\, t_{f'}}{B_f\, B_{f'}}\,. \tag{4.48}$$

For the π^- case we have $B_{\pi^-} \equiv B_e = |eB|$, $f = d$, $f' = u$ and $s_u s_d = -1$. Regarding the π^+, exchanging $d \leftrightarrow u$ and shifting $y \to 1 - y$ one can show that $J_{\pi^+}(\ell, \Pi^2) = J_{\pi^-}(\ell, \Pi^2)$, which implies that both charged pions have the same mass, as expected from charge conservation.

As in the case of the neutral pion, the polarization function in Eq. (4.47) turns out to be divergent and has to be regularized. Once again, this can be done within the MFIR scheme. However, due to quantization in the 1-2 plane this requires some care, viz. the subtraction of the $B = 0$ contribution to the polarization function has to be carried out once the latter has been written in terms of the squared canonical momentum Π^2. Thus, the regularized π^- polarization function is given by

$$J^{\rm reg}_{\pi^-}(\ell, \Pi^2) \;=\; J^{\rm vac}_{\pi}(\Pi^2) + J^{\rm mag}_{\pi^-}(\ell, \Pi^2)\,, \tag{4.49}$$

where $J^{\rm vac}_{\pi}(\Pi^2)$ is given in Eq. (4.31) for the 3D cutoff regularization, replacing $p^2 \to \Pi^2$, and $J^{\rm mag}_{\pi^-}(\ell, \Pi^2) = J_{\pi^-}(\ell, \Pi^2) - J^0_{\pi}(\Pi^2)$, where the $B = 0$ term is given in Eq. (4.29) since in that limit $J^0_\pi(p^2) = c^0_{f,f}(p^2)$. Constructed this way, the magnetic field-dependent contribution is well behaved in the limit $z \to 0$ and therefore finite.

Given the regularized polarization function, we can now derive an equation for the π^- meson pole mass in the presence of the magnetic field. To do this, let us first consider a point-like pion. For such a particle, in Euclidean space, the two-point function will vanish (i.e., the propagator will have a pole) when $\Pi^2 = -m^2_{\pi^-}$. Therefore, in our framework the charged pion pole mass can be obtained for each Landau level ℓ by solving the equation

$$\frac{1}{2G} - J^{\rm reg}_{\pi^-}(\ell, -m^2_{\pi^-}) \;=\; 0\,. \tag{4.50}$$

While for a point-like pion m_{π^-} is a B-independent quantity (the π^- mass in vacuum), in the present model—which takes into account the internal quark structure of the pion—this pole mass turns out to depend on the magnetic field. Instead of dealing with this quantity, it has become customary in the literature to define the π^- "magnetic field-dependent mass" as the lowest quantum-mechanically allowed energy of the π^- meson (see e.g. Ref. [74]), namely

$$E_{\pi^-}(B) \;=\; \sqrt{m^2_{\pi^-} + (2\ell + 1)\, B_e + p_3^2}\,\Big|_{p_3=0,\,\ell=0} \;=\; \sqrt{m^2_{\pi^-} + B_e}\,. \tag{4.51}$$

Notice that this "mass" is magnetic field dependent even for a point-like particle. In fact,

owing to zero-point motion in the 1-2 plane, even for $\ell = 0$ the charged pion cannot be at rest in the presence of the magnetic field.

4.2 Pion field redefinition and quark-meson coupling constants

As usual, the pion field wave function has to be redefined. In the absence of an external magnetic field we have $\vec{\pi}(p) = Z_\pi^{1/2}\,\tilde{\vec{\pi}}(p)$, where Z_π is usually called the "wave function renormalization constant". It is defined by fixing the residue of the two-point function at the pion pole. One has

$$Z_\pi^{-1} \;=\; -\frac{\partial J_\pi(p^2)}{\partial p^2}\bigg|_{p^2=-m_\pi^2} \;\equiv\; g_{\pi qq}^{-2}\,, \tag{4.52}$$

where $J_\pi(p^2)$ is the polarization function. Then, in the vicinity of the pole, the action reads

$$S_\pi \;\simeq\; \frac{1}{2}\int \delta\tilde{\vec{\pi}}(-p)\,(p^2+m_\pi^2)\,\delta\tilde{\vec{\pi}}(p)\,. \tag{4.53}$$

As expected, the energy dispersion relation is isotropic in this context.

We consider now the situation in which the external magnetic field is present. For the neutral pion, as shown in Eq. (4.27), the polarization function $J^{\rm reg}_{\pi^0}(p_\perp^2, p_\parallel^2)$ depends in a different way on the perpendicular and parallel components of p. We expand the action in Eq. (4.25) around the pion pole ($p_\perp = 0$, $p_\parallel^2 = -m_{\pi^0}^2$), factorize out the parallel derivative, and redefine the pion field according to $\pi^0(p) = Z_\parallel^{1/2}\,\tilde{\pi}^0(p)$. This leads to

$$S_{\pi^0} \;\simeq\; \frac{1}{2}\int_p \delta\tilde{\pi}^0(-p)\,\left[u_{\pi^0}^2\,p_\perp^2 + p_\parallel^2 + m_{\pi^0}^2\right]\delta\tilde{\pi}^0(p)\,, \tag{4.54}$$

where we have defined

$$Z_\parallel^{-1} \;=\; -\frac{dJ^{\rm reg}_{\pi^0}}{dp_\parallel^2}\bigg|_{\substack{p_\perp^2\,=\,0\\ p_\parallel^2\,=\,-m_{\pi^0}^2}} \;\equiv\; g_{\pi^0qq}^{-2}\,, \qquad Z_\perp^{-1} \;=\; -\frac{dJ^{\rm reg}_{\pi^0}}{dp_\perp^2}\bigg|_{\substack{p_\perp^2\,=\,0\\ p_\parallel^2\,=\,-m_{\pi^0}^2}}\,, \qquad u_{\pi^0}^2 = \frac{Z_\parallel}{Z_\perp}\,. \tag{4.55}$$

Denoting $M_0(y) = [M^2 - y(1-y)m_{\pi^0}^2]^{1/2}$ and $M_\Lambda(y) = [\Lambda^2 + M_0(y)^2]^{1/2}$, from Eqs. (4.27-

2.53) we obtain

$$Z_{\parallel}^{-1}\,\frac{4\pi^2}{N_c} \;=\; -\,2\int_0^1 dy\,\left[\frac{\Lambda}{M_\Lambda(y)}+\ln\left(\frac{M_0(y)}{\Lambda+M_\Lambda(y)}\right)-\frac{\Lambda^3\,y(1-y)\,m_{\pi^0}^2}{2\,M_0(y)^2\,M_\Lambda(y)^3}\right]-$$
$$\sum_f\int_0^\infty dz\int_0^1 dy\,e^{-zM_0(y)^2}\,y(1-y)\,\times$$
$$\left\{\left[M^2+y(1-y)m_{\pi^0}^2+\frac{2}{z}\right]\left(1-\frac{zB_f}{\tanh(zB_f)}\right)+\frac{1}{z}-\frac{zB_f^2}{\sinh^2(zB_f)}\right\}, \quad (4.56)$$

and

$$Z_{\perp}^{-1}\,\frac{4\pi^2}{N_c} \;=\; -\,2\int_0^1 dy\,\left[\frac{\Lambda}{M_\Lambda(y)}+\ln\left(\frac{M_0(y)}{\Lambda+M_\Lambda(y)}\right)-\frac{\Lambda^3\,y(1-y)\,m_{\pi^0}^2}{2\,M_0(y)^2\,M_\Lambda(y)^3}\right]-$$
$$\sum_f\int_0^\infty dz\int_0^1 dy\,e^{-zM_0(y)^2}\left\{-\,\gamma_f(y,z)\left(\frac{1}{z\tanh(zB_f)}+\frac{2B_f}{\sinh^2(zB_f)}\right)+\right.$$
$$\left.\left[M^2+y(1-y)m_{\pi^0}^2\right]\left[y(1-y)-\frac{\gamma_f(y,z)}{\tanh(zB_f)}\right]+\frac{3y(1-y)}{z}\right\}, \quad (4.57)$$

where $\gamma_f(y,z)$ was defined in Eq. (4.28). It is seen that, owing to the pion internal structure, the energy dispersion relation is anisotropic in the presence of an external magnetic field. Namely, as already stated in Ref. [170], one has

$$E_{\pi^0}^2 \;=\; -p_4^2 \;=\; u_{\pi^0}^2\,p_\perp^2+p_3^2+m_{\pi^0}^2\,. \quad (4.58)$$

The direct comparison of our results for the renormalization constants with those quoted in Ref. [170] is not possible due to the fact that different regularization procedures were followed in each case (we use the MFIR scheme, while in Ref. [170] an ultraviolet cutoff is introduced). However, we have found some discrepancies between both results when comparing the corresponding unregularized expressions. We will come back to this point in section 4.5.

For charged pions, the momentum in the plane perpendicular to the external magnetic field is quantized in Landau levels ℓ. The energy dispersion relation reads in this case

$$E_{\pi^-}^2 \;=\; -p_4^2 \;=\; (2\ell+1)B_e+p_3^2+m_{\pi^-}^2\,. \quad (4.59)$$

The redefined (negative) charged pion field is given by $\pi^-(\bar{p}) = Z_{\pi^-}^{1/2}\,\tilde{\pi}^-(\bar{p})$, where

$$Z_{\pi^-}^{-1} \;=\; -\frac{dJ_{\pi^-}^{\rm reg}(\ell,\Pi^2)}{d\Pi^2}\bigg|_{\Pi^2=-m_{\pi^-}^2} \;\equiv\; g_{\pi^- qq}^{-2}\;. \tag{4.60}$$

Explicitly, denoting $M_-(y) = [M^2 - y(1-y)m_{\pi^-}^2]^{1/2}$ and $M_-^\Lambda(y) = [\Lambda^2 + M_-(y)^2]^{1/2}$, from Eq. (4.49) we find

$$\begin{aligned}
Z_{\pi^-}^{-1}\,\frac{2\pi^2}{N_c} \;=\; &-\int_0^1 dy\,\left[\frac{\Lambda}{M_-^\Lambda(y)} + \ln\left(\frac{M_-(y)}{\Lambda + M_-^\Lambda(y)}\right) - \frac{\Lambda^3\,y(1-y)\,m_{\pi^-}^2}{2\,M_-(y)^2\,M_-^\Lambda(y)^3}\right] + \\
&\int_0^\infty dz \int_0^1 dy\, e^{-zM_-(y)^2}\, z\,y(1-y)\Bigg\{\left[M^2 + y(1-y)\left(m_{\pi^-}^2 + (2\ell+1)B_e\right) + \frac{2}{z}\right]\times \\
&\left[\frac{\alpha_-^\ell}{\alpha_+^{\ell+1}}\,(1 - t_u\,t_d)\; e^{zy(1-y)(2\ell+1)B_e} - \frac{1}{z}\right] - \frac{1}{z}\left[\frac{1}{z} - y(1-y)(2\ell+1)B_e\right] + \\
&\frac{\alpha_-^{\ell-1}}{\alpha_+^{\ell+2}}\,(1-t_u^2)\,(1-t_d^2)\Big[\alpha_- + (\alpha_- - \alpha_+)\,\ell\Big]\; e^{zy(1-y)(2\ell+1)B_e}\Bigg\}\,.
\end{aligned} \tag{4.61}$$

Here, t_u and t_d are defined in Eq. (4.19) for $f = d$ and $f' = u$, while $\alpha_\pm$ are given in Eq. (4.48).

4.3 Pion-to-vacuum vector and axial vector amplitudes and weak decay constants

In order to obtain pion-to-vacuum vector and axial-vector amplitudes, we have to "gauge" the effective action by introducing a set of vector and axial vector gauge fields, $W_{\mu,V}^a(x)$ and $W_{\mu,A}^a(x)$, respectively. This is done by performing the replacement

$$\gamma_\mu\partial_\mu \;\to\; \gamma_\mu\partial_\mu - i\sum_{a=1}^{3}\frac{\tau^a}{2}\sum_{B=V,A}\Gamma_{\mu,B}\;W_{\mu,B}^a(x)\,, \tag{4.62}$$

where $B = V, A$ with $\Gamma_{\mu,V} = \gamma_\mu$ and $\Gamma_{\mu,A} = \gamma_\mu\gamma_5$. Once this extended gauged effective action is built, the corresponding pion-to-vacuum amplitudes are obtained as the derivative of this action with respect to $W_{\mu,B}^a(x)$ and the redefined meson fields, evaluated at $W_{\mu,B}^a(x) = 0$. Therefore, the relevant terms in the action are those linear in the pion and gauge fields. This piece of the action can be written as

$$S_{\pi W} \;=\; \sum_{B=V,A}\;\sum_{\kappa=\pm,3}\int d^4x\,d^4x'\;W_{\mu,B}^{-\kappa}(x)\,F_{\mu,B}^{\kappa}(x,x')\,\delta\pi^\kappa(x')\,, \tag{4.63}$$

where $W^{\pm}_{\mu,B} = (W^1_{\mu,B} \mp i\, W^2_{\mu,B})/\sqrt{2}$. The functions $F^{\kappa}_{\mu,B}(x,x')$ are defined as

$$F^3_{\mu,B}(x,x') \;=\; -\,\frac{i}{4}\sum_f c^{ff}_{\mu,B}(x,x')\,, \tag{4.64}$$

$$F^-_{\mu,B}(x,x') \;=\; -\,\frac{i}{2}\, c^{du}_{\mu,B}(x,x')\,, \tag{4.65}$$

$$F^+_{\mu,B}(x,x') \;=\; -\,\frac{i}{2}\, c^{ud}_{\mu,B}(x,x')\,, \tag{4.66}$$

where, in analogy with Eq. (4.14), we have defined the function

$$c^{f,f'}_{\mu,B}(x,x') \;=\; 2N_c\,\mathrm{Tr}_{\mathrm{D}}\left[\mathcal{S}^f_{\mathrm{MF}}(x,x')\,\gamma_5\,\mathcal{S}^{f'}_{\mathrm{MF}}(x',x)\,\Gamma_{\mu,B}\right]\,. \tag{4.67}$$

Proceeding as in Eqs. (4.14-4.18), this function can be expressed as the product of a Schwinger phase and a translational invariant function

$$c^{f,f'}_{\mu,B}(x,x') \;=\; e^{i\Phi_\pi(x,x')}\int_v e^{iv(x-x')}\,c^{f,f'}_{\mu,B}(v)\,, \tag{4.68}$$

where

$$c^{f,f'}_{\mu,B}(v) \;=\; 2N_c\int_r \mathrm{Tr}_{\mathrm{D}}\left[\bar{\mathcal{S}}^f(q+v/2)\,\gamma_5\,\bar{\mathcal{S}}^{f'}(q-v/2)\,\Gamma_{\mu,B}\right]\,. \tag{4.69}$$

The only difference remains in the calculation of the trace. From Eq. (4.18), we can write the momentum function in a general way as

$$c^{f,f'}_{\mu,B}(v) \;=\; 2N_c\int_0^\infty dz\int_0^1 dy\; z\, e^{-z\phi_0(v)}\int_r e^{-z\phi_1(r,v)}\;T_{\mu,B}(r,v)\,, \tag{4.70}$$

where $T_{\mu,B}(r,v)$ represents the corresponding traces, which can be found in App. A of Ref. [252]. Regarding the momentum integrals, besides Eq. (4.21) we only need

$$\int_r e^{-z\phi_1(r,v)}(r_1+i\epsilon\, r_2) \;=\; -\,\frac{t_-}{t_+}\,\frac{v_1+i\epsilon\, v_2}{2}\,\frac{1}{16\pi^2\, z\, t_+}\,, \tag{4.71}$$

Finally, defining the linear combinations ($\epsilon = \pm 1$)

$$\begin{aligned} c^{f,f',\epsilon}_{\parallel,B}(v) \;&=\; c^{f,f'}_{4,B}(v) + \epsilon\, c^{f,f'}_{3,B}(v)\,,\\ c^{f,f',\epsilon}_{\perp,B}(v) \;&=\; c^{f,f'}_{1,B}(v) + i\epsilon\, c^{f,f'}_{2,B}(v)\,, \end{aligned} \tag{4.72}$$

and assuming $M_f = M_{f'}$ we arrive at

$$\begin{aligned} c_{\parallel,V}^{f,f',\epsilon}(v) &= i\,\frac{N_c\,M}{2\pi^2}\int_0^\infty dz\int_0^1 dy\,e^{-z\phi_0(v)}\,\frac{s_f t_f + s_{f'} t_{f'}}{t_+}\,\epsilon\,v_\parallel^{-\epsilon}\,, \\ c_{\perp,V}^{f,f',\epsilon}(v) &= 0\,, \end{aligned} \tag{4.73}$$

and

$$\begin{aligned} c_{\parallel,A}^{f,f',\epsilon}(v) &= -\,\frac{N_c\,M}{2\pi^2}\int_0^\infty dz\int_0^1 dy\,e^{-z\phi_0(v)}\,\frac{1+s_f s_{f'} t_f t_{f'}}{t_+}\,v_\parallel^\epsilon\,, \\ c_{\perp,A}^{f,f',\epsilon}(v) &= -\,\frac{N_c\,M}{2\pi^2}\int_0^\infty dz\int_0^1 dy\,e^{-z\phi_0(v)}\,\times \\ &\qquad \frac{B_f t_{f'}(1-t_f^2)(1+\epsilon\,s_{f'}t_{f'}) + B_{f'} t_f (1-t_{f'}^2)(1-\epsilon\,s_f t_f)}{B_f B_{f'}\,t_+^2}\,v_\perp^\epsilon\,, \end{aligned} \tag{4.74}$$

where $v_\parallel^\epsilon = v_4 + \epsilon\,v_3$ and $v_\perp^\epsilon = v_1 + i\epsilon\,v_2$.

4.3.1 Neutral pion amplitudes and form factors

As in the analysis of the π^0 mass, we expand the neutral pion field in Eq. (4.63) in the Fourier basis. After redefining the pion field, pion-to-vacuum amplitudes read

$$\begin{aligned} H_{\mu,B}^0(x,\vec{p}) &= \langle 0|\bar{\psi}(x)\,\Gamma_{\mu,B}\,\frac{\tau^3}{2}\,\psi(x)|\tilde{\pi}^0(\vec{p})\rangle \;=\; -\,\frac{\partial S_{\pi W}}{\partial\delta\tilde{\pi}^0(p)\,\partial W_{\mu,B}^3(x)} \\ &= -\,Z_\parallel^{1/2}\int d^4x'\,e^{ipx'}\,F_{\mu,B}^3(x,x')\,. \end{aligned} \tag{4.75}$$

Using Eqs. (4.64) and (4.68), and taking into account that Schwinger phases cancel out in this case, after integrating over x' we get

$$H_{\mu,B}^0(x,\vec{p}) \;=\; \frac{i}{4}\,Z_\parallel^{1/2}\,e^{ipx}\sum_f c_{\mu,B}^{ff}(p)\,. \tag{4.76}$$

For convenience, we consider the linear combinations of Eq. (4.72). Using the relations of Eqs. (4.73) and (4.74), after a straightforward calculation we obtain

$$\begin{aligned} H_{\parallel,V}^{0,\epsilon}(x,\vec{p}) &= -\,\epsilon\,p_\parallel^{-\epsilon}\,e^{ipx}\sum_f s_f\int_0^\infty dz\int_0^1 dy\,\mathcal{F}^0(y,z)\,, \\ H_{\perp,V}^{0,\epsilon}(x,\vec{p}) &= 0\,, \end{aligned} \tag{4.77}$$

and

$$
\begin{aligned}
H^{0,\epsilon}_{\parallel,A}(x,\vec{p}) &= -i\, p^{\epsilon}_{\parallel}\, e^{ipx} \sum_f \int_0^\infty dz \int_0^1 dy\, \mathcal{F}^0(\vec{p},y,z)\, \coth(zB_f)\,, \\
H^{0,\epsilon}_{\perp,A}(x,\vec{p}) &= -i\, p^{\epsilon}_{\perp}\, e^{ipx} \sum_f \int_0^\infty dz \int_0^1 dy\, \mathcal{F}^0(\vec{p},y,z)\, \frac{\cosh[(2y-1)zB_f]}{\sinh(z\,B_f)}\,,
\end{aligned}
\tag{4.78}
$$

where we have defined $p^{\epsilon}_{\parallel} = p_4 + \epsilon\, p_3$, $p^{\epsilon}_{\perp} = p_1 + i\epsilon\, p_2$ and

$$
\mathcal{F}^0(\vec{p},y,z) = Z_{\parallel}^{1/2}\, \frac{N_c M}{8\pi^2}\, B_f\, e^{-z\left[M^2 + y(1-y)p_{\parallel}^2\right]}\, e^{-\gamma_f(y,z)\frac{p_\perp^2}{B_f}}\,. \tag{4.79}
$$

Now, following the notation of Eq. (3.45), we define the neutral pion decay form factors as

$$
\begin{aligned}
H^{0,\epsilon}_{\parallel,V}(x,\vec{p}) &= -\epsilon\, p_{\parallel}^{-\epsilon}\, e^{ipx}\, f^{(V)}_{\pi^0}\,, \\
H^{0,\epsilon}_{\parallel,A}(x,\vec{p}) &= -i\, p^{\epsilon}_{\parallel}\, e^{ipx} f^{(A1)}_{\pi^0}\,, \\
H^{0,\epsilon}_{\perp,A}(x,\vec{p}) &= -i\, p^{\epsilon}_{\perp}\, e^{ipx} \left[f^{(A1)}_{\pi^0} - \epsilon\, f^{(A2)}_{\pi^0} - f^{(A3)}_{\pi^0} \right]\,.
\end{aligned}
\tag{4.80}
$$

Note that, since we are working in Euclidean space, the relations $H_4 = iH^0$ and $p_4 = ip^0$ need to be considered when comparing with the expressions in Eq. (3.45). In this way, for an on-shell pion in its rest frame, i.e. taking $p_\mu = i m_{\pi^0}\delta_{\mu 4}$, the axial decay constants are given by

$$
\begin{aligned}
f^{(A1)}_{\pi^0} &= Z_{\parallel}^{1/2}\, \frac{N_c M}{8\pi^2} \sum_f \int_0^\infty dz \int_0^1 dy\, e^{-zM_0(y)^2}\, \frac{B_f}{\tanh(zB_f)}\,, \\
f^{(A2)}_{\pi^0} &= 0\,, \\
f^{(A3)}_{\pi^0} &= Z_{\parallel}^{1/2}\, \frac{N_c M}{8\pi^2} \sum_f 2\, B_f \int_0^\infty dz \int_0^1 dy\, e^{-zM_0(y)^2}\, \gamma_f(y,z)\,,
\end{aligned}
\tag{4.81}
$$

while the vector decay constant reads

$$
f^{(V)}_{\pi^0} = Z_{\parallel}^{1/2} \frac{N_c M}{8\pi^2} \sum_f s_f B_f \int_0^\infty dz \int_0^1 dy\, e^{-zM_0(y)^2}\,. \tag{4.82}
$$

We recall that $M_0(y) = [M^2 - y(1-y)m_{\pi^0}^2]^{1/2}$ and $\gamma_f(y,z)$ is defined in Eq. (4.28). It is seen that $f^{(A2)}_{\pi^0}$ vanishes, as indicated from the general analysis of Appendix B. Thus, we find that in the presence of the external magnetic field there are in general two axial and one vector nonvanishing form factors for the neutral pion. Notice that in the chosen frame both $H^{0,\epsilon}_{\perp,V}$ and $H^{0,\epsilon}_{\perp,A}$ are zero, hence $f^{(A3)}_{\pi^0}$ will not contribute to the amplitudes.

It can be easily seen that $f_{\pi^0}^{(A3)}$ and $f_{\pi^0}^{(V)}$ are finite and vanish in the $B \to 0$ limit. On the contrary, the expression for $f_{\pi^0}^{(A1)}$ in Eq. (4.81) is divergent. It can be regularized in the context of the MFIR scheme, i.e., subtracting the corresponding divergent contribution in the $B = 0$ limit, f_π^0, and adding it in a regularized form, $f_{\pi^0}^{\rm vac}$. One has

$$f_{\pi^0}^{(A1),\rm reg} \;=\; f_{\pi^0}^{\rm vac} + f_{\pi^0}^{(A1),\rm mag}\,, \tag{4.83}$$

where $f_{\pi^0}^{(A1),\rm mag} = f_{\pi^0}^{(A1)} - f_\pi^0$. The divergent $B = 0$ piece,

$$f_\pi^0 \;=\; Z_\pi^{1/2}\,\frac{N_c M}{4\pi^2}\int_0^\infty dz \int_0^1 \frac{dy}{z}\, e^{-zM_0(y)^2}\,, \tag{4.84}$$

can be regularized using a 3D momentum cutoff scheme, as done in the previous subsections. One has in this way

$$f_{\pi^0}^{\rm vac} \;=\; -2\,Z_{||}^{1/2} N_c M I_2^{\rm vac}(-m_{\pi^0}^2)\,, \tag{4.85}$$

where $I_2^{\rm vac}$ is given in Eq. (2.53). Note that we do not take the $B \to 0$ limit in $Z_{||}$ (strictly, one should first regularize the form factor and then redefine the pion wave function).

Finally, we find it convenient to define "parallel" and "perpendicular" axial decay constants $f_{\pi^0}^{(A||)}$ and $f_{\pi^0}^{(A\perp)}$, given in terms of $f_{\pi^0}^{(A1),\rm reg}$ and $f_{\pi^0}^{(A3)}$ according to

$$f_{\pi^0}^{(A||)} \;=\; f_{\pi^0}^{(A1),\rm reg}\,, \qquad\qquad f_{\pi^0}^{(A\perp)} \;=\; f_{\pi^0}^{(A1),\rm reg} - f_{\pi^0}^{(A3)}\,. \tag{4.86}$$

Our expressions for the π^0 decay constants, taken before any regularization scheme is applied, can be compared with those obtained in Ref. [170]. Although, as mentioned in the previous subsection, we have found some discrepancies in the results for the renormalization constants, it can be checked that the ratios $f_{\pi^0}^{(A||)}/g_{\pi^0 qq}$ and $f_{\pi^0}^{(A\perp)}/g_{\pi^0 qq}$ are in agreement with those quoted in Ref. [170], once different notations have been properly compatibilized.

4.3.2 Charged pion amplitudes and form factors

As in the case of the polarization functions, we expand the charged pion fields using Eq. (4.35). Since charged decay constants are real and equal for both charged pions (see Appendix B), it is sufficient to consider the π^- hadronic amplitudes

$$\begin{aligned} H_{\mu,B}^-(x,\breve{p}) \;&=\; \langle 0|\bar\psi\,\Gamma_{\mu,B}\,\tau^+\,\psi|\tilde\pi^-(\breve{p})\rangle \;=\; -\sqrt{2}\,\frac{\partial S_{\pi W}}{\partial\delta\tilde\pi_{\bar p}^-\,\partial W_{\mu,B}^+(x)} \\ &=\; -\sqrt{2}\,Z_{\pi^-}^{1/2}\int_{x'}\mathcal{B}_{\bar p}^s(x')\,F_{\mu,B}^-(x,x')\,. \end{aligned} \tag{4.87}$$

We recall that $\bar{p} = (\ell, p_2, p_3, p_4) = (\breve{p}, p_4)$, see also Table 3.1, and $s = \text{sign}(Q_{\pi^-} B)$. From Eqs. (4.65) and (4.68) we have

$$H^-_{\mu,B}(x,\breve{p}) \;=\; \frac{i}{\sqrt{2}}\, Z^{1/2}_{\pi^-} \int d^4x'\; \mathcal{B}^s_{\bar{p}}(x')\, e^{i\Phi_{\pi^-}(x,x')} \int_v e^{iv(x-x')}\, c^{du}_{\mu,B}(v)\,, \tag{4.88}$$

which resembles the form of expression (4.37). Integrating first over x' some Dirac deltas appear, leading to

$$H^-_{\mu,C}(x,\breve{q}) = i\frac{4\pi N_\ell}{\sqrt{2}B_e}\, Z^{1/2}_{\pi^-}\, e^{ip_2x_2+ip_{||}x_{||}} \int_{v_\perp} c^{du}_{\mu,B}(v)\, e^{iv_1(x_1-x_1')} D_\ell(\beta_s')\Big|_{\substack{v_{||}=p_{||}\\ x_1'=-x_1+\frac{2s}{B_e}(p_2-v_2)}}\,, \tag{4.89}$$

where we recall $\beta_s' = \sqrt{2B_e}\, x_1' - s\sqrt{2/B_e}\, p_2$. The remaining momentum integrals can be performed with the aid of the following relations, which can be derived from property 7.724 of Ref. [255]

$$\begin{aligned}
\int_{v_\perp} v_\perp^\epsilon\, \mathcal{D}_\ell(x_1,p_2,v_\perp)\, e^{-\gamma v_\perp^2} \;&=\; -is\epsilon\frac{\sqrt{2}B_e^{3/2}}{4\pi}\,\frac{(1-\gamma B_e)^\ell}{(1+\gamma B_e)^{\ell+1}}\,\frac{\ell^{\frac{1+s\epsilon}{2}}}{(1-s\epsilon\gamma B_e)}\, D_{\ell-s\epsilon}(\beta_s)\,,\\
\int_{v_\perp} \mathcal{D}_\ell(x_1,p_2,v_\perp)\, e^{-\gamma v_\perp^2} \;&=\; \frac{B_e}{4\pi}\,\frac{(1-\gamma B_e)^\ell}{(1+\gamma B_e)^{\ell+1}}\, D_\ell(\beta_s)\,,
\end{aligned} \tag{4.90}$$

where $\beta_s = \sqrt{2B_e}\, x_1 - s\sqrt{2/B_e}\, p_2$ and

$$\mathcal{D}_\ell(x_1,p_2,v_\perp) \;=\; e^{2iv_1\left(x_1+s\frac{v_2-p_2}{B_e}\right)}\, D_\ell\left[-\sqrt{2B_e}\, x_1 + s\sqrt{\frac{2}{B_e}}\,(p_2-2v_2)\right]\,. \tag{4.91}$$

For our case, from $\phi_0(v)$ in Eq. (4.20) we have $\gamma = t_+(1-t_-^2/t_+^2)/4$.

For convenience, as in the π^0 case we concentrate on the linear combinations $H^{-,\epsilon}_{||,B}$ and $H^{-,\epsilon}_{\perp,B}$, defined as in Eq. (4.72). After some algebra one arrives at

$$\begin{aligned}
H^{-,\epsilon}_{||,A}(x,\breve{p}) \;&=\; -\,i\,\sqrt{2}\; p_{||}^\epsilon\; \mathcal{B}^s_{\bar{p}}(x) \int_0^\infty dz \int_0^1 dy\; \mathcal{F}^-(\breve{p},y,z)\,(1-t_ut_d)\,,\\
H^{-,\epsilon}_{\perp,A}(x,\breve{p}) \;&=\; -\,s\epsilon\,\sqrt{2}\,\sqrt{(2\ell+1-s\epsilon)B_e}\; \mathcal{B}^s_{\bar{p}-s\epsilon}(x)\,\times\\
&\qquad \int_0^\infty dz \int_0^1 dy\; \mathcal{F}^-(\breve{p},y,z)\,\left(\frac{\alpha_-}{\alpha_+}\right)^{-s\epsilon}\,(1+\epsilon\, s_ut_u)(1-\epsilon\, s_dt_d)\,,\\
H^{-,\epsilon}_{||,V}(x,\breve{p}) \;&=\; -\,\epsilon\,\sqrt{2}\; p_{||}^{-\epsilon}\; \mathcal{B}^s_{\bar{p}}(x) \int_0^\infty dz \int_0^1 dy\; \mathcal{F}^-(\breve{p},y,z)\,(s_ut_u - s_dt_d)\,,\\
H^{-,\epsilon}_{\perp,V}(x,\breve{p}) \;&=\; 0\,,
\end{aligned} \tag{4.92}$$

where $s_d = -s_u = s$ and

$$\mathcal{F}^{-}(\breve{p}, y, z) \;=\; Z_{\pi^-}^{1/2}\,\frac{N_c M}{4\pi^2}\,\frac{\alpha_-^{\ell}}{\alpha_+^{\ell+1}}\,e^{-z[M^2+y(1-y)p_{\parallel}^2]}\,. \tag{4.93}$$

We recall the shorthand notation $\bar{p}+\epsilon = (\ell+\epsilon, p_2, p_3, p_4)$ and $p_{\parallel}^{\epsilon} = p_4 + \epsilon\, p_3$.

As in the neutral pion case we follow the notation of Eq. (3.48), defining the charged pion decay constants in Euclidean space as

$$\begin{aligned}
H^{-;\epsilon}_{\parallel,A}(x,\breve{p}) \;&=\; -\,i\,\sqrt{2}\,f_{\pi^-}^{(A1)}\;p_{\parallel}^{\epsilon}\;\;\mathcal{B}^{s}_{\bar{p}}(x)\,,\\
H^{-;\epsilon}_{\perp,A}(x,\breve{p}) \;&=\; -\,s\epsilon\,\sqrt{2}\,\left[f_{\pi^-}^{(A1)} - s\epsilon\,f_{\pi^-}^{(A2)} - f_{\pi^-}^{(A3)}\right]\sqrt{(2\ell+1-s\epsilon)B_e}\;\mathcal{B}^{s}_{\bar{p}-s\epsilon}(x)\,.\\
H^{-;\epsilon}_{\parallel,V}(x,\breve{p}) \;&=\; -\,\epsilon\,\sqrt{2}\;f_{\pi^-}^{(V)}\;p_{\parallel}^{-\epsilon}\;\mathcal{B}^{s}_{\bar{p}}(x)\,,
\end{aligned} \tag{4.94}$$

From Eqs. (4.92) and (4.94), evaluating at the pion mass $p_{\parallel}^2 + (2\ell+1)B_e = -m_{\pi^-}^2$ we obtain

$$\begin{aligned}
f_{\pi^-}^{(A1)} \;&=\; Z_{\pi^-}^{1/2}\int_0^{\infty}dz\int_0^1 dy\;\frac{N_c M}{4\pi^2}\,\frac{\alpha_-^{\ell}}{\alpha_+^{\ell+1}}\,e^{-z\{M^2-y(1-y)[m_{\pi^-}^2+(2\ell+1)B_e]\}}\,(1-t_u\,t_d)\,,\\
f_{\pi^-}^{(A2)} \;&=\; Z_{\pi^-}^{1/2}\int_0^{\infty}dz\int_0^1 dy\;\frac{N_c M}{4\pi^2}\,\frac{\alpha_-^{\ell}}{\alpha_+^{\ell+1}}\,e^{-z\{M^2-y(1-y)[m_{\pi^-}^2+(2\ell+1)B_e]\}}\,\times\\
&\qquad\left[\frac{\alpha_-}{2\alpha_+}(1+t_u)(1+t_d) - \frac{\alpha_+}{2\alpha_-}(1-t_u)(1-t_d)\right]\,,\\
f_{\pi^-}^{(A3)} \;&=\; Z_{\pi^-}^{1/2}\int_0^{\infty}dz\int_0^1 dy\;\frac{N_c M}{4\pi^2}\,\frac{\alpha_-^{\ell}}{\alpha_+^{\ell+1}}\,e^{-z\{M^2-y(1-y)[m_{\pi^-}^2+(2\ell+1)B_e]\}}\,\times\\
&\qquad\left[1-t_u\,t_d - \frac{\alpha_-}{2\alpha_+}(1+t_u)(1+t_d) - \frac{\alpha_+}{2\alpha_-}(1-t_u)(1-t_d)\right]\,,\\
f_{\pi^-}^{(V)} \;&=\; Z_{\pi^-}^{1/2}\int_0^{\infty}dz\int_0^1 dy\;\frac{N_c M}{4\pi^2}\,\frac{\alpha_-^{\ell}}{\alpha_+^{\ell+1}}\,e^{-z\{M^2-y(1-y)[m_{\pi^-}^2+(2\ell+1)B_e]\}}\,(s_u t_u - s_d t_d)\,.
\end{aligned} \tag{4.95}$$

In the $B \to 0$ limit we have $Z_{\pi^-} \to Z_\pi$ and $f_{\pi^-}^{(A1)} \to f_\pi^0$, the latter given by Eq. (4.84). Meanwhile, $f_{\pi^-}^{(A2)}$, $f_{\pi^-}^{(A3)}$ and $f_{\pi^-}^{(V)}$ are finite and vanish in the limit $B \to 0$. Therefore, as expected, both neutral and charged pion weak form factors tend to the usual pion decay constant in the absence of the external field.

Once again, the expression for $f_{\pi^-}^{(A1)}$ in Eq. (4.95) is divergent and needs to be regularized. Using a 3D cutoff within the MFIR scheme, the regularized expression reads

$$f_{\pi^-}^{(A1),\mathrm{reg}} \;=\; f_{\pi^-}^{\mathrm{vac}} + f_{\pi^-}^{(A1),\mathrm{mag}}\,, \tag{4.96}$$

where $f_{\pi^-}^{(A1),\mathrm{mag}} = f_{\pi^-}^{(A1)} - f_\pi^0$, see Eq. (4.84) for the $B = 0$ expression, and

$$f_{\pi^-}^{\mathrm{vac}} \;=\; -2\, Z_{\pi^-}^{1/2}\, N_c\, M\, I_2^{\mathrm{vac}}(-m_{\pi^-}^2)\,, \tag{4.97}$$

with $I_2^{\mathrm{vac}}(p^2)$ given by Eq. (2.53).

As in the case of the neutral pion, we find it convenient to introduce parallel and perpendicular π^- axial decay form factors. Thus, we define one parallel and two perpendicular decay constants, according to

$$f_{\pi^-}^{(A\parallel)} \;=\; f_{\pi^-}^{(A1),\mathrm{reg}}\,, \qquad\qquad f_{\pi^-}^{(A\perp\pm)} \;=\; f_{\pi^-}^{(A1),\mathrm{reg}} \pm f_{\pi^-}^{(A2)} - f_{\pi^-}^{(A3)}\,. \tag{4.98}$$

It is worth noticing that if the pion lies on the lowest Landau level, i.e. $\ell = 0$, from Eq. (4.94) one has $H_{\perp,A}^{-,-}(x,\breve{p}) = 0$, hence in that case the π^- weak decay amplitude will not depend on $f_{\pi^-}^{(A\perp-)}$. In fact, strictly speaking, for $\ell = 0$ one cannot determine $f_{\pi^-}^{(A\perp-)}$ from Eqs. (4.92) and (4.94).

The π^+ decay constants can be obtained following a similar procedure. As stated in Appendix B, one can check that $f_{\pi^+}^{(j)} = f_{\pi^-}^{(j)}$, where $j = V, A1, A2, A3$. Moreover, by changing $B \to -B$ one can check that

$$\begin{aligned} f_{\pi^\pm}^{(V)}(\ell,B) \;&=\; -\, f_{\pi^\pm}^{(V)}(\ell,-B)\,, \\ f_{\pi^\pm}^{(Ai)}(\ell,B) \;&=\; f_{\pi^\pm}^{(Ai)}(\ell,-B)\,, \qquad i = 1,2,3\,. \end{aligned} \tag{4.99}$$

4.4 Chiral limit relations

It is interesting to discuss the relations satisfied by the quantities studied in the previous section in the chiral limit, i.e., for $m_c \to 0$. First, it should be stressed that even in the presence of an external magnetic field, the neutral pion remains being a pseudo-Nambu-Goldstone (NG) boson. This can be shown by taking into account the polarization function $J_{\pi^0}^{\mathrm{reg}}(p_\parallel^2, p_\perp^2)$ evaluated at $p_\parallel^2 = p_\perp^2 = 0$. After integration by parts it is seen that $J_{\pi^0}^{\mathrm{mag}}(0,0) \;=\; 2N_c\, I_1^{\mathrm{mag}}$, where I_1^{mag} is given by the average of Eq. (2.79). Hence, from Eqs. (4.9), (2.52) and (4.31) one gets

$$J_{\pi^0}^{\mathrm{reg}}(0,0) \;=\; 2N_c\, I_1^{\mathrm{reg}}\,. \tag{4.100}$$

Now, taking into account this result together with the (regularized) gap equation (2.34), in the chiral limit one gets $J_{\pi^0}^{\mathrm{reg}}(0,0)_{\mathrm{ch}} = 1/(2G)$, which implies $m_{\pi^0,\,\mathrm{ch}} = 0$. In this way, associated chiral relations are expected to hold even for nonzero B.

From the expressions for the renormalization constants, Eqs. (4.56-4.57), and the axial

form factors, Eq. (4.81), it is seen that the parallel and perpendicular axial decay constants for the π^0 meson introduced in Eq. (4.86) satisfy the generalized Goldberger-Treiman relations

$$g_{\pi^0 qq}\, f_{\pi^0}^{(A||)} \;=\; M_{\rm ch} + \mathcal{O}(m_{\pi^0}^2)\,, \tag{4.101}$$

$$g_{\pi^0 qq}\, f_{\pi^0}^{(A\perp)} \;=\; u_{\pi^0,\,\rm ch}^2\, M_{\rm ch} + \mathcal{O}(m_{\pi^0}^2)\,. \tag{4.102}$$

Thus, in the chiral limit one has [170]

$$f_{\pi^0,\,\rm ch}^{(A\perp)} \;=\; u_{\pi^0,\,\rm ch}^2\, f_{\pi^0,\,\rm ch}^{(A||)}\,. \tag{4.103}$$

In fact, this equation can be readily obtained from a general effective low energy action for NG bosons in the presence of a magnetic field, see e.g. Ref. [103]. Making use of Eq. (4.101), together with the gap equation, one obtains the generalized Gell-Mann-Oakes-Renner relation [234]

$$\left(m_{\pi^0}\, f_{\pi^0,\,\rm ch}^{(A||)}\right)^2 \;=\; -\,2m_c\,\frac{\langle\bar{u}u+\bar{d}d\rangle_{\rm ch}}{2}\,, \tag{4.104}$$

where we have taken into account that in our model the averaged quark condensate satisfies $\langle\bar{u}u+\bar{d}d\rangle/2 = -M_{\rm ch}/(4G) + \mathcal{O}(m_c)$. Note that a similar relation can be found for $f_{\pi^0,\,\rm ch}^{(A\perp)}$ using Eq. (4.103).

It is also interesting to consider the expression for $f_{\pi^0}^{(V)}$ in the chiral limit. From Eqs. (4.82) and (4.101) it is seen that for $m_c \to 0$ one has

$$f_{\pi^0,\,\rm ch}^{(V)} \;=\; \frac{B_e}{8\pi^2 f_{\pi^0,\,\rm ch}^{(A||)}}\,. \tag{4.105}$$

This relation —to the best of our knowledge—has not been previously stated in the literature. It is worth noticing it can be obtained from the anomalous Wess-Zumino-Witten (WZW) effective Lagrangian [256, 257]. The WZW term that couples a neutral pion to an electromagnetic field and a vector field $W_{\mu,V}^3$ is given by

$$\mathcal{L}_{WZW}\Big|_{\pi^0 A W^V} = \frac{i\,N_c\,e}{48\pi^2 f_\pi}\;\pi^0\,\epsilon_{\mu\nu\alpha\beta}\,\partial_\mu W_{\nu,V}^3\,F_{\alpha\beta}\,, \tag{4.106}$$

where $\epsilon_{4123} = 1$. If one identifies the constant f_π in this effective Lagrangian with $f_{\pi^0}^{(A||)}$, and the electromagnetic field tensor with the external magnetic field ($F_{12} = -F_{21} = B$), taking into account the definitions in Eq. (4.80) one arrives at the chiral relation in Eq. (4.105).

In the case of charged pions, the presence of an external magnetic field leads to the explicit breakdown of chiral symmetry and, in general, $\pi^\pm$ cannot be identified with NG bosons. However, chiral relations should be recovered in the limit of low B. In particular,

	m_c (MeV)	$g = G\Lambda^2$	Λ (MeV)	$-\langle u\bar{u}\rangle^{1/3}$ (MeV)	M (MeV)
Set I	5.6616	2.2501	613.39	243.26	350
Set II	5.4192	2.1364	639.49	246.91	320
Set III	5.7921	2.3642	596.11	241.36	380

Table 4.1: Parameters sets for the two-flavor NJL model.

the coupling of charged pions to the magnetic field and an external vector current arising from the WZW Lagrangian has the same form of Eq. (4.106), taking the $i = 1, 2$ isospin components of the fields π^i and $W^i_{\mu,V}$.

4.5 Numerical results

For definiteness, we consider $B > 0$ and only π^- for the charged pions. Therefore $s_u = -s_d = -s = +1$. In order to obtain numerical results for the different pion properties one has to fix the model parametrization. In addition to the usual requirements for the description of low-energy phenomenological properties, such as the pion mass and decay constant, we find it adequate to choose a parameter set that takes into account LQCD results for the behavior of quark-antiquark condensates under an external magnetic field.

In order to compare with LQCD results given in Refs. [73] we introduce the quantities

$$\Delta\bar{\Sigma}(B) \equiv \frac{\Delta\Sigma_u(B) + \Delta\Sigma_d(B)}{2}\,, \qquad \Sigma^-(B) = \Delta\Sigma_u(B) - \Delta\Sigma_d(B)\,, \tag{4.107}$$

where $\Delta\Sigma_f(B) = -2\,m_c\Big[\langle\bar{f}f\rangle_B - \langle\bar{f}f\rangle_0\Big]/D^4$. Here D is a phenomenological normalization constant given by $D = (135 \times 86)^{1/2}$ MeV.

In order to test the sensitivity of our results to the parametrization, we consider the three parametrization sets listed in Table 4.1. All of these reproduce the phenomenological values $m_\pi = 138$ MeV and $f_\pi = 92.4$ MeV. Moreover, we also explore the possibility of considering a magnetic field dependent coupling $G(B)$, so as to incorporate the sea effect produced by the backreaction of gluons to magnetized quarks loops, as discussed in the introduction. We adopt the expression proposed in Ref. [161], given by

$$G(B) = G\,\frac{\alpha + \beta\, e^{-\gamma B_e^2}}{\alpha + \beta}\,, \tag{4.108}$$

where $\alpha = 1.44373$ GeV^{-2} $\beta = 3.06$ GeV^{-2} and $\gamma = 1.31$ GeV^{-4}. We have normalized the functional dependence so that $G(0) = G$ corresponds to the coupling constant of each set of Table 4.1. Since variations in the parametrization turn out to have a negligible impact on the outcomes, for visual clarity we will show results using $G(B)$ only for set I.

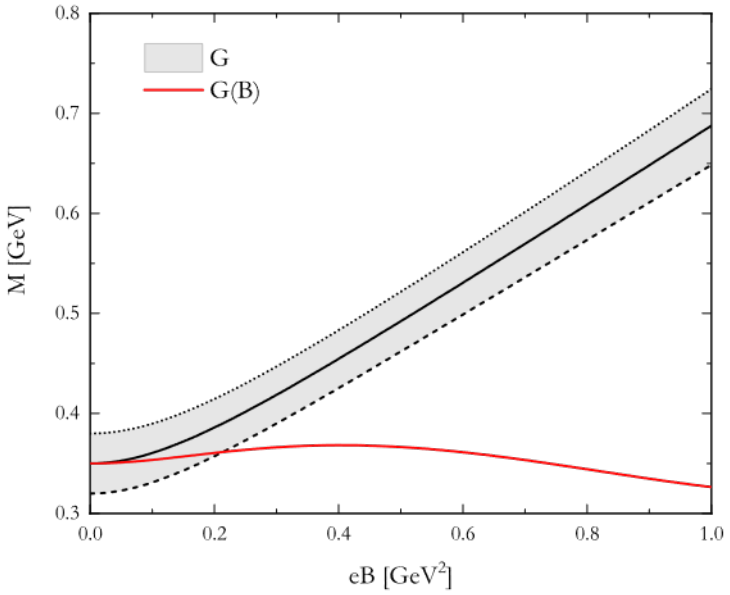

Figure 4.1: Effective quark mass M as function of eB. Solid lines correspond to set I using G (black) and $G(B)$ (red), while the limits of the gray bands correspond to set II (dashed lines) and set III (dotted lines) using a constant coupling.

The effective quark mass M, which is a solution to the gap equation (2.34), is displayed in Figure 4.1 for all three sets of Table 4.1 using a constant coupling G but only for set I using $G(B)$. For the rest of this section, solid lines in the figures indicate the results for parameter set I, while the limits of the gray bands correspond to set II (dashed lines) and set III (dotted lines). As seen, the magnetic-field dependent coupling greatly diminishes the enhancement of M with B, even resulting in a nonmonotonic behavior.

In Figure 4.2 we show the comparison between the sets of Table 4.1, using G and $G(B)$, and LCQD results for the normalized condensates of Eq. (4.107). We see that results obtained using a constant coupling are in good agreement with lattice calculations of Ref. [73] for the normalized average and difference condensate, being set I the closest one. On the other hand, $G(B)$ results show a somewhat larger deviation from lattice simulations. It is also seen that our predictions are not significantly affected by the parameter choice.

4.5.1 Neutral pion

In Figure 4.3 we show our numerical results for the quantities associated with the neutral pion as functions of eB. We observe that the qualitative behavior of all calculated quantities remains basically unaffected by changes in the model parameters within phenomenological reasonable limits.

Panel (a) shows the effect of the magnetic field on the neutral pion mass. It is seen that for a constant coupling G the mass shows a slight non-monotonic decrease with B.

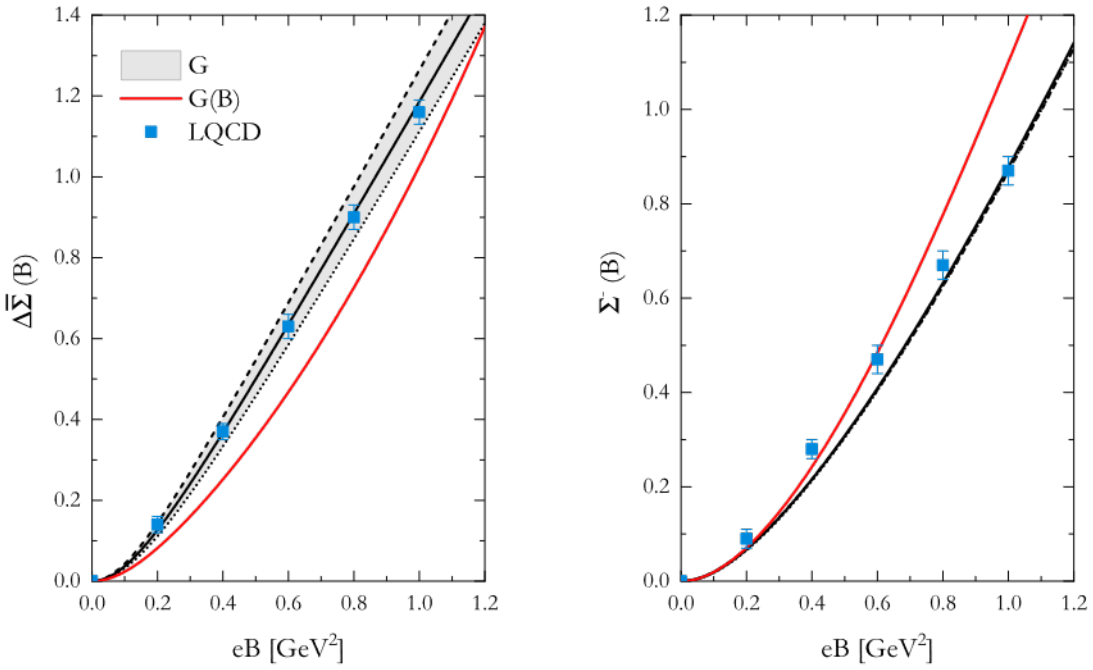

Figure 4.2: Behavior of $\Delta\bar{\Sigma}$ (left) and Σ^- (right) as functions of eB. Solid lines correspond to set I using G (black) and $G(B)$ (red), while the limits of the gray bands correspond to set II (dashed lines) and set III (dotted lines) using a constant coupling. Results from lattice QCD calculations [73] are included as blue squares for comparison.

On the other hand, the decrease is not only monotonic but more pronounced when a magnetic field dependent coupling is used.

In panel (b) we display the pion-to-quark coupling constant $g_{\pi^0 qq}$ and the transverse velocity u_{π^0}, given by Eqs. (4.55-4.57). We observe that for constant G, $g_{\pi^0 qq}$ shows some enhancement if B is increased, in contrast to what happens for the $G(B)$ case. On the other hand, for both type of couplings u_{π^0} decreases monotonously with B, remaining always lower than one guaranteeing the law of causality. This result is consistent with the one obtained in Refs. [100, 153, 217]. It should be also noticed that u_{π^0} is basically insensitive to the parametrization. In fact, it remains almost unchanged if one takes $m_c \to 0$, which implies that for nonzero B neutral pions move at a speed lower than the speed of light even in the chiral limit. We notice that, on the contrary, $u_{\pi^0} > 1$ is found in Ref. [170]. In addition to the already mentioned discrepancies in the expressions for the renormalization constants, this behavior is likely due to the choice of a bad regularization scheme in that work, namely a soft cutoff magnetic function. This claim is supported by the fact that a subluminal behavior is also obtained when using the (non MFIR) Pauli-Villar scheme [153].

Results for the neutral axial decay constants are shown in panel (c). Starting from a common value at $B = 0$, it is seen that while $f_{\pi^0}^{(A^{||})}$ is enhanced for increasing B, $f_{\pi^0}^{(A^{\perp})}$ is reduced. In both cases the B dependence is stronger than for the other quantities

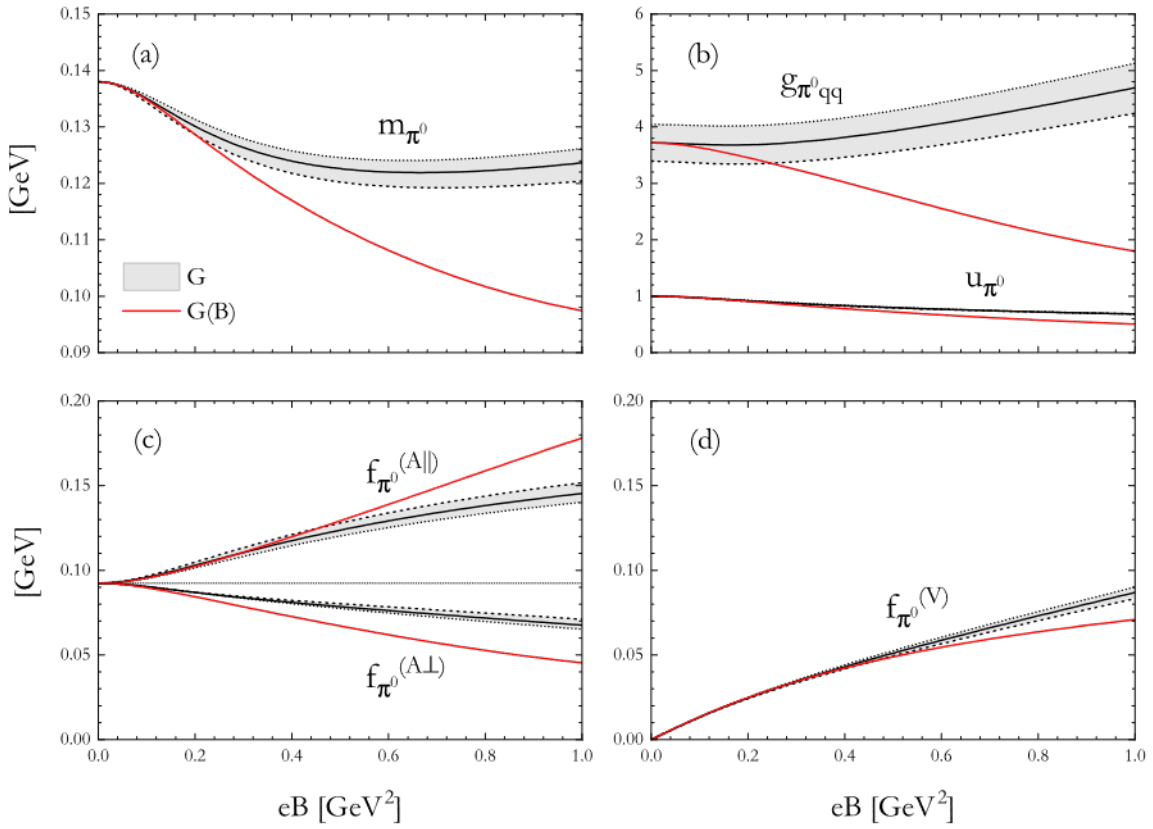

Figure 4.3: Neutral pion properties as functions of eB. Solid lines correspond to set I using G (black) and $G(B)$ (red), while the limits of the gray bands correspond to set II (dashed lines) and set III (dotted lines) using a constant coupling.

discussed previously. Note that our results indicate that $f_{\pi^0}^{(A\perp)} < f_{\pi^0}^{(A\parallel)}$ for all considered values of eB, which differs from the result in Ref. [170]. This seems to be related to the fact that, as stated, in that reference $u_{\pi^0} > 1$ is obtained. Finally, in panel (d) we show the behavior of $f_{\pi^0}^{(V)}$, which grows with B.

It is interesting to notice that the numerical results given above (which have been obtained from parametrization sets leading to $m_\pi = 138$ MeV and $f_\pi = 92.4$ MeV at $B = 0$) satisfy quite well the chiral limit relations in Eqs. (4.101-4.105). In fact, it is found that all these relations are satisfied at a level of less than 2% for all considered values of eB.

To conclude this subsection, in the next figures we show a comparison between our results and others found in the literature. In Figure 4.4 we compare normalized neutral pion masses. For a constant coupling G, it shows a slight decrease with B, in agreement with the analysis of Refs. [161, 248] also done within the NJL model. Moreover, this behavior is nonmonotonic: the mass increases for strong enough fields. In contrast, lattice simulations seem to lean toward a monotonic decrease of m_{π^0} with the magnetic field. Also shown are lattice results obtained using Wilson fermions with a heavy pion mass of

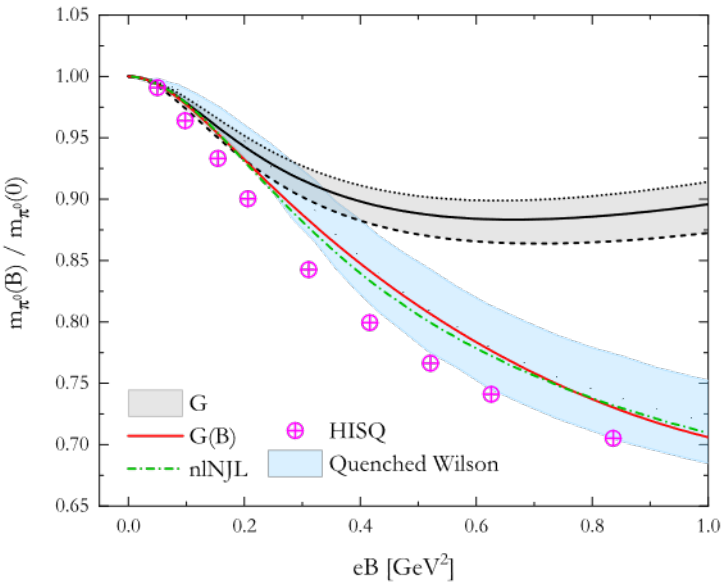

Figure 4.4: Normalized neutral pion mass as a function of eB. Grey band (red solid line) correspond to this work using a constant (magnetic) coupling; light blue band to LQCD results of Ref. [129] employing quenched Wilson quarks; magenta dots to LQCD results of Ref. [258] using highly improved staggered quarks; and green dashed-dotted line to results from the nonlocal-NJL model [251].

$m_\pi(0) = 415$ MeV in vacuum [129], and highly improved staggered quarks with similar to physical pion masses of $m_\pi(0) = 220$ MeV [258]. As seen in the figure, through the introduction of a magnetic coupling $G(B)$, which schematically takes into account the effect of sea quarks on the gluon fields, the NJL model is able to reproduce this monotonic behavior together with an enhancement of the decrease, in agreement with Ref. [161]. It is interesting to note that in the framework of NJL-like models, this behavior can also be reproduced by considering nonlocal interactions (nlNJL) [250, 251], whose results are displayed as well in Figure 4.4.

In Figure 4.5 we compare normalized axial decay constants. In the left panel, the usual parallel component is displayed. Our results using G show a somewhat mild increase with the magnetic field. By putting $G(B)$ the enhancement is magnified, in better agreement with estimations from LQCD [258] and the nonlocal-NJL model [251], which show a steeper enhancement. Lastly, results from the functional renormalization group approach to the quark-meson model (rgQMM) [228] show an even greater increase of $f_{\pi^0}^{(A||)}$. This is likely to be correlated with the fact that in that approach the π^0 mass shows a stronger decrease as the magnetic field increases.

On the other hand, results for the perpendicular component are displayed in the right panel. For constant G our results show a decreasing behavior. The effect is stronger when $G(B)$ is used. An even steeper decrease is obtained in the nlNJL model [251]. In

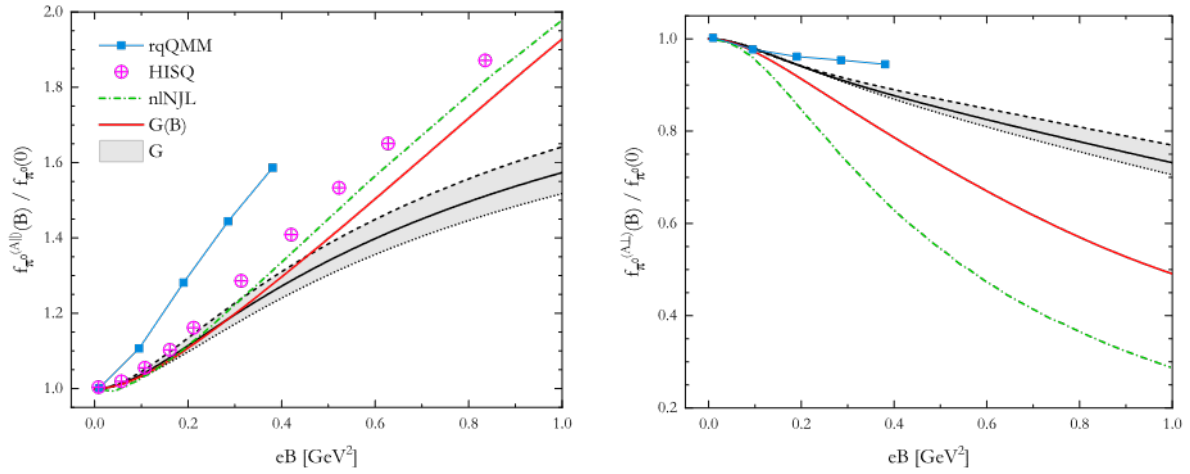

Figure 4.5: Left (right) panel: normalized parallel (perpendicular) neutral axial decay constant as a function of eB. Grey band (red solid line) correspond to this work using a constant (magnetic) coupling; magenta dots to LQCD results of Ref. [258] using highly improved staggered quarks; green dashed-dotted line to results from the nonlocal-NJL model [251]; and blue connected dots to results from the functional renormalization group approach to the quark-meson model [228].

contrast, rgQMM results show a milder decrease with the magnetic field [228]. It should be mentioned that additional calculations for $f_{\pi^0}^{(A||)}$ have been carried out using ChPT [235] and within the effective chiral confinement Lagrangian approach [243]. The latter shows a behavior similar to that of the nlNJL model considered in Ref. [250], while ChPT results, trustable for values of the magnetic field up to say $eB \sim 0.1$ GeV^2, are found to be in reasonable agreement with our curves.

It is worth mentioning that all of the quantities displayed in Figure 4.3 have also been calculated in the nonlocal version of the NJL model, see Ref. [251] for comparison. We briefly outline the remaining results of the nlNJL compared to our study: $g_{\pi qq}$ shows a decreasing behavior, in contrast with our results for G but in agreement when using $G(B)$; u_{π^0} decreases more with B; and $f_{\pi^0}^{(V)}$ displays a milder increase with B.

4.5.2 Charged pions

In Figure 4.6 we show our numerical results for the quantities associated with the charged pions in the lowest Landau level (LLL), as functions of eB. As in the case of the π^0, the qualitative behavior of all calculated quantities is not significantly affected by changes in the model parametrization within the considered limits. The curves corresponding to $g_{\pi^- qq}$ and $f_{\pi^-}^{(V)}$ are very similar to those obtained for the neutral pion in Figure 4.3. Regarding the decay constants, it is interesting to note that while the use of $G(B)$ decreases the value of $f_{\pi^-}^{(i)}$ for $i = A1, A2, V$, the effect is reversed for $f_{\pi^-}^{(A3)}$. All decay constants show an enhancement with the magnetic field. This is particularly interesting for the new

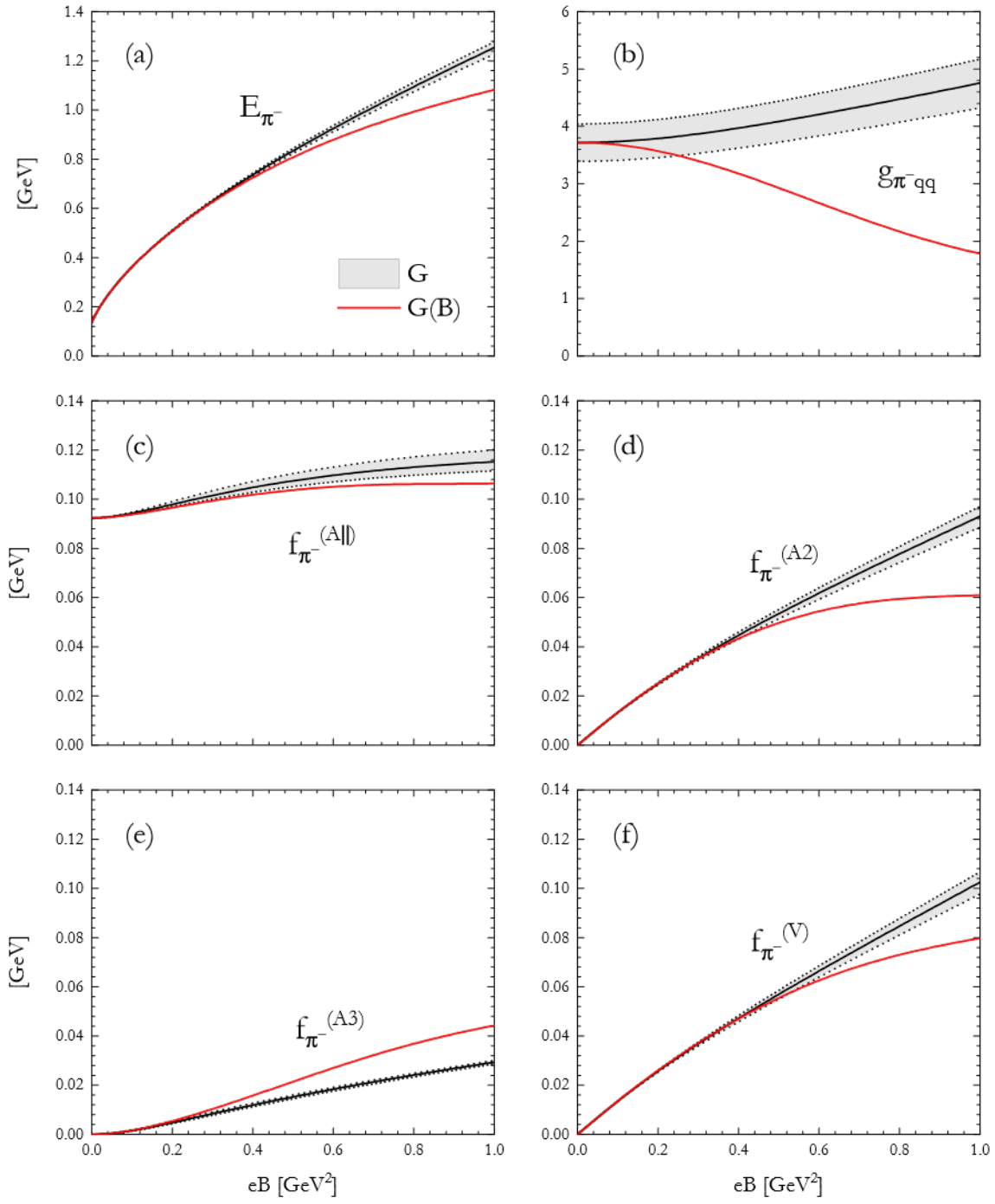

Figure 4.6: Charged pion properties as functions of eB. Solid lines correspond to set I using G (black) and $G(B)$ (red), while the limits of the gray bands correspond to set II (dashed lines) and set III (dotted lines) using a constant coupling.

decay constants, $f_{\pi^-}^{(A2)}$, $f_{\pi^-}^{(A3)}$ and $f_{\pi^-}^{(V)}$. While for low magnetic fields their value is almost negligible, for strong magnetic fields $f_{\pi^-}^{(A2)}$ and $f_{\pi^-}^{(V)}$ can reach values comparable to $f_{\pi^-}^{(A\|)}$, and therefore have a possibly meaningful impact on the decay. Moreover, as discussed in subsection 3.3.2, if the pion lies on the lowest energy state then the combination

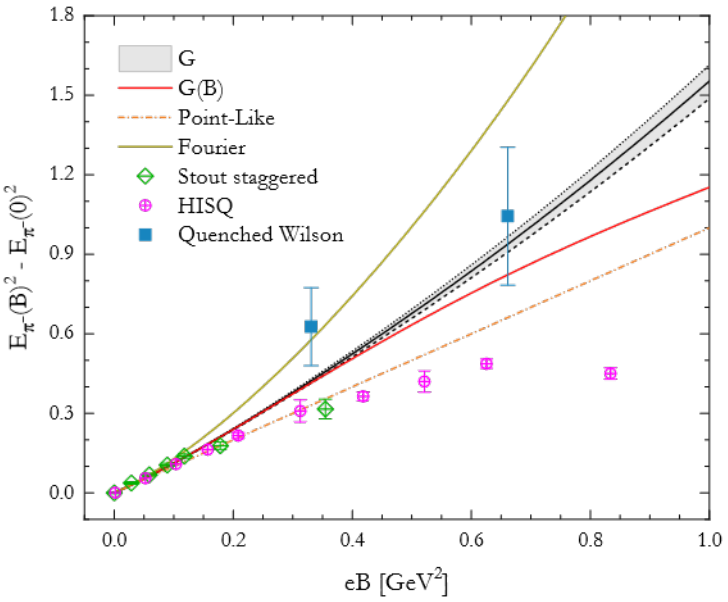

Figure 4.7: Difference of squared lowest energies of charged pions between the case at $B \neq 0$ and $B = 0$ as a function of eB. The grey band (red solid line) correspond to this work using a constant (magnetic) coupling, while the orange dashed-dotted line represents the point-like case (eB). The dark yellow solid line is obtained by disregarding Schwinger phases (Fourier transform) using set I and a constant coupling. LQCD results are displayed as: green rhombus for Ref. [74], magenta dots for Ref. [258], and blue squares for Ref. [129].

$f_{\pi^-}^{(A\perp+)} = f_{\pi^-}^{(A1),\mathrm{reg}} + f_{\pi^-}^{(A2)} - f_{\pi^-}^{(A3)}$ is the only perpendicular form factor relevant for the evaluation of the matrix elements of the axial current. From the above curves, one can check that $f_{\pi^-}^{(A\perp+)}$ exhibits a strong increase with B for a constant coupling G, reaching a magnitude of about 180 MeV for $eB = 1$ GeV^2. In contrast, for $G(B)$ it exhibits a nonmonotic behavior, with $f_{\pi^-}^{(A\perp+)} \simeq 124$ MeV at $eB = 1$ GeV^2.

In Figure 4.7 we compare our results for the charged pion lowest energy with lattice simulations. Instead of normalizing E_{π^-} with respect to its vacuum value, as done for the neutral pion, we find it convenient to compare the difference of squared lowest energies, i.e. $E_{\pi^-}(B)^2 - E_{\pi^-}(0)^2$, see Eq. (4.51). The main advantage lies on the fact that for the point-like case this quantity is just eB and therefore independent of the vacuum mass, which is different for each simulation. Thus, it serves as a common reference for all calculations. We see that our results for constant G are in fair agreement with those obtained in quenched LQCD [129] using heavy pions with $m_{\pi^-}(B = 0) = 415$ MeV. In order to make a more sensible comparison, an alternative procedure was proposed in Ref. [161], which consists of using a parameter set where the current quark mass is increased so that $m_{\pi^-}(B = 0)$ matches the value considered in Ref. [129]. For the charged case, this is discussed in Ref. [233], where it is shown that for the normalized lowest energy the aforementioned procedure provides closer agreement with LQCD results from Ref. [129].

Nevertheless, for the quantity displayed in Figure 4.7 results from both procedures are almost identical. On the other hand, lattice simulations using staggered quarks point to a different behavior. For low magnetic fields, say $eB < 0.2$ GeV^2, our results coincide fairly well with those obtained in lattice simulations using stout smeared [74] and highly improved [258] staggered quarks. However, for large magnetic fields our results start to deviate, showing a steeper enhancement with eB. Moreover, no trace of the non-monotonic behavior found in Ref. [258] is seen.

At this point it is worth mentioning the difference between our results for the lowest energy as compared to those obtained in the literature by simply disregarding the Schwinger phases in the charged pion polarization function [168, 169, 247]. In the latter case, the calculation is analogous to the one performed for the neutral pion, using Fourier transformations. At the end, the polarization is simply given by the function $c_{d,u}(p_\perp^2, p_\parallel^2)$ in Eq. (4.24), evaluated at $p_\mu = im_{\pi^-}\delta_{\mu,4}$. It is interesting to note that, compared to the full result in Eq. (4.47), for $\ell = p_3 = 0$ disregarding Schwinger phases amounts to replace $\alpha_+ \to t_+$ and $m_{\pi^-}^2 + B_e \to m_{\pi^-}^2$. The result is shown in Figure 4.7 for set I and a constant coupling G. As expected, at weak magnetic fields, say $eB \lesssim 0.1$ GeV^2, both methods yield similar results. However, their behavior deviates at high magnetic fields, where disregarding Schwinger phases triggers a much stronger enhancement with B. At $eB = 1$ GeV^2 we get $E_{\pi^-} = 1.65$ GeV for the Fourier transformation, as compared to the lower value $E_{\pi^-} = 1.25$ GeV obtained using the full Ritus method. On the other hand, Schwinger phases are properly accounted for in Refs. [222, 223]. In the former reference, an approach based on the derivative expansion is proposed, while the analysis of the latter work is analogous to ours but using a Landau level expansion for the quark propagator. In both analyses, which share the regularization choice of a non-MFIR Pauli-Villars scheme, an even stronger magnetic enhancement is found at an intermediate $eB < 0.4$ GeV^2 regime.

In the framework of lattice QCD, some results for $f_{\pi^-}^{(A^{||})}$ and $f_{\pi^-}^{(V)}$ in the presence of an external magnetic field have been presented in Ref. [129]. However, a sensible comparison with our results is not possible since in that reference decay constants are defined differently, using a Fourier instead of a Ritus basis. Nevertheless, it can be seen that, although errors are still relatively large, for staggered quarks at the physical point both decay constants shows an overall increase with the magnetic field, in qualitative agreement with our results. In fact, for $f_{\pi^-}^{(V)}$ our NJL predictions are compatible within errors with lattice data, which have been obtained for eB up to 0.3 GeV^2. However, for weak fields a continuum extrapolation seems to indicate that $f_{\pi^-}^{(A^{||})}$ starts out with a negative slope, which differs from our results and also from the neutral case. We find this result difficult to understand, since the decay constants of charged and neutral pions should behave similarly [235] for very small values of eB. In addition, in Ref. [244] the

magnetic field dependence of $f_{\pi^-}^{(A||)}$ has been analyzed in the context of QCD sum rules. In comparison with our results, their analysis shows a steeper enhancement with B, leading to $f_{\pi^-}^{(A||)} \sim 0.17$ GeV for $eB = 1$ GeV^2. In any case, it should be stressed that our results show that, as expected [236, 259], the Goldberger-Treiman and Gell–Mann-Oakes-Renner relations for charged pions [i.e., the equivalent to Eqs. (4.101) and (4.104), obtained for neutral mesons] are violated for $eB \gtrsim m_\pi^2$, for both $f_{\pi^-}^{(A||)}$ and $f_{\pi^-}^{(A\perp+)}$, the latter being defined in Eq. (4.98).

To conclude, let us make an additional comment on the magnetic field dependences of the decay constants. In the chiral limit, it can be seen that for low values of eB the difference $f_{\pi^-}^{(A2)} - f_{\pi^-}^{(A3)}$ is given by

$$f_{\pi^-,\,\mathrm{ch}}^{(A2)} - f_{\pi^-,\,\mathrm{ch}}^{(A3)} \;=\; \frac{B_e}{8\pi^2 f_{\pi^-,\,\mathrm{ch}}^{(A||)}} \left(1 \,-\, \frac{7\,B_e}{45\,M_{\mathrm{ch}}^2} \,+\, \ldots\right). \tag{4.109}$$

On the other hand, in the case of $f_{\pi^-}^{(V)}$, for low values of the magnetic field a relation similar to Eq. (4.105) is expected to be satisfied in the chiral limit. Even though the π^- cannot be considered a pseudo-Goldstone boson in the presence of the magnetic field, from our numerical calculations we find quite remarkable that relations of the same form, i.e.,

$$f_{\pi^-}^{(A2)} - f_{\pi^-}^{(A3)} \;=\; \frac{B_e}{8\pi^2 f_{\pi^-}^{(A||)}} \left(1 \,-\, \frac{7\,B_e}{45\,M^2}\right), \tag{4.110}$$

and

$$f_{\pi^-}^{(V)} \;=\; \frac{B_e}{8\pi^2 f_{\pi^-}^{(A||)}}, \tag{4.111}$$

are in fact valid also for intermediate values of the external magnetic field, up to say $eB \lesssim 0.4$ GeV^2. Moreover, for a constant coupling G we find that $f_{\pi^-}^{(A2)} - f_{\pi^-}^{(A3)}$ and $f_{\pi^-}^{(V)}$ can be approximated by the expressions in Eqs. (4.110) and (4.111) within 15% and 10% accuracy, respectively, for values of eB up to 1 GeV^2. For a magnetic coupling $G(B)$ these expressions deviate, especially the one in Eq. (4.110). It would be interesting to verify if equivalent relations also arise within other theoretical approaches to low energy hadron physics.

4.5.3 Weak decay width of magnetized charged pions

In section 3.3 we have a obtained a general expression for the weak decay width of charged pions under a uniform magnetic field. In that expression, the internal structure of the pions is parametrized in terms of several form factors. In the absence of exact QCD solutions, these are model-dependent. As usual, we will concentrate on the pion lowest energy state (LES) case, i.e. $\ell = 0$ and $p_3 = 0$. The relevant expressions can be found

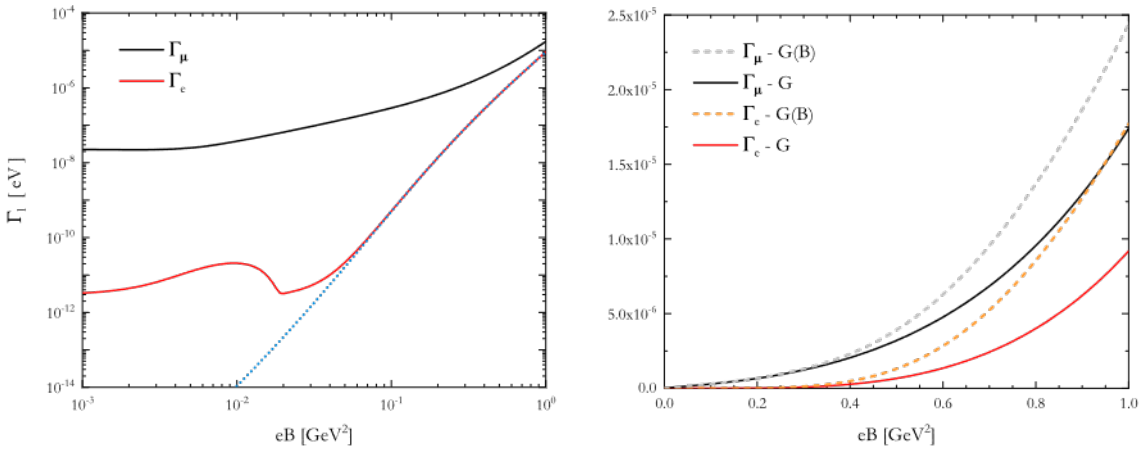

Figure 4.8: π^- partial decay widths into $e^-\bar{\nu}_e$ (red line) and $\mu^-\bar{\nu}_\mu$ (black line) for set I using a constant coupling G, as functions of eB in logarithmic (linear) scale for left (right) panel. Left panel: dotted blue line represents to the $n = 0$ asymptotic contribution for $m_l = 0$. Right panel: dashed lines correspond to results using $G(B)$, in grey (orange) for electron (muon) decay.

in Eqs. (3.71) and (3.72). For the LES, only the perpendicular combination $f_{\pi^-}^{(A2)} - f_{\pi^-}^{(A3)}$ is relevant. Using the masses and decay constants obtained in this chapter within the two-flavor NJL model, we provide actual estimates for the magnetic field dependence of the π^- decay width. For visual clarification we will only display results from set I, since we have checked that results from sets II and III do not differ from by more than 3%.

Our results for the π^- partial decay widths to both $\mu^-\bar{\nu}_\mu$ (Γ_μ) and $e^-\bar{\nu}_e$ (Γ_e) using a constant coupling as functions of eB are shown in Figure 4.8. The effect at weak magnetic fields is better seen using a logarithmic scale, as shown in the left panel. It is seen that the partial widths are strongly enhanced by the magnetic field. This enhancement is more pronounced for the decay to $e^-\bar{\nu}_e$, since for low values of B helicity suppression becomes important. The bump observed in this curve for $eB \sim 10^{-2}$ GeV^2 is due to the fact that this region is dominated by the $n = 1$ Landau level contribution, which disappears at about $eB \sim 2 \times 10^{-2}$ GeV^2 leaving $n = 0$ as the only energetically allowed electron Landau level. The dotted line in the graph corresponds to the asymptotic decay width quoted in Eq. (3.75), corresponding to $n = 0$ and $m_l = 0$. As expected, this curve approximates fairly well the results at $eB \gg m_l^2$ and $eB > m_{\pi^-} - m_l$, especially for the (less massive) electron. Since the effects of using a magnetic coupling take place at high magnetic fields, we compare the results using a linear scale in the right panel, where it is seen that the use of $G(B)$ strongly strengthens the value of the decay compared to the constant coupling case.

In Figure 4.9 we show the behavior of the total decay width $\Gamma_e + \Gamma_\mu$, normalized to its value at $B = 0$. For this effective model the enhancement factor is found to be about 1000

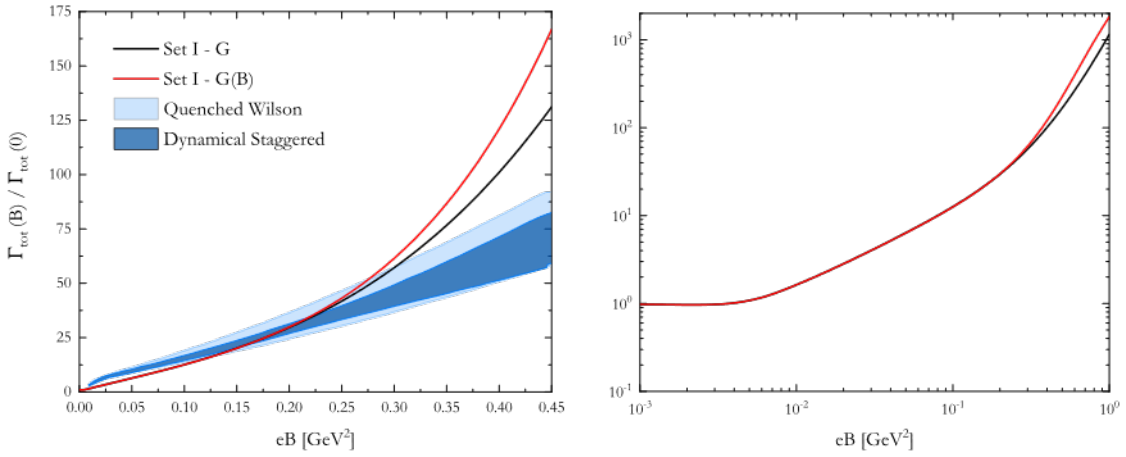

Figure 4.9: Normalized total π^- partial decay width $[\Gamma_e^-(B) + \Gamma_\mu^-(B)]/[\Gamma_e^-(0) + \Gamma_\mu^-(0)]$ using G (black line) and G(B) (red line) as functions of eB in linear (left) and logarithmic scale (right). LQCD bands quoted in Ref. [171] are included in the left panel for comparison.

for $eB \simeq 1$ GeV^2 when using a constant coupling, increasing up to 1800 for $G(B)$. In the left panel we include for comparison results from LQCD calculations quoted in Ref. [171], which cover values of eB up to about 0.45 GeV^2. Dark and light blue regions correspond to staggered and quenched Wilson quarks, respectively. Although these LQCD results also predict a significant growth of the total width with the magnetic field, it is seen that in our case the slope of the curve gets more rapidly enhanced with B. This is, in part, due to the $e^-\bar{\nu}_e$ channel contribution.

The dramatic enhancement of the rate implies a drastic reduction of the mean lifetime $\tau_\pi = 1/\Gamma$. A typical $B > 0$ lifetime and the lowest possible lifetime considered in this work are

$$\begin{cases} \tau_\pi \approx 5 \times 10^{-10}\,\text{s} & \text{for} \quad B \approx 0.3\,\text{GeV}^2/e \approx 5 \times 10^{19}\,\text{G}\,, \\ \tau_\pi \approx 1.5 \times 10^{-11}\,\text{s} & \text{for} \quad B \approx 1\,\text{GeV}^2/e \approx 1.7 \times 10^{20}\,\text{G}\,. \end{cases} \tag{4.112}$$

As noted in Ref. [171], since lifetimes of magnetic fields in off-central heavy-ion collisions are by 13-15 orders of magnitude smaller [51], this effect will not result in any observable predictions for heavy-ion phenomenology. However, the B dependence of weak decays is expected to be relevant in astrophysical environments, since the upper limit for magnetic field strengths in the core of magnetized neutron stars is thought to be around $B = 10^{18} - 10^{20}$ G [59, 61]. Indeed, for $B = 0$ the pion mean lifetime and the time scale for cooling via inverse Compton scattering are roughly comparable [260]. Thus, a reduction in τ_π will inevitably decrease radiation energy loss of pions and result in a harder neutrino spectrum. Neutrino emissivities of meson-condensed matter, even though not as high as

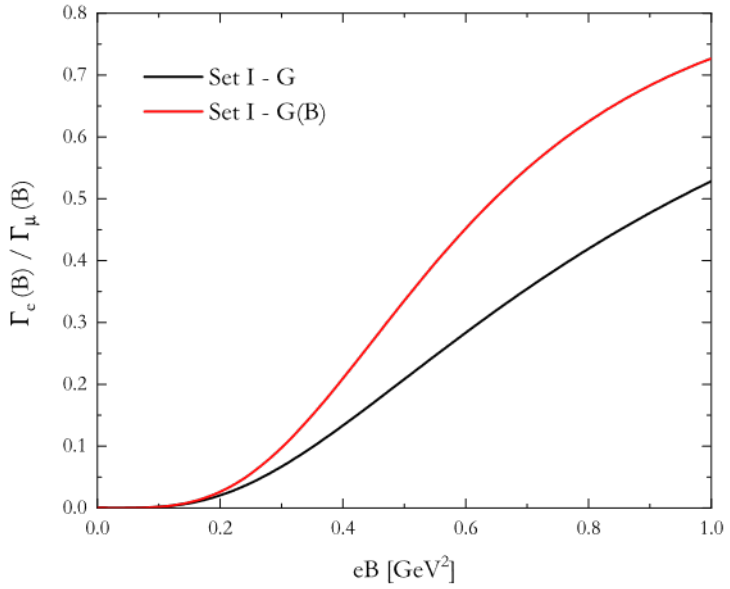

Figure 4.10: Ratio Γ_e/Γ_μ using G (black line) and $G(B)$ (red line) as a function of eB.

the ones of the direct Urca processes, still lead to fast cooling, and could have an impact on the cooling curves of compact stars [261].

Another interesting consequence of the presence of the magnetic fields is the absence of helicity suppression, which yields a stronger $e^-\bar{\nu}_e$ production. As seen in Figure 4.8, at $B \neq 0$ the electron contribution strongly grows with eB. Therefore, while at $B = 0$ muon production dominates, at strong fields both contributions compete. To measure this effect, in Figure 4.10 we quote the ratio Γ_e/Γ_μ as a function of eB. We notice that the presence of the external field leads to a strong increase of this ratio with the strength of the magnetic field, reaching a value of about 0.5 for $eB \simeq 1$ GeV^2 using a constant coupling, increasing to 0.7 when using $G(B)$. In contrast, for $B = 0$ one has $\Gamma_e/\Gamma_\mu \simeq 1.2 \times 10^{-4}$. This could be interesting e.g. regarding the expected flavor composition of neutrino fluxes coming from the cores of magnetars and other stellar objects. It is worth to remark that our estimation for the ratio Γ_e/Γ_μ is different from the one obtained in Ref. [171], where helicity suppression leads to a ratio of the order of 10^{-5} that becomes almost independent of the magnetic field.

4.5.4 Angular distribution of outgoing antineutrinos

Another interesting consequence of the presence of the external magnetic field is its effect on the angular distribution of outgoing antineutrinos. As mentioned in subsection 3.3.4, while for $B = 0$ the distribution is isotropic, this changes significantly for $B \neq 0$. Denoting $w = \cos\theta = k_3/|\vec{k}|$, the relevant expressions are in Eqs. (3.79-3.81).

Our numerical results for the normalized differential partial decay widths are shown

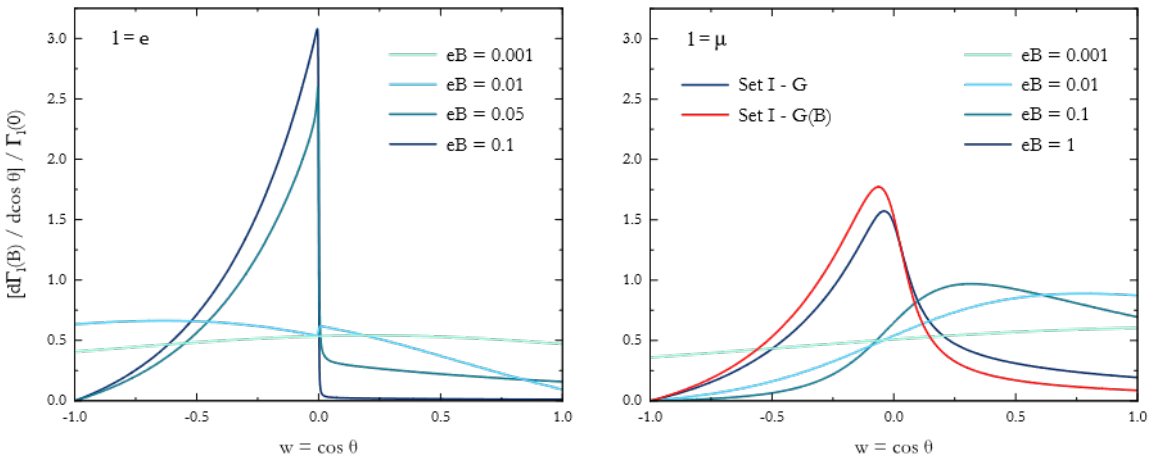

Figure 4.11: Normalized differential partial decay widths of π^- into $e^-\bar{\nu}_e$ (left) and $\mu^-\bar{\nu}_\mu$ (right), as functions of $w = \cos\theta$ for selected values of eB. All results correspond to set I using constant coupling G, except for the red solid line in the right panel which corresponds to set I using $G(B)$ at $eB = 1$ GeV^2.

in Figure 4.11, where several representative values of eB are considered. Left and right panels correspond to π^- decays into $e^-\bar{\nu}_e$ and $\mu^-\bar{\nu}_\mu$, respectively. The inclusion of magnetic effects through the coupling $G(B)$ only has an appreciable impact on the decay constants values of Figure 4.6 for strong magnetic fields, say $eB > 0.4$ GeV^2. Therefore, for the selected values of eB displayed in Figure 4.11, the use of $G(B)$ is only discernible for the greatest chosen value of $eB = 1$ GeV^2, as seen on the red line of the right panel.

It is seen that the fraction of antineutrinos that come out in the upper half-space $w > 0$ fluctuates when the magnetic field is increased, becoming strongly suppressed for values of eB much larger than the lepton mass squared and the difference $m_{\pi^-} - m_l$. This suppression is mildly enhanced by the use of $G(B)$. The anisotropy can be qualitatively understood as follows. When $eB \gg m_{\pi^-} - m_l$, only $n = 0$ is allowed. In addition, for $B_e \gg m_l^2$ the lepton can be considered massless. In the chiral limit, the lepton has to be left-handed. Therefore from Eq. (3.76) one gets $q_3 > 0$. Conservation of the 3 component of total momentum implies $q_3 + k_3 = p_3 = 0$. Hence, for large B, in the $m_l \to 0$ limit all antineutrinos should be produced with momentum in the lower half-space $k_3 < 0$. Indeed, for $m_l = 0$ and $n = 0$ the normalized differential decay width is given by Eq. (3.82).

We conclude that, in contrast to the isotropy seen at $B = 0$, the presence of an external magnetic field induces an anisotropy in the angular distribution of outgoing antineutrinos. The anisotropy is sharpened for strong fields and lower lepton masses, where antineutrinos are mostly produced with momenta in the half-space opposite to the direction of $\vec{B}$. Within the NJL model, a strong anisotropy in the electron production is already seen at $eB = 0.05$ GeV^2, with virtually vanishing antineutrino momentum in the direction of the field for

$eB = 0.1$ GeV^2. The anisotropy is reduced for muon production since they are heavier; even at $eB = 1$ GeV^2 there is still some non-negligible antineutrino momenta in the field direction. In addition, it is worth noticing that for large values of B most antineutrinos come out with low $|k_3|$, i.e. in directions approximately perpendicular to the magnetic field.

CHAPTER 5

Light pseudoscalar meson masses under strong magnetic fields within the SU(3) NJL model

In the previous chapter we have calculated several pion properties in a strongly magnetized medium within the framework of the $SU(2)$ NJL model, using a magnetic field-independent regularization scheme. There are very few calculations of meson properties incorporating the strange quark. In Refs. [262, 263], using a nonrelativistic constituent SU(3) quark model, neutral and charged mesons masses are considered. By using a relativistic Hamiltonian-based formalism, in Refs. [236, 241] pions and kaons are calculated and comparisons with chiral perturbation theory and LQCD results are considered. In Ref. [264], kaons and antikaons are investigated in a chiral SU(3) model.

The aim of this chapter is to extend the pole mass calculation to all mesons of the pseudoscalar nonet. To that end, we work with the $SU(3)$ version of the NJL model. Once again, we employ both a constant and a magnetic field-dependent coupling $G(B)$ so as to include the backreaction of the gluons due to the coupling of the magnetic field to sea quarks. Numerical results for the pole masses are obtained for definite parametrizations of the model, which we compare with previous calculations given in the literature. Results from this chapter are based on Ref. [265].

5.1 Pseudoscalar meson masses

5.1.1 Effective Lagrangian and mean field properties

We consider the Euclidean action of the $SU(3)$ NJL model which includes a scalar-pseudoscalar interaction and the 't Hooft six-fermion interaction in the presence of an external magnetic field. It is written as

$$S = \int d^4x \left[\bar{\psi} \left(-i \not{D} + \hat{m} \right) \psi - G \sum_{a=0}^{8} \left[\left(\bar{\psi} \, \lambda_a \, \psi \right)^2 + \left(\bar{\psi} \, i\gamma_5 \lambda_a \, \psi \right)^2 \right] + K \left(d_+ + d_- \right) \right] , \quad (5.1)$$

where G and K are coupling constants, $\psi = (\psi_u, \psi_d, \psi_s)^T$ represents a quark field with three flavors, $d_\pm = \det \left[\bar{\psi} \left(1 \pm \gamma_5 \right) \psi \right]$ and $\hat{m} = \mathrm{diag} \left(m_u, m_d, m_s \right)$ is the corresponding current quark mass matrix. In addition, $\lambda_0 = \sqrt{2/3} \, I$, where I is the unit matrix in the three-flavor space, and λ_a with $a = 1, ..., 8$ denote the Gell-Mann matrices. The coupling of quarks to the electromagnetic field $\mathcal{A}_\mu$ is implemented through the covariant derivative $D_\mu = \partial_\mu - i\hat{Q}\mathcal{A}_\mu$ where $\hat{Q} = \mathrm{diag} \left(Q_u, Q_d, Q_s \right)$ represents the quark electric charge matrix with $Q_u/2 = -Q_d = -Q_s = e/3$, $e > 0$ being the proton electric charge. As in previous chapters we consider a uniform magnetic field in the 3-direction. Using the Landau gauge we have $\mathcal{A}_\mu = B x_1 \, \delta_{\mu,2}$.

The 't Hooft term explicitly breaks the axial symmetry $U_A(1)$, as expected from the axial anomaly of QCD [173, 174]. This anomaly is in turn responsible for the higher value of the η' mass as compared to the η one. Therefore, this term is necessary in the $SU(3)$ version of the model in order to reproduce physical η and η' mesons. The standard $SU(2)$ version of the model used in Eq. (4.1) corresponds to taking $K = 2G$, i.e. having maximum flavor mixing. In that case, $M_u = M_d$. In contrast, for $K = 0$ quark flavors get fully decoupled.

In order to study meson properties, we proceed as in the $SU(2)$ case by bosonizing the action in terms of scalar $\sigma_a(x)$ and pseudoscalar $\pi_a(x)$ fields and the corresponding auxiliary $\mathsf{s}_a(x)$ and $\mathsf{p}_a(x)$ fields. We follow the standard procedure described in Appendix A, starting with the partition function

$$Z = \int \mathcal{D}\bar{\psi}\mathcal{D}\psi \; e^{-S} \, . \quad (5.2)$$

By introducing functional delta functions, the scalar $(\bar{\psi}\lambda_a\psi)$ and pseudoscalar $(\bar{\psi}i\gamma_5\lambda_a\psi)$ terms present in the action are replaced by $\mathsf{s}_a(x)$ and $\mathsf{p}_a(x)$. The remaining functional gaussian integration on the fermionic fields ψ and $\bar{\psi}$ can be performed by standard methods.

We obtain

$$\mathcal{Z} = \int \mathcal{D}\sigma_a \, \mathcal{D}\pi_a \, \det \mathcal{D}(x,x') \int \mathcal{D}\mathsf{s}_a \, \mathcal{D}\mathsf{p}_a \, e^{\int d^4x [\sigma_a(x)\mathsf{s}_a(x) + \pi_a(x)\mathsf{p}_a(x)]} \times$$
$$e^{\int d^4x \left\{ G[\mathsf{s}_a(x)\mathsf{s}_a(x) + \mathsf{p}_a(x)\mathsf{p}_a(x)] - \frac{K}{6} A_{abc} [\mathsf{s}_a(x)\mathsf{s}_b(x)\mathsf{s}_c(x) - 3\,\mathsf{s}_a(x)\mathsf{p}_b(x)\mathsf{p}_c(x)] \right\}} , \tag{5.3}$$

where

$$\mathcal{D}(x,x') = \delta^{(4)}(x-x') \left[-i\not{\partial} + \hat{m} + \lambda_a \sigma_a(x) + i\gamma_5 \lambda_a \pi_a(x) \right] , \tag{5.4}$$

and the totally symmetric array A_{abc} is given by

$$A_{abc} = \begin{cases} d_{abc} & , \quad a,b,c = 1,...,8 \\ -1/\sqrt{6} & , \quad a = 0 \ , \ b = c = 1,...,8 \\ \sqrt{2/3} & , \quad a = b = c = 0 \end{cases} . \tag{5.5}$$

Here, $d_{abc} = \mathrm{tr}(\lambda_a \{\lambda_b, \lambda_c\})/4$ refer to the totally symmetric structure constants of the $SU(3)$ group.

Since, in contrast to the $SU(2)$ case, the integrals over the auxiliary fields are not gaussian, we perform the stationary phase approximation (SPA). That is, we replace the auxiliary fields by the values $\tilde{\mathsf{s}}_a(x)$ and $\tilde{\mathsf{p}}_a(x)$ that minimize the integrand of the partition function. This yields a set of coupled equations among the bosonic fields; at the end, $\tilde{\mathsf{s}}_a(x)$ and $\tilde{\mathsf{p}}_a(x)$ are to be considered as implicit functions of $\sigma_a(x)$ and $\pi_a(x)$. The bosonized action in the SPA then reads

$$S_{\mathrm{bos}} = -\,\mathrm{Tr}\ln \mathcal{D}(x,x') - \int d^4x \left\{ \sigma_a(x)\tilde{\mathsf{s}}_a(x) + \pi_a(x)\tilde{\mathsf{p}}_a(x) + \right.$$
$$\left. G\,[\tilde{\mathsf{s}}_a(x)\tilde{\mathsf{s}}_a(x) + \tilde{\mathsf{p}}_a(x)\tilde{\mathsf{p}}_a(x)] - \frac{K}{6} A_{abc}\,[\tilde{\mathsf{s}}_a(x)\tilde{\mathsf{s}}_b(x)\tilde{\mathsf{s}}_c(x) - 3\,\tilde{\mathsf{s}}_a(x)\tilde{\mathsf{p}}_b(x)\tilde{\mathsf{p}}_c(x)] \right\} , \tag{5.6}$$

where $\tilde{\mathsf{s}}_a(x)$ and $\tilde{\mathsf{p}}_a(x)$ satisfy the SPA conditions

$$\sigma_a(x) + 2G\,\tilde{\mathsf{s}}_a(x) - \frac{K}{2} A_{abc}\,[\tilde{\mathsf{s}}_b(x)\tilde{\mathsf{s}}_c(x) - \tilde{\mathsf{p}}_b(x)\tilde{\mathsf{p}}_c(x)] = 0\,,$$
$$\pi_a(x) + 2G\,\tilde{\mathsf{p}}_a(x) + K A_{abc}\,\tilde{\mathsf{s}}_b(x)\tilde{\mathsf{p}}_c(x) = 0\,. \tag{5.7}$$

We can now proceed as in subsection 2.2.1, expanding the bosonized action in powers of field fluctuations around the corresponding translationally invariant mean field values $\bar{\sigma}_a$ and $\bar{\pi}_a$, i. e. $\sigma_a(x) = \bar{\sigma}_a + \delta\sigma_a(x)$ and $\pi_a(x) = \bar{\pi}_a + \delta\pi_a(x)$. Due to charge conservation, only

$\bar{\sigma}_0$, $\bar{\sigma}_3$ and $\bar{\sigma}_8$ are different from zero, while the vacuum expectation values of pseudoscalar boson fields are zero, $\bar{\pi}_a = 0$. For convenience, we introduce $\bar{\sigma} = \mathrm{diag}(\bar{\sigma}_u, \bar{\sigma}_d, \bar{\sigma}_s) = \lambda_0\bar{\sigma}_0 + \lambda_3\bar{\sigma}_3 + \lambda_8\bar{\sigma}_8$. Symbolically, the expansion of the action reads

$$S^{\mathrm{bos}} \;=\; S^{\mathrm{bos}}_{\mathrm{MF}} \;+\; S^{\mathrm{bos}}_{\mathrm{quad}} \;+\; \dots \tag{5.8}$$

At the mean field level, the Euclidean action per unit volume or free energy is given by

$$\frac{S^{\mathrm{bos}}_{\mathrm{MF}}}{V^{(4)}} \;=\; -\frac{1}{V^{(4)}}\,\mathrm{Tr}\ln\mathcal{D}_{\mathrm{MF}}(x,x') - \frac{1}{2}\left[\bar{\sigma}_f\;\bar{\mathsf{s}}_f + G\;\bar{\mathsf{s}}_f\;\bar{\mathsf{s}}_f - \frac{K}{2}\,\bar{\mathsf{s}}_u\;\bar{\mathsf{s}}_d\;\bar{\mathsf{s}}_s\right]\,, \tag{5.9}$$

constrained by the SPA conditions

$$\bar{\sigma}_a + 2G\,\bar{\mathsf{s}}_a - \frac{K}{2}\,\epsilon_{abc}\,\epsilon_{abc}\,\bar{\mathsf{s}}_b\,\bar{\mathsf{s}}_c \;=\; 0\,. \tag{5.10}$$

The trace Tr refers to all spaces; color, flavor, Dirac and coordinates. Here, $\bar{\mathsf{s}}_f = \tilde{\mathsf{s}}_f(\bar{\sigma}_a)$ represents the auxiliary field at the mean field level within the SPA approximation (note that $\bar{\mathsf{p}}_f = 0$). The MF fermionic operator is flavor-diagonal

$$\mathcal{D}_{\mathrm{MF}}(x,x') \;=\; \mathrm{diag}\left(\mathcal{D}^u_{\mathrm{MF}}(x,x')\,,\,\mathcal{D}^d_{\mathrm{MF}}(x,x')\,,\,\mathcal{D}^s_{\mathrm{MF}}(x,x')\right)\,, \tag{5.11}$$

where

$$\mathcal{D}^f_{\mathrm{MF}}(x,x') \;=\; \delta^{(4)}(x-x')\left(-i\partial\!\!\!/ - Q_f A\!\!\!/ + M_f\right)\,. \tag{5.12}$$

represents the inverse of the mean field quark propagator $\mathcal{S}^f_{\mathrm{MF}}(x,x')^{-1}$ for each flavor, with effective mass $M_f = m_f + \bar{\sigma}_f$. Once again we choose to write the quark propagator in its Schwinger form, given by Eqs. (2.66) and (2.67). Note, however, that the substitution $M \to M_f$ has to be made, since quark masses are different in this case due to the 't Hooft term in the Lagrangian.

Minimizing the free energy with respect to M_f we obtain the gap equation $\bar{\mathsf{s}}_f = 2\phi_f$, where $\phi_f = -N_c M I^{\mathrm{B}}_{1f}$ is the chiral condensate for each flavor, given in Eq. (4.10). The function I^{B}_{1f} defined in Eq. (2.75) is divergent integral and has to be properly regularized. As in previous chapters, we use the MFIR scheme. Then the quark condensate is given by Eq. (4.11), where I^{mag}_{1f} and I^{vac}_1 were defined in Eqs. (2.79) and (2.52) respectively. Recall that the substitution $M \to M_f$ has to be made for the $SU(3)$ case.

Finally, by combining the equations from the SPA together with the gap equations, we obtain that the regularized form of the set of coupled equations for the effective quarks

masses read

$$\begin{aligned} M_u &= m_u - 4G\ \phi_u^{\rm reg} + 2K\ \phi_d^{\rm reg}\phi_s^{\rm reg}\ , \\ M_d &= m_d - 4G\ \phi_d^{\rm reg} + 2K\ \phi_s^{\rm reg}\phi_u^{\rm reg}\ , \\ M_s &= m_s - 4G\ \phi_s^{\rm reg} + 2K\ \phi_u^{\rm reg}\phi_d^{\rm reg}\ . \end{aligned} \tag{5.13}$$

5.1.2 Meson sector

For the calculation of meson masses, we consider the second-order correction to the mean field bosonized Euclidean action. At the quadratic level we get for the pseudoscalar sector

$$S^{\rm bos}_{\rm quad} = \frac{1}{2}\int d^4x' d^4x \sum_{P,P'}\ \delta P^*(x)\ \mathcal{G}^{-1}_{P,P'}(x,x')\ \delta P'(x')\,, \tag{5.14}$$

where the sum indexes run over the nonet of pseudoscalar mesons. Namely, $P, P' = \pi_3, \pi^\pm, K^0, \bar{K}^0,\ K^\pm, \eta_0, \eta_8$, where we have defined the physical meson fields as

$$\lambda_a \pi_a = \begin{pmatrix} \pi_3 + \sqrt{\frac{2}{3}}\eta_0 + \frac{1}{\sqrt{3}}\eta_8 & \sqrt{2}\pi^+ & \sqrt{2}K^+ \\ \sqrt{2}\pi^- & -\pi_3 + \sqrt{\frac{2}{3}}\eta_0 + \frac{1}{\sqrt{3}}\eta_8 & \sqrt{2}K^0 \\ \sqrt{2}K^- & \sqrt{2}\bar{K}^0 & \sqrt{\frac{2}{3}}\eta_0 - \frac{2}{\sqrt{3}}\eta_8 \end{pmatrix} \tag{5.15}$$

The inverse meson propagator in coordinate space can be written as

$$\mathcal{G}^{-1}_{P,P'}(x,x') = T_{P,P'}\ \delta^{(4)}(x-x') - J_{P,P'}(x,x')\,. \tag{5.16}$$

For $P, P' = \pi^\pm, K^\pm, K^0, \bar{K}^0$ this operator is diagonal

$$T_{P,P'} = T_P\ \delta_{P,P'} \qquad , \qquad J_{P,P'}(x,x') = J_P(x,x')\ \delta_{P,P'}\,, \tag{5.17}$$

where

$$\begin{aligned} T_{\pi^-} &= T_{\pi^+} = [2G - K\phi_s]^{-1} \quad , \quad J_{\pi^-}(x,x') = J_{\pi^+}(x',x) = c_{d,u}(x,x')\,, \\ T_{K^-} &= T_{K^+} = [2G - K\phi_d]^{-1} \quad , \quad J_{K^-}(x,x') = J_{K^+}(x',x) = c_{s,u}(x,x')\,, \\ T_{K^0} &= T_{\bar{K}^0} = [2G - K\phi_u]^{-1} \quad , \quad J_{K^0}(x,x') = J_{\bar{K}^0}(x',x) = c_{d,s}(x,x')\,. \end{aligned} \tag{5.18}$$

The functions $c_{f,f'}(x,x')$ were already defined in Eq. (4.14).

On the other hand, in the $P, P' = \pi_3, \eta_0, \eta_8$ subspace, $\mathcal{G}^{-1}_{P,P'}(x,x')$ is nondiagonal but

symmetric. The corresponding matrix elements of $T_{P,P'}$ are

$$
\begin{aligned}
T_{\pi_3\pi_3} &= \frac{K^2\left(\phi_u+\phi_d\right)^2-4GK\phi_s-8G^2}{f}\,,\\
T_{\eta_0\pi_3} &= \frac{2\left[K^2(\phi_u+\phi_d-\phi_s)-2GK\right](\phi_u-\phi_d)}{\sqrt{6}F}\,,\\
T_{\eta_8\pi_3} &= \frac{\left[K^2(\phi_u+\phi_d+2\phi_s)+4GK\right](\phi_u-\phi_d)}{\sqrt{3}F}\,,\\
T_{\eta_0\eta_0} &= \frac{2K^2\left[(\phi_d-\phi_s)^2+\phi_u(\phi_u-2\phi_d-2\phi_s)\right]+8GK(\phi_u+\phi_d+\phi_s)-24G^2}{3F}\,,\\
T_{\eta_8\eta_0} &= \frac{2K^2\left[(\phi_u-\phi_d)^2+\phi_s(\phi_u+\phi_d-2\phi_s)\right]-4GK\left(\phi_u+\phi_d-2\phi_s\right)}{3\sqrt{2}F}\,,\\
T_{\eta_8\eta_8} &= \frac{K^2\left[(\phi_u-\phi_d)^2+4\phi_s(\phi_u+\phi_d+\phi_s)\right]-4GK\left(2\phi_u+2\phi_d-\phi_s\right)-24G^2}{3F}\,,
\end{aligned}
\tag{5.19}
$$

where

$$
F \;=\; -4K^3\phi_u\phi_d\phi_s+4GK^2\left(\phi_u^2+\phi_d^2+\phi_s^2\right)-16G^3\,. \tag{5.20}
$$

In turn, the polarization function elements can be expressed as

$$
J_{P,P'}(x,x') \;=\; \sum_f \gamma^f_{P,P'}\; c_{f,f}(x,x')\,, \tag{5.21}
$$

where the coefficients $\gamma^f_{P,P'}$ are given by

$$
\begin{aligned}
&\gamma^u_{\pi_3\pi_3} = +\gamma^d_{\pi_3\pi_3} = \frac{1}{2}\quad, \quad \gamma^s_{\pi_3\pi_3} = 0\,, \quad \gamma^u_{\eta_0\eta_0} = \gamma^d_{\eta_0\eta_0} = \gamma^s_{\eta_0\eta_0} = \frac{1}{3}\,,\\
&\gamma^u_{\eta_0\pi_3} = -\gamma^d_{\eta_0\pi_3} = \frac{1}{\sqrt{6}}\quad, \quad \gamma^s_{\eta_0\pi_3} = 0\,, \quad \gamma^u_{\eta_8\eta_0} = \gamma^d_{\eta_8\eta_0} = -\frac{1}{2}\gamma^s_{\eta_8\eta_0} = \frac{1}{3\sqrt{2}}\,,\\
&\gamma^u_{\eta_8\pi_3} = -\gamma^d_{\eta_8\pi_3} = \frac{1}{2\sqrt{3}}\quad, \quad \gamma^s_{\eta_8\pi_3} = 0\,, \quad \gamma^u_{\eta_8\eta_8} = \gamma^d_{\eta_8\eta_8} = +\frac{1}{4}\gamma^s_{\eta_8\eta_8} = \frac{1}{6}\,.
\end{aligned}
\tag{5.22}
$$

For the pseudoscalar mesons we are interested in, the $c_{f,f'}(x,x')$ functions can be worked out leading to the expressions given by Eqs. (4.15) and (4.24).

5.1.2.1 Neutral mesons

For neutral mesons the contributions of Schwinger phases associated with the quark propagators in Eq. (4.14) cancel out. Therefore, the polarization functions depend only on the difference $(x-x')$, which leads to the conservation of momentum, since they are translationally invariant. If we take the Fourier transform of neutral meson fields to

the momentum basis, the corresponding transform of the polarization functions will be diagonal in momentum space. Thus, the neutral meson contribution to the quadratic action in the momentum basis can be written as

$$S^{\text{bos}}_{\text{quad,neutral}} = \frac{1}{2}\sum_{P=K^0,\bar{K}^0}\int_p \delta P^*(-p)\;\mathcal{G}_P^{-1}(p_\perp^2,p_\parallel^2)\;\delta P(p) + \frac{1}{2}\sum_{P,P'=\pi_3,\eta_0,\eta_8}\int_p \delta P^*(-p)\;\mathcal{G}_{P,P'}^{-1}(p_\perp^2,p_\parallel^2)\;\delta P'(p)\,. \tag{5.23}$$

Here, the inverse neutral kaon propagator is given by

$$\mathcal{G}_{K^0}^{-1}(p_\perp^2,p_\parallel^2) = \mathcal{G}_{\bar{K}^0}^{-1}(p_\perp^2,p_\parallel^2) = [2G - K\phi_u]^{-1} - c_{d,s}(p_\perp^2,p_\parallel^2)\,, \tag{5.24}$$

while for $P,P' = \pi_3,\eta_0,\eta_8$ we have

$$\mathcal{G}_{P,P'}^{-1}(p_\perp^2,p_\parallel^2) = T_{P,P'} - \sum_f \gamma^f_{P,P'}\;c_{f,f}(p_\perp^2,p_\parallel^2)\,. \tag{5.25}$$

The values of $T_{P,P'}$ and $\gamma^f_{P,P'}$ can be found in Eqs. (5.19) and (5.22), respectively.

An explicit expression for $c_{f,f'}(p_\perp^2,p_\parallel^2)$ was found in Eq. (4.24). In the neutral case, this function may involve quarks of different flavors as in Eq. (5.24), but of equal charges. Thus, taking $Q_f = Q_{f'}$ we arrive at

$$c_{f,f'}(p_\perp^2,p_\parallel^2) = \frac{N_c B_f}{2\pi^2}\int_0^\infty dz\int_0^1 dy\, e^{-z\left[yM_f^2+(1-y)M_{f'}^2+y(1-y)p_\parallel^2-i\epsilon\right]}\, e^{-\gamma_f(y,z)\frac{p_\perp^2}{B_f}}\times \left\{\left[M_fM_{f'}+\frac{1}{z}-y(1-y)p_\parallel^2\right]\coth(zB_f)+\frac{B_f}{\sinh^2(zB_f)}\left[1-\gamma_f(y,z)\,\frac{p_\perp^2}{B_f}\right]\right\}, \tag{5.26}$$

where $\gamma_f(y,z)$ is given in Eq. (4.28). Expression (5.26) properly reduces to Eq. (4.27) in the particular case $M_{f'} = M_f$.

The function $c_{f,f'}(p_\perp^2,p_\parallel^2)$ is divergent. As in the previous chapter, we regularize it using the MFIR scheme, by adding and subtracting its unregulated contribution in the $B=0$ limit. The calculation of the $B=0$ contribution for different quark masses is outlined in Appendix C, where the relevant expression is given in Eq. (C.2). Regularizing the $B=0$ piece using a 3D cutoff, the function is then separated in a vacuum and a magnetic contribution

$$c^{\text{reg}}_{f,f'}(p_\perp^2,p_\parallel^2) = c^{\text{vac}}_{f,f'}(p^2) + c^{\text{mag}}_{f,f'}(p_\perp^2,p_\parallel^2)\,. \tag{5.27}$$

In contrast to the two-flavor case, in $SU(3)$ the η' mass can overcome the quark threshold

$M_f + M_{f'}$. Therefore, we carefully proceed with the calculation taking into account this possibility. The neutral pole masses are calculated in the rest frame of the mesons, i.e. setting $p_\mu = im_P\delta_{\mu,4}$, with $m_P > 0$. For the vacuum, the calculation is detailed in section C.1 of Appendix C, leading to the expression in Eq. (C.12). In turn, the magnetic contribution is discussed in section C.2. We outline below the strategy followed for the latter case.

Assuming that $m_P < M_f + M_{f'}$, the magnetic term can be integrated by parts to be re-expressed as

$$c^{\rm mag}_{f,f'}(0,-m_P^2) \;=\; 2N_c\left\{\frac{I^{\rm mag}_{1f}+I^{\rm mag}_{1f'}}{2} - \left[m_P^2-(M_f-M_{f'})^2\right] I^{\rm mag}_{2ff'}(-m_P^2)\right\}\,. \tag{5.28}$$

The function $I^{\rm mag}_{1f}$ has already been given in Eq. (2.79), while

$$I^{\rm mag}_{2ff'}(-m_P^2) \;=\; \frac{1}{8\pi^2}\lim_{\epsilon\to 0}\int_0^1 dy\left[\psi(\bar{x}_{f,f'}-i\epsilon) - \ln(\bar{x}_{f,f'}-i\epsilon) + \frac{1}{2(\bar{x}_{f,f'}-i\epsilon)}\right]\,, \tag{5.29}$$

is a generalization of $I^{\rm mag}_{2f}(p_\parallel^2)$ in Eq. (4.34). Here $\psi(x)$ is the digamma function and we have defined

$$\bar{x}_{f,f'} \;=\; \frac{yM_f^2+(1-y)M_{f'}^2-y(1-y)m_P^2}{2B_f}\,. \tag{5.30}$$

For $m_P < M_f + M_{f'}$, $\bar{x}_{f,f'} > 0$ for all values of y within the integration range of the integral of Eq. (5.29). The function $I^{\rm mag}_{2ff'}$ is well-defined then and the limit $\epsilon \to 0$ can be directly taken.

On the other hand, for the η' we expect that $m_P > M_f + M_{f'}$. In this case one has to have special care since $\bar{x}_{ff'}$ can be negative within the interval $0 < y < 1$. We proceed by taking the analytic continuation of both the digamma and logarithm functions. This implies that the inverse propagators become complex functions. Thus, we assume that $p_\parallel$ develops an imaginary part

$$p_\parallel^2 \;=\; -\left(m_P - \frac{i}{2}\Gamma_P\right)^2\,, \tag{5.31}$$

where Γ_P is associated with the decay width of the meson. Following the customary method introduced in Ref. [266], we assume that the width is not too large and neglect its contribution inside the $I^{\rm mag}_{2ff'}$ function (this also applies to the equivalent vacuum contribution)

$$c^{\rm mag}_{f,f'}(m_P,\Gamma_P) \;\simeq\; 2N_c\left\{\frac{I^{\rm mag}_{1f}+I^{\rm mag}_{1f'}}{2} - \left[\left(m_P-\frac{i}{2}\Gamma_P\right)^2-(M_f-M_{f'})^2\right] I^{\rm mag}_{2ff'}(-m_P^2)\right\}\,. \tag{5.32}$$

Note that in Eq. (5.29) one might hit some poles of the digamma function if the limit $\epsilon \to 0$ is naively taken. As detailed in Appendix C, through a careful treatment of these poles one can explicitly calculate the $I^{\rm mag}_{2ff'}$ function. The general result for $f \neq f'$ is given in Eq. (C.22). We remark here that, as a consistency check, we have repeated the calculation using the Landau level representation of the quark propagator, well-defined for all m_P, obtaining the same result. For the determination of the η' mass we only need the $f = f'$ version of the general expression, given by

$$I^{\rm mag}_{2ff}(-m_P^2) \;=\; \frac{1}{8\pi^2}\Bigg\{ \int_0^1 dy\; \psi(\bar{x}_{f,f'} + N + 1) - \ln\left(\frac{M_f^2}{2B_f}\right) - 2\beta_0 \ln\left[\frac{m_P(1+\beta_0)}{2M_f}\right] + 2 - \frac{2B_f}{m_P^2}\sum_{n=0}^{N} \frac{g_n}{\beta_n} \ln\left(\frac{1-\beta_n}{1+\beta_n}\right)\Bigg\} + \frac{i}{8\pi}\left[\beta_0 - \frac{2B_f}{m_P^2}\sum_{n=0}^{N}\frac{g_n}{\beta_n}\right] , \tag{5.33}$$

where $g_n = 2 - \delta_{n0}$ and $N = \text{Floor}\,[m_P^2\beta_0^2/8B_f]$. Moreover,

$$\beta_n \;=\; \sqrt{1 - \frac{4M_f^2}{m_P^2} - \frac{8nB_f}{m_P^2}}\,. \tag{5.34}$$

For the neutral kaons, we expect $m_{K^0} = m_{\bar{K}^0} < M_d + M_s$. In this case the polarization function is real and $I^{\rm mag}_{2ff'}$ is well defined in the $\epsilon \to 0$ limit of Eq. (5.29). Therefore, the pole-mass will be given by the solution of

$$\mathcal{G}^{-1}_{K^0}(p_\perp^2 \;=\; 0, p_\parallel^2 \;=\; -m_{K^0}^2) \;=\; 0\,. \tag{5.35}$$

In the $P, P' = \pi_3, \eta_0, \eta_8$ subspace, the corresponding quadratic action can be expressed in matrix notation through the following inverse matrix propagator

$$\mathcal{M} \;=\; \begin{pmatrix} \mathcal{G}^{-1}_{\pi_3\pi_3} & \mathcal{G}^{-1}_{\pi_3\eta_0} & \mathcal{G}^{-1}_{\pi_3\eta_8} \\ \mathcal{G}^{-1}_{\eta_0\pi_3} & \mathcal{G}^{-1}_{\eta_0\eta_0} & \mathcal{G}^{-1}_{\eta_0\eta_8} \\ \mathcal{G}^{-1}_{\eta_8\pi_3} & \mathcal{G}^{-1}_{\eta_0\eta_8} & \mathcal{G}^{-1}_{\eta_8\eta_8} \end{pmatrix}\,, \tag{5.36}$$

which is actually symmetric. The physical meson pole-masses and widths will be given by the roots of

$$\det[\mathcal{M}(m_P, \Gamma_P)] \;=\; 0\,, \tag{5.37}$$

where the three pair of roots are to be associated with the π^0, η, η'. Of course, one expects to get $\Gamma_{\pi^0} = \Gamma_\eta = 0$, while $\Gamma_{\eta'}$ is expected to be nonvanishing. Note that when $B = 0$, π_3 (i.e. π^0 in this case) decouples from the η_0, η_8 states due to isospin symmetry. However, in the presence of an external magnetic field this symmetry breaks down due to different quark electric charges. In that case, the π^0, η, η' neutral mesons consist of a mix of π_3, η_0, η_8

states, reflected by the fact that nondiagonal terms are present in the inverse propagator of Eq. (5.36).

5.1.2.2 Charged mesons

For charged mesons the contributions of Schwinger phases associated with the quark propagators do not cancel out, leading to a breakdown of translational invariance. As in the previous chapter, in order to diagonalize the charged meson fields we expand them as

$$\delta P(x) \;=\; \sum\!\!\!\!\!\!\int_{\bar{p}} \mathcal{B}^{s}_{\bar{p}}(x)\, \delta P(\bar{p})\,, \tag{5.38}$$

where we have used the shorthand notation of Eq. (2.62). The Euclidean Ritus-type basis function $\mathcal{B}^{s}_{\bar{p}}(x)$ are given in Eq. (2.59) for the Landau gauge. Here, $\bar{p} = (\ell, p_2, p_3, p_4)$, where ℓ labels the charged meson Landau level, and $s = \mathrm{sign}(Q_P B)$. In this subsection, $P = \pi^{\pm}, K^{\pm}$. Thus, the charged meson contribution to the quadratic action in the Ritus basis reads

$$\begin{aligned} S^{\mathrm{bos}}_{\mathrm{quad,charged}} \;=\; & \frac{1}{2} \sum\!\!\!\!\!\!\int_{\bar{p},\bar{p}'} \Big(\delta\pi^{\pm}(\bar{p})\Big)^{*} \left[\frac{1}{2G - K\phi_s}\, \hat{\delta}_{\bar{p},\bar{p}'} - J_{\pi^{\pm}}(\bar{p},\bar{p}')\right] \delta\pi^{\pm}(\bar{p}') \,+ \\ & \frac{1}{2} \sum\!\!\!\!\!\!\int_{\bar{p},\bar{p}'} \Big(\delta K^{\pm}(\bar{p})\Big)^{*} \left[\frac{1}{2G - K\phi_d}\, \hat{\delta}_{\bar{p},\bar{p}'} - J_{K^{\pm}}(\bar{p},\bar{p}')\right] \delta K^{\pm}(\bar{p}')\,, \end{aligned} \tag{5.39}$$

where from Eq. (4.15)

$$J_{\pi^{-}}(\bar{p},\bar{p}') \;=\; \int_v c_{d,u}(v)\, h_{\pi^{-}}(\bar{p},\bar{p}',v)\,, \qquad J_{K^{-}}(\bar{p},\bar{p}') \;=\; \int_v c_{s,u}(v)\, h_{K^{-}}(\bar{p},\bar{p}',v)\,. \tag{5.40}$$

For positively charged mesons, flavors must be interchanged in the $c_{f,f'}(v)$ functions defined in Eq. (4.16). The spatial integral $h_P(\bar{p},\bar{p}',v)$ is given by Eq. (4.38).

Following the same steps of subsection 4.1.3, we can integrate to obtain the generalization of the polarization function found in Eq. (4.47) to the case of different quark masses. These functions are divergent and need to be regularized. Within the MFIR scheme using a 3D cutoff, defining $J_{\pi^{-}}(\bar{p},\bar{p}') \equiv \hat{\delta}_{\bar{p},\bar{p}'}\, J_{\pi^{-}}(\ell,\Pi^2)$ and $J_{K^{-}}(\bar{p},\bar{p}') \equiv \hat{\delta}_{\bar{p},\bar{p}'}\, J_{K^{-}}(\ell,\Pi^2)$ they can be expressed as

$$J^{\mathrm{reg}}_{P}(\ell,\Pi^2) \;=\; J^{\mathrm{vac}}_{P}(\Pi^2) + J^{\mathrm{mag}}_{P}(\ell,\Pi^2)\,. \tag{5.41}$$

Once again, the regularized vacuum contribution is given in Eq. (C.12) of Appendix C,

evaluated at $p^2 \to \Pi^2$. After a long but straightforward calculation, we obtain the following expression for the magnetic contribution

$$
\begin{aligned}
J_P^{\rm mag}(\ell,\Pi^2) \;=\; & \frac{N_c}{2\pi^2}\int_0^\infty dz \int_0^1 dy\, e^{-z\left[yM_f^2+(1-y)M_{f'}^2+y(1-y)\left(\Pi^2-(2\ell+1)B_P\right)\right]} \times \\
& \left\{ \left[M_f M_{f'} + \frac{1}{z} - y(1-y)\left(\Pi^2-(2\ell+1)B_P\right)\right] \times \right. \\
& \left[\frac{(1+s_f\, s_{f'}\, t_f\, t_{f'})}{\alpha_+}\left(\frac{\alpha_-}{\alpha_+}\right)^\ell - \frac{e^{-zy(1-y)(2\ell+1)B_P}}{z}\right] + \\
& \frac{(1-t_f^2)(1-t_{f'}^2)}{\alpha_+^2\alpha_-}\left(\frac{\alpha_-}{\alpha_+}\right)^\ell \left[\alpha_- + \ell(\alpha_- - \alpha_+)\right] - \\
& \left. \frac{e^{-zy(1-y)(2\ell+1)B_e}}{z}\left[\frac{1}{z} - y(1-y)(2\ell+1)B_P\right]\right\}, \qquad (5.42)
\end{aligned}
$$

which properly reduces to (4.47) when $M_f = M_{f'}$. Here $B_P = |Q_P B|$ with $Q_P = Q_f - Q_{f'}$. Also, see Eqs. (4.19) and (4.48) for the definitions of t_f, $t_{f'}$ and $\alpha_\pm$. For charged pions and kaons, $B_P = |eB| \equiv B_e$.

For these mesons we expect them to develop only a real pole-mass, i.e. $\Pi^2 = -m_P^2$ with $m_P < M_f + M_{f'}$. In that case the integrals in Eq. (5.42) are convergent and well-defined. Therefore, for each Landau level the charged mesons pole-masses will be given by the solutions of

$$
\begin{aligned}
& \frac{1}{2G - K\phi_s} - J_{\pi^-}(\ell, \Pi^2 \;=\; -m_{\pi^-}^2) \;=\; 0\,, \\
& \frac{1}{2G - K\phi_d} - J_{K^-}(\ell, \Pi^2 \;=\; -m_{K^-}^2) \;=\; 0\,. \qquad (5.43)
\end{aligned}
$$

For the π^+ and K^+, it is easy to see that $J_{\pi^+}(\ell,\Pi^2) = J_{\pi^-}(\ell,\Pi^2)$ and $J_{K^+}(\ell,\Pi^2) = J_{K^-}(\ell,\Pi^2)$, which implies that for the same charged meson both masses are equal as expected from charge conservation.

5.2 Numerical results

To obtain numerical results for the magnetic field dependence of the meson masses one has to fix the model parametrization. Here, following Ref. [266], we take the parameter set $m_u = m_d = 5.5$ MeV, $m_s = 140.7$ MeV, $\Lambda = 602.3$ MeV, $G\Lambda^2 = 1.835$ and $K\Lambda^5 = 12.36$, which has been determined on fixing that for vanishing external field one gets $m_\pi = 135$ MeV, $m_K = 497.7$ MeV, $m_{\eta'} = 957.8$ MeV and $f_\pi = 92.4$ MeV. This parameter

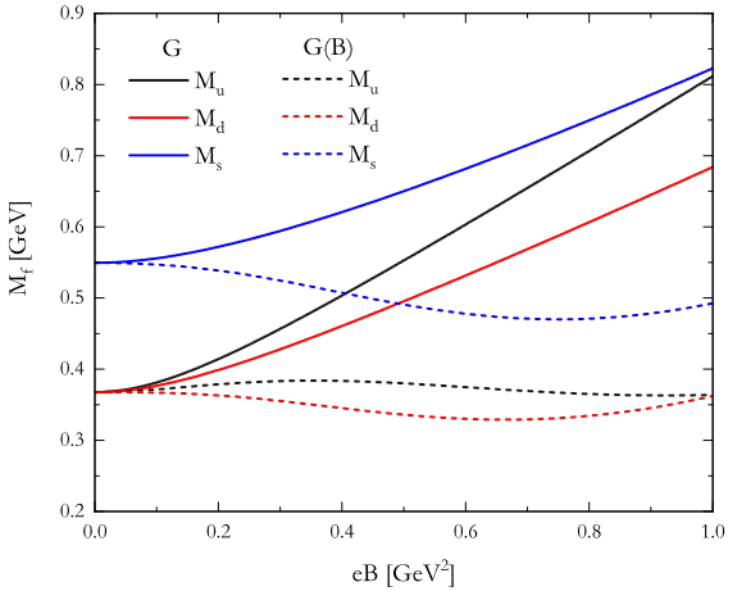

Figure 5.1: Effective quark masses M_u (black), M_d (red) and M_s (blue) as functions of eB for fixed (solid lines) and B-dependent (dashed lines) coupling G.

set gives an η mass of $m_\eta = 514.8$ MeV, which compares reasonably well with the physical value $m_\eta^{ph} = 548.8$ MeV, together with an appropriate value for the chiral condensate of $\langle \bar{f} f \rangle^{1/3} = 242$ MeV for $f = u, d$. As mentioned in the introduction, while local NJL-like models are able to reproduce the MC effect at vanishing temperature, they fail to lead to the IMC effect. As in the previous chapter, to incorporate the backreaction of gluons due to magnetized quark loops, we allow for magnetic field dependence of the coupling constant. In particular, we adopt the expression proposed in Ref. [158] in the context of an $SU(3)$ NJL model with the same parameters that we use. In that work the current quark masses, Λ and K were kept constant while for $G(B)$ the form

$$G(B) \;=\; G\left[\frac{1 + a(eB/\Lambda_{QCD}^2)^2 + b(eB/\Lambda_{QCD}^2)^3}{1 + c(eB/\Lambda_{QCD}^2)^2 + d(eB/\Lambda_{QCD}^2)^4}\right] , \tag{5.44}$$

was introduced. Here, $a = 0.0108805$, $b = -1.0133\ 10^{-4}$, $c = 0.02228$, $d = 1.84558\ 10^{-4}$ and $\Lambda_{\rm QCD} = 300$ MeV. As stated in Ref. [158], this form of the scalar coupling has been fitted so that the lattice QCD pseudocritical chiral transition temperatures are reproduced.

Results for the magnetic field dependence of the dynamical quark masses are shown in Figure 5.1, for both constant and B-dependent coupling G. As we see, for constant G all quark masses increase with B. In contrast, for $G(B)$ they display a nonmonotonous behavior, less affected by the magnetic field. In this case, M_d and M_s initially decrease with B, while about $eB \sim 0.6 - 0.7$ GeV^2 this tendency reverses. On the other hand, M_u has just the opposite behavior. In fact, these dependencies of the dynamical quark masses on the magnetic field are roughly consistent with the results obtained in Ref. [164]. In

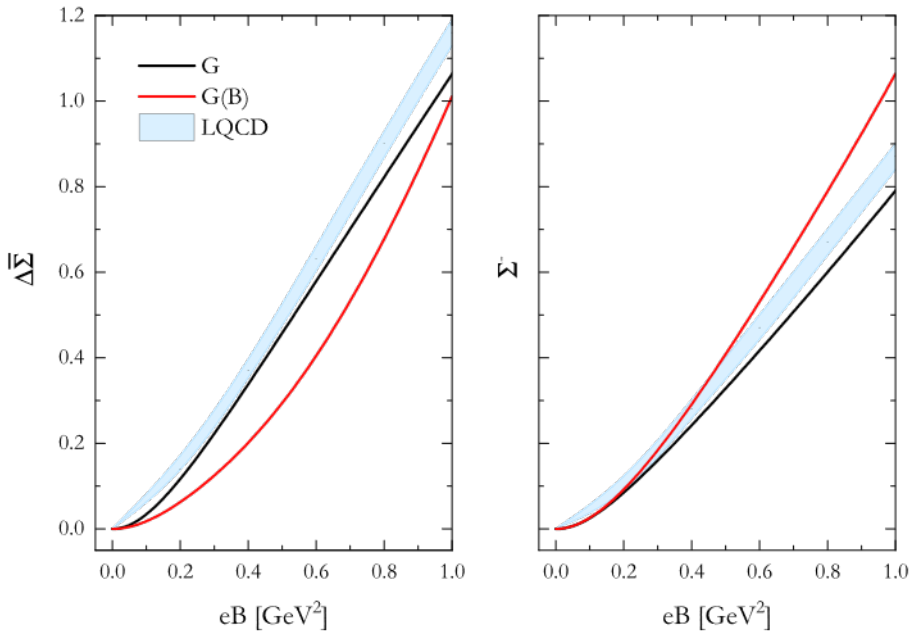

Figure 5.2: Condensate average (left) and difference (right) as functions of eB. Results for constant (black) and B-dependent (red) coupling G are shown in solid lines. LQCD results from Ref. [73] (light blue bands) are added for comparison.

that work these quantities have been extracted from a LQCD calculation of the baryon masses using a simple minded approximation based on the constituent quark model.

It should be stressed that in spite of the rather different behavior between the dynamical quark masses, a magnetic catalysis effect at zero temperature is obtained independently on whether G depends on B or not. This is shown in Figure 5.2, where we display the conveniently normalized light quark condensates defined in Eq. (4.107) for both constant and B-dependent coupling G. In the left panel we plot the average $\Delta\bar{\Sigma} = (\Delta\Sigma_u + \Delta\Sigma_d)/2$ while in the right panel the difference $\Sigma^- = \Delta\Sigma_u - \Delta\Sigma_d$ is shown. We recall that $\Delta\Sigma_f = -2m_f[\phi_f^{\rm reg}(B) - \phi_f^{\rm reg}(0)]/D^4$, where $D = (135 \times 86)^{1/2}$ MeV is a phenomenological normalization constant. We compare our results with LQCD ones, represented in the bands of Figure 5.2. As in the $SU(2)$ case, we observe that although the predictions for constant G are somewhat closer to the LQCD results, those corresponding to $G(B)$ can certainly be considered as acceptable. It is interesting to remark here that other form functions of $G(B)$, such as the ones proposed in Refs. [161, 164], reproduce similar trends for these quantities.

We turn now to our results for the magnetic field dependence of the masses of the nonet of pseudoscalar mesons. They are shown in Figure 5.3, where for charged mesons we instead display their lowest energy states, given by

$$E_{P^\pm} = \sqrt{m_{P^\pm}^2 + (2\ell+1)eB + p_3^2}\Big|_{p_3=\ell=0} = \sqrt{m_{P^\pm}^2 + eB}\,. \tag{5.45}$$

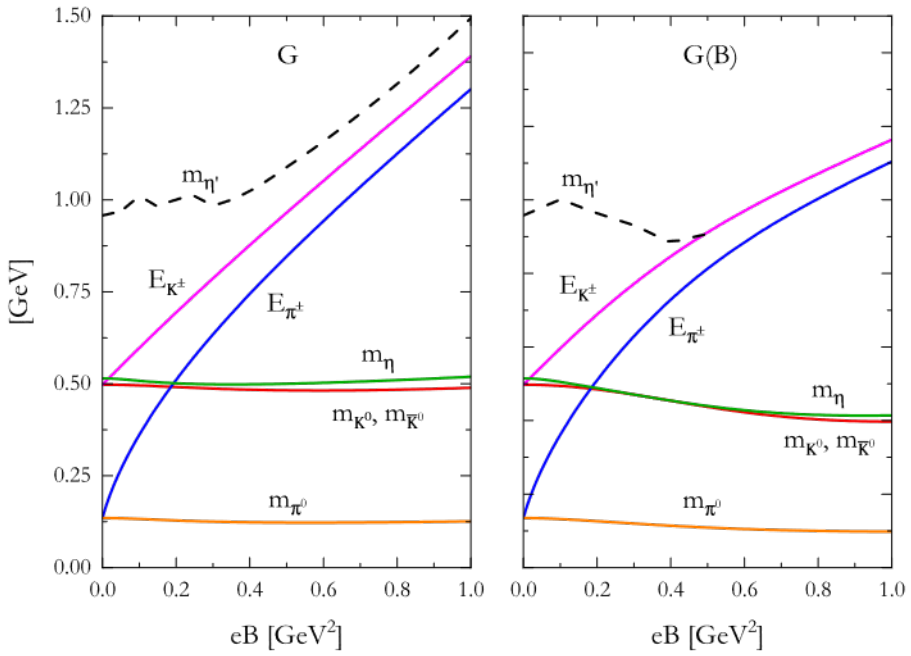

Figure 5.3: Pseudoscalar neutral meson pole-masses and charged mesons lowest energies as functions of eB for constant (left) and B-dependent (right) coupling G.

It should be noticed that both E_P and m_P depend on B, although not explicitly stated. The left (right) panel corresponds to the case of constant coupling G (B-dependent G). We observe that, except for the η'-mass, the B-dependence is rather mild in the case of the neutral mesons. On the other hand a rather strong increase with growing B is found for charged meson masses. These results are analyzed in further detail in what follows.

The case of η' is somewhat special and, therefore, indicated in dashed lines in Figure 5.3. In fact, already at $B = 0$ its mass is above the threshold for $q\bar{q}$-decay and, thus, the associated $q\bar{q}$ polarization diagram receives an unphysical imaginary part. Following Ref. [266] we accept this as an unavoidable feature of the NJL model and define the η'-mass as the real part of the corresponding pole in the complex plane. We should keep in mind, however, that this fact makes the predictions for the η'-mass less reliable as compared to those of the other mesons. The situation worsens for finite magnetic field. First, new divergencies appear at low magnetic fields due the existence of thresholds associated with the Landau levels of the intermediate quark states. Although these divergencies are along the real axis, they originate the kind of oscillatory behavior found for $eB \lesssim 0.2$ GeV^2. In passing, we note that including in the calculation the imaginary part of the polarization function makes these divergences less harmful. If one neglects that contribution, as done in Ref. [147], the determination of $m_{\eta'}$ becomes full of ambiguities making its determination even more troublesome. The other point has to do with the fact that at finite magnetic field the width is in general larger than the already non-negligible

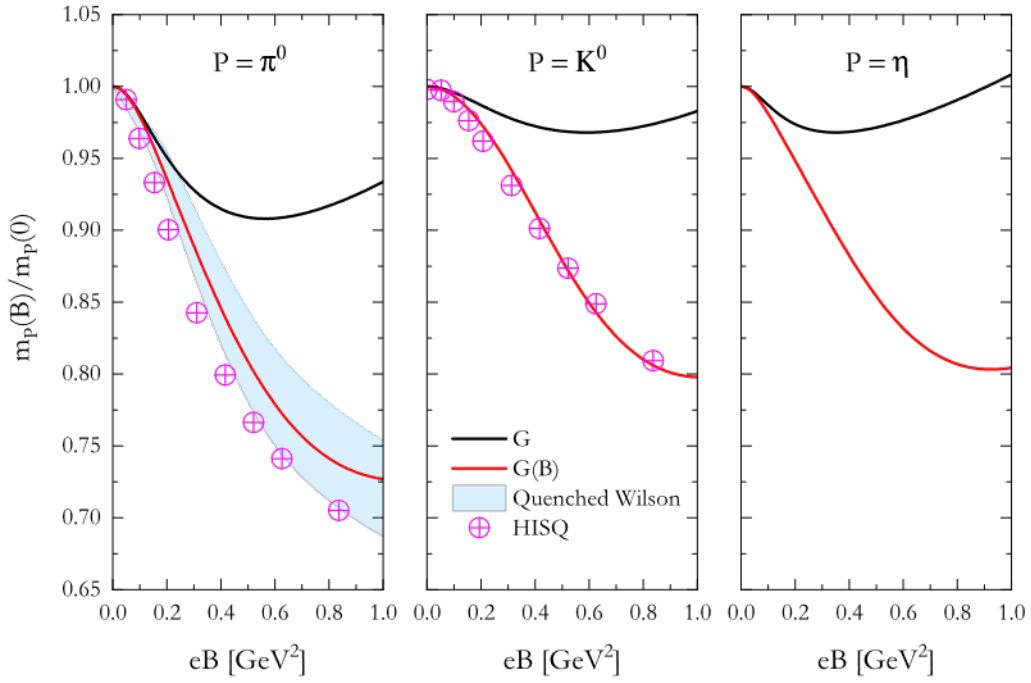

Figure 5.4: Normalized neutral meson masses as functions of eB for constant (black solid lines) and B-dependent (red solid lines) coupling G. LQCD results from Ref. [129] (light blue band) and Ref. [258] (magenta circles) are added for comparison.

value at $B = 0$, $\Gamma_{\eta'}^{B=0} = 269$ MeV. For constant G, we encounter a nonmonotonic behavior of the width, which shows a close-to-vacuum mean value of $\Gamma_{\eta'}^{B,mean} = 332$ MeV but can reach values of $\Gamma_{\eta'}^{B} \sim 590$ MeV at intermediate fields. On the other hand, for $G(B)$ the pace of growth of the width increases. At fields strengths around $eB \sim 0.5$ GeV^2 the width exceeds the mass, with a value of $\Gamma_{\eta'}^{B} \sim 1.46$ GeV. This enhancement of the width, together with the decrease of $G(B)$ as B increases, results in the fact that for $eB \gtrsim 0.5$ GeV^2 no solution of Eq. (5.37) can be found apart from the ones associated with π^0 and η. Namely, above such a value of the magnetic field the coupling strength is not enough to form an η'-resonance in the $q\bar{q}$-continuum.

To discuss our results for the other neutral mesons (π^0, $K^0, \bar{K}^0$ and η) in more detail we display in Figure 5.4 the corresponding masses taken with respect to their values at $B = 0$. We show results using a constant and a B-dependent coupling G, together with LCQD simulations from Refs. [129, 258] for comparison. It should be noticed that these LQCD calculations correspond to unphysical pion masses of 415 and 220 MeV respectively, for vanishing magnetic field. In both cases they point to a stronger decrease of the π^0 mass with increasing B than the one found in our calculation with constant G. On the other hand, the results obtained using $G(B)$ are in reasonable good agreement with LQCD ones. The same conclusion was reached in the previous chapter for the $SU(2)$ case; for both versions of the model results for m_{π^0} are rather similar, although $SU(3)$ values are slightly

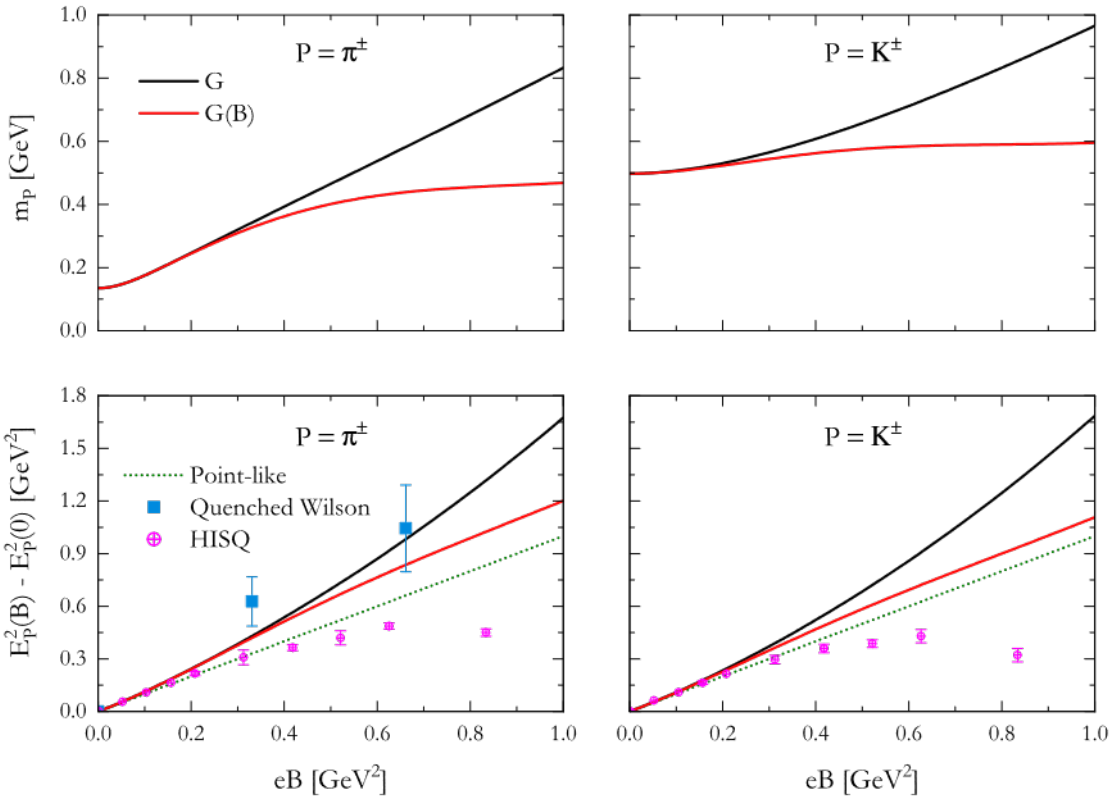

Figure 5.5: Charged meson masses (top) and differences of squared lowest energies between the case at $B \neq 0$ and $B = 0$ (bottom) for charged pions (left) and kaons (right) as a function of eB. Results for constant and B-dependent coupling G are shown in black and red solid lines, respectively. Green dotted lines correspond to energies associated with point-like charged mesons. LQCD results from Ref. [129] (blue squares) and Ref. [258] (magenta circles) are added for comparison.

higher. This seems to also provide further support to the relation between the IMC effect and the reduction of the neutral pion mass at finite B mentioned in Ref. [258]. A similar behavior is observed for K^0 and $\bar{K}^0$ masses (central panel), although the magnitude of the decrease is reduced. For these mesons, the only LQCD result that has been reported is that of Ref. [258]. We observe that, once again, a much better agreement with these results is obtained when a B-dependent coupling G is used in the NJL model. Finally, in the right panel we show our predictions for the behavior of the normalized η-meson mass. They turn out to be quite similar to the ones obtained for the K^0 and $\bar{K}^0$ relative masses.

Finally, we consider the masses of charged pseudoscalar mesons $\pi^\pm$ and $K^\pm$. We display the differences in their squared lowest energies from the case of a zero magnetic field, i.e. $E^2_{P^\pm}(B) - E^2_{P^\pm}(B = 0)$, in Figure 5.5. We also include their masses in the top graphs for completeness. We show results for G and $G(B)$ as compared to a point-like charged meson and LQCD simulations from Refs. [129, 258]. We observe that for both charged pions and kaons, our results show a stronger increase with growing B as compared

with the ones associated with point-like mesons. Those obtained using a B-dependent coupling are, however, somewhat closer to them. Results are very similar to the ones obtained in the $SU(2)$ case in Figure 4.7, although $SU(3)$ values are slightly higher. As for the comparison with LQCD results, we note that in the case of charged pions there are significant differences between the results reported by the two different LQCD groups, specially at large magnetic fields. Although our results seem to be more consistent with those of Ref. [129] it should be recalled that they correspond to a larger (unphysical) value of the $B = 0$ pion mass and have larger error bars. In any case, we see that, for both charged pions and kaons, our NJL results show no sign of the strong nonmonotonous behavior found in the LQCD calculation of Ref. [258]. Results obtained within the $SU(2)$ version of the model seem to indicate that the inclusion of quark anomalous magnetic moments does not modify the trend of the charged pion mass obtained in the present work [157].

CHAPTER 6

Diquark and nucleon masses under strong magnetic fields within the SU(2) NJL model

In the past few years, the effects of a magnetic field on baryon masses has been addressed in the context of ChPT [267, 268], nonrelativistic quark models [269], extended linear sigma model [270], Walecka model [270, 271], soliton models [272], finite energy QCD sum rules [273], and also lattice QCD [164]. It is worth noticing that these theoretical approaches lead to various different results for the behavior of nucleon masses. In this chapter we complement these works by studying the effect of an intense external magnetic field on scalar diquark and nucleon properties within the framework of the two-flavor Nambu–Jona-Lasinio (NJL) model. In the NJL model, diquarks are constructed through the resummation of quark loop chains using the random phase approximation, while nucleons are treated as bound quark-diquark states described by a relativistic Fadeev equation, using the static approximation for quark exchange interactions. For charged particles, analytical calculations are performed using the Ritus-type eigenfunction method presented in previous chapters, which properly takes into account the breakdown of translation invariance that arises from the presence of Schwinger phases. Within this scheme, for definite model parametrizations we obtain numerical predictions for diquark and nucleon masses, which are compared with Chiral Perturbation Theory and Lattice QCD results. In addition, numerical estimations for the nucleon magnetic moments are obtained. Results from this chapter are based on Ref. [274].

6.1 Diquarks and nucleons

6.1.1 Bosonized NJL model with diquark interactions in the presence of an external magnetic field

We start by considering the Euclidean Lagrangian density for the NJL two-flavor model in the presence of an electromagnetic field and color pairing interactions. One has

$$\mathcal{L} \;=\; \bar{\psi}\left(-i\,\not{D} + m_c\right)\psi - G\left[(\bar{\psi}\,\psi)^2 + (\bar{\psi}\,i\gamma_5\tau_a\,\psi)^2\right] - H\left(\bar{\psi}_c\,i\gamma_5\tau_2\lambda_A\,\psi\right)^{\dagger}\left(\bar{\psi}_c\,i\gamma_5\tau_2\lambda_A\,\psi\right)\,, \tag{6.1}$$

where $\psi = (\psi_u, \psi_d)^T$ represents a quark field with two flavors, G and H are coupling constants and m_c is the current quark mass, which is assumed to be equal for u and d quarks. Moreover we have defined $\psi_c = \gamma_2\gamma_4\bar{\psi}^T$, while τ_a and λ_A, with $a = 1, 2, 3$ and $A = 2, 5, 7$, stand for Pauli and Gell-Mann matrices acting on flavor and color spaces, respectively. The interaction between the fermions and the electromagnetic field $\mathcal{A}_\mu$ is driven by the covariant derivative $D_\mu = \partial_\mu - i\,\hat{Q}\mathcal{A}_\mu$, where $\hat{Q} = \mathrm{diag}(Q_u, Q_d)$. As before, we consider the particular case of an uniform stationary magnetic field $\vec{B}$ orientated along the 3-axis, represented in the Landau gauge $\mathcal{A}_\mu = Bx_1\,\delta_{\mu,2}$.

As in previous chapters, it is convenient to bosonize the fermionic action. The procedure follows the idea outlined in Appendix A, taking additional care of the color pairing interactions. Then, the action is rewritten in terms of scalar $\sigma(x)$, pseudoscalar $\pi_a(x)$ and diquark fields $\Delta_A(x)$, while fermion fields are integrated out. The bosonized Euclidean action can be written as

$$S_{\mathrm{bos}} \;=\; -\frac{1}{2}\mathrm{Tr}\,\ln\mathbf{D} + \int d^4x\,\left[\frac{\sigma(x)\,\sigma(x) + \pi_a(x)\,\pi_a(x)}{4G} + \frac{\Delta_A(x)^*\Delta_A(x)}{4H}\right]\,, \tag{6.2}$$

where

$$\mathbf{D}(x,x') \;=\; \delta^{(4)}(x-x')\begin{pmatrix} -i\gamma_\mu D_\mu + m_c + \phi(x) & i\,\gamma_5\,\tau_2\,\lambda_A\,\Delta_A(x) \\ i\,\gamma_5\,\tau_2\,\lambda_A\,\Delta_A(x)^* & -i\gamma_\mu D_\mu^* + m_c + \phi(x)^T \end{pmatrix}\,. \tag{6.3}$$

with $\phi(x) = \sigma(x) + i\gamma_5\tau_a\pi_a(x)$. As customary, we have used here the Nambu-Gorkov formalism, see e.g. [275]. In the former equations, and in what follows, matrices in Nambu-Gorkov space are denoted in boldface.

We proceed by expanding the bosonized action in powers of the fluctuations $\delta\sigma(x)$, $\delta\pi_a(x)$ and $\delta\Delta_A(x)$ around the corresponding mean field (MF) values. As before, we assume that the field $\sigma(x)$ has a nontrivial translational invariant MF value $\bar{\sigma}$, while the

vacuum expectation values of pseudoscalar and diquark fields are zero. Then, one has

$$\mathbf{D}(x,x') \;=\; \mathbf{D}_{\rm MF}(x,x') + \delta\mathbf{D}(x,x')\,. \tag{6.4}$$

The MF piece reads

$$\mathbf{D}_{\rm MF}(x,x') \;=\; \begin{pmatrix} \mathcal{D}(x,x') & 0 \\ 0 & \mathcal{D}_c(x,x') \end{pmatrix}\,, \tag{6.5}$$

where

$$\begin{aligned} \mathcal{D}(x,x') \;&=\; \delta^{(4)}(x-x')\;(-i\gamma_\mu D_\mu + M)\,, \\ \mathcal{D}_c(x,x') \;&=\; \delta^{(4)}(x-x')\;(-i\gamma_\mu {D_\mu}^* + M)\,, \end{aligned} \tag{6.6}$$

Here M denotes the quark effective mass, $M = m_c + \bar{\sigma}$, and we have omitted the MF subindex for visual clarity. The fluctuation piece is given by

$$\delta\mathbf{D}(x,x') = \delta^{(4)}(x-x') \begin{pmatrix} \delta\phi(x) & i\,\gamma_5\,\tau_2\,\lambda_A\,\delta\Delta_A(x) \\ i\,\gamma_5\,\tau_2\,\lambda_A\,\delta\Delta_A(x)^* & \delta\phi(x)^T \end{pmatrix}\,. \tag{6.7}$$

The MF operators $\mathcal{D}(x,x')$ and $\mathcal{D}_c(x,x')$ are flavor-diagonal, and their inverses correspond to the MF quark propagators in the presence of a magnetic field. One has

$$\mathcal{D}^{-1}(x,x') \;=\; \mathcal{S}(x,x') \;=\; \mathrm{diag}\left(\mathcal{S}^u(x,x')\,,\,\mathcal{S}^d(x,x')\right)\,, \tag{6.8}$$

$$\mathcal{D}_c^{-1}(x,x') \;=\; \mathcal{S}_c(x,x') \;=\; \mathrm{diag}\left(\mathcal{S}^{-u}(x,x')\,,\,\mathcal{S}^{-d}(x,x')\right)\,, \tag{6.9}$$

where the minus signs in front of the flavor indices $f = u,d$ indicate that the sign of the corresponding quark electric charge in the propagator has to be reversed. As before, we choose to write the quark propagator in its Schwinger form, given by Eqs. (2.66) and (2.67) (see text below these equations for some shorthand notation).

Replacing the previous relations in the bosonized effective action and expanding in powers of meson fluctuations around the MF values, one gets

$$S^{\rm bos} \;=\; S^{\rm bos}_{\rm MF} \;+\; S^{\rm bos}_{\rm quad} \;+\; \ldots \tag{6.10}$$

The expression of $S^{\rm bos}_{\rm MF}$, together with those of the mesonic contributions to $S^{\rm bos}_{\rm quad}$, are given in Eqs. (2.28) and (4.12) respectively. In each corresponding section, the procedure followed to obtain the regularized gap equation and the expressions required to calculate various meson properties are discussed in detail. In the present case, $S^{\rm bos}_{\rm quad}$ includes an

additional contribution that is quadratic in the diquark fields. This will be discussed in the next subsection.

6.1.2 Diquark mass and propagator

The diquark contribution to $S^{\rm bos}_{\rm quad}$ is given by

$$S^{\rm bos}_{\rm diq} \;=\; S_{\Delta} + S_{\bar{\Delta}} \;=\; \frac{1}{2} \sum_{\mathsf{D}=\Delta,\bar{\Delta}} \int d^4x\, d^4x'\; \delta\mathsf{D}_A(x)^*\; \mathcal{G}^{-1}_{\mathsf{D}}(x,x')\; \delta\mathsf{D}_A(x')\,, \tag{6.11}$$

where

$$\mathcal{G}^{-1}_{\mathsf{D}}(x,x') \;=\; \frac{1}{4H}\,\delta^{(4)}(x-x') - J_{\mathsf{D}}(x,x')\,. \tag{6.12}$$

The polarization functions read

$$J_{\Delta}(x,x') \;=\; \frac{1}{2N_c}\,\mathrm{Tr}_{\rm D}\left[\,c_{u,-d}(x,x') + c_{d,-u}(x,x')\,\right]\,, \tag{6.13}$$

$$J_{\bar{\Delta}}(x,x') \;=\; \frac{1}{2N_c}\,\mathrm{Tr}_{\rm D}\left[\,c_{-u,d}(x,x') + c_{-d,u}(x,x')\,\right]\,, \tag{6.14}$$

where the trace is taken over Dirac space and the functions $c_{f,f'}(x,x')$ were defined in Eq. (4.14). As seen from its quark content, Δ ($\bar{\Delta}$) corresponds to the diquark with charge $Q_{\Delta} = e/3$ ($Q_{\bar{\Delta}} = -e/3$). Since $J_{\Delta}(x,x') = J_{\bar{\Delta}}(x',x)$, both diquarks have the same mass, and we can proceed by considering only the positively charged diquark Δ.

As in the case of charged pions, there is no cancellation of Schwinger phases, leading to the breakdown of translational invariance. Therefore, in order to diagonalize the polarization function we expand the charged diquark field in terms of Ritus-type basis functions

$$\delta\Delta_A(x) \;=\; \sum\!\!\!\!\!\!\int_{\bar{p}}\; \mathcal{B}^s_{\bar{p}}(x)\;\delta\Delta_A(\bar{p})\,, \tag{6.15}$$

where we have used the shorthand notation of Eq. (2.62). The Euclidean Ritus-type basis function $\mathcal{B}^s_{\bar{p}}(x)$ are given in Eq. (2.59) for the Landau gauge. Here, $\bar{p} = (\ell, p_2, p_3, p_4)$, where ℓ labels the diquark Landau level, $s = \mathrm{sign}(Q_{\Delta}B)$ and $B_{\Delta} = |Q_{\Delta}B| = B_e/3$. Replacing this expansion in Eq. (6.11) we have

$$S_{\Delta} \;=\; \frac{1}{2} \sum\!\!\!\!\!\!\int_{\bar{p},\bar{p}'}\; \delta\Delta_A(\bar{p})^*\;\mathcal{G}^{-1}_{\Delta}(\bar{p},\bar{p}')\;\delta\Delta_A(\bar{p}')\,, \tag{6.16}$$

where $\mathcal{G}_\Delta^{-1}(\bar{p},\bar{p}') = \hat{\delta}_{\bar{p},\bar{p}'}/4H - J_\Delta(\bar{p},\bar{p}')$. Then, from Eq. (4.15) we arrive at

$$J_\Delta(\bar{p},\bar{p}\,') \;=\; \frac{1}{2N_c}\int_v \left[c_{u,-d}(v)+c_{d,-u}(v)\right] h_\Delta(\bar{p},\bar{p}\,',v)\,, \tag{6.17}$$

which depends on the $c_{f,f'}(v)$ function defined in Eq. (4.16) and on the spatial integral $h_\Delta(\bar{p},\bar{p}\,',v)$ defined in Eq. (4.38). Notice from the result in Eq. (4.24) that $c_{u,-d}(v) = c_{d,-u}(v)$.

The remaining integrals in the polarization function can be worked out following the same steps as those described in subsection 4.1.3 for the case of charged pions. As a result, the polarization function turns out to be diagonal in the Ritus-type eigenfunction basis, i.e. $J_\Delta(\bar{p},\bar{p}') = \hat{\delta}_{\bar{p},\bar{p}'}\; J_\Delta(\ell,\Pi^2)$, where $\Pi^2 = (2\ell+1)B_\Delta + p_\parallel^2$. The expression for $J_\Delta(\ell,\Pi^2)$ can be obtained from Eq. (4.47) by replacing $P=\Delta$, $f=u$, $f'=-d$ and dividing by N_c.

As in the meson case, the polarization function $J_\Delta(\ell,\Pi^2)$ is divergent and can be regularized within the MFIR scheme, carefully subtracting the $B=0$ contribution once the latter has been written in terms of the squared canonical momentum Π^2. Thus, the regularized diquark polarization function can be written as

$$J_\Delta^{\rm reg}(\ell,\Pi^2) \;=\; J_\Delta^{\rm vac}(\Pi^2) \;+\; J_\Delta^{\rm mag}(\ell,\Pi^2)\,, \tag{6.18}$$

where

$$\begin{aligned} J_\Delta^{\rm mag}(\ell,\Pi^2) \;=\; \frac{1}{2\pi^2}\int_0^\infty dz\int_0^1 dy\; e^{-z\left[M^2+y(1-y)\left(\Pi^2-(2\ell+1)B_\Delta\right)\right]}\times \\ \left\{\left[M^2+\frac{1}{z}-y(1-y)\left(\Pi^2-(2\ell+1)\,B_\Delta\right)\right]\times\right. \\ \left[\frac{\alpha_-^\ell}{\alpha_+^{\ell+1}}\,(1+t_u\,t_d)\;-\;\frac{e^{-zy(1-y)(2\ell+1)B_\Delta}}{z}\right]\;+ \\ \frac{\alpha_-^{\ell-1}}{\alpha_+^{\ell+2}}\,(1-t_u^2)\,(1-t_d^2)\,\left[\alpha_-+(\alpha_--\alpha_+)\,\ell\right]\;- \\ \left.\frac{e^{-zy(1-y)(2\ell+1)B_\Delta}}{z}\left[\frac{1}{z}-y(1-y)(2\ell+1)\,B_\Delta\right]\right\}. \end{aligned} \tag{6.19}$$

This magnetic field-dependent contribution is finite since the integrand in Eq. (6.19) is well behaved in the limit $z\to 0$. On the other hand, we regularize the expression for the added $B=0$ piece by using a 3D cutoff. We get

$$J_\Delta^{\rm vac}(\Pi^2) \;=\; 2\left[I_1^{\rm vac}+\Pi^2 I_2^{\rm vac}(\Pi^2)\right]\,, \tag{6.20}$$

where the explicit expressions of $I_1^{\rm vac}$ and $I_2^{\rm vac}$ are given in Eqs. (2.52) and (2.53), respectively.

After diagonalization, the regulated inverse diquark propagator reads

$$\mathcal{G}_\Delta^{-1}(\bar{p},\bar{p}') \;=\; \hat{\delta}_{\bar{p},\bar{p}'}\,\left[\frac{1}{4H}\;-J_\Delta^{\rm reg}(\ell,\Pi^2)\right]\,. \tag{6.21}$$

Consequently, the diquark pole mass in the presence of the magnetic field can be obtained for each Landau level ℓ by solving the equation

$$\frac{1}{4H}-J_\Delta^{\rm reg}(\ell,-m_\Delta^2)\;=\;0\,. \tag{6.22}$$

Although not explicitly stated, m_Δ depends on the magnetic field. As in the case of the charged pions, instead of dealing with m_Δ one can define the Δ "magnetic field-dependent mass" as the lowest quantum-mechanically allowed energy of the diquark, E_Δ. The latter is given by

$$E_\Delta^2\;=\;m_\Delta^2+(2\ell+1)\,B_\Delta+p_3^2\,\Big|_{\ell=p_3=0}\;=\;m_\Delta^2+\frac{|eB|}{3}\,. \tag{6.23}$$

Notice that this "mass" is magnetic field dependent even for a point-like diquark (in which case the pole mass m_Δ would be independent of B). In fact, owing to zero-point motion in the 1-2 plane, even for $\ell=0$ a diquark cannot be at rest in the presence of the magnetic field.

Since the inverse of the diquark propagator is diagonal in this basis, it can be trivially inverted. We have

$$\mathcal{G}_\Delta(\bar{p},\bar{p}')\;=\;\hat{\delta}_{\bar{p},\bar{p}'}\,\mathcal{G}_\Delta^{\rm reg}(\ell,p_\parallel^2)\,, \tag{6.24}$$

where

$$\mathcal{G}_\Delta^{\rm reg}(\ell,p_\parallel^2)\;=\;\left[\frac{1}{4H}\;-J_\Delta^{\rm reg}(\ell,\Pi^2)\right]^{-1}\,. \tag{6.25}$$

Given the diagonal form of the diquark propagator in Ritus space, see Eq. (6.24), we can transform it back to coordinate space. One obtains

$$\mathcal{G}_\Delta(x,x')\;=\;e^{i\Phi_\Delta(x,x')}\int_p e^{ip(x-x')}\,\bar{\mathcal{G}}_\Delta(p_\perp,p_\parallel)\,, \tag{6.26}$$

where

$$\bar{\mathcal{G}}_\Delta(p_\perp,p_\parallel)\;=\;2\,e^{-\frac{p_\perp^2}{B_\Delta}}\sum_{\ell=0}^{\infty}(-1)^\ell\,\mathcal{G}_\Delta^{\rm reg}(\ell,p_\parallel^2)\,L_\ell\left(\frac{2\,p_\perp^2}{B_\Delta}\right)\,. \tag{6.27}$$

We recall here the notation $p_\perp=(p_1,p_2)$ and $p_\parallel=(p_3,p_4)$.

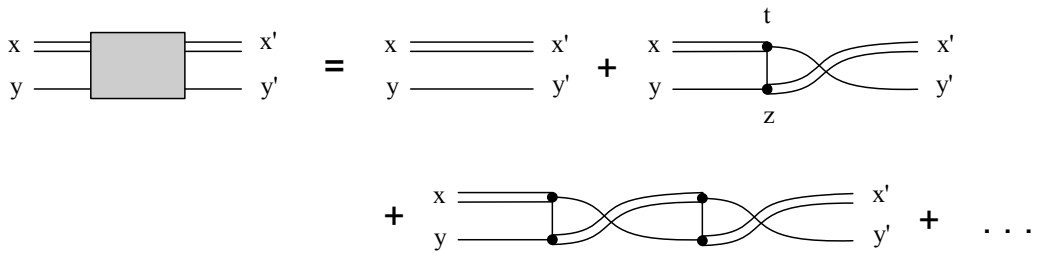

Figure 6.1: Diagrams contributing to the full baryon propagator.

6.1.3 Nucleon masses

The baryon propagator can be obtained consistently with the bound quark-diquark structure following Ref. [276]. From the infinite sum illustrated by the diagrams in Figure 6.1 one arrives at a relation of the form

$$\mathcal{S}^B([x;y],[x';y']) \;=\; \mathcal{S}_0^B([x;y],[x';y']) + \int d^4t\, d^4z\, \mathcal{S}_0^B([x;y],[t;z])\, \mathcal{H}(z,t)\, \mathcal{S}_0^B([z;t],[x';y']) + \ldots \tag{6.28}$$

where, in our case, the kernel $\mathcal{H}$ is given by

$$\mathcal{H}(z,t) \;=\; i\gamma_5\tau_2\lambda_A\, \mathcal{S}_c(z,t)\, i\gamma_5\tau_2\lambda_{A'}\,. \tag{6.29}$$

In Eq. (6.28), $\mathcal{S}^B$ stands for the full baryon propagator, while $\mathcal{S}_0^B$ describes the unperturbed propagation of a diquark and a quark, namely

$$\mathcal{S}_0^B([x;y],[t;z]) \;=\; \mathcal{G}_\Delta(x,t)\, \mathcal{S}(y,z)\,. \tag{6.30}$$

Since the nucleon fields are bilocal, we have introduced the notation of pairs $[x;y]$, where the first and second coordinates correspond to the diquark and the quark, respectively. The resummation of the diagrams in Figure 6.1 leads to a relativistic Fadeev equation that can be written in the form

$$\mathcal{S}_0^B([x;y],[x';y']) \;=\; \int d^4t\, d^4z \Big[\delta^{(4)}(x-z)\delta^{(4)}(y-t) - L([x;y],[z;t])\Big]\, \mathcal{S}^B([z;t],[x';y'])\,, \tag{6.31}$$

where

$$L([x;y],[z;t]) \;=\; \mathcal{S}_0^B([x;y],[t;z])\, \mathcal{H}(z,t)\,. \tag{6.32}$$

The nucleon masses will be given by the poles of the operator in square brackets in

Eq. (6.31). Acting on the baryon field ψ, one has

$$\int d^4z\, d^4t\; L([x;y],[z;t])\,\psi([z;t]) \;=\; \psi([x;y])\,. \tag{6.33}$$

It should be noticed that in our calculation only isocalar-scalar diquark interactions have been considered. This implies that the nucleon isospin is directly given by the flavor of the unpaired quark. Projecting on color singlet baryon states, and using the explicit form of the matrices in flavor space, one gets

$$\begin{aligned} 2\int d^4z\, d^4t\; \mathcal{G}_\Delta(x,t)\,\mathcal{S}^u(y,z)\,\gamma_5\,\mathcal{S}^{-d}(z,t)\,\gamma_5\,\psi_{\mathtt{p}}([z;t]) \;&=\; \psi_{\mathtt{p}}([x;y])\,, \\ 2\int d^4z\, d^4t\; \mathcal{G}_\Delta(x,t)\,\mathcal{S}^d(y,z)\,\gamma_5\,\mathcal{S}^{-u}(z,t)\,\gamma_5\,\psi_{\mathtt{n}}([z;t]) \;&=\; \psi_{\mathtt{n}}([x;y])\,, \end{aligned} \tag{6.34}$$

where $\psi_{\mathtt{p}}$ and $\psi_{\mathtt{n}}$ stand for proton and neutron fields, respectively.

It should be noticed that in the absence of an external magnetic field both equations coincide. Moreover, since in that case both quark and diquark fields are translational invariant, one can perform a Fourier transformation into momentum space. The resulting Fadeev equation, discussed e.g. in Refs. [277, 278], turns out to be a nonseparable integral equation. Given its complexity, in Ref. [277] the so-called "static approximation" was used, in which one disregards the momentum dependence of the exchanged quark. Then, in Ref. [278] the full equation was solved numerically, showing that in fact the static approximation can be taken as a good qualitative approach to the exact results. Having this in mind, and taking into account the additional difficulty introduced by the external magnetic field, we find it appropriate to consider the static approximation to get an estimation of the behavior of nucleon masses with the external field. This means to take

$$\bar{\mathcal{S}}^{-f}(q_\perp, q_\parallel) \;\to\; \frac{1}{M}\,. \tag{6.35}$$

Since in this approximation one has $\mathcal{S}^{-f}(x,y) = \delta^{(4)}(x-y)$ and $\mathcal{H}(x,z) \propto \delta^{(4)}(x-z)$, Eq. (6.34) reduces to

$$\begin{aligned} \frac{2}{M}\int d^4z\; \mathcal{G}_\Delta(x,z)\,\mathcal{S}^u(x,z)\,\psi_{\mathtt{p}}(z) \;&=\; \psi_{\mathtt{p}}(x)\,, \\ \frac{2}{M}\int d^4z\; \mathcal{G}_\Delta(x,z)\,\mathcal{S}^d(x,z)\,\psi_{\mathtt{n}}(z) \;&=\; \psi_{\mathtt{n}}(x)\,. \end{aligned} \tag{6.36}$$

Notice that within this approximation there is no further need to consider coordinate pairs in the arguments of nucleon fields, which become local.

Inserting Eqs. (2.66) and (6.26) into Eq. (6.36), we get

$$\frac{2}{M}\int_{p,q} e^{i(p+q)x}\,\bar{\mathcal{G}}_\Delta(p_\perp,p_\parallel)\,\bar{\mathcal{S}}^u(q_\perp,q_\parallel)\int d^4z\; e^{i\Phi_{\mathtt{p}}(x,z)}\; e^{-i(p+q)z}\;\psi_{\mathtt{p}}(z) \;=\; \psi_{\mathtt{p}}(x)\,,$$

$$\frac{2}{M}\int_{p,q} e^{i(p+q)x}\,\bar{\mathcal{G}}_\Delta(p_\perp,p_\parallel)\,\bar{\mathcal{S}}^d(q_\perp,q_\parallel)\int d^4z\; e^{-i(p+q)z}\;\psi_{\mathtt{n}}(z) \;=\; \psi_{\mathtt{n}}(x)\,, \tag{6.37}$$

where the Schwinger phase appearing in the equation for the proton is given by

$$\Phi_{\mathtt{p}}(x,x') \;=\; \Phi_\Delta(x,x')+\Phi_u(x,x') \;=\; \frac{Q_{\mathtt{p}}B}{2}(x_1+x_1')(x_2-x_2')\,, \tag{6.38}$$

with $Q_{\mathtt{p}}=e>0$. As expected, in the neutron equation the Schwinger phase vanishes. In order to change to a diagonal basis, it is convenient to introduce the transformations

$$\psi_{\mathtt{p}}(x) \;=\; \sum\!\!\!\!\!\!\int_{\bar{P}}\; \mathbb{E}^{s_{\mathtt{p}}}_{\bar{P}}(x)\,\psi_{\mathtt{p}}(\bar{P})\;, \qquad \psi_{\mathtt{n}}(x) \;=\; \int_P e^{iPx}\,\psi_{\mathtt{n}}(P)\,. \tag{6.39}$$

Note that while in the case of the neutron P denotes the usual four-momentum, for the proton field $\bar{P}=(n,P_2,P_3,P_4)$ denotes its corresponding quantum numbers in the Landau gauge, including the Landau level n. The Euclidean Ritus spinor eigenfunctions $\mathbb{E}^{s_{\mathtt{p}}}_{\bar{P}}(x)$ have been defined in Eq. (2.58) for the Landau gauge, with $B_{\mathtt{p}}=|eB|=B_e$ and $s_{\mathtt{p}}=\mathrm{sign}(eB)$.

Inserting the expansions of Eq. (6.39) into Eq. (6.37) one gets

$$\sum\!\!\!\!\!\!\int_{\bar{P}'}\; \mathbb{D}^{(\mathtt{p})}_{\bar{P},\bar{P}'}\,\psi_{\mathtt{p}}(\bar{P}') \;=\; 0 \quad , \qquad \mathbb{D}^{(\mathtt{n})}_{P}\,\psi_{\mathtt{n}}(P) \;=\; 0\,, \tag{6.40}$$

where

$$\mathbb{D}^{(\mathtt{p})}_{\bar{P},\bar{P}'} \;=\; \hat{\delta}_{\bar{P},\bar{P}'}\,\mathbb{1} \;-\; \frac{2}{M}\sum_{\lambda,\lambda'}\int_{p,q} I^{\lambda,\lambda'}_{\bar{P},\bar{P}'}(p,q)\,\bar{\mathcal{G}}_\Delta(p_\perp,p_\parallel)\,\Delta_\lambda\,\bar{\mathcal{S}}^u(q_\perp,q_\parallel)\,\Delta_{\lambda'}\;, \tag{6.41}$$

$$\mathbb{D}^{(\mathtt{n})}_{P} \;=\; \mathbb{1} \;-\; \frac{2}{M}\int_p \bar{\mathcal{G}}_\Delta(p_\perp,p_\parallel)\,\bar{\mathcal{S}}^d(P_\perp-p_\perp,P_\parallel-p_\parallel)\,, \tag{6.42}$$

with $\lambda,\lambda'=\pm$ and

$$I^{\lambda,\lambda'}_{\bar{P},\bar{P}'}(p,q) \;=\; \int d^4x\,d^4z\; e^{i[\Phi_{\mathtt{p}}(x,z)+(p+q)(x-z)]}\,\mathcal{B}^{s_{\mathtt{p}}}_{\bar{P},\lambda}(x)^*\,\mathcal{B}^{s_{\mathtt{p}}}_{\bar{P}',\lambda'}(z)\,. \tag{6.43}$$

The spin projectors, defined below Eq. (3.32), are given by $\Delta_+=\mathrm{diag}(1,0,1,0)$ and $\Delta_-=\mathrm{diag}(0,1,0,1)$. Meanwhile, the Ritus-type basis function $\mathcal{B}^{s_{\mathtt{p}}}_{\bar{P}_\lambda}(x)$ were defined in

Eq. (2.59), with $\bar{P}_\lambda = (n_\lambda, P_2, P_3, P_4)$ where $n_\lambda = n - (1 - s_\mathtt{p}\lambda)/2$ is a non-negative integer. We omit the $s_\mathtt{p}$ subscript in the notation of n_λ for visual clarity.

It is not obvious from Eq. (6.41) that $\mathbb{D}^{(\mathtt{p})}_{\bar{P},\bar{P}'}$ is diagonal in Ritus space. However, after a rather long calculation, it can be shown that $\mathbb{D}^{(\mathtt{p})}_{\bar{P},\bar{P}'}$ is indeed proportional to $\hat{\delta}_{\bar{P},\bar{P}'}$. The main steps of the calculation are detailed in section D.1 of Appendix D. Using the form of the quark and diquark propagator given in Eqs. (2.67) and (6.27) one finally obtains

$$\begin{aligned}
\mathbb{D}^{(\mathtt{p})}_{\bar{P},\bar{P}'} &= \hat{\delta}_{\bar{P},\bar{P}'} \sum_{\lambda=\pm} \left[X^{(\mathtt{p})}_\lambda + Y^{(\mathtt{p})}_\lambda \, P_\parallel \cdot \gamma_\parallel + Z^{(\mathtt{p})}_\lambda \, \gamma_2 \right] \Delta_\lambda \,, \\
\mathbb{D}^{(\mathtt{n})}_{P} &= \sum_{\lambda=\pm} \left[X^{(\mathtt{n})}_\lambda + Y^{(\mathtt{n})}_\lambda \, P_\parallel \cdot \gamma_\parallel + Z^{(\mathtt{n})} \, P_\perp \cdot \gamma_\perp \right] \Delta_\lambda \,,
\end{aligned} \tag{6.44}$$

where

$$X^{(\mathtt{p})}_\lambda = 1 - (-1)^{n_\lambda} \frac{8\pi}{B_\mathtt{p}} \int_{p,q_\perp} e^{-\frac{(p_\perp+q_\perp)^2}{B_\mathtt{p}}} \, \bar{\mathcal{G}}_\Delta(p_\perp, p_\parallel) \, T^u_\lambda(q_\perp, P_\parallel - p_\parallel) \, L_{n_\lambda}\left(\frac{2(q_\perp + p_\perp)^2}{B_\mathtt{p}} \right) , \tag{6.45}$$

$$\begin{aligned}
Y^{(\mathtt{p})}_\lambda = {} & (-1)^{n_\lambda} \frac{8\pi}{M B_\mathtt{p}} \int_{p,q_\perp} e^{-\frac{(p_\perp+q_\perp)^2}{B_\mathtt{p}}} \, \bar{\mathcal{G}}_\Delta(p_\perp, p_\parallel) \times \\
& \left(1 - \frac{p_\parallel \cdot P_\parallel}{P_\parallel^2} \right) T^u_\lambda(q_\perp, P_\parallel - p_\parallel) \, L_{n_\lambda}\left(\frac{2(q_\perp + p_\perp)^2}{B_\mathtt{p}} \right) ,
\end{aligned} \tag{6.46}$$

$$\begin{aligned}
Z^{(\mathtt{p})}_\lambda = {} & (-1)^{n} \frac{8\pi \, s_\mathtt{p}}{M B_\mathtt{p}} \sqrt{\frac{2}{n B_\mathtt{p}}} \int_{p,q_\perp} e^{-\frac{(p_\perp+q_\perp)^2}{B_\mathtt{p}}} \, \bar{\mathcal{G}}_\Delta(p_\perp, p_\parallel) \times \\
& |q_\perp| \, [(q_1 + p_1) - i\lambda(q_2 + p_2)] \, V^u(q_\perp, P_\parallel - p_\parallel) \, L^1_{n-1}\left(\frac{2(q_\perp + p_\perp)^2}{B_\mathtt{p}} \right) ,
\end{aligned} \tag{6.47}$$

for the proton and

$$X^{(\mathtt{n})}_\lambda = 1 - 2 \int_p \bar{\mathcal{G}}_\Delta(p_\perp, p_\parallel) \, T^d_\lambda(P_\perp - p_\perp, P_\parallel - p_\parallel) \,, \tag{6.48}$$

$$Y^{(\mathtt{n})}_\lambda = \frac{2}{M} \int_p \bar{\mathcal{G}}_\Delta(p_\perp, p_\parallel) \, T^d_\lambda(P_\perp - p_\perp, P_\parallel - p_\parallel) \left(1 - \frac{p_\parallel \cdot P_\parallel}{P_\parallel^2} \right) , \tag{6.49}$$

$$Z^{(\mathtt{n})}_\lambda = \frac{2}{M} \int_p \bar{\mathcal{G}}_\Delta(p_\perp, p_\parallel) \, V^d(P_\perp - p_\perp, P_\parallel - p_\parallel) \left(1 - \frac{p_\perp \cdot P_\perp}{P_\perp^2} \right) , \tag{6.50}$$

for the neutron, with

$$T^f_\lambda(q_\perp, q_\parallel) \;=\; \int_0^\infty d\tau\; e^{-\tau\Upsilon_f(\tau,q)}\;\left[1+\lambda\, s_f\,\tanh(\tau B_f)\right]\;,$$
$$V^f(q_\perp, q_\parallel) \;=\; \int_0^\infty d\tau\; e^{-\tau\Upsilon_f(\tau,q)}\;\mathrm{sech}^2(\tau B_f)\,. \tag{6.51}$$

The function $\Upsilon_f(\tau, q)$ was defined in Eq. (2.68). Also, similarly to Eq. (2.24), we have defined the shorthand notation

$$\int_{q_\perp} \;=\; \int \frac{dq_1\, dq_2}{(2\pi)^2}\,. \tag{6.52}$$

In what follows we will concentrate on the determination of the proton and neutron lowest possible energies. Since these quantities are usually interpreted as the nucleon masses, we denote them as $\mathcal{M}_{\mathtt{N}}$, with $\mathtt{N} = \mathtt{p}, \mathtt{n}$. For the neutron we just take, as usual, $P_\perp = P_3 = 0$ and $P_4^2 = -\mathcal{M}_{\mathtt{n}}^2$. In the proton case, as done for diquarks, we consider the squared canonical momentum, $\Pi^2 = 2nB_{\mathtt{p}} + P_\parallel^2$. The lowest energy state corresponds to $P_3 = 0$ and the lowest Landau level (LLL), $n = 0$. Then $P_4^2 = -\mathcal{M}_{\mathtt{p}}^2$, as for the neutron case. Since the determinants of the Dirac operators in Eq. (6.44) have to vanish at the pole masses, the corresponding eigenvalue equations read

$$\left(\hat{X}^{(\mathtt{p})}_{s_{\mathtt{p}}}\right)^2 - \mathcal{M}_{\mathtt{p}}^2\,\left(\hat{Y}^{(\mathtt{p})}_{s_{\mathtt{p}}}\right)^2 \;=\; 0 \quad , \qquad \left(\hat{X}^{(\mathtt{n})}_{\lambda}\right)^2 - \mathcal{M}_{\mathtt{n}}^2\,\left(\hat{Y}^{(\mathtt{n})}_{\lambda}\right)^2 \;=\; 0\,, \tag{6.53}$$

where we have denoted by $\hat{X}^\nu_\pm$ and $\hat{Y}^\nu_\pm$ the coefficients in Eq. (6.44) evaluated at $n = 0$, $P_3 = 0$ and $P_\perp = 0$. Note that for the lowest energy states there is no contribution from the $Z^{(\mathtt{p})}_\lambda$ and $Z^{(\mathtt{n})}_\lambda$ terms. In addition, for the proton case only the projection $\lambda = s_{\mathtt{p}}$ is nonvanishing for $n = 0$. For the neutron, both projections are in principle allowed, and one should take the value of λ that leads to the lowest value of the mass.

To obtain the explicit form of the coefficients $\hat{X}^\nu_\lambda$ and $\hat{Y}^\nu_\lambda$ needed to evaluate –and solve – Eq. (6.53), one has to replace the diquark propagator of Eq. (6.27) into Eqs. (6.45-6.50). For convenience we consider first the form of the coefficients in the absence of the external magnetic field (in this case both nucleons are taken at rest). They are given by

(see section D.2)

$$\hat{X} \;=\; 1 - \frac{1}{4\pi^2 m_{\mathtt{N}}} \int_1^\infty \frac{d\tau}{\tau} \int_0^\infty dp\, p^2 \; \mathcal{G}_\Delta^{\rm vac}(p^2)\, e^{-\tau \frac{M^2+p^2-m_{\mathtt{N}}^2}{\Lambda_B^2}} \; J_1\left(\frac{2\,\tau\, p\, m_{\mathtt{N}}}{\Lambda_B^2}\right) \,, \tag{6.54}$$

$$\begin{aligned}\hat{Y} \;=\; & \frac{1}{4\pi^2 m_{\mathtt{N}} M} \int_1^\infty \frac{d\tau}{\tau} \int_0^\infty dp\, p^2 \; \mathcal{G}_\Delta^{\rm vac}(p^2)\, e^{-\tau \frac{M^2+p^2-m_{\mathtt{N}}^2}{\Lambda_B^2}} \;\times \\ & \left[J_1\left(\frac{2\,\tau\, p\, m_{\mathtt{N}}}{\Lambda_B^2}\right) - \frac{p}{m_{\mathtt{N}}} J_2\left(\frac{2\,\tau\, p\, m_{\mathtt{N}}}{\Lambda_B^2}\right)\right] \,.\end{aligned} \tag{6.55}$$

Here, and below, $m_{\mathtt{N}}$ denotes the nucleon mass at $B = 0$ while $J_n(x)$ are Bessel functions. The $B = 0$ diquark propagator [see Eq. (6.25)] is given by

$$\mathcal{G}_\Delta^{\rm vac}(p^2) \;=\; \left[\frac{1}{4H} \;- J_\Delta^{\rm vac}(p^2)\right]^{-1} \,. \tag{6.56}$$

Notice that Eqs. (6.54) and (6.55) include a cutoff parameter Λ_B, which has been introduced in order to regularize the otherwise divergent quark-diquark loop within the proper time regularization scheme.

For nonzero magnetic field B, in the case of the proton we have

$$\begin{aligned}\hat{X}^{(\mathtt{p})}_{s_{\mathtt{p}}} \;=\; & 1 - \frac{B_u B_\Delta}{2\pi^2 \Lambda_B^2} \int_1^\infty d\tau \; \frac{1+t_u}{B_u + (B_{\mathtt{p}} + B_\Delta) t_u} \; \sum_{\ell=0}^\infty \left[\frac{B_u + (B_{\mathtt{p}} - B_\Delta) t_u}{B_u + (B_{\mathtt{p}} + B_\Delta) t_u}\right]^\ell \;\times \\ & \int_0^\infty dp_\parallel \; p_\parallel \; \mathcal{G}_\Delta^{\rm reg}(\ell, p_\parallel^2)\; e^{-\tau \frac{M^2+p_\parallel^2-\mathcal{M}_p^2}{\Lambda_B^2}} \; J_0\left(\frac{2\,\tau\, p_\parallel\, \mathcal{M}_{\mathtt{p}}}{\Lambda_B^2}\right) \,,\end{aligned}$$

$$\begin{aligned}\hat{Y}^{(\mathtt{p})}_{s_{\mathtt{p}}} \;=\; & \frac{B_u B_\Delta}{2\pi^2 M \Lambda_B^2} \int_1^\infty d\tau \; \frac{1+t_u}{B_u + (B_{\mathtt{p}} + B_\Delta) t_u} \; \sum_{\ell=0}^\infty \left[\frac{B_u + (B_{\mathtt{p}} - B_\Delta) t_u}{B_u + (B_{\mathtt{p}} + B_\Delta) t_u}\right]^\ell \;\times \\ & \int_0^\infty dp_\parallel \; p_\parallel \; \mathcal{G}_\Delta^{\rm reg}(\ell, p_\parallel^2)\; e^{-\tau \frac{M^2+p_\parallel^2-\mathcal{M}_p^2}{\Lambda_B^2}} \; \left[J_0\left(\frac{2\,\tau\, p_\parallel\, \mathcal{M}_{\mathtt{p}}}{\Lambda_B^2}\right) - \frac{p_\parallel}{\mathcal{M}_{\mathtt{p}}} J_1\left(\frac{2\,\tau\, p_\parallel\, \mathcal{M}_{\mathtt{p}}}{\Lambda_B^2}\right)\right] \,,\end{aligned} \tag{6.57}$$

while for the neutron we get

$$\hat{X}_\lambda^{(\mathtt{n})} = 1 - \frac{B_d B_\Delta}{2\pi^2 \Lambda_B^2} \int_1^\infty d\tau \, \frac{1+\lambda s_d t_d}{B_d + B_\Delta t_d} \sum_{\ell=0}^\infty \left[\frac{B_d - B_\Delta t_d}{B_d + B_\Delta t_d}\right]^\ell \times$$
$$\int_0^\infty dp_\parallel \, p_\parallel \, \mathcal{G}_\Delta^{\rm reg}(\ell, p_\parallel^2) \, e^{-\tau \frac{M^2 + p_\parallel^2 - \mathcal{M}_n^2}{\Lambda_B^2}} \, J_0\left(\frac{2\,\tau\, p_\parallel \, \mathcal{M}_\mathtt{n}}{\Lambda_B^2}\right) ,$$

$$\hat{Y}_\lambda^{(\mathtt{n})} = \frac{B_d B_\Delta}{2\pi^2 M \Lambda_B^2} \int_1^\infty d\tau \, \frac{1+\lambda s_d t_d}{B_d B_\Delta t_d} \sum_{\ell=0}^\infty \left[\frac{B_d - B_\Delta t_d}{B_d + B_\Delta t_d}\right]^\ell \times$$
$$\int_0^\infty dp_\parallel \, p_\parallel \, \mathcal{G}_\Delta^{\rm reg}(\ell, p_\parallel^2) \, e^{-\tau \frac{M^2 + p_\parallel^2 - \mathcal{M}_n^2}{\Lambda_B^2}} \left[J_0\left(\frac{2\,\tau\, p_\parallel \, \mathcal{M}_\mathtt{n}}{\Lambda_B^2}\right) - \frac{p_\parallel}{\mathcal{M}_\mathtt{n}} J_1\left(\frac{2\,\tau\, p_\parallel \, \mathcal{M}_\mathtt{n}}{\Lambda_B^2}\right)\right] . \tag{6.58}$$

In these equations we have used the definition $t_f = \tanh(\tau B_f/\Lambda_B^2)$.

6.1.4 Nucleon magnetic moments

We finish this section by noting that in order to study how nucleon masses get modified to lowest order in the magnetic field, the above expressions for $\hat{X}_\lambda^\nu$ and $\hat{Y}_\lambda^\nu$ can be expanded around $B = 0$. Let us define the corresponding slopes $\alpha_\mathtt{N}$ by

$$\mathcal{M}_\mathtt{N} = m_\mathtt{N} + \alpha_\mathtt{N} |B| + \mathcal{O}(B^2) . \tag{6.59}$$

After a rather long calculation, sketched in section D.2, we obtain

$$\alpha_\mathtt{p} = \frac{-Q_u \left[(M + m_\mathtt{N})\,\mathcal{I}_1 - m_\mathtt{N}\,\mathcal{I}_2\right] + Q_\mathtt{p}\,\hat{W}}{M\,\hat{Y} + 2\,m_\mathtt{N}\,\hat{W}} ,$$
$$\alpha_\mathtt{n} = \frac{Q_d \left[(M + m_\mathtt{N})\,\mathcal{I}_1 - m_\mathtt{N}\,\mathcal{I}_2\right]}{M\,\hat{Y} + 2\,m_\mathtt{N}\,\hat{W}} , \tag{6.60}$$

where

$$\hat{W} = (M + m_\mathtt{N})\,\mathcal{I}_1 - (2\,m_\mathtt{N} + M)\,\mathcal{I}_2 + m_\mathtt{N}\,\mathcal{I}_3 , \tag{6.61}$$

and the integrals $\mathcal{I}_k$ are given by

$$\mathcal{I}_k = \frac{1}{4\pi^2\,\Lambda_B^2\,m_\mathtt{N}^k} \int_1^\infty d\tau \int_0^\infty dp\, p^{k+1}\, \mathcal{G}_\Delta^{B=0}(p^2)\, e^{-\tau \frac{M^2 + p^2 - m_\mathtt{N}^2}{\Lambda_B^2}} \, J_k\left(\frac{2\,\tau\, p\, m_\mathtt{N}}{\Lambda_B^2}\right) . \tag{6.62}$$

To find the relation between $\alpha_\mathtt{N}$ and the nucleon magnetic moments we proceed as follows. First, we take into account that to leading order in the magnetic field the change

in the nucleon energy is given by [267, 279]

$$\Delta E_{\mathtt{N}} \;=\; \frac{|Q_{\mathtt{N}}B|}{2m_{\mathtt{N}}} - \vec{\mu}_{\mathtt{N}}\cdot\vec{B} + \mathcal{O}(B^2)\,. \tag{6.63}$$

The first term corresponds to orbital motion. While it vanishes for the neutron, for the proton it provides a contribution due to zero point motion in the plane perpendicular to the magnetic field. The second term represents, for both p and n, the spin contribution leading to the Zeeman effect. Thus, we have

$$\begin{aligned}\Delta E_{\mathtt{p}} \;&=\; (1-\mu_{\mathtt{p}})\,\frac{e|B|}{2m_{\mathtt{N}}} + \mathcal{O}(B^2)\,,\\ \Delta E_{\mathtt{n}} \;&=\; -\,\lambda\,\mu_{\mathtt{n}}\,\frac{eB}{2m_{\mathtt{N}}} + \mathcal{O}(B^2)\,,\end{aligned} \tag{6.64}$$

where, as usual, the nucleon magnetic moments are expressed in units of the nuclear magneton $\mu_{\mathtt{N}} = e/(2m_{\mathtt{N}})$. Note that for the proton we have taken into account the fact that for the lowest energy state one has $\lambda = s_{\mathtt{p}}$. In this way, identifying the corresponding slopes at $B = 0$, the nucleon magnetic moments are given by

$$\mu_p \;=\; 1 - \frac{2m_{\mathtt{N}}}{e}\,\alpha_{\mathtt{p}} \quad , \qquad \mu_n \;=\; -\lambda\,\mathrm{sign}(B)\,\frac{2m_{\mathtt{N}}}{e}\,\alpha_{\mathtt{n}}\,. \tag{6.65}$$

6.2 Numerical results

For definiteness, in what follows we will consider $B > 0$. To obtain numerical results for diquark and baryon properties one has to fix the model parametrization. Here we will consider only set I of Table 4.1, which from the three sets of the table provides the best agreement with lattice QCD results [73] for the normalized average condensate up to $eB \simeq 1$ GeV^2, as seen in Figure 4.2. The effective Lagrangian in Eq. (6.1) also includes the scalar quark-quark coupling constant H. Typical effective approaches for the strong interaction, such as the One Gluon Exchange or the Instanton Liquid Model, lead to $H/G = 0.75$ [181]. However, this value is subject to somewhat large uncertainties from the phenomenological point of view. In fact, larger values for this ratio seem to be favored from the determination of baryon properties within the Fadeev approach [277, 278, 280, 281]. Here we choose to take H/G within the range $0.75 \leq H/G \leq 1.2$, typically considered in the literature. The corresponding values of the diquark mass and binding energies at $B = 0$ are shown in Figure 6.2. We observe that for $H/G \simeq 0.75$ the scalar diquark is barely bound by 5 MeV, while for $H/G = 1.2$ one gets binding energies of about 200 MeV.

Let us consider the effect of an uniform magnetic field on the (LLL) diquark mass,

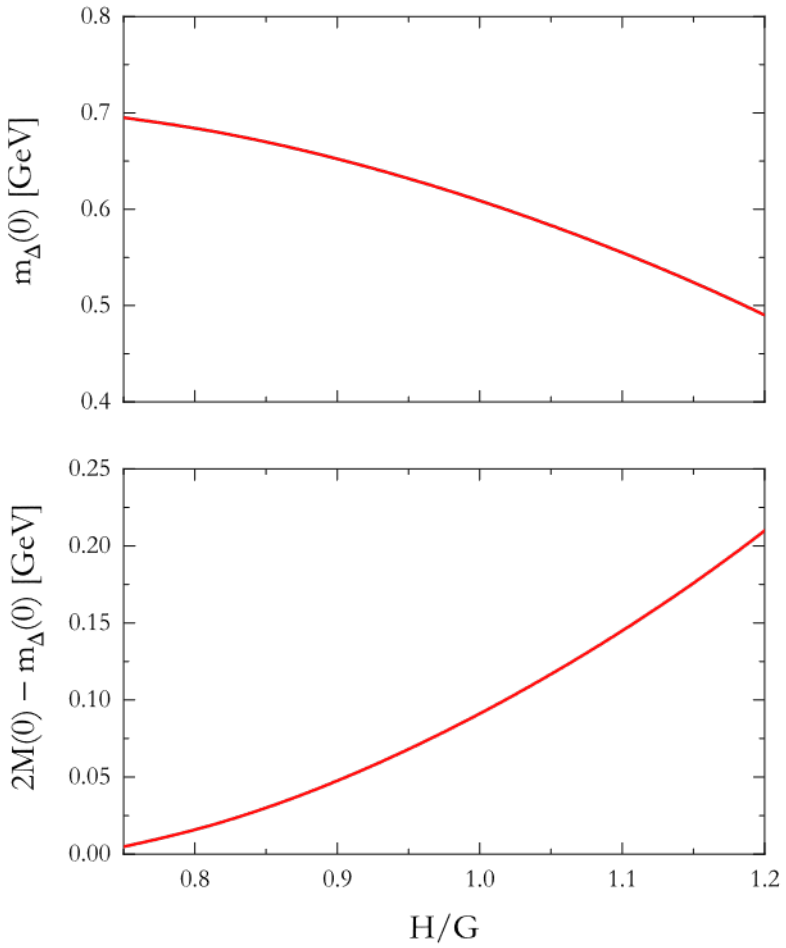

Figure 6.2: Δ mass (top) and binding energy (bottom) at $B = 0$ as functions of H/G.

contained in Eq. (6.22). In the upper panel of Figure 6.3 we show the magnetic dependence of the diquark mass, normalized with respect to its $B = 0$ value. The curves correspond to some selected values of the ratio H/G within the range mentioned above. We get $m_\Delta(B = 0) = 0.685$, 0.653, 0.609 and 0.555 GeV for $H/G = 0.8$, 0.9, 1.0 and 1.1, respectively. It is seen that for all considered values of H/G the normalized mass initially decreases as B increases, attaining a minimum at about $eB \sim 0.2$ GeV^2. Beyond this minimum the curves steadily increase with the magnetic field, reaching a ratio $m_\Delta(B)/m_\Delta(0) = 1$ somewhere in the range $eB \sim 0.4 - 0.6$ GeV^2, depending on the precise value of H/G. Notice that this nonmonotonic behavior differs from the steady charged pion mass increase found in Figure 5.5. Lastly, results obtained disregarding Schwinger phases greatly deviate at high magnetic fields, showing a rather strong enhancement with B.

In the lower panel of Figure 6.3 we show the difference of squared lowest energies, i.e. $E_\Delta(B)^2 - E_\Delta(0)^2$, see Eq. (6.23). For a point-like diquark this difference is simply given by $eB/3$, indicated by the straight dotted black line. It can be observed that, as a consequence of the nonmonotonic behavior of the pole mass, for small (large) values of eB

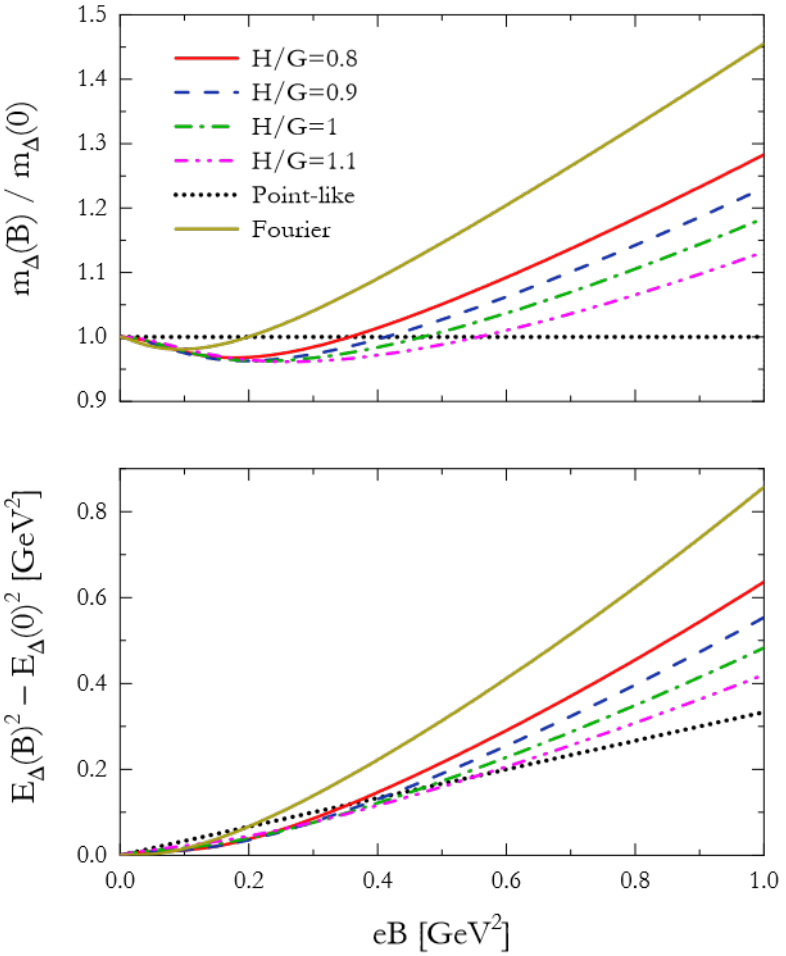

Figure 6.3: Diquark normalized mass (top) and squared energy difference (bottom) as functions of eB for some representative values of H/G. The point-like case is indicated by the dotted line, while results obtained disregarding Schwinger phases are depicted as a dark yellow line for $H/G = 0.8$.

the difference $E_\Delta(B)^2 - E_\Delta(0)^2$ lies below (above) that straight line. A similar behavior was found in the analysis of Ref. [169], where Schwinger phases were not taken into account. As for charged pions, for $\ell = p_3 = 0$ this amounts to replace $\alpha_+ \to t_+$ and $m_\Delta^2 + B_\Delta \to m_\Delta^2$ in the final expression of Eq. (6.19). We see that in this case not only the crossing is found to occur at a lower value of eB, of about 0.2 GeV^2 for $H/G = 0.8$, but also the behavior of the curve deviates at high magnetic fields, showing a rather steep enhancement with B. It is also interesting to note that as H/G increases the behavior of the squared energy difference gets closer to the point-like case. This might be understood by realizing that a larger value of H/G implies a more deeply bound diquark and, consequently, a more localized one.

We turn next to the analysis of nucleon masses. As mentioned in subsection 6.1.3, the calculation of these quantities requires the introduction of an additional cutoff parameter, Λ_B, to regularize the otherwise divergent quark-diquark loop in the proper time

regularization scheme. For a given value of H/G, we adjust this parameter demanding the $B = 0$ eigenvalue equation $|\hat{X}| = m_{\mathtt{N}}\,|\hat{Y}|$ [see Eqs. (6.54) and (6.55)] to be satisfied for the physical value $m_{\mathtt{N}} = 0.938$ GeV. In this way we obtain $\Lambda_B = 1.618$, 1.380 and 1.104 GeV for $H/G = 0.8$, 0.9 and 1.0, respectively. For larger values of H/G, no value of Λ_B is found to be compatible with the physical nucleon mass at zero magnetic field in this model. Having determined all input parameters, one can solve the eigenvalue equations (6.53) to obtain proton and neutron masses for nonvanishing external magnetic field.

Before reporting the corresponding results, we find it convenient to make a few comments concerning the numerical details of the calculation. Firstly, we note that to evaluate the coefficients $\hat{X}_{\pm}^{(\mathtt{N})}$ and $\hat{Y}_{\pm}^{(\mathtt{N})}$ in Eqs. (6.57) and (6.58) one has to perform a sum over Landau levels (LL). In that sum we have taken into account as many LL as needed in order to obtain a stable result for the calculated mass. For low values of eB, this implies the inclusion of a quite large number of LL. For example, at $eB = 0.04$ GeV^2, for $H/G = 1$ about 300 LL are needed in order to obtain an accuracy of about 1 MeV in the nucleon mass. For $H/G = 0.8$ the required number of LL is found to be even larger, of the order of 600. As expected, for larger values of the magnetic field the needed number of LL gets significantly reduced. Still, it is found that for eB as large as 0.8 GeV^2 about 10 LL are needed to obtain the above mentioned accuracy in the mass determination. Another issue that requires some care is the numerical evaluation of the integrals in Eqs. (6.57) and (6.58), due to the highly oscillatory behavior of the Bessel functions for large values of their arguments.

Our results for the behavior of nucleon masses as functions of the external magnetic field are given in Figure 6.4. In the upper (lower) panel we show the magnetic dependence of the proton (neutron) mass, considering $H/G = 0.8$, 0.9 and 1.0. In all cases it is seen that both nucleon masses display a nonmonotonic behavior. While they initially decrease when the magnetic field is increased, a steady growth is observed for larger fields. The decrease becomes less pronounced (and the corresponding minimum occurs at smaller eB) the larger the value of H/G is. It is also seen that the dependence on H/G is weaker in the case of the neutron. Let us recall that for a proton in the LLL only the spin projection $\lambda = s_{\mathtt{p}} = \mathrm{sign}(Q_{\mathtt{p}}B)$ is allowed, while both values of λ are allowed for the neutron. In Figure 6.4 we have plotted the values corresponding to the lower solution of Eq. (6.53), defined as the neutron mass. In our model, for $B > 0$ ($B < 0$) it is found that this lower state corresponds to $\lambda = -1$ ($\lambda = 1$). For the higher state, not shown in the figure, we have seen that the neutron mass initially increases with eB. This solution is found to exist only for $eB \lesssim 0.1 - 0.2$ GeV^2 (the state becomes unbound for larger values of the external field).

As stated, close to $B = 0$ both proton and neutron masses are shown to decrease for

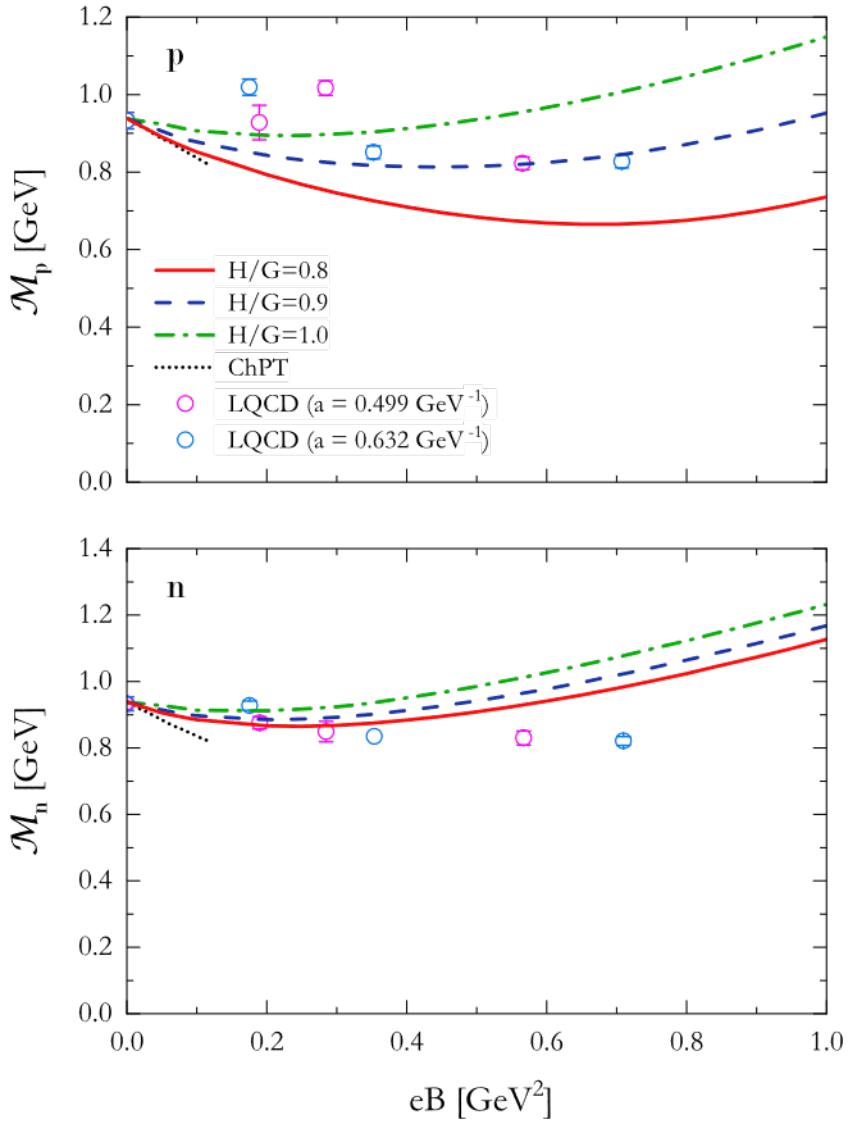

Figure 6.4: Proton and neutron masses as functions of eB for various values of H/G. Open dots and dotted lines correspond to Lattice QCD results given in Ref. [164] and ChPT results given in Ref. [268], respectively.

increasing external field, i.e. the slopes α_{p} and α_{n} obtained from Eq. (6.60) are found to be negative. Taking into account that for the lowest neutron state one has $\lambda\,\mathrm{sign}(B) = -1$, from Eq. (6.65) one gets $\mu_{\mathrm{p}} > 0$ and $\mu_{\mathrm{n}} < 0$, as expected from phenomenology. In addition, the negative slopes found at $B = 0$ are consistent with results from ChPT quoted in Ref. [268]. The latter, which are expected to hold for low values of the external field, are displayed as dotted lines in Figure 6.4. Notice, however, that the slopes obtained within ChPT are in general steeper that those found from our results. The lower slopes in our model imply in turn relatively low results for the absolute values of proton and neutron magnetic moments. From the numerical evaluation of Eq. (6.60) and (6.65) we find the magnetic moments quoted in Table 6.1, to be compared with the empirical values

$\mu_{\mathrm{p}} = 2.79$ and $\mu_{\mathrm{n}} = -1.91$. In this regard, it should be stressed that in our work we have neglected for simplicity the axial-vector diquark correlations. The latter can be important to get an enhancement in $|\mu_{\mathrm{p}}|$ and $|\mu_{\mathrm{n}}|$, as shown in Ref. [282]. Finally, let us compare our results with those obtained from LQCD simulations. In Figure 6.4 we have depicted as open dots the LQCD results quoted in Ref. [164], corresponding to two different values of the lattice spacing a. We observe some qualitative agreement with our results, although LQCD values tend to show a lower dependence on the external field. In the case of the proton, a few lattice points seem to show a mass enhancement for $eB \simeq 0.2 - 0.3$ GeV^2. Presumably, this could be due to the fact that, as mentioned by the authors of Ref. [164], the Zeeman-splitting cannot be fully resolved. We believe that our results exhibit a more trustable initial slope, in view of the results arising from ChPT.

H/G	μ_{p}	μ_{n}
0.8	2.63	-1.19
0.9	2.30	-1.05
1.0	1.99	-0.94

Table 6.1: Predicted values of nucleon magnetic moments for different values of H/G.

CHAPTER 7

Conclusions

In this thesis we have investigated the effect of an external uniform magnetic field on several light hadron properties, composed by strongly interacting quark matter. Since strong magnetic fields can resolve the quark structure of hadrons, the effect on their properties can provide meaningful information about the magnetized QCD phase diagram, relevant for various physical scenarios. Since the nonperturbative character of QCD at low energies render calculations extremely complicated, to calculate hadron properties we have employed the Nambu–Jona-Lasinio effective model, where current-current color interactions mediated by gluon exchanges are approximated by local four-point interactions. The model, introduced in chapter 2, is built upon the symmetries of QCD and is able to reproduce the chiral symmetry breaking phenomenon.

Since pions are the lightest hadrons, they can be easily produced in the aforementioned magnetized systems. However, they are unstable particles, prompt to decay into less heavier ones such as leptons and photons. In the absence of external fields, a unique decay constant is associated to the weak decay of charged pions. In contrast, the presence of a uniform magnetic field modifies the symmetries of the system and opens up the possibility for new decay constants to appear. In chapter 3 we have presented a general method to parametrize the magnetized one-pion-to-vacuum matrix elements of the vector and axial-vector hadronic currents, based on Refs. [230] and [231]. When the magnetic field is present, new gauge-covariant tensor structures are available. We have shown that, in fact, four independent four-vectors can be formed, leading the existence of four form factors or decay constants; three associated to the vector-axial current, and one to the vector current. These are constrained by discrete symmetries. As a result, all form factors are real, and for charged pions they are independent of the charge sign. Moreover, in the neutral pion case, such symmetries prevent the appearance of a particular axial form factor.

Choosing $\vec{B}$ to be orientated along the 3-axis, we have shown that the matrix elements of the parallel (0- and 3-) components of the vector current can be expressed in terms of one single real form factor, $f_{\pi^0}^{(V)}$ or $f_{\pi^\pm}^{(V)}$, while the perpendicular (1- and 2-) components vanish identically. For the matrix elements of the axial-vector current, two real form factors $f_{\pi^0}^{(A1)}$ and $f_{\pi^0}^{(A3)}$ can be defined in the neutral pion case. Alternatively, these can be written in terms of a parallel and a perpendicular form factor, reflecting the anistropy induced by the external field [170]. For charged pions, in contrast, three form factors $f_{\pi^\pm}^{(A1)}$, $f_{\pi^\pm}^{(A2)}$ and $f_{\pi^\pm}^{(A3)}$ are in general required to parametrize the matrix elements of the axial-vector current. While $f_{\pi^0}^{(A3)}$, $f_{\pi^\pm}^{(V)}$ and $f_{\pi^\pm}^{(A2)}$ were already known in the literature [170, 171], the decay constants $f_{\pi^0}^{(V)}$ and $f_{\pi^\pm}^{(A3)}$ are new, first defined in [230].

Using the above results we have introduced a general, model-independent framework to study the weak decay $\pi^- \to l\,\bar{\nu}_l$ in the presence of an uniform external magnetic field. To that end, we described for each involved particle the specific form of the field, taking fully into account the effect of the magnetic field on the corresponding eigenfunctions. By performing calculations in two different gauges, Landau [230] and symmetric [231], we were able to provide an explicit test of gauge independence of our result. Moreover, this has let us clarify on the behavior of the associated quantum numbers. For both gauges, the momentum in the field direction together with the energy are conserved. The remaining quantum numbers are the Landau level and a last one which depends on the chosen gauge. For the Landau gauge it is the canonical momentum along the 2-direction, while for the symmetric gauge it is the canonical total angular momentum along the 3-direction. Although these quantities are conserved, they are gauge dependent and thus do not correspond to physical observables.

For the case in which the decaying pion lies in its state of minimum energy (i.e. in the lowest Landau level, with zero momentum along the 3-direction), we have obtained an explicit expression for the magnetized $\pi^- \to l\,\bar{\nu}_l$ decay width in Eq. (3.71). As expected, this expression coincides for both chosen gauges and does not depend on their corresponding gauge-dependent quantum numbers. Moreover, we have revealed that angular momentum conservation does not imply, as claimed in Ref. [171], that the antineutrino momentum has to be necessarily parallel to the magnetic field. For large magnetic fields, i.e. $eB > m_{\pi^-}^2 - m_l^2 \sim 0.05\ \text{GeV}^2$ but smaller than the squared τ lepton mass, this expression reduces to Eq. (3.73). In fact, a novel result was obtained for strong fields which also satisfy $eB \gg m_l^2$. As seen in the simplified expression of Eq. (3.75), valid for very intense magnetic fields, the magnetized decay width does not vanish in the chiral limit $m_l \to 0$, i.e. it does not show the helicity suppression found in the absence of the external magnetic field. In fact, helicity conservation only implies that the projection of the antineutrino momentum in the magnetic field direction should be

antiparallel to the magnetic field. This implies a highly anisotropic distribution of outgoing antineutrinos,signaling a significant suppression in the direction of the external field.

In order to quantitatively estimate how weak decay rates of charged pions are modified by the magnetic field, the behavior of the decay form factors and pion masses should be determined. In chapter 4, these and other pion properties have been calculated in the framework of the two-flavor NJL model (introduced in chapter 2), based on Refs. [233, 252]. While for neutral pions one can take the usual momentum basis to diagonalize the corresponding polarization functions, this is not possible for charged pions, due to the presence of nonvanishing contributions from Schwinger phases. In chapter 3 we have shown that the Ritus eigenfunction method presented allows us to fully take into account the translational-breaking effects induced by these phases. Calculations of charged meson properties using this method have been performed in [233, 252] for the first time. In our numerical calculations we have used three model parametrization sets that satisfactorily describe not only meson properties in the absence of the magnetic field but also lattice QCD results for the behavior of quark condensates under a magnetic field. Moreover, we have explored the possibility of considering a magnetic field dependent coupling $G(B)$, so as to incorporate the inverse magnetic catalysis effect. Due to the nonrenormalizability of the model, divergent results were regulated using a 3D cutoff in the MFIR scheme, which has been proven to provide more reliable results as compared to other magnetic dependent regularization schemes [212].

We have found that, for a constant coupling G, the magnetic field slightly diminishes the π^0 mass, in agreement with previous NJL results [161, 248]. However, the m_π^0 behavior found is nonmonotonic, in contrast with LQCD [129, 258] and nonlocal NJL [250, 251] results, which display a monotonous decrease of the mass with B. For $eB < 1$ GeV^2 this trend is recovered when a magnetic coupling $G(B)$ is used [161], which mimics the backreaction of sea quarks due to the external field. Meanwhile, the pion-to-quark coupling constant $g_{\pi^0 qq}$ shows some enhancement if B is increased for a constant G, in contrast to what happens for the $G(B)$ case. On the other hand, for both couplings the directional refraction index u_{π^0} decreases monotonously with B, remaining always lower than one (subluminal pions) even in the chiral limit, in agreement with Refs. [100, 217]. Regarding neutral decay constants, in the NJL model $f_{\pi^0}^{(A2)}$ vanishes, as expected from the constraints imposed by the discrete symmetries of the interaction. For both couplings $f_{\pi^0}^{(A\parallel)} = f_{\pi^0}^{(A1)}$ and $f_{\pi^0}^{(V)}$ are enhanced for increasing B, while $f_{\pi^0}^{(A\perp)} = f_{\pi^0}^{(A1)} - f_{\pi^0}^{(A3)}$ is reduced. The use of $G(B)$ leads to better agreement with some other approaches [243, 251, 258], which show a steeper behavior. We have also remarked that our results satisfy quite well several chiral limit relations, such as the well-known generalized Goldberger-Treiman and Gell-Mann-Oakes-Renner equations for $f_{\pi^0}^{(A\parallel)}$ (see e.g. Ref. [234]). Moreover, we have shown

that relations $f_{\pi^0}^{(A\perp)} = u_{\pi^0}^2 f_{\pi^0}^{(A\parallel)}$ and $f_{\pi^0}^{(V)} = eB/(8\pi^2 f_{\pi^0}^{(A\parallel)})$ also hold in the chiral limit. While the former can be derived from Refs. [103, 170, 228], the latter can be related to the anomalous Wess-Zumino-Witten effective Lagrangian, and – to the best of our knowledge – has not been previously stated in the literature.

Turning now to the charged pion case, we remark that calculations have been performed fully accounting for Schwinger phases through the Ritus eigenfunction method. We have obtained $m_{\pi^-} = m_{\pi^+}$, as expected from charge invariance. Moreover, a mass for each Landau level can be obtained; we have considered only the lowest Landau level mass. In particular, we have found that the magnetic-field dependent mass $E_{\pi^\pm}$ (defined as its lowest energy state) steadily increases with the magnetic field [less markedly for $G(B)$], remaining always larger than that of a point-like pion. For low values of eB (say $eB \lesssim 0.15$ GeV^2), results for $E_{\pi^\pm}^2(B) - E_{\pi^\pm}^2(0)$ are in good agreement with LQCD calculations using staggered quarks with realistic pion masses [74, 258]. For larger values of eB, our results are consistent with quenched LQCD simulations at unphysically large pion masses [129]. However, NJL results do not reproduce the nonmonotonic behavior with values below the point-like case found in [258], using highly improved staggered quarks with close-to-physical pion masses. As compared to results obtained disregarding Schwinger phases, as done in previous works, the latter show an even steeper enhancement with B, in further contrast with lattice outputs. On the other hand, as in the neutral case, $g_{\pi^- qq}$ shows some enhancement if B is increased for a constant G, in contrast to what happens for the $G(B)$ case. Regarding the four charged decay constants, they all increase with B – see [171] for some LQCD results obtained in Fourier space. The use of $G(B)$ moderates this enhancement, except for $f_{\pi^-}^{(A3)}$ where it is intensified. We stress that some chiral relations, such as GT and GMOR, are violated for $eB \gtrsim m_\pi^2$, for both $f_{\pi^-}^{(A\parallel)}$ and $f_{\pi^-}^{(A\perp+)}$. However, for a constant coupling G, new relations involving $f_{\pi^-}^{(V)}$ or the difference $f_{\pi^-}^{(A2)} - f_{\pi^-}^{(A3)}$ are approximately satisfied.

From the NJL outcomes for these pion properties, we have obtained an estimation of the effect of an external uniform magnetic field on the magnitude of the decay rate $\Gamma(\pi^- \to l^- \bar{\nu}_l)$ and the angular distribution of the antineutrinos in the final state, based on Ref. [253]. Our estimation took into account the contribution of all four possible π^- decay form factors. It also considered the π^- in its lowest possible energy state. Then, from the two possible form factors combinations $f_{\pi^-}^{(A\perp\pm)} = f_{\pi^-}^{(A1)} \pm f_{\pi^-}^{(A2)} - f_{\pi^-}^{(A3)}$ which parametrize the matrix elements of the axial current, only $f_{\pi^-}^{(A\perp+)}$ contributes. Our results show that the total decay rate $\Gamma_e + \Gamma_\mu$ becomes strongly increased with respect to its $B = 0$ value, with the enhancement factor reaching a value of 1000 at $eB \simeq 1$ GeV^2 when using a constant coupling, increased up to 1800 for $G(B)$. Moreover, owing to the presence of the new decay constants and the features of nonzero B kinematics, it was found that

the decay width Γ_l does not vanish in the limit $m_l = 0$. As a consequence, for large values of B the ratio Γ_e/Γ_μ changes dramatically with respect to the $B = 0$ value (of about 1.2×10^{-4}), reaching a magnitude of ~ 0.5 at $eB \simeq 1$ GeV^2. This could be interesting e.g. regarding the expected flavor composition of neutrino fluxes coming from the cores of magnetars and other stellar objects. Also, a reduction in the pion mean lifetime will inevitably decrease radiation energy loss of pions and result in a harder neutrino spectrum. On the other hand, it was found that for large B the angular distribution of outgoing antineutrinos becomes highly anisotropic, showing a significant suppression in the direction of the external field. In addition, most antineutrinos come out with low momentum in the field direction, i.e. in directions approximately perpendicular to the magnetic field.

It is worth noticing that for the three parametrization sets used, we have found that all mentioned results are rather insensitive to variations in the parametrization.

The Ritus eigenfunction method presented for the calculation of charged pion properties can be straightforwardly extended to calculate properties for all charged mesons of the pseudoscalar nonet. To that end, we worked with the three-flavor version of the NJL model, including the 't Hooft-Maekawa six-fermion interaction which explicitly breaks axial symmetry $U(1)_A$. Results are based on Ref. [265]. Bosonization is performed using the stationary phase approximation. Once again we considered a magnetic field dependent coupling $G(B)$ and regularized divergent results using a 3D cutoff in the MFIR scheme.

For neutral mesons the magnetic field breaks isospin symmetry, leading to a mixing between all three $\pi^0 - \eta - \eta'$ states [105] in contrast to the $B = 0$ case, where π^0 is decoupled. As known, the η' meson comes out in the model as a resonance or unstable particle. In this regard, we have developed a new formalism to deal with the multiple complex magnetic poles. Nevertheless, results for this meson are less reliable, approaching the limit of applicability of the NJL model due to the lack of confinement. In fact, its width increases with B and we have found that when using $G(B)$ the coupling strength is not enough to form an η'-resonance for $eB \gtrsim 0.5$ GeV^2. Results for the π^0 mass are rather similar to those obtained in the two-flavor case, although $SU(3)$ values are slightly higher. For constant G, the mass displays a non-monotonous behavior with B, while the monotonous decreasing behavior found in LQCD [129, 258] is reproduced using $G(B)$. A similar behavior is found for K^0, $\bar{K}^0$ and η masses. From the behavior of neutral pseudoscalar meson masses, we conclude that the incorporation of the inverse magnetic catalysis effect in the NJL model, as done e.g. in this thesis through the magnetic field dependent coupling $G(B)$, is fundamental to qualitatively reproduce the available LQCD results.

Concerning charged mesons, for their lowest energies $E_{P^\pm}(B)$ $(P = \pi, K)$ a strong enhancement with B was found, surpassing the energy associated with a point-like charged

meson. Once again, pion results are very similar to the ones obtained in the two-flavor case. Our NJL results for $E^2_{P^\pm}(B) - E^2_{P^\pm}(0)$ are in reasonable agreement with LQCD results of Ref. [129] within error bars for $P = \pi$, being closer for the constant coupling case. On the other hand, no sign of the non-monotonous behavior found in the LQCD calculation of Ref. [258] is observed for $P = \pi, K$.

Lastly, the Ritus eigenfunction method has been applied to the calculation of diquark and nucleon masses, within the two-flavor NJL model. To account for diquarks, scalar quark-quark color pairing interactions were included, driven by a constant coupling H. We have considered values of the interaction strength ratio in the usually studied range $0.75 \leq H/G \leq 1.2$. Bosonization has been performed using the Nambu-Gorkov formalism.

Diquarks can be treated in a very similar fashion as charged pions. As before, the regularization has been performed using a 3D cutoff within the MFIR scheme. At $B = 0$, the (LLL) mass m_Δ decreases with H/G. Inversely, the binding energy $2M - m_\Delta$ increases: while for $H/G = 0.75$ the scalar diquark is barely bound by 5 MeV, at $H/G = 1.2$ the binding energy is about 200 MeV. At $B \neq 0$, results for m_Δ and the lowest energy state E_Δ showed that, for low values of B, both curves lie below those corresponding to a point-like diquark. This is reversed for $eB \gtrsim 0.3 - 0.5$ GeV^2, where the growth gets steeper in comparison with the point-like case. In fact, the increase becomes even more pronounced for lower values of the ratio H/G. In comparison, results obtained disregarding Schwinger phases show an early crossing of the point-like curve and a rather strong enhancement at high magnetic fields.

Regarding the analysis of baryon states, in our framework nucleons have been built as bound quark-diquark states following a relativistic Fadeev approach. Given the complexity of the problem, we have considered a static approximation in which one disregards the momentum dependence of the exchanged quark. This approximation has been shown to lead to an adequate description of nucleon properties in the absence of external fields [278]. In addition, we have introduced a further model parameter Λ_B to regularize the otherwise divergent quark-diquark loops, for which we have chosen the proper time regularization scheme. We have found that for values of H/G larger than 1 no value of Λ_B is compatible with a physical value of the nucleon mass at zero external magnetic field.

We have obtained numerical results for the magnetic field dependence of the lowest energy nucleon states, usually interpreted as the nucleon masses. In general, it is seen that the masses initially decrease for increasing magnetic field, whereas they show a steady growth for large values of eB. In the proton case, results strongly depend on the ratio H/G. It was also seen that the negative slopes of the mass curves at $B = 0$ lead to the phenomenologically correct signs for the nucleon magnetic moments. Moreover, there is a qualitative agreement with ChPT results [268], although the slopes in our model are found

to be somewhat lower. This leads to numerical absolute values for the proton and neutron magnetic moments that are relatively small in comparison with the empirical ones. An improvement on the predictions of nucleon magnetic moments is expected to be obtained by including axial-vector diquark interactions [282]. Moreover, a full calculation would require to take into account the momentum dependence of the exchanged quark.

In this thesis we have introduced a method to deal with uniformly magnetized charged systems which fully takes into account the translational breaking effect of Schwinger phases, induced by the gauge choice representation of an external uniform magnetic field. The method is based on the use of Ritus-type eigenfunctions, which allow for a proper diagonalization of the system. Concerning the future outlook on this subject, it is clear that the method introduced in this thesis can be used to provide a consistent determination of other light charged hadron properties. In fact, charged vector and axial-vector mesons can be readily studied within the NJL model using this method, see Ref. [283] for recent advances in this direction. Moreover, the range of applicability can be extended to study magnetized systems in dense and/or hot mediums, relevant for different physical scenarios. In that regard, a natural improvement would be to consider inhomogeneous magnetic fields, as suggested by heavy ion collision studies. Although in this thesis we have mainly applied the Ritus method to the particular case of the NJL effective model, other approaches could benefit from the insights gained using this strategy.

Conclusiones

En esta tesis hemos investigado el efecto de un campo magnético uniforme externo sobre varias propiedades de los hadrones ligeros, compuestos por materia de quarks fuertemente interactuante. Dado que los campos magnéticos fuertes pueden resolver la estructura de quarks de los hadrones, el efecto sobre sus propiedades puede proporcionar información significativa sobre el diagrama de fases magnetizado de QCD, relevante para varios escenarios físicos. Dado que el carácter no perturbativo de QCD a bajas energías hace que los cálculos sean extremadamente complicados, para calcular propiedades hadrónicas hemos empleamos el modelo efectivo de Nambu–Jona-Lasinio, donde las interacciones de color corriente-corriente mediadas por el intercambio de gluones se aproximan mediante interacciones locales de cuatro puntos. El modelo, introducido en el capítulo 2, está construido sobre las simetrías de QCD y es capaz de reproducir el fenómeno de ruptura de la simetría quiral.

Dado que los piones son los hadrones más ligeros, pueden producirse fácilmente en los sistemas magnetizados antes mencionados. Sin embargo, son partículas inestables, propensas a decaer en otras menos pesadas, como leptones y fotones. En ausencia de campos externos, el decaimiento de los piones cargados se asocia con una única constante de decaimiento. En cambio, la presencia de un campo magnético uniforme modifica las simetrías del sistema y abre la posibilidad de que aparezcan nuevas constantes de decaimiento. En el capítulo 3 hemos presentamos un método general para parametrizar los elementos matriciales magnetizados de un pión a vacío de las corrientes hadrónicas vectoriales y axiales-vectoriales, basado en las Refs. [230] y [231]. Cuando el campo magnético está presente, nuevas estructuras tensoriales covariantes de gauge se vuelven disponibles. Hemos mostrado que, de hecho, pueden formarse cuatro cuadrivectores independientes, lo que conduce a la existencia de cuatro factores de forma o constantes de decaimiento; tres asociados a la corriente vectorial-axial, y uno a la corriente vectorial. Estos factores están limitados por simetrías discretas. Como resultado, todos los factores de forma son reales, y para los piones cargados son independientes del signo de la carga. Además, en el caso del pión neutro, dichas simetrías impiden la aparición de un factor de forma axial en particular.

Escogiendo $\vec{B}$ orientado a lo largo del eje 3, hemos mostrado que los elementos matriciales de las componentes paralelas (0- y 3-) de la corriente vectorial pueden expresarse en términos de un único factor de forma real, $f_{\pi^0}^{(V)}$ o $f_{\pi^\pm}^{(V)}$, mientras que las componentes perpendiculares (1- y 2-) desaparecen idénticamente. Para los elementos matriciales de la corriente axial-vectorial, pueden definirse dos factores de forma reales $f_{\pi^0}^{(A1)}$ y $f_{\pi^0}^{(A3)}$ en el caso del pión neutro. Alternativamente, estos pueden escribirse en términos de un factor de forma paralelo y otro perpendicular, reflejando la anistropía inducida por el campo externo [170]. Para piones cargados, en cambio, se requieren en general tres factores de forma $f_{\pi^\pm}^{(A1)}, f_{\pi^\pm}^{(A2)}$ y $f_{\pi^\pm}^{(A3)}$ para parametrizar los elementos matriciales de la corriente axial-vectorial. Mientras que $f_{\pi^0}^{(A3)}$, $f_{\pi^\pm}^{(V)}$ y $f_{\pi^\pm}^{(A2)}$ ya eran conocidos en la literatura [170, 171], las constantes de decaimiento $f_{\pi^0}^{(V)}$ y $f_{\pi^\pm}^{(A3)}$ son nuevas, definidas por primera vez en [230].

Utilizando los resultados anteriores, hemos introducido un marco general, independiente del modelo, para estudiar el decaimiento débil $\pi^- \to l\,\bar{\nu}_l$ en presencia de un campo magnético externo uniforme. Para ello, describimos para cada partícula implicada la forma específica del campo, teniendo plenamente en cuenta el efecto del campo magnético sobre las correspondientes autofunciones. Mediante la realización de cálculos en dos gauges diferentes, Landau [230] y simétrico [231], hemos sido capaces de proporcionar una prueba explícita de la independencia de gauge de nuestro resultado. Además, esto nos ha permitido aclarar el comportamiento de los números cuánticos asociados. Para ambos gauges, el momento en la dirección del campo junto con la energía se conservan. Los números cuánticos restantes son el nivel de Landau y un último que depende del gauge elegido. Para el gauge de Landau es el momento canónico a lo largo de la dirección 2, mientras que para el gauge simétrico es el momento angular canónico total a lo largo de la dirección 3. Aunque estas cantidades se conservan, al depender del gauge elegido no corresponden a observables físicos.

Para el caso en que el pión que decae se encuentra en su estado de mínima energía (es decir, en el nivel más bajo de Landau, con momento cero a lo largo de la dirección 3), hemos obtenido una expresión explícita para el ancho de decaimiento magnetizado $\pi^- \to l\,\bar{\nu}_l$ en la Ec. (3.71). Como era de esperar, esta expresión coincide para ambos gauges elegidos y no depende de sus correspondientes números cuánticos dependientes del gauge. Además, hemos revelado que la conservación del momento angular no implica, como se afirma en la Ref. [171], que el momento del antineutrino tenga que ser necesariamente paralelo al campo magnético. Para campos magnéticos grandes, es decir $eB > m_{\pi^-}^2 - m_l^2 \sim 0.05\ \text{GeV}^2$, pero menores que la masa del leptón τ al cuadrado, esta expresión se reduce a la Ec. (3.73). De hecho, se obtuvo un resultado novedoso para campos fuertes que también satisfacen $eB \gg m_l^2$. Como se observa en la expresión simplificada de la Ec. (3.75), válida para

campos magnéticos muy intensos, el ancho de decaimiento magnetizado no desaparece en el límite quiral $m_l \to 0$, es decir, no muestra la supresión de helicidad encontrada en ausencia del campo magnético externo. De hecho, la conservación de la helicidad sólo implica que la proyección del momento del antineutrino en la dirección del campo magnético debe ser antiparalela al campo magnético. Esto implica una distribución altamente anisotrópica de los antineutrinos salientes, señalando una supresión significativa en la dirección del campo externo.

Para estimar cuantitativamente cómo las tasas de decaimiento débil de los piones cargados se ven modificadas por el campo magnético, es necesario determinar el comportamiento de los factores de forma del decaimiento y de las masas de los piones. En el capítulo 4, estas y otras propiedades de los piones se han calculado en el marco del modelo NJL de dos sabores (introducido en el capítulo 2), basado en las Refs. [233, 252]. Mientras que para los piones neutros se puede tomar la base de momento habitual para diagonalizar las funciones de polarización correspondientes, esto no es posible para los piones cargados, debido a la presencia de contribuciones no nulas de las fases de Schwinger. En el capítulo 3 hemos demostrado que el método de autofunciones de Ritus presentado nos permite tener plenamente en cuenta los efectos de ruptura traslacional inducidos por estas fases. Los cálculos de las propiedades de los mesones cargados utilizando este método se han realizado en [233, 252] por primera vez. En nuestros cálculos numéricos hemos utilizado tres conjuntos de parametrización del modelo que describen satisfactoriamente no solo las propiedades de los mesones en ausencia del campo magnético, sino también los resultados de QCD en la red para el comportamiento de los condensados de quarks bajo un campo magnético. Además, hemos explorado la posibilidad de considerar un acoplamiento $G(B)$ dependiente del campo magnético, con el fin de incorporar el efecto de catálisis magnética inversa. Debido a la no renormalizabilidad del modelo, los resultados divergentes se han regulado utilizando un corte 3D en el esquema MFIR, que ha demostrado proporcionar resultados más fiables en comparación con otros esquemas de regularización dependientes del campo magnético [212].

Hemos encontrado que, para un acoplamiento constante G, el campo magnético disminuye ligeramente la masa del π^0, de acuerdo con resultados previos obtenidos en el modelo NJL [161, 248]. Sin embargo, el comportamiento encontrado de m_π^0 no es monótono, en contraste con los resultados de LQCD [129, 258] y NJL no local [250, 251], que muestran una disminución monótona de la masa con B. Para $eB < 1$ GeV^2 esta tendencia se recupera cuando se utiliza un acoplamiento magnético $G(B)$ [161], que imita la retroreacción del mar de quarks debida al campo externo. Mientras tanto, la constante de acoplamiento pión-quark $g_{\pi^0 qq}$ muestra cierto aumento si se incrementa B para un G constante, en contraste con lo que ocurre para el caso $G(B)$. Por otro lado, para

ambos acoplamientos el índice de refracción direccional u_{π^0} decrece monótonamente con B, permaneciendo siempre menor que uno (piones subluminales) incluso en el límite quiral, de acuerdo con las Refs. [100, 217]. En cuanto a las constantes de decaimiento neutras, en el modelo NJL $f_{\pi^0}^{(A2)}$ desaparece, como era de esperarse de las restricciones impuestas por las simetrías discretas de la interacción. Para ambos acoplamientos $f_{\pi^0}^{(A||)} = f_{\pi^0}^{(A1)}$ y $f_{\pi^0}^{(V)}$ aumentan con B, mientras que $f_{\pi^0}^{(A\perp)} = f_{\pi^0}^{(A1)} - f_{\pi^0}^{(A3)}$ se reduce. El uso de $G(B)$ conduce a un mejor acuerdo con algunos otros enfoques [243, 251, 258], que muestran un comportamiento más pronunciado. Tambipén hemos observado que nuestros resultados satisfacen bastante bien varias relaciones en límite quiral, como las conocidas ecuaciones generalizadas de Goldberger-Treiman y Gell-Mann-Oakes-Renner para $f_{\pi^0}^{(A||)}$ (véase por ejemplo la Ref. [234]). Además, hemos demostrado que las relaciones $f_{\pi^0}^{(A\perp)} = u_{\pi^0}^2 f_{\pi^0}^{(A||)}$ y $f_{\pi^0}^{(V)} = eB/(8\pi^2 f_{\pi^0}^{(A||)})$ también se cumplen en el límite quiral. Mientras que la primera puede deducirse de las Refs. [103, 170, 228], la segunda puede relacionarse con el lagrangiano efectivo anómalo de Wess-Zumino-Witten, y – hasta donde sabemos – no se ha establecido previamente en la literatura.

Pasando ahora al caso del pión cargado, remarcamos que los cálculos se han realizado teniendo plenamente en cuenta las fases de Schwinger mediante el método de autofunciones de Ritus. Hemos obtenido $m_{\pi^-} = m_{\pi^+}$, como era de esperar a partir de la invariancia de carga. Además, se puede obtener una masa para cada nivel de Landau; nosotros hemos considerado sólo la masa del nivel de Landau más bajo. Las masas de piones cargados se obtuvieron utilizando este método por primera vez en la Ref. [233]. En particular, hemos encontrado que la masa dependiente del campo magnético $E_{\pi^\pm}$ (definida como su estado de energía más bajo) aumenta constantemente con el campo magnético [menos marcadamente para $G(B)$], permaneciendo siempre mayor que la de un pión puntual. Para valores bajos de eB (digamos $eB \lesssim 0.15$ GeV^2), los resultados para $E_{\pi^\pm}^2(B) - E_{\pi^\pm}^2(0)$ están en buen acuerdo con los cálculos de LQCD usando quarks 'staggered' con masas de piones realistas [74, 258]. Para valores mayores de eB, nuestros resultados son consistentes con simulaciones de LQCD que utilizan masas de piones mayores que las físicas [129]. Sin embargo, los resultados de NJL no reproducen el comportamiento no monótono con valores por debajo del caso puntual encontrado en [258], utilizando quarks 'staggered' altamente mejorados con masas de piones cercanas a la física. En comparación con los resultados obtenidos sin tener en cuenta las fases de Schwinger, como se hizo en trabajos anteriores, estos últimos muestran un realzamiento aún más pronunciado con B, en mayor contraste con los resultados de la red. Por otra parte, como en el caso neutro, $g_{\pi^- qq}$ muestra cierto incremento si se aumenta B para un G constante, en contraste con lo que ocurre para el caso $G(B)$. En cuanto a las cuatro constantes de decaimiento cargadas, todas aumentan con B – véase la Ref. [171] para algunos resultados de LQCD obtenidos en el espacio de

Fourier. El uso de $G(B)$ modera este aumento, excepto para $f_{\pi^-}^{(A3)}$ donde se intensifica. Destacamos que algunas relaciones quirales, como GT y GMOR, se violan para $eB \gtrsim m_\pi^2$, tanto para $f_{\pi^-}^{(A||)}$ como para $f_{\pi^-}^{(A\perp+)}$. Sin embargo, para un acoplamiento constante G, se satisfacen aproximadamente nuevas relaciones que implican a $f_{\pi^-}^{(V)}$ o a la diferencia $f_{\pi^-}^{(A2)} - f_{\pi^-}^{(A3)}$.

A partir de los resultados de NJL para estas propiedades piónicas, hemos obtenido una estimación del efecto que un campo magnético uniforme externo tiene sobre la magnitud de la tasa de decaimiento $\Gamma(\pi^- \to l^- \bar{\nu}_l)$ y la distribución angular de los antineutrinos en el estado final, basándonos en la Ref. [253]. Nuestra estimación tuvo en cuenta la contribución de los cuatro posibles factores de forma del decaimiento π^-. También se consideró el pión cargado en su estado de energía más bajo posible. Entonces, de las dos posibles combinaciones de factores de forma $f_{\pi^-}^{(A\perp\pm)} = f_{\pi^-}^{(A1)} \pm f_{\pi^-}^{(A2)} - f_{\pi^-}^{(A3)}$ que parametrizan los elementos matriciales de la corriente axial, sólo contribuye $f_{\pi^-}^{(A\perp+)}$. Nuestros resultados muestran que la tasa de decaimiento total $\Gamma_e + \Gamma_\mu$ se incrementa fuertemente con respecto a su valor $B = 0$, alcanzando el factor de incremento un valor de 1000 para $eB \simeq 1$ GeV^2 cuando se utiliza un acoplamiento constante, aumentado hasta 1800 para $G(B)$. Además, debido a la presencia de las nuevas constantes de decaimiento y a las características de la cinemática a B finito, se encontró que el ancho de decaimiento Γ_l no desaparece en el límite $m_l = 0$. Como consecuencia, para valores grandes de B la relación Γ_e/Γ_μ cambia drásticamente con respecto al valor de $B = 0$ (de aproximadamente $1,2 \times 10^{-4}$), alcanzando una magnitud de $\sim 0,5$ a $eB \simeq 1$ GeV^2. Esto podría ser interesante, por ejemplo, para la composición de sabores esperada de los flujos de neutrinos procedentes de los núcleos de magnetares y otros objetos estelares. Además, una reducción de la vida media del pión disminuirá inevitablemente la pérdida de energía de radiación de los piones y dará lugar a un espectro de neutrinos más duro. Por otro lado, se encontró que para grandes B la distribución angular de los antineutrinos salientes se vuelve altamente anisotrópica, mostrando una supresión significativa en la dirección del campo externo. Además, la mayoría de los antineutrinos salen con bajo momento en la dirección del campo, es decir, en direcciones aproximadamente perpendiculares al campo magnético.

Cabe señalar que, para los tres conjuntos de parametrización utilizados, hemos comprobado que todos los resultados mencionados son bastante insensibles a las variaciones de la parametrización.

El método de autofunciones de Ritus presentado para el cálculo de las propiedades de los piones cargados puede extenderse directamente para calcular las propiedades de todos los mesones cargados del nonete pseudoescalar. Para ello, trabajamos con la versión de tres sabores del modelo NJL, incluyendo la interacción 't Hooft-Maekawa de seis fermiones que rompe explícitamente la simetría axial $U(1)_A$. Los resultados se basan en la Ref. [265].

La bosonización se realiza utilizando la aproximación de fase estacionaria. Una vez más consideramos un acoplamiento $G(B)$ dependiente del campo magnético y regularizamos los resultados divergentes utilizando un corte 3D en el esquema MFIR.

Para los mesones neutros, el campo magnético rompe la simetría de isospín, dando lugar a una mezcla entre los tres estados $\pi^0-\eta-\eta'$ [105], en contraste con el caso $B=0$ donde π^0 está desacoplado. Sus masas polares y anchos se obtienen como las raíces del determinante inverso de la matriz de propagación de 3x3. Como es sabido, el mesón η' sale en el modelo como una resonancia o partícula inestable. A este respecto, hemos desarrollado un nuevo formalismo para tratar los múltiples polos magnéticos complejos. Sin embargo, los resultados para este mesón son menos fiables, acercándose al límite de aplicabilidad del modelo NJL debido a la falta de confinamiento. De hecho, su ancho aumenta con B y hemos encontrado que cuando se usa $G(B)$ la fuerza del acoplamiento no es suficiente para formar una resonancia η' para $eB \gtrsim 0.5$ GeV^2. Los resultados para la masa π^0 son bastante similares a los obtenidos en el caso de dos sabores, aunque los valores en $SU(3)$ son ligeramente superiores. Para G constante, la masa muestra un comportamiento no monótono con B, mientras que el comportamiento monótono decreciente encontrado en LQCD [129, 258] se reproduce usando $G(B)$. Un comportamiento similar se encuentra para las masas K^0, $\bar{K}^0$ y η. A partir del comportamiento de las masas de mesones pseudoescalares neutros, concluimos que la incorporación del efecto de catálisis magnética inversa en el modelo NJL, como se hace por ejemplo en esta tesis a través del acoplamiento $G(B)$ dependiente del campo magnético, es fundamental para reproducir cualitativamente los resultados de LQCD disponibles.

Con respecto a los mesones cargados, para sus energías más bajas $E_{P^\pm}(B)$ $(P=\pi,K)$ se encontró un fuerte incremento con B, superando la energía asociada a un mesón cargado puntual. Una vez más, los resultados de los piones son muy similares a los obtenidos en el caso de dos sabores. Nuestros resultados en el modelo NJL para $E^2_{P^\pm}(B)-E^2_{P^\pm}(0)$ están razonablemente de acuerdo con los resultados de LQCD de la Ref. [129] dentro de las barras de error para $P=\pi$, estando más cerca para el caso de acoplamiento constante. Por otro lado, no se encontró ningún signo del comportamiento no monótono encontrado en el cálculo de LQCD de la Ref. [258] para $P=\pi,K$.

Por último, se ha aplicado el método de autofunciones de Ritus al cálculo de las masas de diquarks y nucleones, dentro del modelo NJL de dos sabores. Para dar cuenta de los diquarks, se incluyeron interacciones escalares quark-quark de emparejamiento de color, conducidas por un acoplamiento constante H. Hemos considerado valores de la razón entre interacciones en el rango usualmente estudiado de $0,75 \leq H/G \leq 1,2$. La bosonización se ha realizado utilizando el formalismo de Nambu-Gorkov.

Los diquarks pueden tratarse de forma muy similar a los piones cargados. Como antes,

la regularización se ha realizado utilizando un corte 3D dentro del esquema MFIR. Para $B = 0$, la masa (LLL) m_Δ disminuye con H/G. Inversamente, la energía de ligadura $2M - m_\Delta$ aumenta: mientras que para $H/G = 0,75$ el diquark escalar se encuentra apenas ligado por 5 MeV, a $H/G = 1,2$ la energía de ligadura es de unos 200 MeV. A $B \neq 0$, los resultados para m_Δ y el estado de menor energía E_Δ muestran que, para valores bajos de B, ambas curvas se sitúan por debajo de las correspondientes a un diquark puntual. Esto se invierte para $eB \gtrsim 0,3 - 0,5$ GeV^2, donde el crecimiento se hace más pronunciado en comparación con el caso puntual. De hecho, el aumento se hace aún más pronunciado para valores más bajos de la relación H/G.

En cuanto al análisis de los estados bariónicos, en nuestro marco los nucleones se han construido como estados ligados quark-diquark siguiendo una aproximación relativista de Fadeev. Dada la complejidad del problema, hemos considerado una aproximación estática en la que se desprecia la dependencia del momento del quark intercambiado. Se ha demostrado que esta aproximación conduce a una descripción adecuada de las propiedades de los nucleones en ausencia de campos externos [278]. Además, hemos introducido un parámetro modelo adicional Λ_B para regularizar los lazos quark-diquark, que de otro modo serían divergentes, para lo cual hemos elegido el esquema de regularización de tiempo propio. Hemos encontrado que para valores de H/G mayores que 1 ningún valor de Λ_B es compatible con un valor físico de la masa del nucleón a campo magnético externo cero.

Hemos obtenido resultados numéricos para la dependencia del campo magnético de los estados nucleónicos de más baja energía, normalmente interpretados como las masas nucleónicas. En general, se observa que las masas disminuyen inicialmente al aumentar el campo magnético, mientras que muestran un crecimiento constante para valores grandes de eB. En el caso del protón, los resultados dependen fuertemente de la relación H/G. También se observó que las pendientes negativas de las curvas de masa en $B = 0$ conducen a signos fenomenológicamente correctos para los momentos magnéticos de los nucleones. Además, existe un acuerdo cualitativo con los resultados de ChPT [268], aunque las pendientes en nuestro modelo resultan ser algo menores. Esto conduce a valores absolutos numéricos para los momentos magnéticos del protón y del neutrón que son relativamente pequeños en comparación con los empíricos. Se espera obtener una mejora en las predicciones de los momentos magnéticos de los nucleones incluyendo interacciones axiales-vectoriales entre diquarks [282]. Además, un cálculo completo requeriría tener en cuenta la dependencia del momento del quark intercambiado.

En esta tesis hemos introducido un método para tratar sistemas cargados uniformemente magnetizados que tiene plenamente en cuenta el efecto de ruptura traslacional de las fases de Schwinger, inducido por un campo magnético uniforme externo. El método se basa en el uso de funciones propias de tipo Ritus, que permiten una diagonalización adecuada del

sistema. Con respecto a las perspectivas futuras en esta área, está claro que el método introducido en esta tesis puede utilizarse para proporcionar una determinación consistente de otras propiedades de hadrones ligeros cargados. De hecho, los mesones vectoriales y axiales-vectoriales cargados pueden ser fácilmente estudiados dentro del modelo NJL usando este método, ver Ref. [283] para avances recientes en esta dirección. Además, el rango de aplicabilidad puede extenderse para estudiar sistemas magnetizados en medios densos y/o calientes, relevantes para diferentes escenarios físicos. En este sentido, una mejora natural sería considerar campos magnéticos no homogéneos, como sugieren los estudios de colisiones de iones pesados. Aunque en esta tesis hemos aplicado principalmente el método de Ritus al caso particular del modelo efectivo NJL, otros enfoques podrían beneficiarse de los conocimientos obtenidos utilizando esta estrategia.

Agradecimientos

En el largo viaje de este doctorado quisiera agradecer principalmente a mi director Norberto, quien me guió en este camino siempre con buena energía y predisposición. Sus explicaciones, los debates en conjunto y su manera constante de involucrarme lograban empujarme hacia la mejor versión de mí mismo. Además su manera de trabajar, iluminando caminos oscuros con su conocimiento e intuición, empujando la frontera de la ciencia todos los días un poquito más, fue a lo largo del doctorado una fuente de gran inspiración para mí.

Otros investigadores también formaron parte importante de mi doctorado, con quienes tuve el privilegio de realizar investigaciones que culminaron en la publicación de varios artículos. En este sentido le estoy agradecido a Daniel, quien también colaboró en gran medida con mi formación como doctor y con quien entre otras cosas aprendí la importancia que los pequeños detalles tienen en la calidad final de un trabajo. Por otro lado le agradezco a Santiago, que me invitó a realizar una estadía con él en Valencia, a Sidney y a Joana; todos ellos colaboraron con mi formación y me enseñaron sobre el trabajo en equipo.

En cuanto al apoyo emocional, quisiera agradecerle enormemente a mi familia; mis padres, mi hermano y Orne (y Cochis). Por su cariño, su contención, su acompañamiento; en fin, su incondicionalidad, que es su forma de amar. A ellos les dedico este logro, ya que ellos me dieron el apoyo para alcanzarlo. También le agradezco al JS por acompañarme, siempre interesados en lo que estudio y en cómo me esta yendo, y por la distensión que me ofrecen. Ya al final del doctorado uno está cansado, aunque ustedes mejor que nadie saben bien de qué. Por último quisiera nombrar a todas las personas que indirectamente formaron parte de este proceso y de mi vida. Mi tío, que quiere lo mejor para mí. Mis compañeras Flor y Cin que hicieron de los almuerzos y la oficina un lugar mucho más agradable. Gaby que siempre anda por ahí dando una mano. Personas muy valiosas que conocí en la facultad y aún me acompañan. Mis tíos, mi primo, mi madrina del corazón.

En memoria de mis abuelos, en especial de mi querida Oma.

APPENDIX

Bosonization procedure

The starting point is the generating functional associated to the Euclidean NJL Lagrangian given in Eq. (2.12). It reads

$$\mathcal{Z} \;=\; \int \mathcal{D}\bar{\psi}\mathcal{D}\psi \; e^{-\int d^4x_E \, \mathcal{L}_E(\psi,\bar{\psi})} \,. \tag{A.1}$$

We omit the Euclidean subscript E hereafter. Next, we rewrite the interactions in (2.12) in terms of bosonic fields that will represent the scalar and pseudoscalar mesons $\sigma(x)$ and $\vec{\pi}(x)$, respectively. The treatment for each interaction term is equivalent, so we will only detail the one corresponding to the scalar case. Using the equality

$$f\left[j_{\mathrm{s}}(x)\right] \;=\; \int \mathcal{D}\mathsf{s} \; \delta\left[\mathsf{s}(x) - j_{\mathrm{s}}(x)\right] \;\; f\left[\mathsf{s}(x)\right] \,, \tag{A.2}$$

we can rewrite the interaction term as follows

$$e^{G\int d^4x \, j_{\mathrm{s}}(x) j_{\mathrm{s}}(x)} \;=\; \int \mathcal{D}\mathsf{s} \; \delta\left[\mathsf{s}(x) - j_{\mathrm{s}}(x)\right] \;\; e^{G\int d^4x \, \mathsf{s}(x)\mathsf{s}(x)} \,, \tag{A.3}$$

where $\mathsf{s}(x)$ is an auxiliary field which will be later removed by integration and $j_{\mathrm{s}}(x) = \bar{\psi}(x)\psi(x)$ is the scalar quark current. Then, using

$$\delta\left(\mathsf{s}(x) - j_{\mathrm{s}}(x)\right) \;=\; N_{\mathsf{s}} \int \mathcal{D}\sigma \; e^{\int d^4x \, \sigma(x)[\mathsf{s}(x) - j_{\mathrm{s}}(x)]} \,, \tag{A.4}$$

the contribution to the action from the scalar interaction term is re-expressed as

$$e^{G\int d^4x\, j_{\mathsf{s}}(x) j_{\mathsf{s}}(x)} \;=\; N_{\mathsf{s}} \int \mathcal{D}\mathsf{s}\, \mathcal{D}\sigma\; e^{\int d^4x \left\{\sigma(x)[\mathsf{s}(x) - j_{\mathsf{s}}(x)] + G\,\mathsf{s}(x)^2\right\}}\,, \tag{A.5}$$

where N_{s} is a normalization factor. Repeating this procedure for the pseudoscalar field introduces a vector of fields $\vec{\mathsf{p}}(x)$ analogous to $\mathsf{s}(x)$, resulting in the partition function

$$\begin{aligned}\mathcal{Z} \;=\; N_{\mathsf{s}} N_{\mathsf{p}} \int \mathcal{D}\bar{\psi}\, \mathcal{D}\psi\; e^{-\int d^4x\, \bar{\psi}(-i\partial\!\!\!/ + m_0)\psi} \;\times \\ \int \mathcal{D}\mathsf{s}\, \mathcal{D}\sigma\; e^{\int d^4x \{\sigma(x)[\mathsf{s}(x) - j_{\mathsf{s}}(x)] + G\,\mathsf{s}(x)\mathsf{s}(x)\}} \;\times \\ \int \mathcal{D}\vec{\mathsf{p}}\, \mathcal{D}\vec{\pi}\; e^{\int d^4x \left\{\vec{\pi}(x)\cdot\left[\vec{\mathsf{p}}(x) - \vec{j}_p(x)\right] + G\,\vec{\mathsf{p}}(x)\cdot\vec{\mathsf{p}}(x)\right\}}\,,\end{aligned} \tag{A.6}$$

where $\vec{j}_p(x) = \bar{\psi}\, i\gamma_5 \vec{\pi}\, \psi$.

We can evaluate the integrals over $\mathsf{s}(x)$, $\vec{\mathsf{p}}(x)$, $\psi(x)$ and $\bar{\psi}(x)$, leaving the action expressed in terms of the bosonic degrees of freedom $\sigma(x)$ and $\vec{\pi}(x)$. To that end, we rearrange the terms in (A.6) so as to factorize the integrals, which can be performed since they are Gaussian. The Gaussian integral over continuous fields is written as

$$\int \mathcal{D}\mathsf{s}\; e^{-\frac{1}{2}\mathsf{s}\,K\,\mathsf{s} + \sigma\,\mathsf{s}} \;=\; N'_{\mathsf{s}}\; e^{\frac{1}{2}\sigma K^{-1}\sigma}\,, \tag{A.7}$$

where N'_{s} is a factor that does not depend on σ and the field product notation implies $\mathsf{s}\,K\,\mathsf{s} = \int d^4x\, d^4x' \mathsf{s}(x) K(x,x') \mathsf{s}(x')$, with the inverse of K given by the relation $\int d^4x'' K(x,x'') K^{-1}(x'',x') = \delta^{(4)}(x-x')$. In our case, $K(x,x') = -2G\,\delta^{(4)}(x-x')$. Then, for the scalar field we have

$$\begin{aligned}&\int \mathcal{D}\sigma\; e^{-\int d^4x\, \sigma(x) j_{\mathsf{s}}(x)} \int \mathcal{D}\mathsf{s}\; e^{\int d^4x\, [G\,\mathsf{s}(x)\mathsf{s}(x) + \sigma(x)\mathsf{s}(x)]} \;= \\ &\int \mathcal{D}\sigma\; e^{-\int d^4x\, \sigma(x) j_{\mathsf{s}}(x)}\; N'_{\mathsf{s}}\, e^{\frac{1}{2}\int d^4x\, d^4x'\, \sigma(x)\left[\frac{-\delta^{(4)}(x-x')}{2G}\right]\sigma(x')} \;= \\ &N'_{\mathsf{s}} \int \mathcal{D}\sigma\; e^{-\int d^4x \left[\frac{\sigma(x)\sigma(x)}{4G} + \sigma(x) j_{\mathsf{s}}(x)\right]}\,.\end{aligned} \tag{A.8}$$

Repeating this calculation for $\vec{\mathsf{p}}(x)$ we obtain the analogous expression

$$N'_{\mathsf{p}} \int \mathcal{D}\vec{\pi}\; e^{-\int d^4x \left[\frac{\vec{\pi}(x)\cdot\vec{\pi}(x)}{4G} + \vec{\pi}(x)\cdot\vec{j}_p(x)\right]}\,. \tag{A.9}$$

After replacing these expressions, we can group all fermionic field contributions to the

actions under the single term

$$S_F = \int d^4x \left[\bar{\psi}(x)(-i\partial\!\!\!/ + m_0)\psi(x) + \sigma(x) j_{\mathrm{s}}(x) + \vec{\pi}(x)\cdot\vec{j}_p(x)\right] \tag{A.10}$$

$$= \int d^4x\, d^4x'\ \bar{\psi}(x)\ \mathcal{D}(x,x')\ \psi(x')\,, \tag{A.11}$$

where we have defined the fermionic operator

$$\mathcal{D}(x,x') = \delta^{(4)}(x-x')\left[-i\partial\!\!\!/ + m_0 + \sigma(x) + i\gamma_5\vec{\tau}\cdot\vec{\pi}(x)\right]\,. \tag{A.12}$$

Finally, the semibosonized generating functional reads

$$\mathcal{Z} = \int \mathcal{D}\sigma\,\mathcal{D}\vec{\pi}\int \mathcal{D}\bar{\psi}\,\mathcal{D}\psi\ e^{-S_F}\ e^{-\frac{1}{4G}\int d^4x\,[\sigma(x)^2+\vec{\pi}(x)^2]}\,, \tag{A.13}$$

where we have omitted the unphysical normalization factors N_{s}, N_{p}, N'_{s} and N'_{p}.

APPENDIX

Discrete symmetries

In the Landau gauge, the electromagnetic interaction term between the light quarks and the external field (chosen to be orientated along the z axis) is given by

$$\mathcal{L}(x) \;=\; -\sum_f \, Q_f \, B \, x^1 \, \bar{\psi}_f(x) \, \gamma_2 \, \psi_f(x) \;, \tag{B.1}$$

where the sum extends over $f = u, d$, and Q_f are the corresponding electric charges. As can be checked, the action is separately invariant under $\mathcal{P}$, $\mathcal{CT}$ and $\mathcal{PCT}$, where $\mathcal{P}$, $\mathcal{C}$ and $\mathcal{T}$ stand for parity, charge conjugation and time reversal transformations acting on the quark fields. Moreover, it can be seen that the Lagrangian density in Eq. (B.1) is invariant under the transformation $\mathcal{CR}_1$, where $\mathcal{R}_1$ is a spatial rotation by angle π about the 1 axis (i.e., a rotation that inverts the orientation of the magnetic field $\vec{B}$).

The existence of these symmetries imposes constraints on the form factors of the pion-to-vacuum hadronic matrix elements discussed in chapter 3. As in the case of no external field, parity is responsible for selecting which Lorentz structures in Eq. (3.42) contribute to the matrix elements of the vector and axial-vector currents, as quoted in Eqs. (3.43) and (3.47). Moreover, it is possible to use $\mathcal{CT}$ and $\mathcal{CR}_1$ symmetries to show that the form factors are real and equal for both charged pions.

We start by using $\mathcal{CT}$ symmetry to show that the form factor $f_{\pi^0}^{(V)}$ in Eq. (3.45) is real.

One has

$$\begin{aligned}\langle 0|\bar{\psi}_f(x)\gamma^\mu\psi_f(x)|\pi^0(\vec{p})\rangle &= \langle 0|(\mathcal{CT})^\dagger\mathcal{CT}\,\bar{\psi}_f(x)\gamma^\mu\psi_f(x)\,(\mathcal{CT})^\dagger\mathcal{CT}|\pi^0(\vec{p})\rangle \\ &= \eta_T\,\langle 0|\mathcal{C}^\dagger\mathcal{C}\,\bar{\psi}_f(-\tilde{x})\gamma_\mu\psi_f(-\tilde{x})\,\mathcal{C}^\dagger\mathcal{C}|\pi^0(-\vec{p})\rangle^* \\ &= \langle 0|\bar{\psi}_f(-\tilde{x})\gamma_\mu\psi_f(-\tilde{x})|\pi^0(-\vec{p})\rangle^*\,, \end{aligned} \tag{B.2}$$

where $\tilde{x}^\mu = (x^0, -\vec{x}\,)$, and the phase η_T, arising from the action of the time reversal operator on the pion state, has been taken to be equal to -1 due to $\mathcal{PCT}$ invariance. From Eqs. (3.45) and (B.2) it can be seen that $f_{\pi^0}^{(V)}$ is real. For example, from the definition of $H_V^{0,\mu}(x,\vec{p})$, Eq. (B.2) implies $H_V^{0,0}(x,\vec{p}) = H_V^{0,0}(-\tilde{x},-\vec{p})^*$, which according to the relation in Eq. (3.45) leads to

$$-if_{\pi^0}^{(V)}\,p^3\,e^{-ip\cdot x} \;=\; \left(-if_{\pi^0}^{(V)}\right)^*\,(-p^3)\,e^{i\tilde{p}\cdot(-\tilde{x})}\,, \tag{B.3}$$

i.e. $f_{\pi^0}^{(V)} = f_{\pi^0}^{(V)\,*}$. For matrix elements of the axial-vector current, a similar analysis leads to $f_{\pi^0}^{(Ai)} = f_{\pi^0}^{(Ai)\,*}$, for $i = 1,2,3$.

On the other hand, taking into account the invariance of the action under $\mathcal{CR}_1$ one has

$$\begin{aligned} H_{\perp,A}^{0,\epsilon}(x,\vec{p}) &= \langle 0|(\mathcal{CR}_1)^\dagger\mathcal{CR}_1\bar{\psi}_f(x)(\gamma^1 + i\epsilon\,\gamma^2)\gamma_5\psi_f(x)(\mathcal{CR}_1)^\dagger\mathcal{CR}_1|\pi^0(\vec{p})\rangle \\ &= \langle 0|\mathcal{C}^\dagger\mathcal{C}\bar{\psi}_f(x')(\gamma^1 - i\epsilon\,\gamma^2)\gamma_5\psi_f(x')\mathcal{C}^\dagger\mathcal{C}|\pi^0(\vec{p}\,')\rangle \\ &= \langle 0|\bar{\psi}_f(x')(\gamma^1 - i\epsilon\,\gamma^2)\gamma_5\psi_f(x')|\pi^0(\vec{p}\,')\rangle = H_{\perp,A}^{0,-\epsilon}(x',\vec{p}\,')\,, \end{aligned} \tag{B.4}$$

where $x'^\mu = (x^0, x^1, -x^2, -x^3)$ and $\vec{p}\,' = (p^1, -p^2, -p^3)$. From Eqs. (3.43) and (3.44), this hadronic amplitude reads

$$H_{\perp,A}^{0,\,\epsilon}(x,\vec{p}) \;=\; -i\left[f_{\pi^0}^{(A1)} - \epsilon f_{\pi^0}^{(A2)} - f_{\pi^0}^{(A3)}\right](p^1 + i\epsilon\,p^2)\,e^{-ip\cdot x}\,. \tag{B.5}$$

Therefore Eq. (B.4) leads to

$$\begin{aligned} -\,i\left[f_{\pi^0}^{(A1)} - \epsilon\,f_{\pi^0}^{(A2)} - f_{\pi^0}^{(A3)}\right](p^1 + i\epsilon\,p^2)\,e^{-ip\cdot x} \;=& \\ -\,i\left[f_{\pi^0}^{(A1)} + \epsilon\,f_{\pi^0}^{(A2)} - f_{\pi^0}^{(A3)}\right](p'^1 - i\epsilon\,p'^2)\,e^{-ip'\cdot x'}\,, & \end{aligned} \tag{B.6}$$

which implies $f_{\pi^0}^{(A2)} = 0$.

We consider next matrix elements with charged pion initial states. Proceeding in a

similar way as in the neutral case, from Eq. (3.47) we get

$$\begin{aligned} H_V^{\sigma,\mu}(x,\breve{p}) &= \langle 0|(\mathcal{CT})^\dagger \mathcal{CT}\,\bar{\psi}(x)\gamma^\mu \tau^{-\sigma}\psi(x)\,(\mathcal{CT})^\dagger \mathcal{CT}|\pi^\sigma(\breve{p})\rangle \\ &= -\,\langle 0|\mathcal{C}^\dagger\mathcal{C}\,\bar{\psi}(-\tilde{x})\gamma_\mu \tau^{-\sigma}\psi(-\tilde{x})\,\mathcal{C}^\dagger\mathcal{C}|\pi^\sigma(\breve{p}\,')\rangle^* \\ &= \langle 0|\bar{\psi}(-\tilde{x})\gamma_\mu \tau^{\sigma}\psi(-\tilde{x})|\pi^{-\sigma}(\breve{p}\,')\rangle^* = g_{\mu\nu}\, H_V^{-\sigma,\nu}(-\tilde{x},\breve{p}\,')^* \,, \end{aligned} \tag{B.7}$$

where we have used $\mathcal{C}|\pi^\pm(\breve{p})\rangle = |\pi^\mp(\breve{p})\rangle$ and defined $\breve{p}\,' = (\ell, -p^2, -p^3)$. Since $\mathcal{B}^\sigma_{\bar{p}}(x) = \mathcal{B}^{-\sigma}_{\bar{p}'}(-\tilde{x})^*$ for $\bar{p}\,' = (E_{\pi^-}, \breve{p}\,')$, taking $\mu = 0$ and $\sigma = -$ one obtains [see Eq. (3.48)]

$$-if^{(V)}_{\pi^-}\, p^3\, \mathcal{B}^-_{\bar{p}}(x) \;=\; \left[-if^{(V)}_{\pi^+}\, p'^3\, \mathcal{B}^+_{\bar{p}'}(-\tilde{x})\right]^* \;=\; -i\, f^{(V)\,*}_{\pi^+}\, p^3\, \mathcal{B}^-_{\bar{p}}(x)\;, \tag{B.8}$$

which leads to $f^{(V)\,*}_{\pi^+} = f^{(V)}_{\pi^-}$. Now, from the invariance of the action under $\mathcal{CR}_1$ one has

$$\begin{aligned} H_V^{\sigma,0}(x,\breve{p}) &= \langle 0|(\mathcal{CR}_1)^\dagger \mathcal{CR}_1 \bar{\psi}(x)\gamma^0 \tau^{-\sigma}\psi(x)(\mathcal{CR}_1)^\dagger \mathcal{CR}_1|\pi^\sigma(\breve{p})\rangle \\ &= \langle 0|\mathcal{C}^\dagger\mathcal{C}\bar{\psi}(x')\gamma^0 \tau^{-\sigma}\psi(x')\mathcal{C}^\dagger\mathcal{C}|\pi^\sigma(\breve{p}\,')\rangle \\ &= -\,\langle 0|\bar{\psi}(x')\gamma^0\tau^\sigma\psi(x')|\pi^{-\sigma}(\breve{p}\,')\rangle \;=\; -H_V^{-\sigma,0}(x',\breve{p}\,')\,. \end{aligned} \tag{B.9}$$

Since $\mathcal{B}^\sigma_{\bar{p}}(x) = \mathcal{B}^{-\sigma}_{\bar{p}'}(x')$, taking $\sigma = -$ one obtains $f^{(V)}_{\pi^-} = f^{(V)}_{\pi^+}$ and then $\mathrm{Im}\left(f^{(V)}_{\pi^\sigma}\right) = 0$.

For the matrix elements of the axial-vector current, the analysis of the zeroth and third components of the pion-to-vacuum amplitude leads to $f^{(A1)}_{\pi^-} = f^{(A1)}_{\pi^+}$ and $\mathrm{Im}\left(f^{(A1)}_{\pi^\sigma}\right) = 0$. To constrain the form factors $f^{(A2)}_{\pi^\sigma}$ and $f^{(A3)}_{\pi^\sigma}$ one needs to study the first and second components. Taking into account the invariance under $\mathcal{CT}$ one has ($\epsilon = \pm$)

$$\begin{aligned} H^{\sigma,\epsilon}_{\perp,A}(x,\breve{p}) &= \langle 0|(\mathcal{CT})^\dagger \mathcal{CT}\,\bar{\psi}(x)(\gamma^1 + i\epsilon\gamma^2)\gamma_5 \tau^{-\sigma}\psi(x)\,(\mathcal{CT})^\dagger \mathcal{CT}|\pi^\sigma(\breve{p})\rangle \\ &= -\,\langle 0|\mathcal{C}^\dagger\mathcal{C}\,\bar{\psi}(-\tilde{x})(\gamma_1 - i\epsilon\gamma_2)\gamma_5 \tau^{-\sigma}\psi(-\tilde{x})\,\mathcal{C}^\dagger\mathcal{C}|\pi^\sigma(\breve{p}\,')\rangle^* \\ &= +\,\langle 0|\bar{\psi}(-\tilde{x})(\gamma^1 - i\epsilon\gamma^2)\gamma_5 \tau^{\sigma}\psi(-\tilde{x})|\pi^{-\sigma}(\breve{p}\,')\rangle^* \\ &= \left[H_A^{-\sigma,1}(-\tilde{x},\bar{p}\,') - i\epsilon\, H_A^{-\sigma,2}(-\tilde{x},\breve{p}\,')\right]^* \;=\; \left[H_{\perp,A}^{-\sigma,-\epsilon}(-\tilde{x},\breve{p}\,')\right]^*\,. \end{aligned} \tag{B.10}$$

In this way, taking $\sigma = -$ in Eqs. (3.48) and (B.10) one obtains

$$\left[f^{(A1)}_{\pi^-} + \epsilon f^{(A2)}_{\pi^-} - f^{(A3)}_{\pi^-}\right]\, \mathcal{B}^-_{\bar{p}+\epsilon}(x) \;=\; \left[f^{(A1)}_{\pi^+} + \epsilon f^{(A2)}_{\pi^+} - f^{(A3)}_{\pi^+}\right]^*\, \mathcal{B}^+_{\bar{p}'+\epsilon}(-\tilde{x})^*\,, \tag{B.11}$$

which implies $f^{(A2)}_{\pi^-} = f^{(A2)\,*}_{\pi^+}$ and $f^{(A3)}_{\pi^-} = f^{(A3)\,*}_{\pi^+}$ (we have used the fact that $f^{(A1)}_{\pi^-} = f^{(A1)\,*}_{\pi^+}$).

Finally, considering $\mathcal{CR}_1$ transformations, one has

$$\begin{aligned} H^{\sigma,\epsilon}_{\perp,A}(x,\breve{p}) &= \langle 0|(\mathcal{CR}_1)^\dagger \mathcal{CR}_1\, \bar{\psi}(x)(\gamma^1 + i\epsilon\gamma^2)\gamma_5\tau^{-\sigma}\psi(x)\,(\mathcal{CR}_1)^\dagger \mathcal{CR}_1|\pi^\sigma(\breve{p})\rangle \\ &= \langle 0|\mathcal{C}^\dagger\mathcal{C}\,\bar{\psi}(x')(\gamma^1 - i\epsilon\gamma^2)\gamma_5\tau^{-\sigma}\psi(x')\,\mathcal{C}^\dagger\mathcal{C}|\pi^\sigma(\breve{p}\,')\rangle \\ &= \langle 0|\bar{\psi}(x')(\gamma^1 - i\epsilon\gamma^2)\gamma_5\tau^{\sigma}\psi(x')|\pi^{-\sigma}(\breve{p}\,')\rangle \\ &= H^{-\sigma,1}_A(x',\breve{p}\,') - i\,\epsilon H^{-\sigma,2}_A(x',\breve{p}\,') = H^{-\sigma,-\epsilon}_{\perp,A}(x',\breve{p}\,')\,, \end{aligned} \tag{B.12}$$

which leads to $f^{(A2)}_{\pi^-} = f^{(A2)}_{\pi^+}$ and $f^{(A3)}_{\pi^-} = f^{(A3)}_{\pi^+}$, together with $\mathrm{Im}\Big(f^{(A2)}_{\pi^\sigma}\Big) = \mathrm{Im}\Big(f^{(A3)}_{\pi^\sigma}\Big) = 0$.

The calculation done in this Appendix was carried out in the Landau gauge. However, taking into account the gauge invariance of the form factors, the same conclusions applied for the symmetric gauge.

APPENDIX C

Flavor polarization functions

C.1 Vacuum polarization function

The functions $c^{\rm vac}_{ff'}$ appear in Eqs. (5.27) and (5.41). In their unregularized form they are defined by the $B = 0$ contribution

$$c^0_{ff'}(p^2) \;=\; 2N_c \int_q \mathrm{Tr}_{\rm D}\left[\bar{\mathcal{S}}^{f,0}(q_-)\,\gamma_5\,\bar{\mathcal{S}}^{f',0}(q_+)\,\gamma_5\right] , \tag{C.1}$$

where $\bar{\mathcal{S}}^{f,0}(q) = (\not{q} + M_f)^{-1}$ is the usual vacuum propagator for a quark of mass M_f and $q_\pm = q \pm p/2$. We recall that all four-momenta are defined in Euclidean space. By taking the trace and integrating over q one obtains

$$c^0_{ff'}(p^2) \;=\; \frac{N_c}{2\pi^2}\int_0^\infty dz \int_0^1 dy\; e^{-z\left[yM_f^2+(1-y)M_{f'}^2+y(1-y)p^2-i\epsilon\right]}\,\frac{1}{z}\left[M_f M_{f'} + \frac{2}{z} - y(1-y)p^2\right] . \tag{C.2}$$

We have expressed this function in the proper time formalism. Through some algebraic manipulation, it can also be written in the following standard form

$$c^0_{ff'}(p^2) \;=\; 2N_c\left\{\frac{I^0_{1f}+I^0_{1f'}}{2} + \left[p^2 + (M_f - M_{f'})^2\right] I^0_{2ff'}(p^2)\right\} , \tag{C.3}$$

where the integrals I^0_{1f} and $I^0_{2ff'}$ are defined by

$$\begin{aligned} I^0_{1f} &= 4\int_q \frac{1}{q^2+M_f^2}\,, \\ I^0_{2ff'}(p^2) &= -2\int_q \frac{1}{(q_-^2+M_f^2-i\epsilon)(q_+^2+M_{f'}^2-i\epsilon)}\,. \end{aligned} \tag{C.4}$$

In order to regularize the vacuum loop integrals we introduce a 3D cutoff Λ. For I^0_{1f} one gets the regularized function of Eq. (2.52) by replacing $M \to M_f$. For $I^0_{2ff'}(p^2)$ we note that in order to determine meson masses, the external momenta p in the loop integrals has to be extended to the region $p^2 < 0$. Hence, we find it convenient to introduce $p^2 = -p_m^2$, with $p_m > 0$. In this case the function has several poles. To treat them, we go from Euclidean to the original Minkowski space by taking $q_4 = -iq_0$ for the quarks momenta. Then, by choosing appropriate contours the q_0 integral can be calculated in the complex plane to yield

$$I^{\rm vac}_{2ff'}(p^2) = -\frac{1}{8\pi^2 p_m^2}\int_0^\Lambda dq\,\frac{q^2}{q^2-r-i\epsilon}\left[\frac{p_m^2+M_f^2-M_{f'}^2}{\sqrt{q^2+M_f^2}}+\frac{p_m^2-M_f^2+M_{f'}^2}{\sqrt{q^2+M_{f'}^2}}\right], \tag{C.5}$$

where

$$r = \frac{1}{4p_m^2}\left[(M_f-M_{f'})^2-p_m^2\right]\left[(M_f+M_{f'})^2-p_m^2\right]. \tag{C.6}$$

When $M_f = M_{f'}$ and $p_m < 2M_f$, this expression can be brought to the usual form of $I_2^{\rm vac}(p^2)$ in Eq. (2.53). In the general case, depending on the value of p_m this expression may still have a pole in a point of the integration line if $r > 0$. For those regions of p_m where a pole exists, we proceed by employing a generalized version of the Sokhotski-Plemelj formula. Assuming there exists a function $f(x)$ that has single poles at a set of values x_j, for which exist two other functions $g(x)$ and $h(x)$ such that $g(x_j) \neq 0$ and $h(x_j) \neq 0$, then

$$\lim_{\epsilon\to 0^+}\int_a^b dx\,\frac{h(x)}{f(x)+i\epsilon g(x)} = {\rm PV}\int_a^b dx\,\frac{h(x)}{f(x)} - i\pi\sum_j \frac{h(x_j)}{|f'(x_j)|}\,{\rm sign}[g(x_j)]\,, \tag{C.7}$$

where PV denotes the Cauchy principal value of the integral. By using this property we can fully calculate the complex function $I^{\rm vac}_{2ff'}$ in the most general case. For the regularized

real part we get

$$\mathrm{Re}\left[I^{\mathrm{vac}}_{2ff'}(-p_m^2)\right] = -\frac{1}{8\pi^2 p_m^2}\Bigg\{(p_m^2+M_f^2-M_{f'}^2)\left[\mathrm{arcsinh}\left(\frac{\Lambda}{M_f}\right)-F_f\right]+ (p_m^2-M_f^2+M_{f'}^2)\left[\mathrm{arcsinh}\left(\frac{\Lambda}{M_{f'}}\right)-F_{f'}\right]\Bigg\}, \tag{C.8}$$

where

$$F_f = \begin{cases} \dfrac{y_+}{\sqrt{M_f^2+y_+^2}}\,\mathrm{arctanh}\left(\dfrac{\Lambda}{y_+}\sqrt{\dfrac{M_f^2+y_+^2}{M_f^2+\Lambda^2}}\right) & \text{for } p_m < p_m^{(0)} \text{ or } p_m > p_m^{(3)} \\ \dfrac{y_+}{\sqrt{M_f^2+y_+^2}}\,\mathrm{arccoth}\left(\dfrac{\Lambda}{y_+}\sqrt{\dfrac{M_f^2+y_+^2}{M_f^2+\Lambda^2}}\right) & \text{for } p_m^{\binom{0}{2}} < p_m < p_m^{\binom{1}{3}} \\ \dfrac{y_-}{\sqrt{M_f^2-y_-^2}}\,\arctan\left(\dfrac{\Lambda}{y_-}\sqrt{\dfrac{M_f^2-y_-^2}{M_f^2+\Lambda^2}}\right) & \text{for } p_m^{(1)} < p_m < p_m^{(2)} \end{cases}. \tag{C.9}$$

Here $y_\pm = \sqrt{\pm r}$, with r defined in Eq. (C.6), and

$$p_m^{\binom{0}{3}} = \left[M_f^2+M_{f'}^2+2\Lambda^2 \mp 2\sqrt{(\Lambda^2+M_f^2)(\Lambda^2+M_{f'}^2)}\right]^{1/2}, \qquad p_m^{\binom{1}{2}} = |M_f \mp M_{f'}|. \tag{C.10}$$

For the regularized imaginary part we get

$$\mathrm{Im}\left[I^{\mathrm{vac}}_{2ff'}(-p_m^2)\right] = \begin{cases} -\dfrac{y_+}{4\pi p_m} & \text{for } p_m^{(2)} < p_m < p_m^{(3)} \\ 0 & \text{otherwise} \end{cases}. \tag{C.11}$$

Putting all together, the regularized version of the vacuum $c^0_{ff'}$ function defined in Eq. (C.3) is given by

$$c^{\mathrm{vac}}_{ff'}(p^2=-p_m^2) = 2N_c\left\{\frac{I^{\mathrm{vac}}_{1f}+I^{\mathrm{vac}}_{1f'}}{2}-\left[p_m^2-(M_f-M_{f'})^2\right]I^{\mathrm{vac}}_{2ff'}(-p_m^2)\right\}. \tag{C.12}$$

C.2 Neutral magnetic polarization function

The unregularized magnetic function $c^{\mathrm{mag}}_{ff'}(p_\perp^2, p_\parallel^2)$ was defined for the neutral case in (5.26). The $B \to 0$ limit of this expression $c^0_{ff'}$ is given by Eq. (C.2). Then, the finite magnetic

contribution is defined within the MFIR scheme as the difference

$$\begin{aligned} c^{\rm mag}_{ff'}(p_\perp^2,p_\parallel^2) &= c_{ff'}(p_\perp^2,p_\parallel^2) - c^0_{ff'}(p^2) \\ &= \frac{N_c}{2\pi^2}\int_0^\infty dz \int_0^1 dy\, e^{-z\left[yM_f^2+(1-y)M_{f'}^2+y(1-y)p_\parallel^2-i\epsilon\right]} \times \\ &\quad \left\{ \left[M_f M_{f'} + \frac{1}{z} - y(1-y)p_\parallel^2\right] \left[\frac{B_f\, e^{-\gamma_f(y,z)\frac{p_\perp^2}{B_f}}}{\tanh(zB_f)} - \frac{e^{-zy(1-y)p_\perp^2}}{z}\right] + \right. \\ &\quad \frac{B_f^2\, e^{-\gamma_f(y,z)\frac{p_\perp^2}{B_f}}}{\sinh^2(zB_f)}\left[1-\gamma_f(y,z)\,\frac{p_\perp^2}{B_f}\right] - \\ &\quad \left. \frac{e^{-zy(1-y)p_\perp^2}}{z^2}\left[1-zy(1-y)p_\perp^2\right]\right\}, \end{aligned} \tag{C.13}$$

where $\gamma_f(y,z)$ is given in Eq. (4.28). Pole masses are calculated in the rest frame of the meson, i.e. setting $p_\mu = im_P\delta_{\mu,4}$, with $m_P > 0$. Assuming that $m_P < M_f + M_{f'}$, one can integrate by parts to write this function in the form

$$c^{\rm mag}_{ff'}(0,-m_P^2) = 2N_c\left\{\frac{I^{\rm mag}_{1f}+I^{\rm mag}_{1f'}}{2} - \left[m_P^2-(M_f-M_{f'})^2\right] I^{\rm mag}_{2ff'}(-m_P^2)\right\}, \tag{C.14}$$

where $I^{\rm mag}_{1f}$ is defined in Eq. (2.79). On the other hand, $I^{\rm mag}_{2ff'}$ is given by

$$I^{\rm mag}_{2ff'}(-m_P^2) = -\frac{1}{8\pi^2}\int_0^1 dy \int_0^\infty dz\, e^{-2z(\bar{x}_{ff'}-i\epsilon)}\left(\coth z - \frac{1}{z}\right) \tag{C.15}$$

with

$$x_{ff'} = \frac{yM_f^2+(1-y)M_{f'}^2-y(1-y)m_P^2}{2B_f}. \tag{C.16}$$

When $m_P < M_f + M_{f'}$ we always have that $x_{ff'} > 0$. In that case, the function $I^{\rm mag}_{2ff'}$ as given in Eq. (C.15) is well-defined and can alternatively written as

$$I^{\rm mag}_{2ff'}(-m_P^2) = \frac{1}{8\pi^2}\int_0^1 dy\left[\psi(\bar{x}_{ff'}-i\epsilon) - \ln(\bar{x}_{ff'}-i\epsilon) + \frac{1}{2(\bar{x}_{ff'}-i\epsilon)}\right], \tag{C.17}$$

where $\psi(x)$ is the digamma function. Note that in this case one can safely take the $\epsilon \to 0$ limit, recovering expression (4.34) in the $M_f = M_{f'}$ case.

On the other hand, if $m_P > M_f + M_{f'}$ then $\bar{x}_{ff'}$ can be negative in the integration domain. In this case, the integral in Eq. (C.15) is not convergent. However, one can still proceed by considering the analytic extension of the form given in Eq. (C.17). Since $\bar{x}_{ff'}$

is a positive quadratic function of y, it is immediate to see that $\psi(\bar{x}_{ff'})$ has $N+1$ poles, where

$$N \;=\; \text{Floor}\left\{\frac{1}{2B_f}\left[1-\left(\frac{M_f-M_{f'}}{m_P}\right)^2\right]\left[\frac{m_P^2}{4}-\left(\frac{M_f+M_{f'}}{2}\right)^2\right]\right\}. \tag{C.18}$$

To proceed we first isolate the poles by using the digamma recurrence relation

$$\psi(\bar{x}_{ff'}-i\epsilon) \;=\; \psi(\bar{x}_{ff'}+N+1)-\sum_{n=0}^{N}\frac{1}{\bar{x}_{ff'}+n-i\epsilon}\,. \tag{C.19}$$

Expressed this way, the first term in the right-hand side is pole-free. Then

$$I^{\text{mag}}_{2ff'}(-m_P^2) \;=\; \frac{1}{8\pi^2}\int_0^1 dy\left[\psi(\bar{x}_{ff'}+N+1)-\ln(\bar{x}_{ff'}-i\epsilon)-\frac{1}{2}\sum_{n=0}^{N}\frac{g_n}{\bar{x}_{ff'}+n-i\epsilon}\right], \tag{C.20}$$

where $g_n = 2-\delta_{n,0}$. The complex logarithm is defined by taking the principal branch. For the region where $\bar{x}_{ff'}<0$ we have

$$\lim_{\epsilon\to 0}\ln(-|\bar{x}_{ff'}|-i\epsilon) \;=\; \ln(|\bar{x}_{ff'}|)-i\pi\,. \tag{C.21}$$

Lastly, the third term on the right-hand side of Eq. (C.20) contains two simple poles, which once again can be handled using the generalization of the Sokhotski-Plemelj formula presented in Eq. (C.7). After some algebra we finally obtain that for $m_P > M_f + M_{f'}$

$$\begin{aligned} I^{\text{mag}}_{2ff'}(p_\parallel^2=-m_P^2) \;=\; &-\frac{1}{8\pi^2}\Bigg\{\ln\left[\frac{(M_f)^{1-\alpha}\,(M_{f'})^{1+\alpha}}{2B_f}\right]+\frac{\beta_0}{2}\ln\left[\frac{\alpha^2-(1+\beta_0)^2}{\alpha^2-(1-\beta_0)^2}\right] \\ &\qquad -2+\frac{B_f}{m_P^2}\sum_{n=0}^{N}\frac{g_n}{\beta_n}\ln\left[\frac{\alpha^2-(1-\beta_n)^2}{\alpha^2-(1+\beta_n)^2}\right]\Bigg\} \\ &+\frac{1}{8\pi^2}\int_0^1 dy\;\psi(\bar{x}_{ff'}+N+1)+\frac{i}{8\pi}\left(\beta_0-\frac{2B_f}{m_P^2}\sum_{n=0}^{N}\frac{g_n}{\beta_n}\right), \end{aligned} \tag{C.22}$$

with

$$\alpha=\frac{M_{f'}^2-M_f^2}{m_P^2}\,,\qquad \beta_n=\sqrt{\left[1-\left(\frac{M_{f'}-M_f}{m_P}\right)^2\right]\left[1-\left(\frac{M_{f'}+M_f}{m_P}\right)^2\right]-\frac{8nB_f}{m_P^2}}\,. \tag{C.23}$$

We remark that the calculation of $I^{\text{mag}}_{2ff'}$ was performed here within the proper time formalism, which is well-defined for $m_P < M_f + M_{f'}$ and leads to Eq. (C.17). For $m_P > M_f + M_{f'}$ we have taken the analytic continuation of this equation. As a consistency

check, we have repeated the calculation using the Landau level representation for the quark propagator in Minkowski space, which is well-defined for all m_P, obtaining the same final result of Eq. (C.22).

APPENDIX D

Diagonalization and $B = 0$ expansion for nucleons

D.1 Diagonalization of $\mathbb{D}^{(\mathtt{p})}_{\bar{P},\bar{P}'}$ in Ritus space

In this section of the appendix we briefly sketch how to prove that the Dirac operator $\mathbb{D}^{(\mathtt{p})}_{\bar{P},\bar{P}'}$ in Eq. (6.41) is diagonal. Let us start by taking into account the integral $I^{\lambda,\lambda'}_{\bar{P},\bar{P}'}(p,r)$ in Eq. (6.43). Denoting $w = x_1 - z_1$ and integrating over the remaining space variables, it can be show that

$$I^{\lambda,\lambda'}_{\bar{P},\bar{P}'}(p,r) \;=\; (2\pi)^6\,\delta^{(2)}(P_{\parallel} - P'_{\parallel})\,\delta(P_2 - P'_2)\,\delta^{(2)}(p_{\parallel} + r_{\parallel} - P_{\parallel})\,G_{n_\lambda,n'_{\lambda'}}(p_\perp + r_\perp)\,, \tag{D.1}$$

where

$$\begin{aligned} G_{n_\lambda,n'_{\lambda'}}(p_\perp + r_\perp) \;=\; & \frac{(-1)^{n_\lambda + n'_{\lambda'}}}{B_{\mathtt{p}}}\,N_{n_\lambda}\,N_{n'_{\lambda'}}\int_0^\infty dw\; e^{i(p_1+r_1)w}\;\times \\ & D_{n_\lambda}\left(s_{\mathtt{p}}\sqrt{\frac{2}{B_{\mathtt{p}}}}\,(p_2+r_2) - \sqrt{\frac{B_{\mathtt{p}}}{2}}\,w\right)\;\times \\ & D_{n'_{\lambda'}}\left(s_{\mathtt{p}}\sqrt{\frac{2}{B_{\mathtt{p}}}}\,(p_2+r_2) + \sqrt{\frac{B_{\mathtt{p}}}{2}}\,w\right)\,. \end{aligned} \tag{D.2}$$

The integral over w can be carried out using the property of Eq. (4.40) for the cylindrical parabolic functions. Assuming that $n_{\lambda'} \geq n_\lambda$ (the analysis is similar for the other case),

one has

$$G_{n_\lambda,n'_{\lambda'}}(p_\perp + r_\perp) \;=\; (-)^{n'_{\lambda'}}\,\frac{4\pi}{B_\mathtt{p}}\,\sqrt{\frac{n_\lambda!}{n'_{\lambda'}!}}\;e^{-\frac{(p_\perp+r_\perp)^2}{B_\mathtt{p}}}\;\left[\frac{i(p_1+r_1)+s_\mathtt{p}(p_2+r_2)}{\sqrt{B_\mathtt{p}/2}}\right]^{n'_{\lambda'}-n_\lambda}\;\times$$
$$L_{n_\lambda}^{n'_{\lambda'}-n_\lambda}\left(\frac{2(p_\perp+r_\perp)^2}{B_\mathtt{p}}\right)\,. \tag{D.3}$$

We now use this result to carry out the integral over perpendicular momenta in Eq. (6.41), which can be defined as

$$I_\perp \;=\; \int_{p_\perp\,r_\perp}\,\sum_{\lambda,\lambda'}\,G_{n_\lambda,n'_{\lambda'}}(p_\perp+r_\perp)\,\tilde{\mathcal{G}}_\Delta(p_\perp,p_\parallel)\,\Delta_\lambda\,\mathcal{S}^u(r_\perp,P_\parallel-p_\parallel)\,\Delta_{\lambda'}\,. \tag{D.4}$$

Using the form of the quark propagator in Eq. (2.67), it can be seen that the product $\Delta_\lambda\,\mathcal{S}^u(r_\perp,P_\parallel-p_\parallel)\,\Delta_{\lambda'}$ can be written as

$$\Delta_\lambda\,\mathcal{S}^u(r_\perp,P_\parallel-p_\parallel)\,\Delta_{\lambda'} \;=\; \mathcal{A}(r_\perp,P_\parallel-p_\parallel)\,\delta_{\lambda,\lambda'}\,\Delta_\lambda \;+\; \mathcal{B}(r_\perp,P_\parallel-p_\parallel)\,r_\perp\cdot\gamma_\perp\,\delta_{-\lambda,\lambda'}\,\Delta_{-\lambda}\,, \tag{D.5}$$

where $\mathcal{A}(r_\perp,P_\parallel-p_\parallel)$ and $\mathcal{B}(r_\perp,P_\parallel-p_\parallel)$ are functions of $r_\perp^2$. Then we get

$$I_\perp \;=\; \int_{p_\perp\,r_\perp}\,\tilde{\mathcal{G}}_\Delta(p_\perp,p_\parallel)\,\sum_\lambda\,\Big[G_{n_\lambda,n'_\lambda}(p_\perp+r_\perp)\,\mathcal{A}(r_\perp,P_\parallel-p_\parallel)\,\Delta_\lambda\,+$$
$$G_{n_\lambda,n'_{-\lambda}}(p_\perp+r_\perp)\,\mathcal{B}(r_\perp,P_\parallel-p_\parallel)\,(r_1-i\lambda\,r_2)\gamma_\lambda\,\Delta_{-\lambda}\Big]\,, \tag{D.6}$$

where $\gamma_\lambda=(\gamma_1+i\lambda\gamma_2)/2$. To carry out the angular integrals in Eq. (D.6) it is convenient to use polar coordinates, namely $p_\perp=(\tilde{p}_\perp\cos\theta,\tilde{p}_\perp\sin\theta)$ and $r_\perp=(\tilde{r}_\perp\cos\varphi,\tilde{r}_\perp\sin\varphi)$. Noticing that the diquark propagator depends only on the squared momenta $p_\parallel^2$ and $p_\perp^2$ [see Eq. (6.27)], from Eq. (D.3) we get

$$I_\perp \;=\; \int_0^\infty\frac{\tilde{p}_\perp\,d\tilde{p}_\perp}{(2\pi)^2}\int_0^\infty\frac{\tilde{r}_\perp\,d\tilde{r}_\perp}{(2\pi)^2}\;\tilde{\mathcal{G}}_\Delta(\tilde{p}_\perp,p_\parallel)\;\times$$
$$\sum_\lambda\,\Big[\mathcal{A}(\tilde{r}_\perp,P_\parallel-p_\parallel)\,\Delta_\lambda\int_0^{2\pi}d\varphi\,e^{-is_\mathtt{p}(n'_\lambda-n_\lambda)\varphi}\int_0^{2\pi}d\theta\,F_{n_\lambda,n'_\lambda}(\tilde{p}_\perp,\tilde{r}_\perp,\theta-\varphi)\,+$$
$$\tilde{r}_\perp\,\mathcal{B}(\tilde{r}_\perp,P_\parallel-p_\parallel)\,\gamma_\lambda\,\Delta_{-\lambda}\int_0^{2\pi}d\varphi\,e^{-i[s_\mathtt{p}(n'_{-\lambda}-n_\lambda)+\lambda]\varphi}\int_0^{2\pi}d\theta\,F_{n_\lambda,n'_{-\lambda}}(\tilde{p}_\perp,\tilde{r}_\perp,\theta-\varphi)\Big]\,, \tag{D.7}$$

where $F_{n_\lambda,n'_{\lambda'}}$ is a function that depends on $\theta-\varphi$ only through periodic functions $\sin(\theta-\varphi)$,

$\cos(\theta - \varphi)$. Taking into account that

$$n'_\lambda - n_\lambda \;=\; n' - n \;, \qquad\qquad s_{\mathtt{p}}(n'_{-\lambda} - n_\lambda) + \lambda \;=\; s_{\mathtt{p}}(n' - n) \;, \tag{D.8}$$

and using the periodicity of the function $F_{n_\lambda, n'_{\lambda'}}$, it is seen that

$$\int_0^{2\pi} d\varphi \, e^{-i s_{\mathtt{p}}(n'-n)} \;=\; 2\pi \, \delta_{n,n'} \;, \tag{D.9}$$

and therefore $I_\perp \propto 2\pi \, \delta_{n,n'}$. Together with the result of Eq. (D.1), this shows that $\mathbb{D}^{(\mathtt{p})}_{\bar{P},\bar{P}'}$ is proportional to $\hat{\delta}_{\bar{P},\bar{P}'}$.

D.2 Expansion around $B = 0$

In this section of the appendix we provide some hints for the expansions of the coefficients $\hat{X}^\nu_\pm$ and $\hat{Y}^\nu_\pm$ in Eq. (6.53) around $B = 0$. These expansions allow us to obtain the expressions for $\hat{X}$ and $\hat{Y}$ in Eqs. (6.54 - 6.55), as well as the slopes $\alpha_{\mathtt{N}}$ in Eq. (6.60).

The coefficients $\hat{X}^\nu_\pm$ and $\hat{Y}^\nu_\pm$ depend on B both explicitly and implicitly, through $\mathcal{M}_{\mathtt{N}}$ and M. In fact, it can be seen that $dM/dB|_{B=0} = 0$, hence the effective quark mass M can be taken as a constant at the lowest order in an expansion in powers of $|B|$. In this way, from Eq. (6.53) the slopes $d\mathcal{M}_{\mathtt{N}}/d|B|$ at $B = 0$ are given by

$$\alpha_{\mathtt{N}} \;=\; \frac{\dfrac{\partial \hat{X}^\nu_\lambda}{\partial |B|}\Big|_{B=0} - m_{\mathtt{N}} \, \dfrac{\partial \hat{Y}^\nu_\lambda}{\partial |B|}\Big|_{B=0}}{\hat{Y} - \dfrac{\partial \hat{X}}{\partial m_{\mathtt{N}}} + m_{\mathtt{N}} \, \dfrac{\partial \hat{Y}}{\partial m_{\mathtt{N}}}} \;, \tag{D.10}$$

where appropriate values of λ should be taken for $N = \mathtt{p}$ and $N = \mathtt{n}$ (see discussion in the main text).

In particular, the partial derivatives in the numerator of the rhs of Eq. (D.10) have to be calculated with some care due to the sums over Landau levels in Eqs. (6.57) and (6.58). As an example, let us consider the expression for $\hat{X}^{(\mathtt{p})}_{s_{\mathtt{p}}}$ in Eq. (6.57). The factors that

depend explicitly on the magnetic field can be expanded as

$$\mathcal{G}_\Delta^{\rm reg}(\ell, p_\parallel^2) \;=\; \mathcal{G}_\Delta^{\rm vac}(p_\parallel^2 + 2\ell B_\Delta) \;+ \left.\frac{d\mathcal{G}_\Delta^{\rm vac}(p^2)}{dp^2}\right|_{p^2 = p_\parallel^2 + 2\ell B_\Delta} B_\Delta + \mathcal{O}(B^2, \ell B^3)\,,$$

$$\frac{B_u\,(1+t_u)}{B_u + (B_{\rm p} + B_\Delta)\,t_u} \;=\; 1 + \frac{\tau}{\Lambda_B^2}\,(B_u - B_{\rm p} - B_\Delta) \;+ \mathcal{O}(B^2)\,,$$

$$B_\Delta \left[\frac{B_u + (B_{\rm p} - B_\Delta)t_u}{B_u + (B_{\rm p} + B_\Delta)t_u}\right]^\ell \;=\; B_\Delta\; e^{-\frac{2\tau\ell B_\Delta}{\Lambda_B^2}} \left[1 + \frac{2\tau^2 \ell B_\Delta B_{\rm p}}{\Lambda_B^4} + \mathcal{O}(B^2, \ell B^3)\right]. \tag{D.11}$$

For the evaluation of the sum over Landau levels in the limit of low magnetic field, one can use the relation

$$B\sum_{\ell=0}^{\infty} e^{-\alpha\,\ell B}\,F(\ell B) \;=\; \int_0^\infty dx\; e^{-\alpha\,x}\;F(x) + \frac{1}{2}\,F(0)\,B + \mathcal{O}(B^2)\,, \tag{D.12}$$

which is valid for $\alpha > 0$ if the function $F(x)$ allows a Taylor expansion around $x = 0$ and is well behaved at $x \to \infty$. In this way, after an integration by parts one arrives at

$$B_\Delta\,\frac{B_u\,(1+t_u)}{B_u + (B_{\rm p} + B_\Delta)}\sum_{\ell\,=\,0}^{\infty}\left[\frac{B_u + (B_{\rm p} - B_\Delta)t_u}{B_u + (B_{\rm p} + B_\Delta)t_u}\right]^\ell \mathcal{G}_\Delta^{\rm reg}(\ell, p_\parallel^2) \;=$$

$$\frac{1}{2}\int_0^\infty d\omega\, e^{-\tau\,\frac{\omega}{\Lambda_B^2}}\,\mathcal{G}_\Delta^{\rm vac}(p_\parallel^2 + \omega)\left[1 + \frac{\tau}{\Lambda_B^2}\,(B_u - B_{\rm p}) + \frac{\omega\,\tau^2\,B_{\rm p}}{\Lambda_B^4} + \mathcal{O}(B^2)\right]. \tag{D.13}$$

The variable ω can be identified with $p_\perp^2$ in the $B \to 0$ limit. In addition, with the aid of some properties of the Bessel functions one can prove the relations

$$\int_0^\infty d\tilde{p}_{\parallel} \int_0^\infty d\tilde{p}_\perp\, J_0(\alpha\,\tilde{p}_{\parallel})\,f(\tilde{p}_{\parallel}^2 + \tilde{p}_\perp^2) \;=\; \frac{4}{\alpha}\int_0^\infty d\tilde{p}_\perp\,\tilde{p}_\perp^2\,J_1(\alpha\,\tilde{p}_\perp)\,f(\tilde{p}_\perp^2)\,,$$

$$\int_0^\infty d\tilde{p}_{\parallel} \int_0^\infty d\tilde{p}_\perp\,\tilde{p}_\perp^2\,J_0(\alpha\,\tilde{p}_{\parallel})\,f(\tilde{p}_{\parallel}^2 + \tilde{p}_\perp^2) \;=\; \frac{8}{\alpha^2}\int_0^\infty d\tilde{p}_\perp\,\tilde{p}_\perp^3\,J_2(\alpha\,\tilde{p}_\perp)\,f(\tilde{p}_\perp^2)\,, \tag{D.14}$$

where $\tilde{p}_\perp = |p_\perp|$ and $\tilde{p}_{\parallel} = |p_{\parallel}|$. Now, using Eqs. (D.13) and (D.14) it can be seen that

$$\hat{X}_{s_{\rm p}}^{({\rm p})}\Big|_{B=0} \;=\; \hat{X}\,, \qquad\qquad \left.\frac{\partial \hat{X}_{s_{\rm p}}^{({\rm p})}}{\partial|B|}\right|_{B=0} \;=\; (Q_{\rm p} - Q_u)\,\mathcal{I}_1 - Q_{\rm p}\,\mathcal{I}_2\,, \tag{D.15}$$

where $\hat{X}$ and $\mathcal{I}_k$ are given by Eqs. (6.54) and (6.62), respectively.

A similar procedure can be followed in order to obtain the expansions for $\hat{Y}_{s_{\rm p}}^{({\rm p})}$, $\hat{X}_\lambda^{({\rm n})}$ and $\hat{Y}_\lambda^{({\rm n})}$. The evaluation of the derivatives in the denominator of Eq. (D.10) is straightforward, leading to the final expressions of $\alpha_{\rm p}$ and $\alpha_{\rm n}$ in Eq. (6.60).

Bibliography

[1] S. Weinberg, "Non-abelian gauge theories of the strong interactions", Phys. Rev. Lett. **31**, 494 (1973).

[2] H. Fritzsch, M. Gell-Mann, and H. Leutwyler, "Advantages of the color octet gluon picture", Phys. Rev. B **47**, 365 (1973).

[3] W. N. Cottingham and D. A. Greenwood, *An introduction to the standard model of particle physics* (Cambridge University Press, 2007).

[4] H. D. Politzer, "Reliable perturbative results for strong interactions?", Phys. Rev. Lett. **30**, 1346 (1973).

[5] D. J. Gross and F. Wilczek, "Ultraviolet behavior of non-abelian gauge theories", Phys. Rev. Lett. **30**, 1343 (1973).

[6] D. Rischke, "The quark–gluon plasma in equilibrium", Prog. Part. Nucl. Phys. **52**, 197 (2004).

[7] N. Cabibbo and G. Parisi, "Exponential hadronic spectrum and quark liberation", Phys. Rev. B **59**, 67 (1975).

[8] J. C. Collins and M. J. Perry, "Superdense matter: neutrons or asymptotically free quarks?", Phys. Rev. Lett. **34**, 1353 (1975).

[9] E. V. Shuryak, "Quantum chromodynamics and the theory of superdense matter", Phys. Rep. **61**, 71 (1980).

[10] K. Fukushima and T. Hatsuda, "The phase diagram of dense QCD", Rep. Prog. Phys. **74**, 014001 (2011).

[11] J. N. Guenther, "Overview of the QCD phase diagram: Recent progress from the lattice", Eur. Phys. J. A **57**, 136 (2021).

[12] G. Aarts et al., "Phase transitions in particle physics – results and perspectives from lattice quantum chromo-dynamics", arXiv2301.04382 [hep-lat] (2023).

[13] H. Satz, *Extreme states of matter in strong interaction physics*, Lecture Notes in Physics (Springer International Publishing, 2018).

[14] Y. Nambu and G. Jona-Lasinio, "Dynamical model of elementary particles based on an analogy with superconductivity. I", Phys. Rev. **122**, 345 (1961).

[15] J. Goldstone, A. Salam, and S. Weinberg, "Broken symmetries", Phys. Rev. **127**, 965 (1962).

[16] R. D. Pisarski and F. Wilczek, "Remarks on the chiral phase transition in chromodynamics", Phys. Rev. D **29**, 338 (1984).

[17] A. Bazavov et al., "Chiral and deconfinement aspects of the QCD transition", Phys. Rev. D **85**, 054503 (2012).

[18] T. Bhattacharya et al., "QCD phase transition with chiral quarks and physical quark masses", Phys. Rev. Lett. **113**, 082001 (2014).

[19] S. Borsányi, Z. Fodor, C. Hoelbling, S. D. Katz, S. Krieg, and K. K. Szabó, "Full result for the QCD equation of state with 2+1 flavors", Phys. Lett. B **730**, 99 (2014).

[20] A. Bazavov et al., "Equation of state in (2+1)-flavor QCD", Phys. Rev. D **90**, 094503 (2014).

[21] H.-T. Ding, F. Karsch, and S. Mukherjee, "Thermodynamics of strong-interaction matter from lattice QCD", Int. J. Mod. Phys. E **24**, 1530007 (2015).

[22] A. Bazavov et al., "Chiral crossover in QCD at zero and non-zero chemical potentials", Phys. Lett. B **795**, 15 (2019).

[23] S. Iso, P. D. Serpico, and K. Shimada, "QCD-electroweak first-order phase transition in a supercooled universe", Phys. Rev. Lett. **119**, 141301 (2017).

[24] T. Hambye, A. Strumia, and D. Teresi, "Super-cool dark matter", J. High Energy Phys. **2018**, 188 (2018).

[25] F. Gao and I. M. Oldengott, "Cosmology meets functional QCD: first-order cosmic QCD transition induced by large lepton asymmetries", Phys. Rev. Lett. **128**, 131301 (2022).

[26] D. Blaschke, N. Glendenning, and A. Sedrakian, *Physics of neutron star interiors*, Lecture Notes in Physics (Springer Berlin Heidelberg, 2008).

[27] G. Baym, T. Hatsuda, T. Kojo, P. D. Powell, Y. Song, and T. Takatsuka, "From hadrons to quarks in neutron stars: a review", Rep. Progr. Phys. **81**, 056902 (2018).

[28] M. Alford, K. Rajagopal, and F. Wilczek, "QCD at finite baryon density: nucleon droplets and color superconductivity", Phys. Lett. B **422**, 247 (1998).

[29] R. Rapp, T. Schäfer, E. Shuryak, and M. Velkovsky, "Diquark bose condensates in high density matter and instantons", Phys. Rev. Lett. **81**, 53 (1998).

[30] M. Alford, K. Rajagopal, and F. Wilczek, "Color-flavor locking and chiral symmetry breaking in high density QCD", Nucl. Phys. B **537**, 443 (1999).

[31] I. Giannakis, D. Hou, H.-c. Ren, and D. H. Rischke, "Gauge field fluctuations and first-order phase transition in color superconductivity", Phys. Rev. Lett. **93**, 232301 (2004).

[32] T. Matsuura, K. Iida, T. Hatsuda, and G. Baym, "Thermal fluctuations of gauge fields and first order phase transitions in color superconductivity", Phys. Rev. D **69**, 074012 (2004).

[33] M. G. Alford, A. Schmitt, K. Rajagopal, and T. Schäfer, "Color superconductivity in dense quark matter", Rev. Mod. Phys. **80**, 1455 (2008).

[34] R. Anglani, R. Casalbuoni, M. Ciminale, N. Ippolito, R. Gatto, M. Mannarelli, and M. Ruggieri, "Crystalline color superconductors", Rev. Mod. Phys. **86**, 509 (2014).

[35] M. Buballa and S. Carignano, "Inhomogeneous chiral condensates", Progr. Part. Nucl. Phys. **81**, 39 (2015).

[36] W. Busza, K. Rajagopal, and W. van der Schee, "Heavy ion collisions: the big picture and the big questions", Ann. Rev. Nucl. Part. Sci. **68**, 339 (2018).

[37] G. Odyniec, "Probing the QCD phase diagram with heavy-ion collision experiments", in *Understanding the origin of matter: perspectives in quantum chromodynamics*, edited by D. Blaschke, K. Redlich, C. Sasaki, and L. Turko (Springer International Publishing, Cham, 2022), pp. 3–29.

[38] R. Nouicer, "New state of nuclear matter: nearly perfect fluid of quarks and gluons in heavy-ion collisions at rhic energies", Eur. Phys. J. Plus **131**, 70 (2016).

[39] X. Luo and N. Xu, "Search for the QCD critical point with fluctuations of conserved quantities in relativistic heavy-ion collisions at RHIC: an overview", Nucl. Sci. Tech. **28**, 112 (2017).

[40] U. Heinz and M. Jacob, "Evidence for a new state of matter: an assessment of the results from the CERN lead beam programme", ArXiv:nucl-th/0002042 (2000).

[41] I. Arsene et al., "Quark-gluon plasma and color glass condensate at RHIC? The perspective from the BRAHMS experiment", Nucl. Phys. A **757**, First Three Years of Operation of RHIC, 1 (2005).

[42] B. B. Back et al., "The PHOBOS perspective on discoveries at RHIC", Nucl. Phys. A **757**, First Three Years of Operation of RHIC, 28 (2005).

[43] C. Ratti, "Lattice QCD and heavy ion collisions: a review of recent progress", Rep. Progr. Phys. **81**, 084301 (2018).

[44] P. Kovtun, D. Son, and A. Starinets, "Viscosity in strongly interacting quantum field theories from black hole physics", Physical Review Letters **94**, 111601 (2005).

[45] A. Andronic, P. Braun-Munzinger, K. Redlich, and J. Stachel, "Decoding the phase structure of QCD via particle production at high energy", Nature **561**, 321 (2018).

[46] M. Stephanov, "QCD phase diagram: an overview", PoS **LAT2006**, 024 (2006).

[47] L. Hernandez, A. Ayala, and S. Hernandez-Ortiz, "QCD phase diagram from chiral symmetry restoration: analytic approach at high and low temperature using the linear sigma model with quarks", Revista Mexicana de Física **64**, 302 (2018).

[48] A. Ayala, L. A. Hernández, M. Loewe, and C. Villavicencio, "QCD phase diagram in a magnetized medium from the chiral symmetry perspective: the linear sigma model with quarks and the Nambu–Jona-Lasinio model effective descriptions", Eur. Phys. J. A **57**, 234 (2021).

[49] C. Ratti, "Equation of state for QCD from lattice simulations", Progr. Part. Nucl. Phys. **129**, 104007 (2023).

[50] A. Bzdak, S. Esumi, V. Koch, J. Liao, M. Stephanov, and N. Xu, "Mapping the phases of quantum chromodynamics with beam energy scan", Phys. Rep. **853**, 1 (2020).

[51] D. Kharzeev, K. Landsteiner, A. Schmitt, and H.-U. Yee, eds., *Strongly interacting matter in magnetic fields*, Vol. 871 (Lect. Notes Phys (Springer, Berlin), 2013).

[52] V. A. Miransky and I. A. Shovkovy, "Quantum field theory in a magnetic field: From quantum chromodynamics to graphene and Dirac semimetals", Phys. Rept. **576**, 1 (2015).

[53] J. O. Andersen, W. R. Naylor, and A. Tranberg, "Phase diagram of QCD in a magnetic field: A review", Rev. Mod. Phys. **88**, 025001 (2016).

[54] D. Grasso and H. R. Rubinstein, "Magnetic fields in the early universe", Phys. Rept. **348**, 163 (2001).

[55] J. Navarro, A. Sánchez, M. E. Tejeda-Yeomans, A. Ayala, and G. Piccinelli, "Symmetry restoration at finite temperature with weak magnetic fields", Phys. Rev. D **82**, 123007 (2010).

[56] R. C. Duncan and C. Thompson, "Formation of very strongly magnetized neutron stars: implications for gamma-ray bursts", Astrophys. J. Lett. **392**, L9 (1992).

[57] B. Paczynski, "GB 790305 as a very strongly magnetized neutron star", Acta Astronomica **42**, 145 (1992).

[58] C. Kouveliotou et al., "An X-ray pulsar with a superstrong magnetic field in the soft gamma-ray repeater SGR 1806-20.", Nature **393**, 235 (1998).

[59] D. Lai and S. L. Shapiro, "Cold equation of state in a strong magnetic field - Effects of inverse beta-decay", Astrophys. J. **383**, 745 (1991).

[60] D. Bandyopadhyay, S. Chakrabarty, and S. Pal, "Quantizing magnetic field and quark-hadron phase transition in a neutron star", Phys. Rev. Lett. **79**, 2176 (1997).

[61] E. J. Ferrer, V. de la Incera, J. P. Keith, I. Portillo, and P. L. Springsteen, "Equation of state of a dense and magnetized fermion system", Phys. Rev. C **82**, 065802 (2010).

[62] D. Chatterjee, T. Elghozi, J. Novak, and M. Oertel, "Consistent neutron star models with magnetic-field-dependent equations of state", Monthly Notices of the Royal Astronomical Society **447**, 3785 (2015).

[63] S. A. Olausen and V. M. Kaspi, "The McGill magnetar catalog", Astrophys. J., Suppl. Ser. **212**, 6 (2014).

[64] A. P. Igoshev, S. B. Popov, and R. Hollerbach, "Evolution of neutron star magnetic fields", Universe **7**, 351 (2021).

[65] E. J. Ferrer and V. de la Incera, "Magnetism in dense quark matter", in *Strongly interacting matter in magnetic fields*, edited by D. Kharzeev, K. Landsteiner, A. Schmitt, and H. Yee (Lect. Note Phys. (Springer, Berlin), 2013), pp. 399–432.

[66] D. E. Kharzeev, L. D. McLerran, and H. J. Warringa, "The Effects of topological charge change in heavy ion collisions: 'Event by event P and CP violation´ ", Nucl. Phys. A **803**, 227 (2008).

[67] V. Skokov, A. Y. Illarionov, and V. Toneev, "Estimate of the magnetic field strength in heavy-ion collisions", Int. J. Mod. Phys. A **24**, 5925 (2009).

[68] V. Voronyuk, V. D. Toneev, W. Cassing, E. L. Bratkovskaya, V. P. Konchakovski, and S. A. Voloshin, "Electromagnetic field evolution in relativistic heavy-ion collisions", Phys. Rev. C **83**, 054911 (2011).

[69] A. Bzdak and V. Skokov, "Event-by-event fluctuations of magnetic and electric fields in heavy ion collisions", Phys. Lett. B **710**, 171 (2012).

[70] W.-T. Deng and X.-G. Huang, "Event-by-event generation of electromagnetic fields in heavy-ion collisions", Phys. Rev. C **85**, 044907 (2012).

[71] K. Tuchin, "Particle production in strong electromagnetic fields in relativistic heavy-ion collisions", Adv. High Energy Phys. **2013**, 490495 (2013).

[72] M. D'Elia, L. Maio, F. Sanfilippo, and A. Stanzione, "Phase diagram of QCD in a magnetic background", Phys. Rev. D **105**, 034511 (2022).

[73] G. S. Bali, F. Bruckmann, G. Endrődi, Z. Fodor, S. D. Katz, and A. Schäfer, "QCD quark condensate in external magnetic fields", Phys. Rev. D **86**, 071502 (2012).

[74] G. S. Bali, F. Bruckmann, G. Endrődi, Z. Fodor, S. D. Katz, S. Krieg, A. Schafer, and K. K. Szabo, "The QCD phase diagram for external magnetic fields", J. High Energy Phys. **2012**, 044 (2012).

[75] G. S. Bali, F. Bruckmann, G. Endrődi, S. D. Katz, and A. Schäfer, "The QCD equation of state in background magnetic fields", J. High Energy Phys. **2014**, 177 (2014).

[76] V. G. Bornyakov, P. V. Buividovich, N. Cundy, O. A. Kochetkov, and A. Schäfer, "Deconfinement transition in two-flavor lattice QCD with dynamical overlap fermions in an external magnetic field", Phys. Rev. D **90**, 034501 (2014).

[77] G. Endrődi, "Critical point in the QCD phase diagram for extremely strong background magnetic fields", J. High Energy Phys. **2015**, 173 (2015).

[78] I. A. Shovkovy, "Magnetic catalysis: a review", in *Strongly interacting matter in magnetic fields*, edited by D. Kharzeev, K. Landsteiner, A. Schmitt, and H.-U. Yee (Springer Berlin Heidelberg, Berlin, Heidelberg, 2013), pp. 13–49.

[79] J. Andersen, "QCD phase diagram in a constant magnetic background: Inverse magnetic catalysis: where models meet the lattice", Eur. Phys. J. A **57**, 189 (2021).

[80] A. Bandyopadhyay and R. L. S. Farias, "Inverse magnetic catalysis – how much do we know about?", Eur. Phys. J. Spec. Top. **230**, 719 (2021).

[81] K. Fukushima, D. Kharzeev, and H. Warringa, "The Chiral Magnetic Effect", Phys. Rev. D **78**, 074033 (2008).

[82] D. E. Kharzeev and H. J. Warringa, "Chiral Magnetic conductivity", Phys. Rev. D **80**, 034028 (2009).

[83] D. T. Son and A. R. Zhitnitsky, "Quantum anomalies in dense matter", Phys. Rev. D **70**, 074018 (2004).

[84] M. A. Metlitski and A. R. Zhitnitsky, "Anomalous axion interactions and topological currents in dense matter", Phys. Rev. D **72**, 045011 (2005).

[85] D. E. Kharzeev and H. Yee, "Chiral Magnetic Wave", Phys. Rev. D **83**, 085007 (2011).

[86] Y. Burnier, D. E. Kharzeev, J. Liao, and H. Yee, "Chiral magnetic wave at finite baryon density and the electric quadrupole moment of quark-gluon plasma in heavy ion collisions", Phys. Rev. Lett. **107**, 052303 (2011).

[87] H. Yee and Y. Yin, "Realistic Implementation of Chiral Magnetic Wave in Heavy Ion Collisions", Phys. Rev. C **89**, 044909 (2014).

[88] L. Adamczyk et al. (STAR), "Observation of charge asymmetry dependence of pion elliptic flow and the possible chiral magnetic wave in heavy-ion collisions", Phys. Rev. Lett. **114**, 252302 (2015).

[89] I. A. Shovkovy, D. O. Rybalka, and E. V. Gorbar, "The overdamped chiral magnetic wave", PoS **Confinement2018**, 029 (2018).

[90] M. N. Chernodub, "Superconductivity of QCD vacuum in strong magnetic field", Phys. Rev. D **82**, 085011 (2010).

[91] M. N. Chernodub, "Spontaneous electromagnetic superconductivity of vacuum in a strong magnetic field: evidence from the Nambu–Jona-Lasinio model", Phys. Rev. Lett. **106**, 142003 (2011).

[92] D. Kharzeev, J. Liao, S. Voloshin, and G. Wang, "Chiral magnetic and vortical effects in high-energy nuclear collisions—A status report", Prog. Part. Nucl. Phys. **88**, 1 (2016).

[93] W. Li and G. Wang, "Chiral magnetic effects in nuclear collisions", Ann. Rev. Nucl. Part. Sci. **70**, 293 (2020).

[94] S. P. Klevansky and R. H. Lemmer, "Chiral symmetry restoration in the Nambu-Jona-Lasinio model with a constant electromagnetic field", Phys. Rev. D **39**, 3478 (1989).

[95] H. Suganuma and T. Tatsumi, "On the behavior of symmetry and phase transitions in a strong electromagnetic field", Ann. Phys. **208**, 470 (1991).

[96] K. G. Klimenko, "Three-dimensional gross-neveu model in an external magnetic field. i", Theor. Math. Phys. **89**, 1161 (1991).

[97] K. G. Klimenko, "Three-dimensional gross-neveu model at nonzero temperature and in an external magnetic field", Theor. Math. Phys. **90**, 1 (1992).

[98] V. P. Gusynin, V. A. Miransky, and I. A. Shovkovy, "Catalysis of dynamical flavor symmetry breaking by a magnetic field in 2 + 1 dimensions", Phys. Rev. Lett. **73**, 3499 (1994).

[99] V. P. Gusynin, V. A. Miransky, and I. A. Shovkovy, "Dimensional reduction and dynamical chiral symmetry breaking by a magnetic field in 3 + 1 dimensions", Phys. Lett. B **349**, 477 (1995).

[100] V. P. Gusynin, V. A. Miransky, and I. A. Shovkovy, "Dimensional reduction and catalysis of dynamical symmetry breaking by a magnetic field", Nucl. Phys. B **462**, 249 (1996).

[101] J. Bardeen, L. N. Cooper, and J. R. Schrieffer, "Theory of superconductivity", Phys. Rev. **108**, 1175 (1957).

[102] J. Bardeen, L. N. Cooper, and J. R. Schrieffer, "Microscopic theory of superconductivity", Phys. Rev. **106**, 162 (1957).

[103] V. A. Miransky and I. A. Shovkovy, "Magnetic catalysis and anisotropic confinement in QCD", Phys. Rev. D **66**, 045006 (2002).

[104] A. Bandyopadhyay, R. L. S. Farias, B. S. Lopes, and R. O. Ramos, "Quantum chromodynamics axion in a hot and magnetized medium", Phys. Rev. D **100**, 076021 (2019).

[105] G. Cao, "Recent progresses on QCD phases in a strong magnetic field: views from Nambu–Jona-Lasinio model", Eur. Phys. J. A **57**, 264 (2021).

[106] F. Bruckmann, G. Endrődi, M. Giordano, S. Katz, T. Kovács, F. Pittler, and J. Wellnhofer, "Landau levels in QCD", Phys. Rev. D **96**, 074506 (2017).

[107] M. D'Elia, F. Manigrasso, F. Negro, and F. Sanfilippo, "QCD phase diagram in a magnetic background for different values of the pion mass", Phys. Rev. D **98**, 054509 (2018).

[108] G. Endrődi, M. Giordano, S. D. Katz, T. G. Kovács, and F. Pittler, "Magnetic catalysis and inverse catalysis for heavy pions", J. High Energy Phys. **2019**, 007 (2019).

[109] F. Bruckmann, G. Endrődi, and T. G. Kovács, "Inverse magnetic catalysis and the polyakov loop", J. High Energy Phys. **2013**, 112 (2013).

[110] C. Bonati, M. D'Elia, M. Mariti, F. Negro, and F. Sanfilippo, "Magnetic susceptibility and equation of state of $N_f = 2 + 1$ QCD with physical quark masses", Phys. Rev. D **89**, 054506 (2014).

[111] C. Bonati, M. D'Elia, M. Mariti, M. Mesiti, F. Negro, A. Rucci, and F. Sanfilippo, "Magnetic field effects on the static quark potential at zero and finite temperature", Phys. Rev. D **94**, 094007 (2016).

[112] M. D'Elia, L. Maio, F. Sanfilippo, and A. Stanzione, "Confining and chiral properties of QCD in extremely strong magnetic fields", Phys. Rev. D **104**, 114512 (2021).

[113] C. Bonati, S. Calì, M. D'Elia, M. Mesiti, F. Negro, A. Rucci, and F. Sanfilippo, "Effects of a strong magnetic field on the QCD flux tube", Phys. Rev. D **98**, 054501 (2018).

[114] H.-T. Ding, S.-T. Li, Q. Shi, and X.-D. Wang, "Fluctuations and correlations of net baryon number, electric charge and strangeness in a background magnetic field", Eur. Phys. J. A **57**, 202 (2021).

[115] M. D'Elia and F. Negro, "Chiral Properties of Strong Interactions in a Magnetic Background", Phys. Rev. D **83**, 114028 (2011).

[116] T. Banks and A. Casher, "Chiral symmetry breaking in confining theories", Nucl. Phys. B **169**, 103 (1980).

[117] G. S. Bali, F. Bruckmann, G. Endrődi, F. Gruber, and A. Schäefer, "Magnetic field-induced gluonic (inverse) catalysis and pressure (an)isotropy in QCD", J. High Energy Phys. **2013**, 130 (2013).

[118] S. Schramm, B. Müller, and A. J. Schramm, "Quark-antiquark condensates in strong magnetic fields", Mod. Phys. Lett. A **07**, 973 (1992).

[119] A. Broderick, M. Prakash, and J. M. Lattimer, "The equation of state of neutron star matter in strong magnetic fields", The Astrophysical Journal **537**, 351 (2000).

[120] C. Giunti and A. Studenikin, "Neutrino electromagnetic interactions: a window to new physics", Rev. Mod. Phys. **87**, 531 (2015).

[121] C. Bonati, M. D'Elia, and A. Rucci, "Heavy quarkonia in strong magnetic fields", Phys. Rev. D **92**, 054014 (2015).

[122] K. Fukushima and Y. Hidaka, "Magnetic shift of the chemical freeze-out and electric charge fluctuations", Phys. Rev. Lett. **117**, 102301 (2016).

[123] C. D. Roberts, "Strong QCD and Dyson-Schwinger Equations", arXiv:1203.5341 (2012).

[124] C. S. Fischer, "QCD at finite temperature and chemical potential from dyson–schwinger equations", Prog. Part. Nucl. Phys. **105**, 1 (2019).

[125] N. Dupuis, L. Canet, A. Eichhorn, W. Metzner, J. M. Pawlowski, M. Tissier, and N. Wschebor, "The nonperturbative functional renormalization group and its applications", Phys. Rep. **910**, 1 (2021).

[126] W. Fu, "QCD at finite temperature and density within the fRG approach: an overview", Commun. Theor. Phys. **74**, 097304 (2022).

[127] O. Philipsen, "Lattice constraints on the QCD chiral phase transition at finite temperature and baryon density", Symmetry **13**, 2079 (2021).

[128] S. Borsányi, Z. Fodor, J. Guenther, R. Kara, S. Katz, P. Parotto, A. Pásztor, C. Ratti, and K. K. Szabó, "Lattice QCD equation of state at finite chemical potential from an alternative expansion scheme", Phys. Rev. Lett. **126**, 232001 (2021).

[129] G. S. Bali, B. B. Brandt, G. Endrődi, and B. Gläßle, "Meson masses in electromagnetic fields with Wilson fermions", Phys. Rev. D **97**, 034505 (2018).

[130] A. Ayala, C. A. Dominguez, and M. Loewe, "Finite temperature QCD sum rules: a review", Adv. High Energy Phys. **2017**, 1 (2017).

[131] C. A. Dominguez, *Quantum chromodynamics sum rules*, SpringerBriefs in Physics (Springer International Publishing, 2018).

[132] P. Gubler and D. Satow, "Recent progress in QCD condensate evaluations and sum rules", Prog. Part. Nucl. Phys. **106**, 1 (2019).

[133] S. Weinberg, "Phenomenological lagrangians", Phys. A: Stat. Mech. Appl. **96**, 327 (1979).

[134] S. Scherer, "Introduction to chiral perturbation theory", in *Adv. nucl. phys.* Vol. 27, edited by J. W. Negele and E. W. Vogt (Kluwer Academic Publishers, 2003), pp. 277–538.

[135] A. Chodos, R. L. Jaffe, K. Johnson, C. B. Thorn, and V. F. Weisskopf, "New extended model of hadrons", Phys. Rev. D **9**, 3471 (1974).

[136] A. Chodos, R. L. Jaffe, K. Johnson, and C. B. Thorn, "Baryon structure in the bag theory", Phys. Rev. D **10**, 2599 (1974).

[137] L. L. Lopes, C. Biesdorf, and D. P. Menezes, "Modified MIT bag models—part I: thermodynamic consistency, stability windows and symmetry group", Phys. Scr **96**, 065303 (2021).

[138] L. L. Lopes, C. Biesdorf, K. D. Marquez, and D. P. Menezes, "Modified MIT bag models—part II: QCD phase diagram and hot quark stars", Phys. Scr. **96**, 065302 (2021).

[139] J. Schwinger, "A theory of the fundamental interactions", Ann. Phys. **2**, 407 (1957).

[140] M. Gell-Mann and M. Lèvy, "The axial vector current in beta decay", Il Nuovo Cimento **16**, 705 (1960).

[141] M. Scadron, G. Rupp, and R. Delbourgo, "The quark-level linear σ model", Fortschritte der Physik **61**, 994 (2013).

[142] T. Sakai and S. Sugimoto, "Low energy hadron physics in holographic QCD", Prog. Theor. Phys. **113**, 843 (2005).

[143] T. Sakai and S. Sugimoto, "More on a holographic dual of QCD", Prog. Theor. Phys. **114**, 1083 (2005).

[144] Y. Nambu and G. Jona-Lasinio, "Dynamical model of elementary particles based on an analogy with superconductivity. II", Phys. Rev. **124**, 246 (1961).

[145] S. P. Klevansky, "The Nambu-Jona-Lasinio model of quantum chromodynamics", Rev. Mod. Phys. **64**, 649 (1992).

[146] U. Vogl and W. Weise, "The Nambu and Jona Lasinio model: Its implications for hadrons and nuclei", Prog. Part. Nucl. Phys. **27**, 195 (1991).

[147] T. Hatsuda and T. Kunihiro, "QCD phenomenology based on a chiral effective Lagrangian", Phys. Rept. **247**, 221 (1994).

[148] P. N. Meisinger and M. C. Ogilvie, "Chiral symmetry restoration and ZN symmetry", Phys. Rev. B **379**, 163 (1996).

[149] R. D. Pisarski, "Quark-gluon plasma as a condensate of $Z(3)$ Wilson lines", Phys. Rev. D **62**, 111501 (2000).

[150] K. Fukushima, "Chiral effective model with the Polyakov loop", Phys. Lett. B **591**, 277 (2004).

[151] E. Megías, E. R. Arriola, and L. L. Salcedo, "Polyakov loop in chiral quark models at finite temperature", Phys. Rev. D **74**, 065005 (2006).

[152] D. Gomez Dumm, J. P. Carlomagno, and N. N. Scoccola, "Strong-interaction matter under extreme conditions from chiral quark models with nonlocal separable interactions", Symmetry **13**, 121 (2021).

[153] S. Mao, "Inverse magnetic catalysis in Nambu–Jona-Lasinio model beyond mean field", Phys. Lett. B **758**, 195 (2016).

[154] S. Fayazbakhsh and N. Sadooghi, "Anomalous magnetic moment of hot quarks, inverse magnetic catalysis, and reentrance of the chiral symmetry broken phase", Phys. Rev. D **90**, 105030 (2014).

[155] J. Mei and S. Mao, "Inverse catalysis effect of the quark anomalous magnetic moment to chiral restoration and deconfinement phase transitions", Phys. Rev. D **102**, 114035 (2020).

[156] N. Chaudhuri, S. Ghosh, S. Sarkar, and P. Roy, "Effects of quark anomalous magnetic moment on the thermodynamical properties and mesonic excitations of magnetized hot and dense matter in PNJL model", Eur. Phys. J. A **56**, 213 (2020).

[157] K. Xu, J. Chao, and M. Huang, "Effect of the anomalous magnetic moment of quarks on magnetized QCD matter and meson spectra", Phys. Rev. D **103**, 076015 (2021).

[158] M. Ferreira, P. Costa, O. Lourenço, T. Frederico, and C. Providência, "Inverse magnetic catalysis in the (2+1)-flavor Nambu-Jona-Lasinio and Polyakov-Nambu-Jona-Lasinio models", Phys. Rev. D **89**, 116011 (2014).

[159] R. L. S. Farias, K. P. Gomes, G. I. Krein, and M. B. Pinto, "Importance of asymptotic freedom for the pseudocritical temperature in magnetized quark matter", Phys. Rev. C **90**, 025203 (2014).

[160] R. L. S. Farias, V. S. Timóteo, S. S. Avancini, M. B. Pinto, and G. Krein, "Thermo-magnetic effects in quark matter: Nambu–Jona-Lasinio model constrained by lattice QCD", Eur. Phys. J. A **53**, 101 (2017).

[161] S. S. Avancini, R. L. S. Farias, M. B. Pinto, W. R. Tavares, and V. S. Timóteo, "π_0 pole mass calculation in a strong magnetic field and lattice constraints", Phys. Lett. B **767**, 247 (2017).

[162] S. S. Avancini, R. L. S. Farias, and W. R. Tavares, "Neutral meson properties in hot and magnetized quark matter: a new magnetic field independent regularization scheme applied to NJL-type model", Phys. Rev. D **99**, 056009 (2019).

[163] S. S. Avancini, R. L. S. Farias, M. B. Pinto, T. E. Restrepo, and W. R. Tavares, "Regularizing thermo and magnetic contributions within nonrenormalizable theories", Phys. Rev. D **103**, 056009 (2021).

[164] G. Endrődi and G. Markó, "Magnetized baryons and the QCD phase diagram: NJL model meets the lattice", J. High Energy Phys. **2019**, 036 (2019).

[165] V. Pagura, D. Gomez Dumm, S. Noguera, and N. Scoccola, "Magnetic catalysis and inverse magnetic catalysis in nonlocal chiral quark models", Phys. Rev. D **95**, 034013 (2017).

[166] D. Gomez Dumm, M. F. Izzo Villafañe, S. Noguera, V. P. Pagura, and N. N. Scoccola, "Strong magnetic fields in nonlocal chiral quark models", Phys. Rev. D **96**, 114012 (2017).

[167] J. S. Schwinger, "On gauge invariance and vacuum polarization", Phys. Rev. **82**, 664 (1951).

[168] R. Zhang, W.-j. Fu, and Y.-x. Liu, "Properties of mesons in a strong magnetic field", Eur. Phys. J. C **76**, 307 (2016).

[169] H. Liu, X. Wang, L. Yu, and M. Huang, "Neutral and charged scalar mesons, pseudoscalar mesons, and diquarks in magnetic fields", Phys. Rev. D **97**, 076008 (2018).

[170] S. Fayazbakhsh and N. Sadooghi, "Weak decay constant of neutral pions in a hot and magnetized quark matter", Phys. Rev. D **88**, 065030 (2013).

[171] G. S. Bali, B. B. Brandt, G. Endrődi, and B. Gläßle, "Weak decay of magnetized pions", Phys. Rev. Lett. **121**, 072001 (2018).

[172] R. L. Workman et al., "Review of particle physics", Prog. Theor. Exp. Phys. **2022**, 083C01 (2022).

[173] G. 't Hooft, "Computation of the quantum effects due to a four-dimensional pseudoparticle", Phys. Rev. D **14**, Erratum: [Phys. Rev. D 18 (1978) 2199], 3432 (1976).

[174] G. 't Hooft, "How instantons solve the U(1) problem", Phys. Rep. **142**, 357 (1986).

[175] H. G. Dosch and S. Narison, "Direct extraction of the chiral quark condensate and bounds on the light quark masses", Phys. Rev. B **417**, 173 (1998).

[176] L. Giusti, F. Rapuano, M. Talevi, and A. Vladikas, "The QCD chiral condensate from the lattice", Nucl. Phys. B **538**, 249 (1999).

[177] D. Ebert, "Bosonization in particle physics", in *Field theoretical tools for polymer and particle physics*, edited by H. Meyer-Ortmanns and A. Klümper (Springer Berlin Heidelberg, Berlin, Heidelberg, 1998), pp. 103–114.

[178] W. Greiner, D. A. Bromley, and J. Reinhardt, *Field Quantization* (Springer Berlin Heidelberg, 2013).

[179] G. Ripka, *Quarks Bound by Chiral Fields: The Quark Structure of the Vacuum and of Light Mesons and Baryons*, Oxford science publications (Clarendon Press, 1997).

[180] C. Christov, A. Blotz, H.-C. Kim, P. Pobylitsa, T. Watabe, T. Meissner, E. R. Arriola, and K. Goeke, "Baryons as non-topological chiral solitons", Prog. Part. Nucl. Phys. **37**, 91 (1996).

[181] M. Buballa, "NJL-model analysis of dense quark matter", Phys. Rept. **407**, 205 (2005).

[182] M. L. Goldberger and S. B. Treiman, "Decay of the Pi Meson", Phys. Rev. **110**, 1178 (1958).

[183] M. Gell-Mann, R. J. Oakes, and B. Renner, "Behavior of Current Divergences under SU_3ÖSU_3", Phys. Rev. **175**, 2195 (1968).

[184] S. Noguera and N. N. Scoccola, "Nonlocal chiral quark models with wavefunction renormalization: Sigma properties and π-π scattering parameters", Phys. Rev. D **78**, 114002 (2008).

[185] M. Jamin, "Flavour-symmetry breaking of the quark condensate and chiral corrections to the Gell-Mann–Oakes–Renner relation", Phys. Lett. B **538**, 71 (2002).

[186] R. Jora, "Quark and gluon condensates in QCD reevaluated", Acta Phys. Pol. B **51**, 937 (2020).

[187] Y. Aoki et al., "FLAG Review 2021", Eur. Phys. J. C **82**, 869 (2022).

[188] V. I. Ritus, "Radiative corrections in quantum electrodynamics with intense field and their analytical properties", Ann. Phys. **69**, 555 (1972).

[189] V. I. Ritus, "Method of eigenfunctions and mass operator in quantum electrodynamics of a constant field", Sov. Phys. JETP **48**, 788 (1978).

[190] N. Mueller, J. A. Bonnet, and C. S. Fischer, "Dynamical quark mass generation in a strong external magnetic field", Phys. Rev. D **89**, 094023 (2014).

[191] S. Chakrabarty, "Quark matter in a strong magnetic field", Phys. Rev. D **54**, 1306 (1996).

[192] K. Fukushima, M. Ruggieri, and R. Gatto, "Chiral magnetic effect in the Polyakov-Nambu-Jona-Lasinio model", Phys. Rev. D **81**, 114031 (2010).

[193] R. Gatto and M. Ruggieri, "Deconfinement and chiral symmetry restoration in a strong magnetic background", Phys. Rev. D **83**, 034016 (2011).

[194] M. Frasca and M. Ruggieri, "Magnetic susceptibility of the quark condensate and polarization from chiral models", Phys. Rev. D **83**, 094024 (2011).

[195] S. Ghosh, N. Chaudhuri, P. Roy, and S. Sarkar, "Thermomagnetic modification of the anomalous magnetic moment of quarks using the NJL model", Phys. Rev. D **103**, 116008 (2021).

[196] N. Chaudhuri, S. Ghosh, P. Roy, and S. Sarkar, "Anisotropic pressure of magnetized quark matter with anomalous magnetic moment", Phys. Rev. D **106**, 056020 (2022).

[197] H. Liu, L. Yu, M. Chernodub, and M. Huang, "Possible formation of high temperature superconductor at an early stage of heavy-ion collisions", Phys. Rev. D **94**, 113006 (2016).

[198] K. Fukushima and H. J. Warringa, "Color superconducting matter in a magnetic field", Phys. Rev. Lett. **100**, 032007 (2008).

[199] S. Fayazbakhsh and N. Sadooghi, "Color neutral two-flavor superconducting phase of cold and dense quark matter in the presence of constant magnetic fields", Phys. Rev. D **82**, 045010 (2010).

[200] S. Fayazbakhsh and N. Sadooghi, "Phase diagram of hot magnetized two-flavor color-superconducting quark matter", Phys. Rev. D **83**, 025026 (2011).

[201] J. L. Noronha and I. A. Shovkovy, "Color-flavor locked superconductor in a magnetic field", Phys. Rev. D **76**, 105030 (2007).

[202] J. L. Noronha and I. A. Shovkovy, "Erratum: color-flavor locked superconductor in a magnetic field", Phys. Rev. D **86**, 049901 (2012).

[203] J.-c. Wang, V. de la Incera, E. J. Ferrer, and Q. Wang, "Magnetic tuning of the relativistic BCS-BEC crossover", Phys. Rev. D **84**, 065014 (2011).

[204] T. Mandal and P. Jaikumar, "Neutrality of a magnetized two-flavor quark superconductor", Phys. Rev. C **87**, 045208 (2013).

[205] T. Mandal and P. Jaikumar, "Effect of strong magnetic field on competing order parameters in two-flavor dense quark matter", Adv. High Energy Phys. **2017**, 1 (2017).

[206] D. C. Duarte and R. L. S. Farias, "Phase transitions of cold and dense quark matter in an external magnetic field", J. Phys. Conf. Ser. **1291**, 012014 (2019).

[207] P. Allen, A. G. Grunfeld, and N. N. Scoccola, "Magnetized color superconducting cold quark matter within the $SU(2)_f$ NJL model: A novel regularization scheme", Phys. Rev. D **92**, 074041 (2015).

[208] M. Morimoto, Y. Tsue, J. da Providência, C. Providência, and M. Yamamura, "Spontaneous magnetization under a pseudovector interaction between quarks in high density quark matter", Int. J. Mod. Phys. E **27**, 1850028 (2018).

[209] N. Chaudhuri, S. Ghosh, S. Sarkar, and P. Roy, "Effect of the anomalous magnetic moment of quarks on the phase structure and mesonic properties in the NJL model", Phys. Rev. D **99**, 116025 (2019).

[210] W. J. de Haas and P. M. van Alphen, "The dependence of the susceptibility of diamagnetic metals upon the field", Proc. Acad. Sci. Amsterdam **33**, 1106 (1930).

[211] L. D. Landau and E. M. Lifshitz, *Statistical physics, Volume 5* (Elsevier Science & Technology Books, 2013).

[212] S. S. Avancini, R. L. S. Farias, N. N. Scoccola, and W. R. Tavares, "NJL-type models in the presence of intense magnetic fields: the role of the regularization prescription", Phys. Rev. D **99**, 116002 (2019).

[213] L. Campanelli and M. Ruggieri, "Probing the QCD vacuum with an Abelian chromomagnetic field: a study within an effective model", Phys. Rev. D **80**, 034014 (2009).

[214] R. Gatto and M. Ruggieri, "Quark matter in a strong magnetic background", in *Strongly interacting matter in magnetic fields*, Vol. 871 (Lect. Notes Phys., 2013), pp. 87–119.

[215] D. Menezes, M. Benghi Pinto, S. Avancini, A. Perez Martinez, and C. Providência, "Quark matter under strong magnetic fields in the Nambu-Jona-Lasinio Model", Phys. Rev. C **79**, 035807 (2009).

[216] D. Ebert, K. G. Klimenko, M. A. Vdovichenko, and A. S. Vshivtsev, "Magnetic oscillations in dense cold quark matter with four fermion interactions", Phys. Rev. D **61**, 025005 (2000).

[217] K. Fukushima and Y. Hidaka, "Magnetic Catalysis Versus Magnetic Inhibition", Phys. Rev. Lett. **110**, 031601 (2013).

[218] B. Sheng, X. Wang, and L. Yu, "Impacts of inverse magnetic catalysis on screening masses of neutral pions and sigma mesons in hot and magnetized quark matter", Phys. Rev. D **105**, 034003 (2022).

[219] G. Cao and P. Zhuang, "Effects of chiral imbalance and magnetic field on pion superfluidity and color superconductivity", Phys. Rev. D **92**, 105030 (2015).

[220] G. Cao and A. Huang, "Solitonic modulation and lifshitz point in an external magnetic field within nambu–jona-lasinio model", Phys. Rev. D **93**, 076007 (2016).

[221] S. Mao, "From inverse to delayed magnetic catalysis in a strong magnetic field", Phys. Rev. D **94**, 036007 (2016).

[222] Z. Wang and P. Zhuang, "Meson properties in magnetized quark matter", Phys. Rev. D **97**, 034026 (2018).

[223] S. Mao, "Pions in magnetic field at finite temperature", Phys. Rev. D **99**, 056005 (2019).

[224] B. Sheng, Y. Wang, X. Wang, and L. Yu, "Pole and screening masses of neutral pions in a hot and magnetized medium: A comprehensive study in the Nambu–Jona-Lasinio model", Phys. Rev. D **103**, 094001 (2021).

[225] D. C. Duarte, P. G. Allen, R. L. S. Farias, P. H. A. Manso, R. O. Ramos, and N. N. Scoccola, "BEC-BCS crossover in a cold and magnetized two color NJL model", Phys. Rev. D **93**, 025017 (2016).

[226] M. Coppola, P. G. Allen, A. G. Grunfeld, and N. N. Scoccola, "Magnetized color superconducting quark matter under compact star conditions: phase structure within the SU(2)f NJL model", Phys. Rev. D **96**, 056013 (2017).

[227] W. Dittrich and H. Gies, *Probing the quantum vacuum: pertubative effective action approach in quantum electrodynamics and its application*, Vol. 166 (Springer Berlin Heidelberg, Jan. 2000).

[228] K. Kamikado and T. Kanazawa, "Chiral dynamics in a magnetic field from the functional renormalization group", J. High Energy Phys. **2014**, 009 (2014).

[229] Y. Nagashima and Y. Nambu, *Elementary Particle Physics: Quantum Field Theory and Particles [Volume 1], Quantum field theory and particles v1* (Wiley & Sons, Incorporated, John, 2011), p. 964.

[230] M. Coppola, D. Gomez Dumm, S. Noguera, and N. N. Scoccola, "Pion-to-vacuum vector and axial vector amplitudes and weak decays of pions in a magnetic field", Phys. Rev. D **99**, 054031 (2019).

[231] M. Coppola, D. Gomez Dumm, S. Noguera, and N. N. Scoccola, "Weak decays of magnetized charged pions in the symmetric gauge", Phys. Rev. D **101**, 034003 (2020).

[232] M. E. Peskin and D. V. Schroeder, *An introduction to quantum field theory*, Frontiers in Physics (Westview Press, 1995), p. 842.

[233] M. Coppola, D. Gomez Dumm, and N. N. Scoccola, "Charged pion masses under strong magnetic fields in the NJL model", Phys. Lett. B **782**, 155 (2018).

[234] N. O. Agasian and I. A. Shushpanov, "Gell-Mann-Oakes-Renner relation in a magnetic field at finite temperature", J. High Energy Phys. **2001**, 006 (2001).

[235] J. O. Andersen, "Chiral perturbation theory in a magnetic background - finite-temperature effects", J. High Energy Phys. **2012**, 005 (2012).

[236] V. D. Orlovsky and Y. A. Simonov, "Nambu-Goldstone mesons in strong magnetic field", J. High Energy Phys. **2013**, 136 (2013).

[237] G. Colucci, E. S. Fraga, and A. Sedrakian, "Chiral pions in a magnetic background", Phys. Lett. B **728**, 19 (2014).

[238] A. Ayala, R. L. S. Farias, S. Hernández-Ortiz, L. A. Hernández, D. Manreza Paret, and R. Zamora, "Magnetic field-dependence of the neutral pion mass in the linear sigma model coupled to quarks: The weak field case", Phys. Rev. D **98**, 114008 (2018).

[239] A. Das and N. Haque, "Neutral pion mass in the linear sigma model coupled to quarks at arbitrary magnetic field", Phys. Rev. D **101**, 074033 (2020).

[240] A. Ayala, J. L. Hernández, L. A. Hernández, R. L. S. Farias, and R. Zamora, "Magnetic field dependence of the neutral pion mass in the linear sigma model with quarks: The strong field case", Phys. Rev. D **103**, 054038 (2021).

[241] M. A. Andreichikov, B. O. Kerbikov, E. V. Luschevskaya, Y. A. Simonov, and O. E. Solovjeva, "The Evolution of Meson Masses in a Strong Magnetic Field", J. High Energy Phys. **2017**, 007 (2017).

[242] Y. A. Simonov, "Pion decay constants in a strong magnetic field", Phys. Atom. Nucl. **79**, 455 (2016).

[243] M. A. Andreichikov and Y. A. Simonov, "Chiral physics in the magnetic field with quark confinement contribution", Eur. Phys. J. C **78**, 902 (2018).

[244] C. Dominguez, M. Loewe, and C. Villavicencio, "QCD determination of the magnetic field dependence of QCD and hadronic parameters", Phys. Rev. D **98**, 034015 (2018).

[245] N. Callebaut and D. Dudal, "A magnetic instability of the non-abelian sakai-sugimoto model", J. High Energy Phys. **2014**, 55 (2014).

[246] S. Fayazbakhsh, S. Sadeghian, and N. Sadooghi, "Properties of neutral mesons in a hot and magnetized quark matter", Phys. Rev. D **86**, 085042 (2012).

[247] J. Li, G. Cao, and L. He, "Gauge independence of pion masses in a magnetic field within the Nambu–Jona-Lasinio model", Phys. Rev. D **104**, 074026 (2021).

[248] S. S. Avancini, W. R. Tavares, and M. B. Pinto, "Properties of magnetized neutral mesons within a full RPA evaluation", Phys. Rev. D **93**, 014010 (2016).

[249] S. Mao and Y. Wang, "Effect of discrete quark momenta on the Goldstone mode in a magnetic field", Phys. Rev. D **96**, 034004 (2017).

[250] D. Gomez Dumm, M. F. Izzo Villafañe, and N. N. Scoccola, "Neutral meson properties under an external magnetic field in nonlocal chiral quark models", Phys. Rev. D **97**, 034025 (2018).

[251] D. Gomez Dumm, M. F. Izzo Villafañe, and N. N. Scoccola, "Properties of magnetized neutral pions at zero and finite temperature in nonlocal chiral quark models", Phys. Rev. D **101**, 116018 (2020).

[252] M. Coppola, D. Gomez Dumm, S. Noguera, and N. N. Scoccola, "Neutral and charged pion properties under strong magnetic fields in the NJL model", Phys. Rev. D **100**, 054014 (2019).

[253] M. Coppola, D. Gomez Dumm, S. Noguera, and N. N. Scoccola, "Magnetic field driven enhancement of the weak decay width of charged pions", J. High Energy Phys. **2020**, 58 (2020).

[254] S. P. Klevansky, J. Jaenicke, and R. H. Lemmer, "Collective modes of the Nambu–Jona-Lasinio model with an external U(1) gauge field", Phys. Rev. D **43**, 3040 (1991).

[255] I. S. Gradshteyn and I. M. Ryzhik, *Table of Integrals, Series, and Products*, edited by D. Zwillinger, Eight (Elsevier, Sept. 2014).

[256] J. Wess and B. Zumino, "Consequences of anomalous ward identities", Phys. Lett. B **37**, 95 (1971).

[257] E. Witten, "Global aspects of current algebra", Nuclear Physics B **223**, 422 (1983).

[258] H.-T. Ding, S.-T. Li, A. Tomiya, X.-D. Wang, and Y. Zhang, "Chiral properties of (2+1)-flavor QCD in strong magnetic fields at zero temperature", Phys. Rev. D **104**, 014505 (2021).

[259] I. A. Shushpanov and A. V. Smilga, "Quark condensate in a magnetic field", Phys. Lett. B **402**, 351 (1997).

[260] B. Zhang, Z. G. Dai, P. Meszaros, E. Waxman, and A. K. Harding, "High-energy neutrinos from magnetars", Astrophys. J. **595**, 346 (2003).

[261] D. Page, U. Geppert, and F. Weber, "The cooling of compact stars", Nucl. Phys. A **777**, 497 (2006).

[262] K. Hattori, T. Kojo, and N. Su, "Mesons in strong magnetic fields: (I) General analyses", Nucl. Phys. A **951**, 1 (2016).

[263] T. Kojo, "Neutral and charged mesons in magnetic fields", Eur. Phys. J. A **57**, 317 (2021).

[264] A. Mishra and S. P. Misra, "Strange mesons in strong magnetic fields", Int. J. Mod. Phys. E **30**, 2150014 (2021).

[265] S. S. Avancini, J. C. Sodré, M. Coppola, and N. N. Scoccola, "Light pseudoscalar meson masses under strong magnetic fields within the SU(3) Nambu–Jona-Lasinio model", Phys. Rev. D **104**, 094040 (2021).

[266] P. Rehberg, S. P. Klevansky, and J. Hufner, "Hadronization in the SU(3) Nambu-Jona-Lasinio model", Phys. Rev. C **53**, 410 (1996).

[267] B. C. Tiburzi, "Hadrons in strong electric and magnetic fields", Nucl. Phys. A **814**, 74 (2008).

[268] A. Deshmukh and B. C. Tiburzi, "Octet baryons in large magnetic fields", Phys. Rev. D **97**, 014006 (2018).

[269] H. Taya, "Hadron masses in strong magnetic fields", Phys. Rev. D **92**, 014038 (2015).

[270] A. Haber, F. Preis, and A. Schmitt, "Magnetic catalysis in nuclear matter", Phys. Rev. D **90**, 125036 (2014).

[271] A. Mukherjee, S. Ghosh, M. Mandal, S. Sarkar, and P. Roy, "Effect of external magnetic fields on nucleon mass in a hot and dense medium: Inverse magnetic catalysis in the Walecka model", Phys. Rev. D **98**, 056024 (2018).

[272] B.-R. He, "Skyrme model study of proton and neutron properties in a strong magnetic field", Phys. Lett. B **765**, 109 (2017).

[273] C. A. Dominguez, L. A. Hernández, M. Loewe, C. Villavicencio, and R. Zamora, "Magnetic field dependence of nucleon parameters from QCD sum rules", Phys. Rev. D **102**, 094007 (2020).

[274] M. Coppola, D. G. Dumm, and N. N. Scoccola, "Diquarks and nucleons under strong magnetic fields in the NJL model", Phys. Rev. D **102**, 094020 (2020).

[275] D. H. Rischke, "Debye screening and the Meissner effect in a two-flavor color superconductor", Phys. Rev. D **62**, 034007 (2000).

[276] H. Reinhardt, "Hadronization of quark flavor dynamics", Phys. Rev. B **244**, 316 (1990).

[277] A. Buck, R. Alkofer, and H. Reinhardt, "Baryons as bound states of diquarks and quarks in the Nambu-Jona-Lasinio model", Phys. Lett. B **286**, 29 (1992).

[278] N. Ishii, W. Bentz, and K. Yazaki, "Faddeev approach to the nucleon in the Nambu-Jona-Lasinio (NJL) model", Phys. Rev. B **301**, 165 (1993).

[279] T. Primer, W. Kamleh, D. Leinweber, and M. Burkardt, "Magnetic properties of the nucleon in a uniform background field", Phys. Rev. D **89**, 034508 (2014).

[280] S. Huang and J. Tjon, "Nucleon solution of the Faddeev equation in the Nambu–Jona-Lasinio model", Phys. Rev. C **49**, 1702 (1994).

[281] N. Ishii, W. Bentz, and K. Yazaki, "Baryons in the NJL model as solutions of the relativistic Faddeev equation", Nucl. Phys. A **587**, 617 (1995).

[282] H. Mineo, W. Bentz, N. Ishii, and K. Yazaki, "Axial vector diquark correlations in the nucleon: structure functions and static properties", Nucl. Phys. A **703**, 785 (2002).

[283] J. P. Carlomagno, D. Gomez Dumm, M. F. Izzo Villafañe, S. Noguera, and N. N. Scoccola, "Charged pseudoscalar and vector meson masses in strong magnetic fields in an extended NJL model", Phys. Rev. D **106**, 094035 (2022).